Universidade de Aveiro
2021

Pedro Gonçalo Pereira Duarte

# Produção de peças de porcelana por manufatura aditiva

# Production of porcelain parts by additive manufacturing

Universidade de Aveiro
2021

Pedro Gonçalo Pereira Duarte

# Produção de peças de porcelana por manufatura aditiva

# Production of porcelain parts by additive manufacturing

**Universidade de Aveiro**
**2021**

Departamento de Engenharia de Materiais e Cerâmica

**Pedro Gonçalo Pereira Duarte**

# Produção de peças de porcelana por manufatura aditiva

Tese apresentada à Universidade de Aveiro para cumprimento dos requisitos necessários à obtenção do grau de Doutor em Ciência e Engenharia de Materiais, realizada sob a orientação científica da Doutora Paula Maria Lousada Silveirinha Vilarinho, Professora Associada do Departamento de Engenharia de Materiais e Cerâmica da Universidade de Aveiro, e do Doutor José Martinho Marques de Oliveira, Professor Coordenador da Escola Superior de Aveiro Norte da Universidade de Aveiro, e orientação empresarial do Engenheiro Jorge Miguel Simões Marinheiro, responsável da divisão técnica da empresa Porcelanas da Costa Verde, S.A. situada em Vagos, Aveiro.

Apoio financeiro da FCT e do FSE no âmbito do III Quadro Comunitário de Apoio

Este trabalho foi desenvolvido sob financiamento da FCT através da bolsa com referência SFRH/BDE/97497/2013.

**o júri**

presidente

Doutora Ana Margarida Corujo Ferreira Lima Ramos
Professora Catedrática, Universidade de Aveiro

vogais

Doutor António José Vilela Pontes
Professor Associado, Universidade do Minho

Doutora Begoña Ferrari Fernández
Investigadora Titular, Conselho Superior de Investigações Científicas, Madrid

Doutor Fernando Jorge Lino Alves
Professor Associado, Universidade do Porto

Doutora Ana Maria de Oliveira e Rocha Senos
Professora Associada, Universidade de Aveiro

Doutora Paula Maria Lousada Silveirinha Vilarinho (Orientadora)
Professora Associada, Universidade de Aveiro

**agradecimentos**

Começo por agradecer à Fundação para a Ciência de Tecnologia e à empresa Porcelanas da Costa Verde pelo apoio financeiro que possibilitou o desenvolvimento do trabalho. Também aos meus orientadores, professora Dr.ª Paula Vilarinho, professor Dr. Martinho Oliveira e engenheiro Jorge Marinheiro, por todo o conhecimento transmitido e pelas suas contribuições ao longo deste trabalho.

Quero agradecer também ao corpo técnico do Departamento de Engenharia de Materiais e Cerâmica e da Escola Superior de Aveiro Norte, ambos da Universidade de Aveiro, pelo apoio prestado no desenvolvimento do trabalho. A todos os colaboradores da Porcelanas da Costa Verde, em especial da divisão técnica e do departamento de IDI por todo o apoio prestado.

Agradeço também a todos os meus amigos por toda a amizade, apoio e paciência que sempre demonstraram ao longo destes anos.

Finalmente o agradecimento mais importante aos meus pais, à minha irmã e à minha avó por toda o amor, educação e valores que me transmitiram.

**palavras-chave**

Manufatura aditiva, industrialização, porcelana, pós tratados térmicamente, impressão por jato de ligante, sinterização seletiva a laser

**resumo**

A manufatura aditiva é um meio disruptivo para a produção de objetos tridimensionais que tem como maior vantagem a possibilidade de produzir objetos de formas complexas que de outra forma seriam impossíveis de produzir ou com um custo elevado. Com o rápido crescimento e desenvolvimento destas tecnologias, o interesse da indústria tem crescido nos últimos anos, como é o caso da Porcelanas da Costa Verde, um produtor de objetos de porcelana e que procura sempre novas tecnologias para atingir novos mercados, produzir novos produtos ou melhorar a sua produtividade.

Neste trabalho foram exploradas as tecnologias de base de pó como *Binder Jet Printing (BJP)* e *Selective Laser Sintering (SLS)* com vista à sua potencial industrialização. Tendo disponível a tecnologia de BJP nas suas instalações, o maior foco deste trabalho é o BJP. Para isso estudaram-se diferentes ligantes em pó com o objetivo de produzir objetos em verde com resistência mecânica em verde para poderem ser manipulados em etapas pós-conformação. Considerando os ligantes estudados (PVA, maltodextrina, alginato de sódio e CMC), o PVA apresentou os melhores resultados para a produção de objetos de porcelana por BJP, em quantidades que variam entre 10 e 15 wt.% na mistura a utilizar. Depois de identificado o ligante em pó a usar, o uso de pós de porcelana tratados termicamente foi estudado com o objetivo de melhorar a impressibilidade dos pós de porcelana, ou seja, produzir objetos livres de defeitos. Os resultados mostram que uma formulação com quantidades iguais de pós tratados e não tratados evita a produção de objetos com defeitos.

Relativamente às etapas de pós conformação, foram testados os ciclos de sinterização industrial disponíveis na Costa Verde, bem como o uso de prensagem isostática a frio e a infiltração de objetos impressos com suspensão aquosa de porcelana. Os resultados mostram que os ciclos térmicos são adequados para produzir objetos de geométrica complexa, no entanto sem atingir 100% de densificação. Por outro lado, a prensagem isostática a frio permitiu produzir objetos com 97 % de densificação, no entanto mostrou-se ser inapropriada para objetos de geometria complexa. A infiltração com suspensão de porcelana mostrou ser ineficaz para os objetos impressos. Finalmente, foi explorada a possibilidade de industrialização das técnicas com foco na produção de matéria prima e etapas de pós conformação industriais que mostraram ser adequadas.

Como conclusão, foi provada a capacidade de produzir objetos de porcelana por manufatura aditiva a nível industrial, no entanto foram identificados alguns problemas para serem abordados em trabalhos futuros, com vista à completa implementação da tecnologia na Porcelanas da Costa Verde.

**keywords** Additive manufacturing, industrialization, porcelain, heat-treated powders, binder jet printing, selective laser sintering

**abstract**

Additive manufacturing is a disruptive way to produce three dimensional objects with the main advantage being the ability to produce highly complex geometries and designs which are impossible or expensive to produce in other conventional way. With the fast development and growth of AM technologies the interest from the industry has grown. This is the case of *Porcelanas da Costa Verde*, a porcelain producer looking for new technologies that allow to reach new markets, produce new objects and improve its productivity.

In this work two powder bed AM technologies were used: Binder Jet Printing (BJP) and Selective Laser Sintering (SLS). As BJP is already available at industrial facilities of Costa Verde, this technique was the main focus of these work. To accomplish so, the study of a proper *in-bed* binder, which allows the manipulation of the printed parts in post-conformation processes was crucial. Among the *in-bed* binders studied (PVA, maltodextrin, sodium alginate and CMC), PVA exhibit the best results in amounts of 10 to 15 wt.% in the powder formulation. Once the *in-bed* binder was identified, the improvement in the printability of the powders, i.e., the ability to produce defect free printed parts was assessed by studying the use of heat-treated porcelain powders. The results shown that the use of equal fractions of raw and heat-treated porcelain powders leads to the elimination of defects in the printed parts.

Concerning the use of post-conformation processes in order to improve the density of the produced parts, the thermal industrial cycles of *Porcelanas da Costa Verde* were studied and cold isostatic pressing (CIP) and pressureless infiltration of parts with porcelain suspension as well. The final results highlight the ability to produced complex shaped parts with the industrial thermal cycles, however, the full densification of the parts was not obtained. In the case of CIP, the final parts reached 97 % of relative density but shown to be not appropriate for complex shaped parts. In the case of the pressureless infiltration, the process shown to be not appropriate for the infiltration of porcelain printed parts. Finally, the industrialization of the techniques was explored with focus in the raw materials production and the post-conformation processes and both shown to be adequate for the industrialization.

Concluding, the possibility of producing defect free porcelain objects through powder bed AM technologies was proven, however, several challenges were identified to be assessed in future work in order to reach full industrialization.

## List of figures

## List of tables

## List of main abbreviations

| | |
|---|---|
| AM | Additive Manufacturing |
| AP | Apparent Porosity |
| ASTM | American Society for Testing and Materials |
| BJ | Binder Jetting |
| BJP | Binder Jet Printing |
| CAD | Computer Aided Design |
| CIP | Cold Isostatic Pressing |
| CMC | Carboxymethylcellulose |
| DED | Directed Energy Deposition |
| DLP | Digital Light Processing |
| DMD | Direct Metal Deposition |
| DMLS | Direct Metal Laser Sintering |
| DSC | Differential Scanning Calorimetry |
| EBAM | Electron Beam Additive Manufacturing |
| EBM | Electron Beam Melting |
| FDM | Fused Deposition Modelling |
| FFF | Fused Filament Fabrication |
| FM | Formative Manufacturing |
| HIP | Hot Isostatic Pressing |
| HR | Hausner Ratio |
| ISO | International Organization for Standardization |
| JM | Joining Manufacturing |
| LENS | Laser Engineered Net Shaping |
| LOM | Laminated Object Manufacturing |
| LT | Layer Thickness |
| ME | Material Extrusion |
| MJ | Material Jetting |
| PA | Polyamide |
| PBF | Powder Bed Fusion |
| PSD | Particle Size Distribution |
| PVA | Polyvinyl Alcohol |
| SEM | Scanning Electron Microscopy |
| SL | Stereolithography |
| SLA | Stereolithography Apparatus |
| SLS | Selective Laser Sintering |
| SM | Subatractive Manufacuturing |
| SSA | Specific Surface Area |
| STL | Standard Tessellation Language |

| | |
|---|---|
| TG | Thermogravimetric Loss |
| VP | Vat Photopolymerization |
| WA | Water Absorption |
| WIP | Warm Isostatic Pressing |
| XRD | X-Ray Difraction |

## List of main symbols

| | |
|---|---|
| $\%\rho_{Arc}$ | Relative density assessed by Archimedes method |
| $\%\rho_{geom}$ | Relative geometric density |
| $D_f$ | Diameter of the part |
| $D_i$ | Diameter of the virtual design |
| $D_{max}$ | Maximum dimension of a particle |
| $D_{min}$ | Minimum dimension of a particle |
| Dv10 | 10 vol.% of powder under the measured value in micrometers |
| Dv50 | 50 vol.% of powder under the measured value in micrometers |
| Dv90 | 90 vol.% of powder under the measured value in micrometers |
| l | Length of the cylindrical part |
| $L_f$ | Length of the part |
| $L_i$ | Length of the virtual design |
| m | Mass of the part |
| $m_{dry}$ | Mass of the dry part |
| $m_{imp}$ | Mass of the part immersed in water |
| $m_{powder}$ | Mass of powder |
| $m_{soak}$ | Mass of the part after immersion in water |
| r | Radius of the cylindrical part |
| $\rho_{free\ settled}$ | Density of powder free settled |
| $\rho_{tapped}$ | Density of powder after tapping |
| Tc | Crystallization temperature |
| $t_{f\,1}$ | Time of liquid binder first drop complete absorption |
| $t_{f\,2}$ | Time of liquid binder second drop complete absorption |
| Tg | Glass transition temperature |
| $t_{i\,1}$ | Time of liquid binder first drop contact with powder surface |
| $t_{i\,2}$ | Time of liquid binder second drop contact with powder surface |
| Tm | Melting temperature |
| $V_b$ | Volume of binder fraction |
| $V_{free\ settled}$ | Volume of free settled powder |
| vol.% | Volume percentage |
| $V_p$ | Volume of porcelain fraction |

| | |
|---|---|
| $V_{tapped}$ | Volume of tapped powder |
| wt.% | Weight percentage |
| $\Delta D$ | Diameter variation |
| $\Delta L$ | Length variation |
| $\rho_{Arc}$ | Density assessed by Archimedes method |
| $\rho_b$ | Density of binder |
| $\rho_c$ | Reference density of the green parts |
| $\rho_{geom}$ | Geometric density |
| $\rho_p$ | Reference density of porcelain from Costa Verde |

## Motivation and objectives

Additive manufacturing (here after designated as AM) is a disruptive technique to produce objects. This technique allows production of functional, complex shaped and highly customized objects/products. AM is currently well known for the fabrication of polymeric and metallic materials due to its easier adaptation to a broad range of AM processes and applications. Nevertheless, for ceramics production is far behind its scientific and technical interest. There is yet a long way to go to turn AM of ceramics an industrial reality and more research and development is of utmost importance.

AM started as a rapid prototyping tool, used by industries to quickly create a system or object representation before its commercialization. However, the interest in the use of this process as a production route was immediately recognized and currently increasing in all engineering areas. AM is considered a disruptive manufacturing technique expected to change completely the production landscape of the world, due to the design freedom and customization of new products, the high efficiency in the use of resources and the flexibility in the production process. However, from the industrial point of view, one limitation is the inadequacy of the existent raw materials for AM processes, which can be a hampering drawback for its wide implementation. Although, if limitations are overcome, the fully economical potential of AM will be released.

A ceramic whiteware is defined by ASTM as a glazed or unglazed ceramic body which is commonly white and comprise products as porcelain, china, earthenware, tile and semivitreous ware [1]. Although the term is porcelain is generally used for ceramic bodies with technical applications and china is the term used for non-technical applications [1], in this work the noun porcelain will be used to refer to a ceramic whiteware body for dinnerware or tableware [2]. Porcelains are typically white, translucent, fully dense and hard. Although in this work we refer to porcelain as a ceramic whiteware for tableware applications, it also has technical applications such as electrical, chemical, mechanical, structural and thermal wares [1][3].

Porcelain is one of the most complex ceramics due to its composition based in the three-part folded system of clay, feldspar and quartz (Table 1). Clays are responsible to provide plasticity and mechanical strength to the green part. Feldspars are fluxes used to decrease the sintering temperature. These feldspars are usually potash (microcline) and sodium

feldspar (albite) [4]. Finally, the quartz is used as filler and provides resistance to cracking during drying and forms a skeleton network during firing [4].

**Table I:** Most common materials used in the production of porcelain. (adapt. from [4])

| Raw material | Nominal composition |
|---|---|
| Ball (plastic) clay | $Al_2O_3.2SiO_2.2H_2O$ |
| Kaolin (china) clay | $Al_2O_3.2SiO_2.2H_2O$ |
| Soda feldspar | $Na_2O.\ Al_2O_3.6SiO_2$ |
| Potash feldspar | $K_2O.\ Al_2O_3.6SiO_2$ |
| Quartz | $SiO_2$ |

The conformation processes for porcelain bodies started with slip casting and jiggering, however with the development in automation, the processes of dry powder pressing and pressure casting appeared as routes for porcelain products manufacturing [5]. After the ceramic body is conformed, thermal processing, i.e. firing, is required for the microstructural chemical reactions to occur and densification to take place. Typically, the range of temperatures for porcelain fabrication is 1300 - 1400 °C [3]. Porcelain for tableware applications are glazed in order to improve its sanitary safety, increase the surface hardness and improve the aesthetic of the ceramic bodies.

*Porcelanas da Costa Verde, S.A.* (here after designated as Costa Verde) is a Portuguese company that produces porcelain parts, for tableware, via conventional processes such as slip casting, high pressure casting, plastic molding and isostatic pressing. Always looking for ways to add value to their products and for new processes that can reduce manufacturing time, improve the efficiency, reduce waist, be more sustainable and open new markets, Costa Verde is currently very interested in the use of AM to produce porcelain parts.

The process of Binder Jet Printing (BJP) is already used in the company for the development of prototypes and shape validation. In this sense, the interest in exploiting the use of BJP as a production route increased in the last years in the company. However, the feedstocks, i.e., the mixture of raw materials and additives, produced by Costa Verde for the conventional fabrication processes are not suitable for the use of BJP for production of

porcelain parts. If BJP of porcelain is to be implemented, it is of paramount relevance to develop optimized feedstock for this process. This fact raised the need to study and develop the feedstock for BJP, and, consequently, the post conformation steps adaptation, as well.

Industrial applications of these techniques in the ceramics sector require knowledge of both the process itself and the feedstock and post printing steps. It is precisely within this context that lies the main goal of this industrial PhD project: to explore and study the use of powder bed AM techniques to produce porcelain parts, as BJP and Selective Laser Sintering (SLS) techniques, with special emphasis on the first one, keeping as much as possible the raw materials, composition, post-conformation processes and facilities of Costa Verde's current porcelain production.

Due to its availability in the company and ease to scale up, the main technique exploited in this work is BJP. In this process a printhead deposits a liquid binder to bond particles in a powder bed for each layer of the object to be constructed. After the depositions of the liquid binder, a roller is responsible to spread a new layer of powder and the process is repeated. The exceeding powder acts as support, allowing the production of highly complex shaped parts. Another advantage of this technique is the highly use of powder, due to the possibility of recovery of the powder. The fragility and porosity of the green parts arise as main drawbacks of the technique. However, for comparison purposes, the technique of SLS, where a laser is used to melt/sinter the material in powder form, was also used in this work.

Four main objectives were identified for this thesis: i) printability of porcelain powders in BJP, ii) printability of porcelain powders in SLS, iii) post-conformation processing of porcelain printed parts and iv) exploitation of the industrialization of powder-bed AM techniques.

In what concerns the study of the printability of the porcelain powders in BJP (Objective 1), a major challenge lies in finding the appropriate *in-bed* binders to use and their amount. Due to its nature the interaction of the liquid binders with the porcelain powder will not lead to green parts with enough strength, creating the need to study the role of an *in-bed* binder which provides enough mechanical strength for post conformation processing steps. Four different *in-bed* binders are addressed in this work and the printability of the feedstock is evaluated, i.e., the ability to produce defect free printed parts. The role of particle size, the

particle size distribution and the pre-processing treatment of the porcelain powders towards optimized printability of the feedstock is also aimed in this study.

An alternative AM powder bed technique of powders to BJP is SLS. With comparison purposes the printability of porcelain powders in SLS is also addressed (Objective 2). The effect of pre-processing treatment of porcelain powders, the amount of binder and the reuse of powders are investigated and the benchmark with BJP is presented.

Post-conformation processing steps are needed to reach a high density of additively manufactured ceramic parts. Hence, post-conformation processing steps, such as infiltration, isostatic pressing and industrial thermal cycles need to be systematically investigated (Objective 3). Parts produced either by BJP and SLS are addressed and comparisons are established.

To conclude and within the main goal of this industrial PhD work, a main objective (Objective 4) is to assess the industrialization of powder bed AM techniques as production route for porcelain objects. In this sense, the industrial preparation of the feedstock, with focus in the production of porcelain powders by industrial spray drying process, the AM process and the post-conformation processes, already used for conventionally produced porcelain parts, are discussed.

## References


[1] ASTM, “C 242 - 01 - Standard Terminology of Ceramic Whitewares and Related Products.” pp. 1–11, 2001.

[2] H. Boussak, H. Chemani, and A. Serier, “Characterization of porcelain tableware formulation containing bentonite clay,” *Int. J. Phys. Sci.*, vol. 10, no. 1, pp. 38–45, 2015.

[3] C. Barry Carter and M. Grant Norton, *Ceramic materials: Science and engineering*. 2007.

[4] W. M. Cam and U. Senapati, “Porcelain-Raw Materials, Processing, Phase Evolution, and Mechanical Behavior,” *J. Am. Ceram. Sociaty*, vol. 81, no. 1, pp. 3–20, 1998.

[5] D. W. Richerson, *Modern Ceramic Engineering*, Seond Edit. 2001.

# *Chapter 1: Introduction and state of the art*

## 1.1. Additive Manufacturing

### *1.1.1. Classification and terminology of additive manufacturing*

Additive manufacturing (AM) is a disruptive technology to produce parts with complex shapes and functional features, based on a layer by layer construction. Due to the high interest in this process from diverse areas of technology and science several different designations have been used to refer to AM, such as Rapid Prototyping, Rapid Manufacturing, Rapid Tooling, 3D Printing, Layer Manufacturing, among others, until the more recent and standard designation of Additive Manufacturing, what reflects as well the evolutionary process of AM. Due to the need to normalize and regulate, as a direct consequence of the growing importance and the commoditization tendency an universal designation and a general definition was required. In 2009, ASTM (American Society for Testing and Materials) published the first norm for AM related nomenclature, ASTM F2792 − 12a [6].

According to ASTM, AM is the process of joining materials, usually in a layer by layer process, in order to produce a 3D (three dimensional) object from digital data as opposed to subtractive manufacturing processes [6]. In 2015, in order to standardize the nomenclature used by both institutions (ASTM and ISO), the ASTM/ISO 52900 [7] was published, using the same definition for AM.

The popular term 3D Printing should not be used as synonymous of AM. In fact, according with ASTM the term 3D Printing refers to the fabrication of an object by the deposition of material through printhead, nozzle or another printer technology [6]. Currently, the term 3D Printing is mainly used by media, operators and non-technical public. For that reason, in this work the term Binder Jet Printing (BJP) will be used to refer to the technique in which a liquid binder is deposited in a powder bed to join the powder materials [6].

The ASTM F2792 – 12a standard classifies and defines the terminology for all the different additive manufacturing technologies, including terms and brief descriptions, definitions, nomenclature and acronyms [6]. Accordingly, ASTM F2792 – 12a standard orders the AM technology in seven classes based on the method of joining the materials and layers, as: (1) Vat Photopolymerization, (2) Sheet Lamination, (3) Powder Bed Fusion, (4) Material

Extrusion, (5) Binder Jetting, (6) Directed Energy Deposition and (7) Material Jetting. In Table 1.I the AM processes are presented, grouped by categories, with brief descriptions of each one and enumerates the different techniques of each AM categories, the feedstock form and type of materials used by each one. The working principle of each process will be further presented in detail, as well as its main advantages and disadvantages.

The general process flow for AM techniques, as illustrated in Figure 1.1, starts with a virtual design model, drawn by CAD (Computer Aided Design), which is a digital file of a 3D draw [6]. This design is then converted in to a STL (Standard Tessellation Language) file, which defines the surface of the 3D model using only triangles [6]. The original designation of this acronym was Stereolithography, referring to the first AM technology. However, nowadays is accepted by AM community as Standard Tessellation Language. This file is then uploaded to the slicing software, that defines geometrically each layer and printing parameters of the model. The printing process starts with the first layer and in a layer by layer process, every layer is deposited on the top of the previous one. At the end of this cyclic process, the object is completely produced. In some cases, post-conformation steps, such as support structures removal, depowdering and sintering, are required in order to achieve the object with the final properties required [8].

**Table 1.I:** AM processes categories, techniques, feedstock form and materials used [6].

| **AM Process Categories** [6] | **Description** [6] | **Techniques** | **Feedstock** | **Materials** |
|---|---|---|---|---|
| Vat Photopolymeri-zation | Liquid photopolymer in a vat is selectively cured by light-activated polymerization | SLA®<br>Micro-SLA®<br>DLP<br>CLIP | Liquid | Resins and waxes<br>Polymers<br>Ceramic suspensions |
| Sheet Lamination | Sheets of material are bonded to form an object | UC/UAM<br>LOM | Solid | Metals<br>Ceramics<br>Polymers |
| Powder Bed Fusion | Thermal energy selectively fuses regions of a powder bed | SLS<br>SLM<br>DMLS<br>EBM<br>MJF | Powder | Polymers<br>Metals<br>Ceramics<br>Composites |
| Material Extrusion | Material is selectively dispensed through a nozzle or orifice | FFF/FDM®<br>Robocasting<br>Bioplotting<br>Contour crafting | Filament<br><br>Paste | Polymers<br>Ceramics<br>Composites |
| Binder Jetting | Liquid bonding agent is selectively deposited to join powder materials | BJP<br>MJP | Powder | Metals and metal alloys<br>Ceramics<br>Composites |
| Directed Energy Deposition | Focused thermal energy is used to fuse materials by melting as they are being deposited | LENS<br>EBAM<br>LMD | Powder | Metals<br>Polymers |
| Material Jetting | Droplets of build material are selectively deposited | DOD<br>Polyjet<br>NP Jetting™<br>CIJ<br>RIJ | Liquid | Polymers |

**Note: SLA®** - *Stereolithography Apparatus*; **DLP** – *Digital Light Processing*; **CLIP** – *Continuous Liquid Interphase Printing*; **LOM** – *Laminated Object Manufacturing*; **UC/UAM** - *Ultrassonic Consolidation/Ultrassonic Additive Manufacturing*; **SLS** – *Selective Laser Sintering*; **SLM** – *Selective Laser Melting*; **DMLS** – *Direct Metal Laser Sintering*; **EBM** – *Electron Beam Melting;* **MJF** – *Multi Jet Fusion*; **FFF** – *Fused Filament Fabrication*; **FDM®** – *Fused Deposition Modelling*; **BJP** – *Binder Jet Printing*; **MJP** – *Multi Jet Printing*; **LENS** – *Laser Engineered Net Shaping*; **EBAM** – *Electron Beam Additive Manufacturing*; **LMD** – *Laser Metal Deposition*; **DOD** – *Drop on Demand*; **NP Jetting™** - *NanoParticle Jetting*; C**IJ –** *Continuous Inkjet Printing;* **RIJ –** *Reactive Inkjet Printing*


**Figure 1.1:** General flow of a AM process from the CAD model to the final object [9].

### *1.1.2. History*

The first process reported, that is considered an AM process, was published in 1981 by Hideo Kodama [10] in which is successfully produced an object in a layer by layer process, using ultraviolet (UV) light to solidify layers of a photosensitive polymer. However, Charles W. Hull is considered by many as the father of AM, once in 11$^{th}$ of March of 1986 his patent for the Stereolithography (SL) process was granted (US Patent 4575330) and is the first one known [11]. Charles Hull invented SL technique in 1984 and the first commercial AM device based in SL, named SLA-1 (Stereolithography Apparatus), produced by the company 3D Systems, of which he is one of the founders, appeared in 1987 [12]. The process of SLA-1 uses an UV light to solidify layers of photosensitive liquid polymers as well [12].

By the end of 80's and early 90's, several patents were also filled: Scott Crump and the company Stratasys Inc. filled a patent for the nowadays known Fused Filament Fabrication in 1989 [13], in which a material such as thermoplastics, are fused and deposited in each that adheres to the previous one; Sachs *et al.* [14] at Massachusetts Institute of Technology, USA filled the patent in 1989, for the nowadays known 3D Printing techniques, in this work defined as BJP, in which a liquid binder is deposited in a powder material to join particles; and in 1990 Carl Deckard *et al.* [15] at the University of Texas at Austin, USA, developed the first SLS technique, in which a laser fuses a powder material in a powder bed to join the powder for each cross section of the object being printed. Between 1991 and 1996 the first commercial 3D Printers based in these processes were developed and available commercially [12]. In the 00's several new machines were launched into the market with

features such as BJP with full colour, BJP with nozzles that deposit resins as liquid binder which is solidified by an UV light, Laminated Object Manufacturing (LOM) printers were sold by different providers, in which the laminated material such as metal foils is used each layer and an energy source cuts the correspondent cross section and Direct Metal Deposition (DMD) is created to repair metal parts by using Directed Energy Deposition (DED) with metal powders, in which the powder material, such as metallic powders, are deposited in the same spot where an energy source is focused to fuse the powder [12]. More advanced AM processes, such as Electron Beam Melting (EBM), which works as SLS using an electron beam as energy source was introduced in 2007 by Arcam and Laser Engineered Net Shaping (LENS) based in DED technology, was introduced by Optomec in the same decade [12].

The most used AM technique worldwide is Fused Filament Fabrication (FFF), also known as Fused Deposition Modelling (FDM), which uses a polymeric or composite filament which is melted and deposited in a layer by layer process to construct the object. Due to its price, cleanness and ease of use this technique is suitable to have at home or office, being the choice of most of the end users. In the 2010's, due to the expiration of the initial patents several companies start producing FFF/FDM printers reducing the cost and turning it available to end users from different fields, such as designers, architects, engineers and hobbyists.

Summarizing, throughout the years new machines, new techniques and new materials have been used and exploited in AM. This is an industry currently in fast development and always reaching more and more new applications, users and industries.

### *1.1.3. Comparison with conformation methods*

One of the most important steps in the production of an object is its conformation. The conformation of an object may be done in four distinctive ways: additive manufacturing (AM), subtractive manufacturing (SM), formative manufacturing (FM) and joining manufacturing (JM) [8]. In Figure 1.2 the four groups are schematically represented and their working principle, main advantages and limitations are presented.

In AM processes the object is produced by adding material, usually in a layer by layer cyclic process, using a digital model of the object. The main advantages of AM is the ability to

produce highly complex shaped and personalized objects with reduction in the number of post-conformation assemblies, the reduced use of material and reduced tool costing and, from the commercial point of view, the low volume production number of parts and the reduction in the time from the idea concept until the first produced object as opposed to SM and FM which requires the development of tools. These advantages highlight the flexibility in the production and shape of the object combined with the efficiency in the materials use. However, in the limitations the ability to produce parts with comparable properties to the ones produced in SM and FM ways, such as density and mechanical strength, the reproducibility of parts with the same properties, which can be affected by feedstock morphology and reused and printing parameters [16], and the surface finishing inherent to the layer by layer process which may require post-conformation methods [8][17].

The SM processes, where a tool is used to remove material from a material block to give the final shape to the object. In the case of ceramic industry, subtractive manufacturing is sporadically used in already conformed ceramic parts, to make features such as holes, however for metals, polymers and composites is often used, with processes such as CNC milling, drilling and grinding. The main advantages of SM are the dimensional accuracy, the reproducibility of the parts, the surface finishing of the object and the broad range of materials capable of being machined. On the other hand the high waste of materials and the production of complex shapes, which required specific tools and tool paths to reach all the surfaces of the object are the main limitations of SM [8][17].

In the FM processes a tool, usually a mold, is used to give the shape to the product. Isostatic pressing slip casting and jiggering are examples of formative manufacturing processes used in the production of porcelain parts, however, is frequently used for plastics as injection molding and with metallic materials in casting. Formative processes are commonly used in mass production due to unrivaled cost per part, the waste of materials is reduced and it has high production and reproducibility rate, however, the cost of tooling is high and its development is time consuming, increasing the leading times from the concept until the production [8][17].

JM processes are characterized by joining two parts, already produced, to give the shape of the final object. This type of processes are used in the porcelain production, for example to bond handles in holloware. For other materials, such as metallic objects, welding is an example of this type of processes. Bonding processes are used to produce parts with

shapes difficult or impossible to produce by any other ways, however, the production rate is low, when it is done manually, or the tooling is expensive, when it is done automatically. In addition, the joining zone may promote the development of defects and regards in the bond strength between the two parts [17].

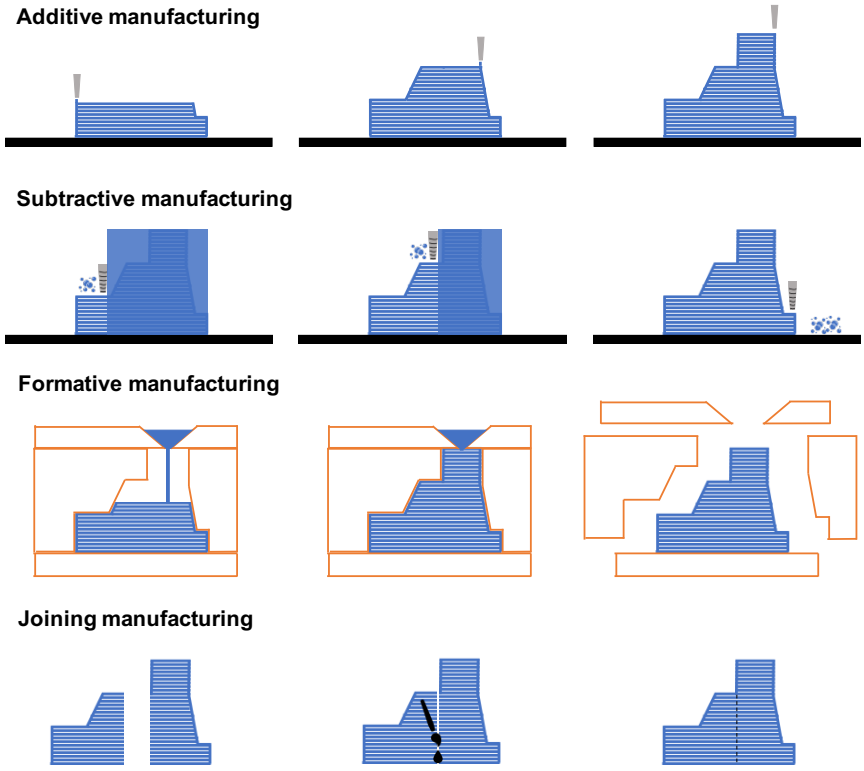


**Figure 1.2:** Conformation manufacturing of additive, subtractive, formative and joining processes (adapted from [17]).

Due to the type of products and its implementation at the industrial scale, with different types of materials, SM and FM processes are the most comparable to AM ones. When compared with SM and FM conformation processes, AM fills the gap for small production series, reducing the cost per part and highly complex shaped parts, keeping the same price per part regardless of its shape complexity, considering only the process itself (Figure 1.3). However, it is also necessary to take in consideration that the cost per part will depend on the AM technique being used: for instance, the process of Selective Laser Sintering is more energy consuming than BJP, leading to higher cost for each part. Regarding the shape complexity one should also consider that parts with high complex shape may lead to a more costly post-conformation steps, such as depowdering of the parts. SM processes, also allows the production of complex shaped parts, but when compared with AM processes,

there are complex shapes of parts that will be impossible to produce through SM. It also has a limitation regarding the waste of material, which, most of the times, cannot be reused. AM is more cost efficient than FM, mainly due to the high cost of tooling for FM. However, when there is a need for high number of parts in the production run, FM starts to be cheaper than AM. Regarding geometrical complexity, AM is cheaper than FM for parts with a very complex shape. In fact, for some shapes, the FM would need a high number of tooling parts, even if feasible, which can increase drastically the cost per part [8][17].

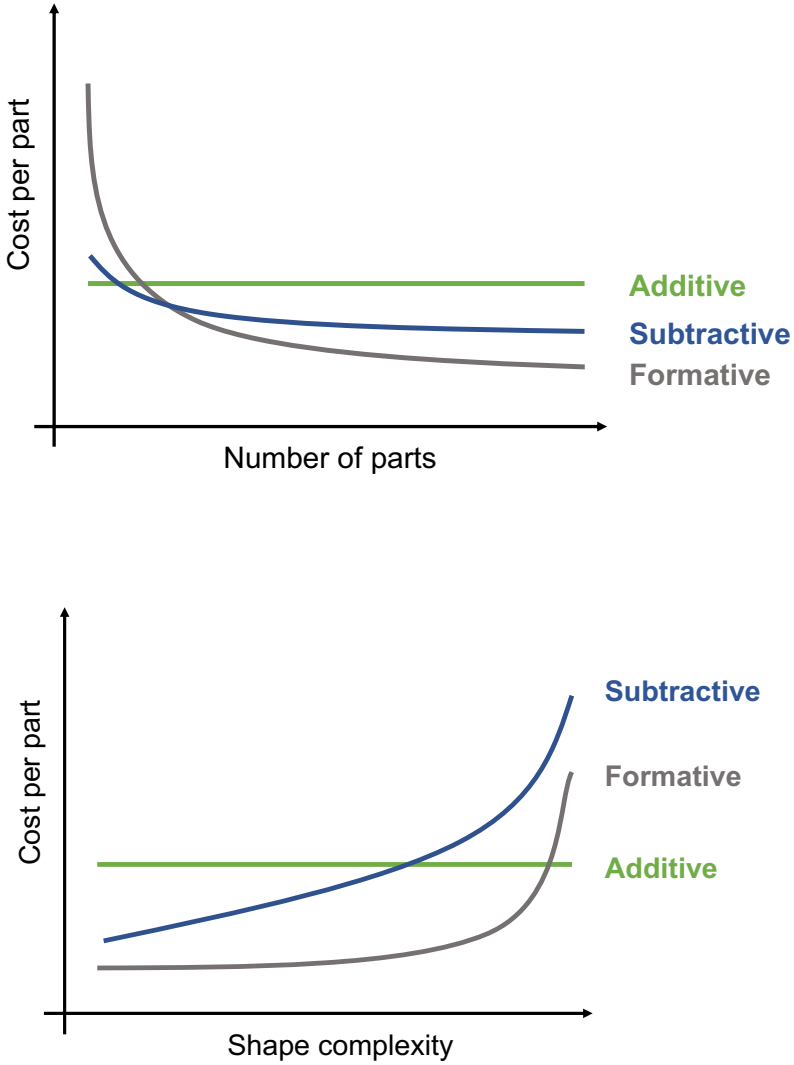


**Figure 1.3:** Comparative plot of the cost per part as function of the number of parts and as function of the shape complexity of additive, subtractive and formative processes (adapted from [17]).

From the industrial production point of view, the use of all the processes described above are complementary to each other, allowing to produce different objects and reach new

markets and costumers. The choose of a conformation method for a specific object will depend in the design of the object, which may be impossible to produce in some processes, the production cost, which depends in the number of objects to be produced in the production batch and in the type of material used, which needs to be able to be processed by the conformation method [17]. In this sense, the study, development and adaptation of existent materials for different conformation methods. One example of this fact is the adaptation of the powders used for isostatic pressing to be used in powder bed AM techniques.

In this sense the AM distinguish from SM and FM by its high customization of products, the high efficiency in material usage, the flexibility of production runs, the near final products stage, depending on the material and application of the object, and the reduced time from the concept to the product.

### *1.1.4. Additive Manufacturing technologies*

In this section we present the working principle, the main advantages and limitations of each AM class. Binder Jetting (BJ), which comprises BJP, and Powder Bed Fusion (PBF), which comprises SLS, will be discussed in detail further in this document.

#### *1. Vat Photopolymerization*

Vat photopolymerization (VP) is the AM class in which a liquid photosensitive polymer, contained in a vat, is selectively cured by a light-activation polymerization [6]. The main advantages of VP processes are printing resolution and accuracy, materials and energy usage efficiency and the surface finishing [18] and its limitations include the cost of photosensitive materials and the unrecyclable material used, for instance, in the support structures [8] [18]. This class includes techniques such as Stereolithography (SL), Figure 1.4, and Digital Light Processing (DLP), Figure 1.5. These techniques differ from each other by using a laser or a group of lasers to cure the material, i.e., point by point, in the case of SL, and a mask to cure a whole layer at once, in the case of DLP [19]. This difference in the process as the advantage of geometric accuracy in the case of SL and the reduction in printing time for the case of DLP. After the curing of each layer, the build platform moves up and another layer is cured. The more important parameters for this group of techniques comprise the laser power, scanning speed, exposure time, resin composition and the

photoinitiator [18]. The typical materials used in VP are photosensitive epoxy and acrylate based monomers/oligomers, which polymerize by interaction with light through cationic and radical polymerization [18].

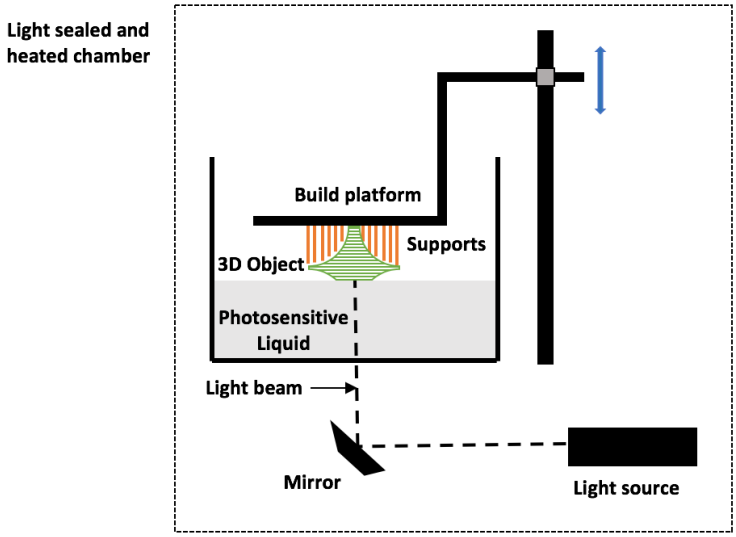


**Figure 1.4:** Schematic representation of Stereolithography Apparatus (Vat Photopolymerization).

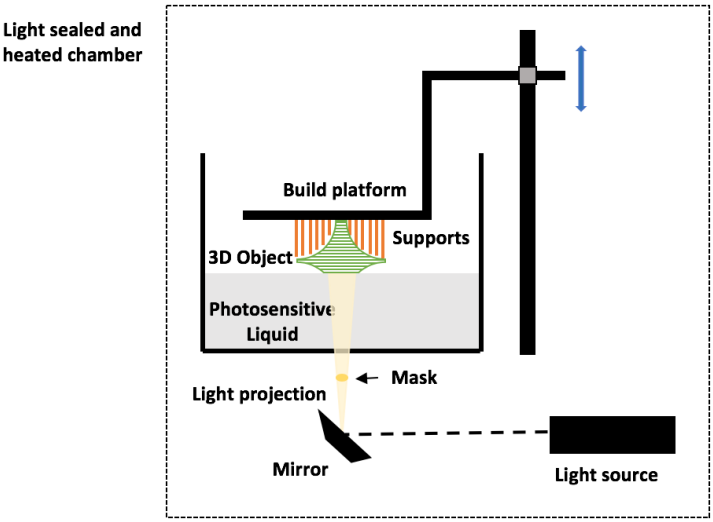


**Figure 1.5:** Schematic representation of Digital Light Processing (Vat Photopolymerization).

In order to produce ceramic objects through VP techniques it is required the preparation of a ceramic suspension with fine ceramic particles suspended in a liquid medium, which ca be aqueous or non-aqueous medium, with photosensitive monomers, once ceramic

particles are usually inert to light emission [19]. After curing, the ceramic particles are surrounded by the organic cured polymer which requires further steps to full removal of the organic part [19]. The rheological behavior of the suspensions plays a crucial role in the successful VP printing [20], however ceramics are well dispersed in acrylate monomers which are a suitable choice for the suspension medium [21], with a ceramic content ranging between 50-65 vol.% [22].

Griffith *et al.* [22] used silica ($SiO_2$), silicon nitride ($Si_3N_4$) and alumina ($Al_2O_3$) to prepare ceramic suspensions in acrylamide-based and diacrylate mediums and study the solid content and the refractive index of ceramic particles in the printing of ceramic parts. The authors found that the suspensions prepared with $Si_3N_4$, which has the highest refractive index, affects the curing depth and the printing of the parts, and reached fully dense alumina parts after sintering at 1550 °C. The mechanical properties of zirconia ($ZrO_2$) parts produced through VP was assessed by Harrer *et al.* [23] by producing $ZrO_2$ suspensions in a mixture of acrylates and methacrylates, founding that the it is possible to produce parts with similar strength to the ones conventionally produced (1000 - 1500 MPa), while Wang *et al.* [24] were able to produce $ZrO_2$ parts with relative density above 99 % after sintering at 1600 °C, using methyl alcohol medium with commercial photopolymer. Schwentenwein *et al.* [25] were able to produce final alumina parts with relative density above 99 % with a commercial alumina suspension. Alumina ($Al_2O_3$) was also used in VP processes to study the rheological behavior of suspensions [26], process parameters [27] and post-conformation steps [28]. Other materials such as SiC and SiOC [29], PZT [30] and biomaterials [31][32] were also used in VP processes. For complete information, reviews of the VP class can be found in [18][20].

Summarizing, the high price of photosensitive resins, that are needed to add to the ceramic suspensions, is a huge drawback to the application of this technique for industrial production, however the final parts properties, such as fully dense bodies and comparable mechanical strength to conventional methods, may be suitable for industries such as dentistry [33].

### 2. ***Sheet Lamination***

The Sheet Lamination class, in which a sheets of material are cut and bonded to form the object [6], comprises Laminated Object Manufacturing (LOM), which is the most

representative technique (Figure 1.6). This process uses the material in sheet form and an energy source (which can be laser, water jet, ultrasound, among others) to cut the sheet for each cross section. Then a heated roller is responsible to press and heat the new layer to the previous one, bonding both together, usually using an adhesive in the bottom side of the sheet [8][34]. The main process parameters comprise among others the heat temperature, the roller pressure, speed and temperature and the laser speed [34]. The major advantages of this process are the low cost of the equipment, the needlessness of support structures and little distortions created. However, the main limitations are the requirement of the material form (sheet), the limitation in complex shapes and the non-recyclable exceeding material from each print [8].

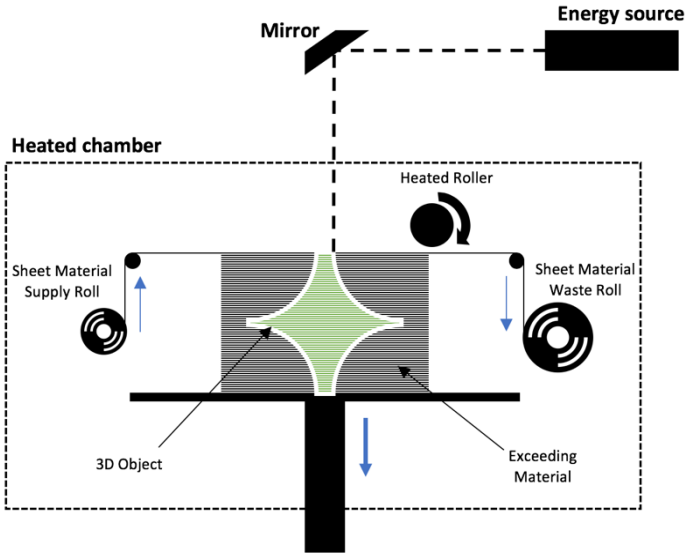


**Figure 1.6:** Schematic representation of Laminated Object Manufacturing (Sheet Lamination).

The materials that can be used in LOM technique need to be able to form a sheet or foil and can be paper, thermoplastic polymers, metal foils and ceramics [8]. Although the material form required by this process is a huge limitation for ceramics, the use of additives allows the processing of ceramics by sheet lamination. Zhong *et al.* [35] used LOM to produce silicon carbide (SiC) objects, by producing SiC green tapes with 0,15 mm of thickness with polyvinyl butyral (PVB) and butyl benzyl phthalate (BBP) used as binder and plasticizer respectively, reaching above 98 % of relative density after binder removal and pressureless sintering. Zhang *et al.* [36] prepared green tapes of alumina with 0,7 mm of thickness with PVB as binder, and using LOM produced alumina bodies with 65 % of relative

density, which increased up to 97 % after pressureless sintering at 1580 °C. Although there is limited reviews in the sheet lamination class, a book chapter focusing in the state of the art of LOM can be found in [34].

In conclusion, the Sheet Lamination processes, especially the LOM technique may be used to produced highly dense ceramics, however, its limitation regarding the production of highly complex shaped objects, which is one of the main advantages of AM in general, is a huge drawback for its use.

### 3. ***Material Extrusion***

The ME class is defined as the AM process in which the material is selectively dispensed through a nozzle or orifice [6]. Two major techniques belong to this class: Fused Filament Fabrication (FFF), represented in Figure 1.7, in which the material is in a filament form and is melted and deposited and Robocasting, represented in Figure 1.8, in which the material is in suspension or paste form. This class differentiates from the others by the feeding system, where a continuous extrusion through an orifice is performed. Then a movable nozzle is responsible to selectively deposit the material in the print bed [8]. The same principle is applied in robocasting, where the material in paste form is feed into the extrusion head. Then the extrusion head will deposit the material for each crossection. In the case of robocasting, this movable extruder can be piston type, if a piston is responsible to feed the material, for instance a syringe, or screw type, if a crew is responsible to feed the paste, such as a typical extrusion system. The most important process parameters comprise the nozzle diameter, the layer thickness and the environmental temperature, as the properties of the ceramic pastes play a crucial role focusing in the viscoelastic behavior for a proper printing process. The main advantages of this class is the broad range of materials able to be used, the low cost of equipment and reduce waste of materials, among others, while in the other hand the surface finishing, especially in the case of robocasting, and the need to control environmental characteristics, such as temperature and moisture, in order to promote a proper printing process, are, among others, limitations of the process [8].

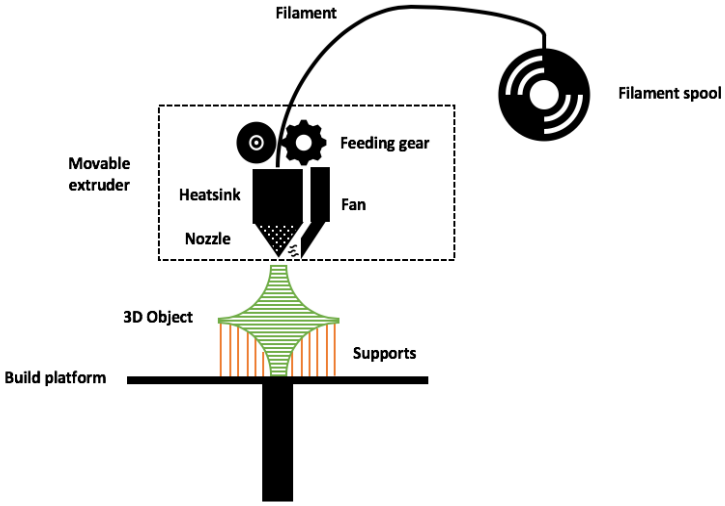


**Figure 1.7:** Schematic representation of Fused Filament Fabrication (Material Extrusion).

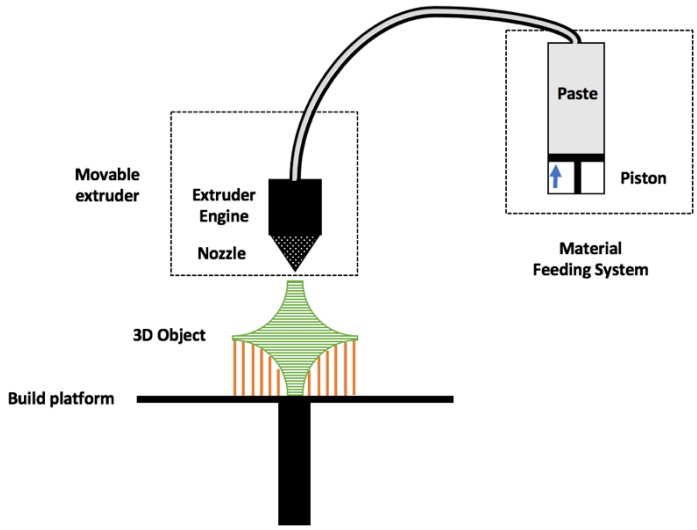


**Figure 1.8:** Schematic representation of Robocasting (Material Extrusion).

Robocasting has been used to produce porcelain parts. Although in the literature the term porcelain often refers to dental porcelain, opposed to this thesis, which refers to porcelain for tableware applications, the constitution is similar. Tian *et al.* [37] used a porcelain composed of quartz, kaolin, soda feldspar and illite to produce porcelain objects through material extrusion process. The authors were able to produce porcelain parts with similar porosity values (13 %) to the ones produced by slip casting, using the same suspension, after sintering at 900 °C. Lima *et al.* [38] used a porcelain composed by quartz, kaolinite, albite, orthoclase and muscovite to produce ceramic parts by slurry deposition. The authors found that printed parts have comparable mechanical properties to the ones produced

through slip casting, and comparable density (2,36 g/cm$^3$ for AM produced parts and 2,38 g/cm$^3$ for slip casted ones). Mullite parts were successfully produced by ME techniques, by Stuecker *et al.* [39], reaching 55 % of relative density as green parts, and increasing up to 96 % after sintering at 1650 °C. Other ceramic and ceramic composite materials were also subject of study in ME techniques, such as alumina [40]–[42], zirconia [43]–[45], tricalcium phosphate [46], bioactive glass [47], hydroxyapatite [48], graphene/SiC composites [49], WC [50], $B_4C$ [51]. Recent review papers in ME processes can be found in [52][53].

In conclusion, ME techniques are well developed for the different class of materials (polymers, metals, ceramics and composites) and are one of the most used worldwide. In the case of ceramics, ME processes present promising results, such as comparable densities and mechanical properties of printed parts to the ones produced through conventional ways and may be an option for industrialization of the techniques.

## 4. Directed Energy Deposition

In Directed Energy Deposition (DED) focused thermal energy, from an energy source that can be laser, electron beam or plasma arc, is used to fuse powder or wire materials as they are being deposited [6][54]. Laser-engineered Net Shaped (LENS) is one of the techniques from this class, and is schematically represented in Figure 1.9, and works by depositing the material in powder form in the same point where the energy is focused, fusing or sintering the material, creating bonds both between the particles being deposit and the previous layer [54]. The main process parameters are laser power, laser beam spot size, material feed rate scanning speed and layer thickness [54]. The main advantages of this process is the zero waste of material, once the material is selectively deposited, and comparable properties of objects to the ones produced conventionally [19] [54]. The main disadvantages are the high energy consumption, required to reach high melting temperatures, the surface finishing and the dimensional accuracy [19] [54].

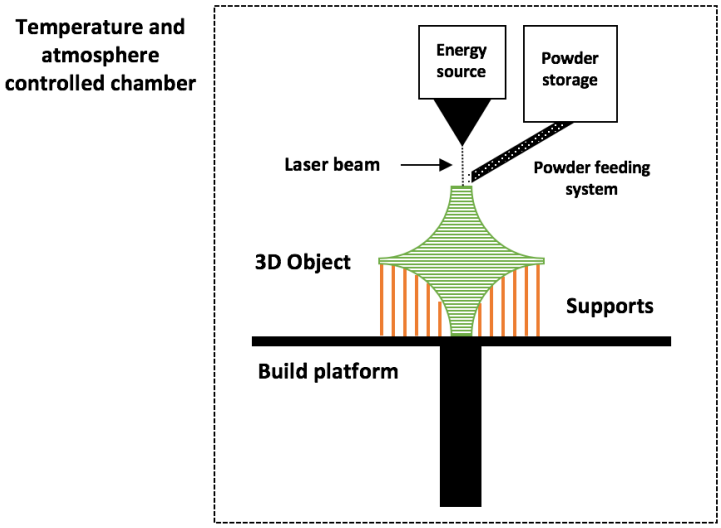


**Figure 1.9:** Schematic representation of Laser-engineered Net Shaping (Directed Energy Deposition).

Although the work in DED of ceramics is limited due to the high temperature needed to fuse the materials, there are still some work using ceramic materials. Li *et al.* [55] studied the effect of LENS printing parameters in the quality (layer geometry, surface roughness, powder efficiency among others) of alumina parts, founding that an increase in laser power leads to an increase in microhardness, improving the quality the surface roughness and powder efficiency among others, in addition, with the increase in the powder feeding rate, the hardness decrease. The high temperatures needed to fuse ceramic materials leads to crack formation due to thermal gradients, in this sense, Niu *et al.* [56] studied the optimization of the process parameters in the printing of alumina concluding that the increase in the laser scan speed reduces the crack formation in the ceramic bodies. Alumina blends, such as $Al_2O_3$-YAG [57] and $Al_2O_3$-$ZrO_2$ [58][59], composite materials with hydroxyapatite [60] and other ceramic materials such as PZT [61]. A recent review in the DED technology can be assessed in [54].

Summarizing, DED processes have promising applications in the AM field, however, due to the high temperatures needed to fuse the materials, the industrial application to ceramic materials is limited due to crack formation based in the temperature gradients and by the energy consumption required for the process.

### 5. Material Jetting

In the MJ class, the material in liquid form is selectively deposited in a drop by drop process [6], while an energy source, either an UV light or heat, promotes solvent evaporation, crosslinking or crystallization of the material in order to solidify the object [62], as schematically represented in Figure 1.10 . This class comprises techniques such as Continuous Inkjet printing (CIJ) and Drop-on-Demand (DoD). The main difference between the two is that in CIJ a stream of drops is generated and deposited in the substrate and in DoD a single drop can be generated and deposited individually [62]. The main parameters in this techniques are the drop volume, speed and diameter and the viscosity of the material [62]. The most used materials used in MJ comprise thermoplastics, photosensitive polymers and biologically active fluids, among others [63].

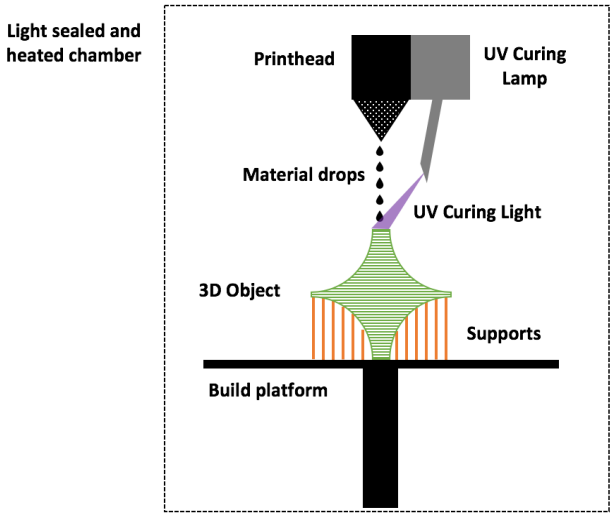


**Figure 1.10:** Schematic representation of Inkjet printing (Material Jetting).

In the case of the use of ceramic materials in material jetting systems, the is a requirement to produce suspension. Ainsley *et al.* [64] produced ceramic suspensions for MJ by dispersing fine particles of alumina (< 2,4 μm) in alkane, producing alumina parts with 80 % of relative density and linear shrinkage of 18 %, after sintering at 1600 °C for 1 h. Serdeen *et al.* [65] also dispersed alumina powders in alkane wax. The authors were able to print small design features with a minimum of 100 μm with a suspension of 30 vol.% fraction of alumina powders. In addition, in the same study a suspension with 40 vol.% fraction of alumina was able to be printed but only with applied pressure in order to avoid clog of the printhead. Zirconia [66][67] and PZT [68] were also subject of study of MJ with ceramic

materials. In addition it was proved that, due to the working principle, the material jetting systems is suitable to produce ceramic parts with graded functionalization [66]. For more information, reviews regarding the MJ class are available at [62][63].

The MJ class can be used with ceramic materials by preparing suspensions of fine ceramic powders, however, from the industrial point of view, especially in traditional ceramics such as porcelain, the technology is far from being interesting due to the size of objects able to be printed and the cost of materials required for a successful printing.

With the main advantages and disadvantages overviewed for the several classes (for BJ and PBF it will be discussed in detail further in the document), the comparison between the classes regarding the energy consumption, the printing speed and the printing resolution is presented in Figure 1.11 [69]. Regarding the energy consumption, as expected the classes that use melting or sintering of materials as bonding mechanism (DED and PBF) are also the most energy consumers. The sheet lamination class is also energy consuming, however it depends on the type of energy source used to cut each section and the use of heat to bond layers. Concerning the printing resolution MJ is the class with higher value, mainly due to its working principle (use of drops). The use of laser or light sources, such as in VP, sheet lamination and PBF also promotes higher printing resolution. The case of BJ, which uses piezoelectric print heads has also a good printing resolution. Finally, the printing speed is higher for classes that use materials in powder form (BJ, DED and PBF) and an intermediate speed for the case of VP, which depends in the method used to cure the photopolymer: laser or mask, as discussed above.

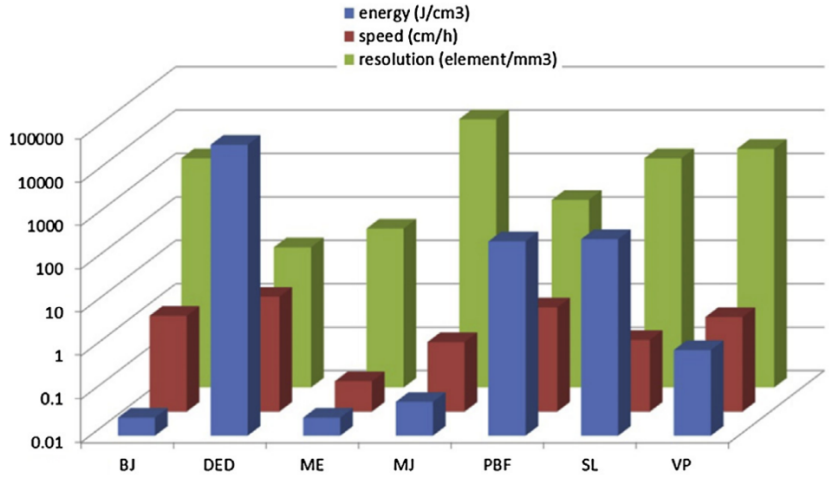


***Note: BJ** – Binder Jetting; **DED** – Directed Energy Deposition; **ME** – Material Extrusion; **MJ** – Material Jetting; **PBF** – Powder Bed Fusion; **SL** – Sheet Lamination; **VP** – Vat Photopolymerization*

**Figure 1.11:** Comparison among AM classes regarding the energy consumption, resolution and printing speed [69].

In the case of ceramics, some of these processes have limited used in research and production, such as DED and MJ, either because of processes limitations, energy consumption or incompatibility with properties of ceramic materials. The class of sheet lamination also lost its interest to produce ceramic parts, mainly due to the material form, but also due to the complex design limitations. Concerning the relative density of the produced parts, VP and ME may lead to ceramic parts with high relative density, however, in the case of VP the high cost of photopolymers and, in the case of ME, the surface finishing may be a limitations for its industrial scale applications for traditional ceramics such as porcelain for tableware applications. In this sense, powder bed AM techniques, such as BJP from BJ class, appear as an opportunity to implement at industrial scale for production of ceramic objects, even though it may require post-conformations steps [70].

### *1.1.5. Materials for Additive Manufacturing*

Metallic and polymeric materials are the type of materials mostly used for AM, however this is not the case of ceramics. As a matter of fact, the Wohlers Report 2019 (Figure 1.12), highlights that in 2018 only 1,6 % of materials used in AM were classified as “Other”, where the ceramic materials belong among materials for binder jet printing and materials for sheet lamination [71], as opposed to photopolymers with 39 %, polymeric powders for laser

sintering with 25 %, filaments with 20,4 % and metals with 14 %. According with the same report, the market of materials for AM reached 1495 $ millions in sales in the year 2018.

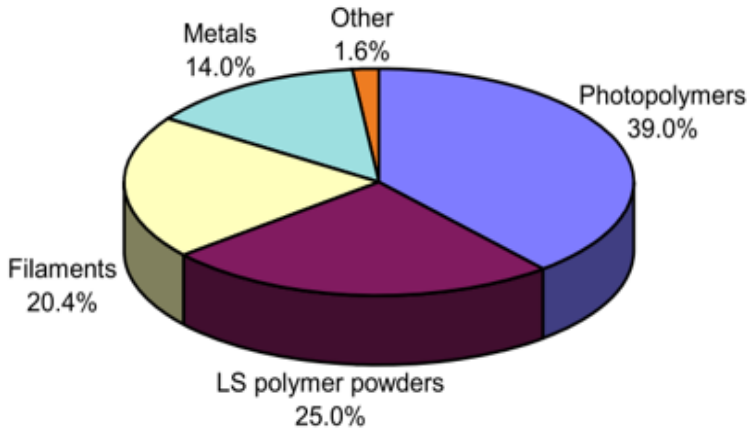


**Figure 1.12:** Materials used in additive manufacturing worldwide in 2018 [71].

According to Ngo *et al.* [72] in a recent review paper, and supporting the statements above, polymers are the most common class of materials for AM and have been subject of investigation and development for several years, however, for fully industrialization, there is still challenges, as the speed of printing and repeatability of printed parts, to overcome. The most typical application for AM of polymers is the development of prototypes for several industries leading to an increase in the research concerning polymers reinforced with fibbers and nano materials to enhance the mechanical properties, lead to development of polymer based materials for industries such as aerospace, automotive and sports among others [72]. This is the same trend as in metals, as the last years, consequence of the investment done, there is an increase in the number of metals and metallic alloys for AM. Used mainly in powder form for technologies such as SLS, SLM and DED, the target industries for AM of metals have been aerospace, automotive and defense [72]. In the case of ceramics, the authors reveal a limited number of different ceramic materials able to be processed through AM techniques, and raising the challenge and opportunity to expand the ceramic materials selection [72]. Singh *et al.* [73], after an analysis regarding materials issues for AM, conclude that commercial AM techniques leads to a rigid choice in the materials characteristics to be processing, leading to an increase in the interest of adapt existent materials and develop new ones. This is the case of traditional ceramic materials, such as porcelain, especially for industrialization in traditional industry sectors, such as tableware production.

The term feedstock is used to refer to the materials or mixture of materials used in AM [74]. In the case of ceramics, due to the high melting point and low toughness, it is difficult to process directly in AM technologies. In this sense, it is common to use additives for ceramic feedstock, such as binders. In this work, the dry powder mixtures composed by porcelain powder and *in-bed* binders are referred as feedstock.

It is clear that up today the use of ceramic materials in AM is limited. However, some ceramic materials have been used and Table 1.II presents a list of ceramics used in the different AM classes. Alumina ($Al_2O_3$) and zirconia ($ZrO_2$) are among the most used ceramic materials, mainly due to its broad range of applications. Biomaterials have been also the focus of some AM processes; the growing need of customised biomaterials products targeted to the specific needs of the patient, justifies the interest and impact of AM for biomedical applications and tissue engineering [75]. The limitation in the number of ceramics used in sheet lamination, directed energy deposition and material jetting supports the difficulty of processing this class of materials. In the case of BJ and PBF classes, the ceramic materials used will be presented further in detail.

**Table 1.II:** Ceramic materials used in techniques from different AM classes.

| Class | Ceramic materials |
|---|---|
| Vat Photpolymerization | $SiO_2$ [22] $Si_3N_4$ [22] $ZrO_2$ [23][24] $Al_2O_3$ [22], [25]–[28], [33] bioactive glass [31] hydroxyapatite [32] SiC and SiOC [29] PZT [30] |
| Sheet Lamination | SiC [35] $Al_2O_3$ [36] |
| Material Extrusion | Porcelain [37] [38] mullite [39] $Al_2O_3$ [40]–[42] $ZrO_2$ [43]–[45] $\beta$-tricalcium phosphate [46] bioactive glass [47] hydroxyapatite [48] WC [50] $B_4C$ [51] |
| Directed Energy Deposition | $Al_2O_3$ [55][56] $Al_2O_3$-YAG [57] $Al_2O_3$- $ZrO_2$ [58][59] hydroxyapatite composite [60] PZT [61] |
| Material Jetting | $Al_2O_3$ [64][65] $ZrO_2$ [66][67] PZT [68] |

Summarizing, while for metallic and polymers the AM is already in advanced stage, driven through the ease to process when comparing with ceramics, and by the interest growth of several industries such as aerospace and automotive, in the case of ceramics the selection

of materials is limited and further investigation to adapt existent ceramic materials and develop new ones is required. In addition, there is often the need to use additives such as binders to prepare a ceramic feedstock in order to process through AM, which requires post-conformation steps.

### *1.1.6. Industrialization and future trends of Additive Manufacturing*

One of the future trends of AM is its industrialization in different types of industries. Although for some industries, such as aerospace, automotive and medical, its use is already happening, in the case of more traditional ones it is still far behind other conventional conformation technologies. As discussed before, the use of AM may lead companies to reach new markets and customers, by manufacturing products that are not able to be produced through FM and SM technologies, or that could turn expensive due to tooling cost, waste of materials or production time, among others. Although for the full industrialization of AM processes there is still to overcome, this technology is still young especially when compared with CNC milling (SM) and injection molding (FM), for instance. These technologies also spent a long time of maturation until they were fully implemented for continuous production. The injection molding was first invented by John Wesley Hyatt in 1872 [76]. However, it took until 1970s until new machines were developed by James Watson Hendry, and the plastics industries overtook the steel production in 1979 [77], creating a gap of around 100 years since the first invention until its fully industrialization. In the case of CNC milling, it was invented in 1950's by American Air Force and with the development of programming, it started to be accepted in industries, and by 1980's several industries were using the process for manufacturing. In this case, CNC machining had a faster development because it was a combination of machining and numerical control. Once the AM was only developed in 80's, it is still a young technology with several years until it reaches the requirements for fully industrialization

Hu [78] discussed the future of manufacturing, concerning mass customization. According with the author, the manufacturing started with the craft manufacturing, where the product, highly customized, was produced by customer request, however, this type of production was confined to localized regions and limited in scale up production, what increases the price of the product. The mass production was driven by low cost products, however with very limited number of products or derivate products. In this sense, the mass customization

appears in the late 80's as an option for products produced in mass production, but features that the customers can choose and differentiate from similar products.

Due to its ability to produce highly complex shaped and functional parts/objects faster or even impossible to be fabricated trough the conventional routes, AM, quickly attracted the interest of several different industries. In Figure 1.13 it is illustrated the different industries already using AM processes; the ones leading in 2018 are the aerospace, with almost 18 %, and automotive, with almost 20 %, besides the market of the machines itself. In addition, the medical/dental industry represents already more than 11 % of the market. , In these industries AM is already used as a production route of ceramic, metallic and polymeric products, due to the high customization (and low number of parts), in order to fabricate some specific parts for their patients and products. However, the use of AM processes and its industrialization is still residual for traditional industries.

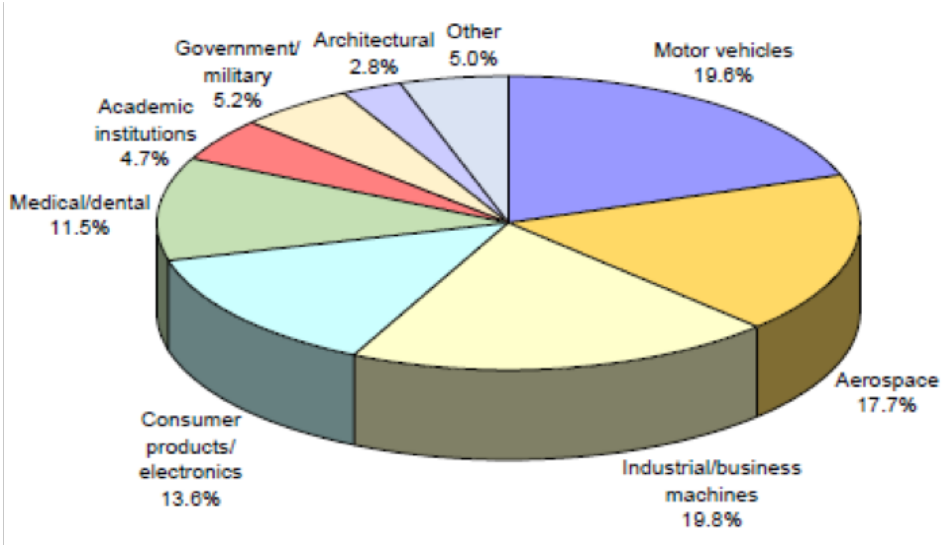


**Figure 1.13:** Use of AM by different industries and markets in 2018, by Wohlers Associates [71].

In 2015, Oropallo *et al.* [79] defined the ten challenges to overcome in AM based on the expectative for industrial AM. Based on the opinion of the authors (1) shape optimization, (2) design for 3D printing, (3) pre and postprocessing, (4) printing methodologies, (5) error control, (6) multi-material printing, (7) hardware and maintenance issues, (8) part orientation, (9) slicing and (10) speed, are the most subjects to overcome. In addition, Singh *et al.* [73] also identified the limited choice in materials and limitation in the use of commercial 3D printers. Costa *et al.* [70] identified two major limitations for the

implementation of AM for tableware production with commercial 3D printers: i) the part volume, i.e., the maximum volume of the printed object which is limited by the size of commercial equipment and ii) the cost of the final objects, once the commercial equipments are most suitable for alumina based ceramic materials for technical applications. In addition, the use of typical materials for tableware production are not recommended to use with commercial 3D printers due to the possibility of damage of the printer.

The AM technology started as an engineering tool for rapid prototyping. However, quickly the technology showed to be an opportunity for several industries as production route. The trend of AM is clearly from prototyping or molding fabrication to continuous defect free product fabrication, to compete with all the conventional fabrication techniques. However, there are several challenges to be overcome before the fully industrialization, being one of them its reproducibility, i.e., producing objects with the same characteristics in different production runs. In order to implement AM as a production route, the company must to conduct a full evaluation of the entire supply chain and the product life cost. This step will lead to major cost savings, but also enable the company to understand which AM metrics should be track during the production [80]. The variables with highest impact in the total cost of use and implementation of AM in a company are the material cost, part volume, AM machine cost and AM machine throughput [80].

Based on this discussion we identify several key aspects to have in consideration for the industrialization of AM for traditional ceramics: 1) adaptation of the existent ceramic materials for AM processes, 2) adequation of commercial 3D printers, 3) requirement of post conformation steps in order to reach full densification, 4) reproducibility of the objects properties and 5) a cost-benefit analysis, which is always a key parameter for implementation of a new production process.

Another topic that has increased in interest is the 4D Printing technology. Coined by Skylar Tibbits in 2014 [81]. In this process, based in 3D printing, special materials are used to produce a 3D object, where the fourth dimension is an external output that makes the object change its shape. The external output that triggers the shape modification can be pH changing, UV light, temperature and pressure among others [82]. Bioprinting is also considered one of the AM segments in continuous growth. In this process cells and biomaterials are used to produce organs and other biological tissues for regenerative medicine such as skin, cartilage, bones and cardiac tissue, among others [83]. With the

high personalization provided by AM, the production of artificial organs and prosthesis is suitable in this production route. Other applications such as the production of artificial organs, mimicking the bio tissues, can be used to test drug medicines, aesthetic procedures and drastically decrease the number of animal tests. Recent reviews in the printing of objects using multi-material [84] and functionally graded materials (FGM) and functionally graded structures (FGS) [85] represent one of the AM trends: the possibility to produce an object with different properties in different sections of its body, allowing to produce objects for specific applications.

## 1.2. Powder bed AM techniques

Binder Jet Printing (BJP) and Selective Laser Sintering (SLS) are the two main powder bed AM techniques and are aim of study in this work, with higher focus on BJP than in SLS. Direct Metal Laser Sintering (DMLS), which is similar to SLS but aimed for metal powders, and Electron Beam Additive Manufacturing (EBAM) [86], which uses an high energy electron beam to sinter/melt the material, are also powder bed AM techniques and both belong to the PBF AM class. Other powder-based technique is Laser Engineered Net Shaping (LENS) [87], which uses a laser to bind powder material fed directly to sintered zone and belong to the DED AM class.

The main advantage of powder bed AM techniques is the use of exceeding powder as support material, which leads to highly complex shaped products, when comparing with other techniques. However, the porosity in the green part is a limitation for ceramic parts where full densification is a requirement. Powder characteristics, such as particle size and shape, particle size distribution, flowability and packing, the use of binders, in the case of BJP *in-bed* and liquid binders and in the case of SLS *in-bed* binders, and the printing parameters have impact in the density, strength and dimensional accuracy of the green printed parts. Powder characteristics and binders will be discussed in detail in sections 1.4 and 1.5 respectively. In this section we present and discuss the working principle and variations of BJP and SLS and the effect of its main printing parameters, as binder saturation, layer thickness and drying time, in the case of BJP, and layer thickness, laser power and laser scan speed, in the case of SLS.

### 1.2.1. Binder Jet Printing (BJP)

Binder Jet Printing, also known as 3D Printing, belongs to the Binder Jetting AM class, in which a liquid binder is deposited to bond the particles in the powder bed [6]. The BJP process, schematically represented in Figure 1.14, starts with the spread of a powder layer, by the moving roller. Then a printing head deposits the liquid binder in the powder bed, in the area corresponding to the layer section. Once the liquid binder is deposited for the whole cross section of the layer, the part bed will move down one layer and the feed bed will move up one layer. The roller pushes another layer of powder from one bed to another, and the liquid binder deposition process is repeated. This cyclic process is repeated until the part is completely printed. Usually, the parts are left in the bed during a binder drying period. After the removal of the parts, the excess powder is removed from the surface of the part. [8] The most important printing parameters in BJP are the binder saturation, layer thickness and drying time. The binder saturation is defined as the ratio between the liquid binder volume to the volume of void space in the section to be printed in the powder bed [88] [89]. The binder saturation may be distinguished in two parts of the printed object: shell saturation and core saturation. The shell saturation is higher than the core saturation in order to provide enough mechanical resistance to the ceramic body and is applied to the outer sections of the printed object, while the core saturation is applied to the interior of the part [89], as schematically represented in Figure 1.15. The layer thickness is the height of each printing layer and the drying time is used in order to dry the printed part or to cure the liquid binder.

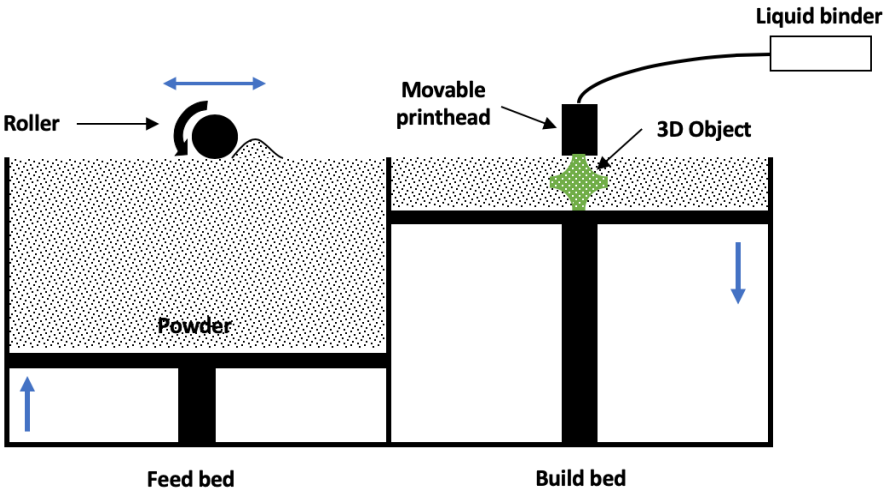


**Figure 1.14:** Schematic representation of Binder Jet Printing apparatus.

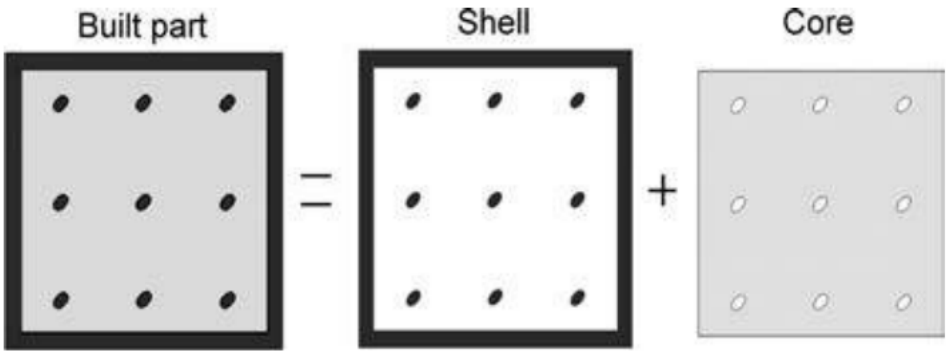


**Figure 1.15:** Schematic illustration of shell and core sections in the printed part. The black area represents higher binder saturation than the grey zone [89].

The effect of layer thickness and printing orientation was studied by Farzadi *et al.* [90] using the commercial powder ZP150, a plaster based powder, and the commercial binder ZB63, a water-based liquid binder. The results, as presented in Figure 1.16 (left), demonstrate the importance of the printing direction. In this case, the authors concluded that printing in X direction, i.e., with the cylinder in the horizontal position, would avoid some layers shifting, comparing with Z direction, i.e., with the cylinder in the vertical position. The authors also demonstrate a more dimensional accurate part, printed with 0,125 mm of layer thickness (Figure 1.16, right). Vaezi *et al.* [91] also studied the effect of binder saturation and layer thickness in the printing of commercial powders. The group found that with higher binder saturation (125 %) the parts have higher mechanical strength, but lower binder saturations (90 %) promotes better surface finishing quality. In the same study is concluded that lower layer thickness (from 0,1 to 0,087 mm) increases the tensile strength but decreased the flexural strength and the surface finishing quality. The effect of printing direction (Figure 1.17) in the shrinkage and mechanical strength of the printed parts was aim of study by Shanjani *et al.* [92] with calcium polyphosphate powders. The authors found anisotropy in the shrinkage of the printed part after thermal annealing at 950 °C, with a shrinkage of of 17 % in the direction parallel to the printed layers and 12 % in the direction perpendicular to the layer deposition. In addition, the authors found higher uniaxial compressive strength in the parallel direction to the printed layers (50 MPa) than in the perpendicular one (34 MPa). The effect of printing parameters as binder saturation, layer thickness and drying time (without specifying if the drying time is considered between each layer or at the end of the printing process) in the density of lithium alumino-silicate (LAS) scaffolds was studied by Zocca *et al.* [93]. The authors found the highest density (1,57 g/cm$^3$) with a layer thickness of 100 μm, a binder saturation of 1,47 and a drying time of 100 s, followed by the

printed part using a layer thickness of 80 μm, a binder saturation of 1,38 and a drying time of 60 s. In addition, the authors conclude that a low binder saturation combined with low drying time leads to defective parts, without mechanical strength to be removed from the powder bed, and as consequence, the increase in binder saturation and drying time leads to denser printed parts. Castilho *et al.* [89] studied the effect of shell/core binder saturation in the dimensional accuracy and mechanical properties of calcium phosphate printed parts. The authors found that with the increase of binder saturation, the dimensional accuracy increased, reducing the deviation of dimensions to the virtual design for a minimum of 2,3 % in diameter of cylinders and 0,1 % in the height, while for all the printing tests anisotropy was found with higher deviation in the diameter than in the height. the increase in the binder saturation both in shell and in core sections, decreased the porosity of the parts to a minimum of 43 %, and increased the compressive strength to a maximum of 24 MPa, and was reached for equal shell and core saturations of 200 %. In addition, the authors found that the increase in the binder saturation lead to an increase in the density of the previous layers, as the liquid binder acts as carrier for small particles from the printing layer to the previous one, and filling void spaces with ceramic particles. In the case of low binder saturation this phenomenon is residual as the amount of liquid binder is not enough.

In the case of porcelain for tableware applications, the works reported in the literature were not found, however, with dental porcelain which as the same material system ($SiO_2$-$Al_2O_3$-$K_2O$-$Na_2O$) was subject of study by Miyanaji *et al.* [94] with focus in the effect of binder saturation in the printability (defect free printed parts) and compressive strength, using 50 % and 75 % levels. The authors found that with 75 % of binder saturation, deformations were observed in the printed parts and were attributed to the roller action combined with insufficient drying of the printed layer, and, on the other hand, using the 45 % binder saturation leads to parts with insufficient mechanical strength to be handled. Concerning the drying time, the authors found that an excessive drying time (60 s) increases deformations in the top of the printed parts, while it avoids deformations in the bottom section of the printed part.

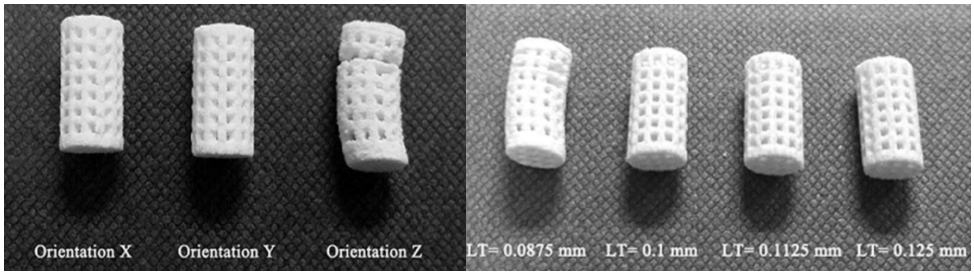


**Figure 1.16:** Effect of printing orientation (left) and layer thickness (right) in the dimensional stability of printed parts by binder jetting printing [90].

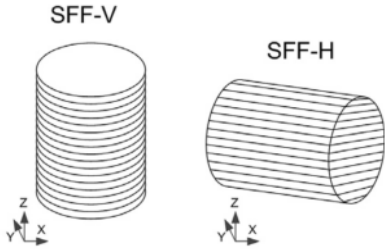


**Figure 1.17:** Stack of layers in different printing directions [92].

Summarizing, the layer thickness and binder saturation are the most impactfull printing parameters in BJP for a sucessful printing, with defect free parts. The binder saturation plays a crucial role in the mechanical strength of the printed parts and often, a low binder saturation leads to low strength printed parts. As most of the available commercial powders for BJP are plaster based powders, it is easy to understand that the interaction between the liquid binder and the powder material will lead to a plaster part, that can be easyli removed from the powder bed. However, for some ceramic materials there is a need to mix an *in-bed* binder, that is responsible to react with the liquid binder and bond ceramic particles together. This subject is detailed further in the document.

### *1.2.2. Selective Laser Sintering (SLS)*

The Selective Laser Sintering (SLS) is a technique that belongs to the Powder Bed Fusion (PBF) AM class, in which thermal energy is used to fuse the material in the powder bed to bond the particles [6]. In the case of SLS, schematically represented in Figure 1.18, a laser is used to melt/sinter the material for each 2D cross-section of the part to be printed. After each layer sintering, a roller pushes another layer of powder from the feed bed to the part

bed. This process is repeated until the part is fully printed. The whole process is performed in a chamber with inert atmosphere, avoiding the combustion of the materials, once the process is usually used with polymeric materials, and the interaction of the material powder with the laser beam, in air, leads to oxidation and burning of the material. After the entire process, parts need to be clean in order to remove the remaining powder in the surface of the parts. Post processing steps may be used either to improve superficial properties and densification of parts as well [8]. The main process parameters to be controlled during SLS process is the build bed and feed bed temperatures and laser parameters as laser powder, laser scan speed and hatching space. The laser beam diameter is also an important parameter, however, typically it is not controlled and depends on the equipment and its features. The temperatures of the beds regard on the surface temperature of the powder and is controlled by heaters inside the chamber. The laser scan speed concerns in the velocity of the laser is scanned in the powder bed and the hatching space is the space between parallel lines of the laser scan [95].

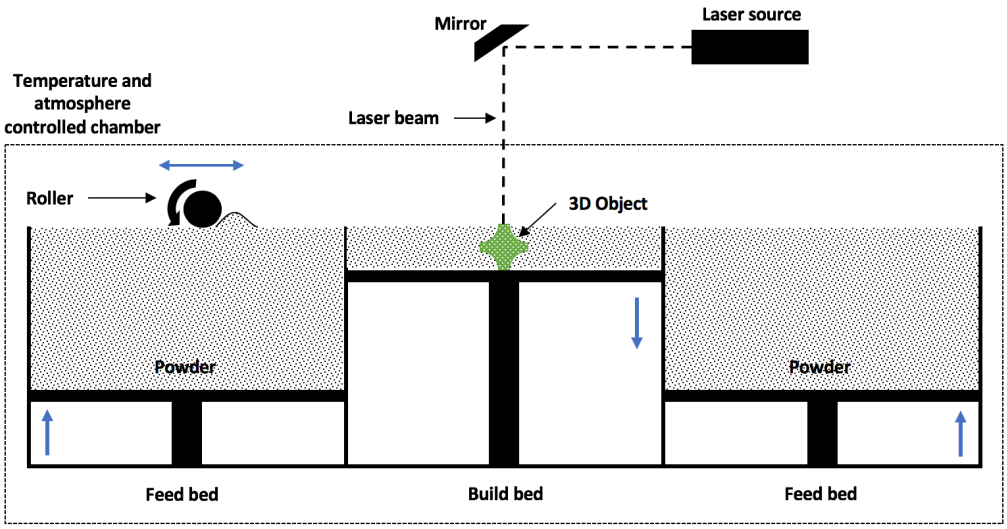


**Figure 1.18:** Schematic representation of Selective Laser Sintering apparatus.

In SLS the type of laser has an important role. In Table 1.III the most common types of laser used in SLS are presented. The wavelength of the laser directly influences the absorptance of the material as reported by Tolochko *et al.* [96] and directly translates in the maximum temperature reached by the powder materials, essential for melting or sintering. The author studied the absorptance of different class of materials (metals, ceramics and polymers) using a Nd:YAG laser with a wavelength of 1,06 μm and a $CO_2$ laser with 10,6 μm. The results exhibit a higher absorptance of metallic materials with the 1,06 μm wavelength than

for the 10,6 μm, while for polymeric materials the opposite trend was observed. In the case of ceramic materials, carbide ceramics exhibit higher absorptance with the 1,06 μm, while oxide ceramics have higher absorptance for 10,6 μm wavelength. The highest absorptance registered by the authors occurs for oxide ceramics, such as $Al_2O_3$, $SiO_2$ and SnO, with an absorptance higher than 95 %, using the $CO_2$ laser. The particle size of the powder used can also affect the powder absorptivity as demonstrated by Zhang *et al.* [97]. The authors found that increasing the particle size of tungsten powders from 5 μm to 45 μm, decreased the absorptivity from 60 % to 50 %. Comparing the three types of lasers regarding its efficiency, it is possible to conclude that Yb-fiber lasers presents the highest efficiency at the same time as it has the highest maintenance time. However, for the case of ceramic materials, its use is limited to the poor absorptance in the 1,07 μm wavelength.

**Table 1.III:** Most common types of lasers used in SLS and its characteristics. (adapt. from [98])

| Laser | $CO_2$ | Nd:YAG | Yb-fiber |
|---|---|---|---|
| Operation wavelength (μm) | 9,4<br>10,6 | 1,06 | 1,07 |
| Efficiency (%) | 5 - 20 | Lamp pump: 1 - 3<br>Diode pump: 10 - 20 | 10 - 30 |
| Maximum output power (kW) | 20 | 16 | 10 |
| Pump source | Electrical discharge | Flashlamp or laser diode | Laser diode |
| Maintenance periods (h) | 2000 | 200 (Lamp pump)<br>10000 (Diode pump) | 25000 |

Another important parameter to control is the chamber temperature. In the case of semi crystalline polymers, such as polyamide 12, the surface of the part bed should be heated above the onset crystallization temperature (Tc) and under the onset melting temperature (Tm) of the material. This range is called SLS window [99], represented in Figure 1.19. The heating of the powder bed is responsible to avoid the curling effect, i.e., deformation defects in the part, usually of polymers, during cooling. Thus, it is important to have a larger SLS window in order to avoid defects promoted from the temperature gradient in the powder bed. The heating temperature should be as closer as possible to the onset of melting temperature, but if it is higher than the Tm all the powder will melt and it will be impossible

to remove the printed part [99]. If the temperature is too close to the Tc, a premature crystallization will occur leading to defective parts [99]. The feeding bed are also pre heated, usually slightly lower temperature than the part bed, in order to avoid temperature gradients between the new layer and the layers already sintered. The temperature gradients also occur in the part bed area, where the maximum temperature is achieved in the center and may decrease towards the part bed edges.

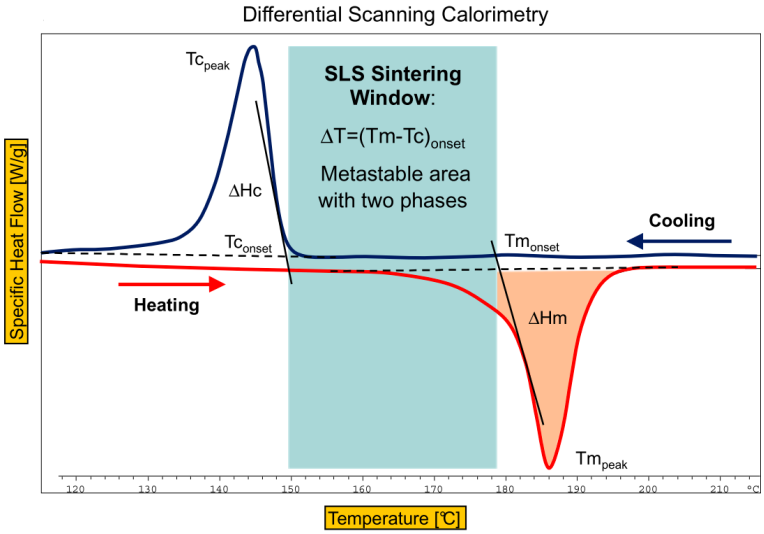


**Figure 1.19:** Representation of SLS window, using Differential Scanning Calorimetry. (adapted from [99])

There are two different approaches to use SLS to produce printed objects: direct and indirect. Direct SLS is when the powder material is directly sintered by the laser beam. This approach reduces production time and post processing steps. However, regarding the case of ceramic materials, due to its high melting temperature, the difference in the temperatures of the cross section being sintered and the adjacent layers and loose powder, leads to residual stress and crack formation, poor surface finish and geometric irregularities [100][101]. One way to avoid these issues is pre-heating the powder bed up to close of sintering temperature, as demonstrated by Hagedorn and Wilkes [102][103] (Figure 1.21) and repeated by Liu *et al* [104] with Yttria-stabilised Zirconia powders. One of the disadvantages of preheating the ceramic powders is the thermal shock induce by the deposition of the new layer with cold ceramic powders, as demonstrated by Hagedorn *et al.* [102]. Also, commercial machines, usually prepared for polymers and metals, aren't set for those temperatures (> 1500 °C). Deckers *et al.* [105] used the direct SLS approach to produce alumina parts. The authors heated the powder bed at 800 °C and with a low laser

power (2 W) were able to produce printed parts with 85 % of densification. Commercial porcelain, with a mean particle size of 5 μm, was also subject of study by Danezan *et al.* [106] for direct SLS. The authors used different laser energy densities (E), proposed by Nelson *et al.* [107], defined in the following equation,

$$E = \frac{P}{D \times V} \qquad [J/cm^2] \qquad \text{(Eq 1.1)}$$

where P is the laser power, D is the laser beam diameter and V is the laser scanning speed, finding that E should be comprised between 180 and 280 J/cm$^2$, as higher energy densities leads to the melt of the material and lower ones leads to no densification of the parts. The authors reached a minimum of total porosity in the green porcelain bodies of 57 ± 5 %, which was decreased to 45 ± 5 %, after sintering at 1350 ºC for 2 h, under vacuum atmosphere. Tian *et al.* [95] assessed the effect of direct SLS process parameters of commercial porcelain in shrinkage, bulk density and bending strength of the ceramic bodies. For that, the authors used a Taguchi method approach defining three levels for each process parameter: laser power (40, 50 and 60 W), scan speed (85, 100 and 150 mm/s) and hatching space (0,3, 0,45 and 0,6 mm). The effect of the energy density (Eq. 1.1.) was also assessed. The authors found that the volume shrinkage of the green ceramic body increases with the decrease of laser power, the increase in laser scan and the increase in the hatching space, varying between 30 and 40 % in all the cases. The bending strength increases with the decrease of laser power, the increase in the scan speed and hatching space, reaching a maximum of 24 MPa and a minimum of 16 MPa. Finally, the bulk density reaches a minimum for the intermediate value of laser powder (50 W) and increases for lower and higher values of laser power, varying between 2,01 and 2,08 g/cm$^3$. The bulk density also increases with the increase in the scan speed and hatching space, varying between 1,95 g/cm$^3$ and 2,11 g/cm$^3$. Concerning the energy density and the hatching space and its influence in the temperature of the sintering zone (measured by a pyrometer directed to the sintering zone), as illustrated in Figure 1.20, the authors found that delamination occurs for temperatures < 1050 °C (low energy density and high hatching space) due to inadequate sintering and cracks formation are observed for sintering temperatures > 1400 °C (high energy density and low hatching space). The optimal range of temperatures for defect free parts is compressed between 1050 °C and 1400 °C. As conclusion, the group found that ceramic bodies produced using 50 W, 85 mm/s and 0,6 mm of laser power, laser scan speed and hatching space, respectively, reached the best results.

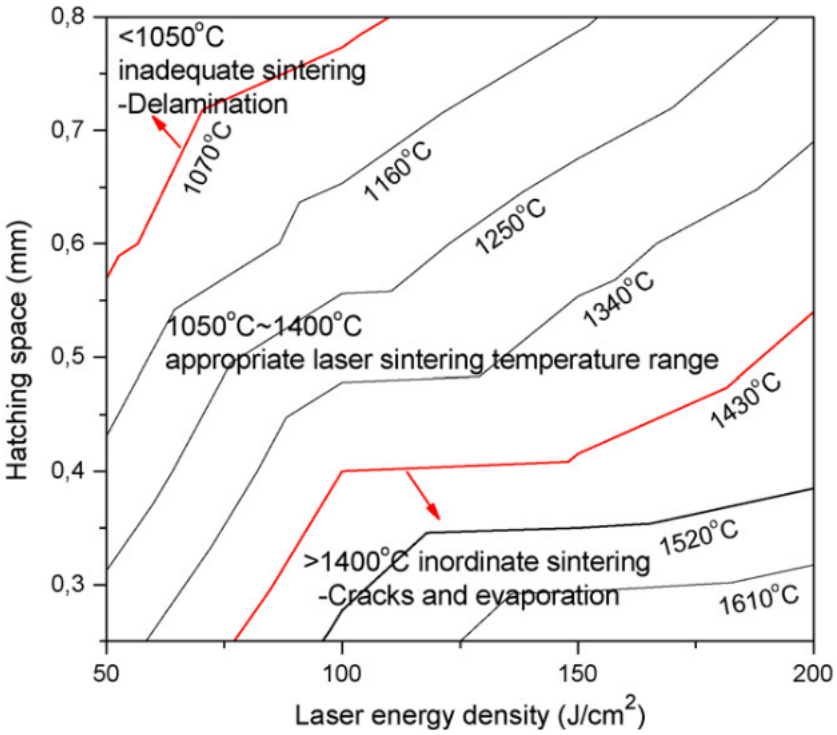


**Figure 1.20:** Influence of energy density and hatching space in the temperature of the sintering zone, in SLS of commercial porcelain [95].

In this sense, the indirect SLS appears as an option for ceramic materials. In this approach, a sacrificial binder, usually polymeric material, is mixed with ceramic powder. This binder will be the material to be sintered, instead of the ceramic powder. This approach uses lower working temperatures than the direct one, improving the surface finish of printed parts, avoid crack and thermal stress formation and better dimensional control. However, the green parts have higher porosity and post processing steps are needed in order to remove the binder and improve density of printed parts. Post processing steps, such as infiltration and isostatic pressing, are also required in order to improve density of printed parts. The indirect SLS approach will be discussed in detail in the section dedicated to the *in-bed* binders for SLS (section 1.5)

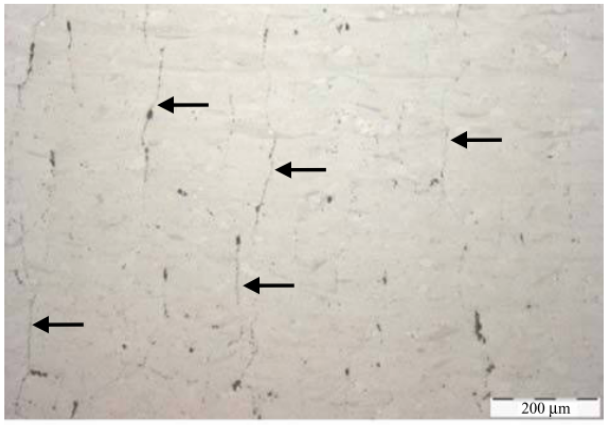


**(a)** No preheating

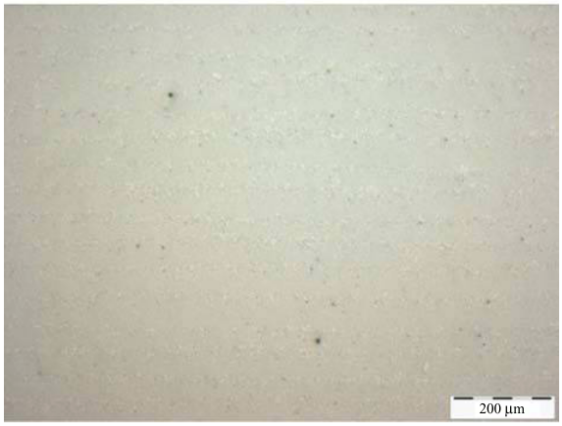


**(b)** 1,715°C preheating temperature

**Figure 1.21:** Effect in the microstructure of preheating of powder bed. [103]

Summarizing, the chamber temperature and the laser characteristics have an important impact in the SLS of ceramics. The direct approach may lead to thermal stresses, due to thermal gradients and, as consequence, crack formation in the ceramic body, as opposed to the indirect SLS via, in which a sacrificial *in-bed* binder is used, but post conformation steps are required to remove the binder and reach full densification of the ceramic body.

## 1.3. Powders for AM

Powders for AM techniques have some requirements regarding properties such as particle size, particle size distribution, morphology and flowability. These are the properties described in the literature as the ones with higher influence, whether in the process itself and in the properties of green and final parts, such as porosity, density, mechanical behavior and dimensional stability. The concept of printability of powders for AM has been used in the literature with different definitions. Mukherjee *et al.* [108] defined the printability of

metallic alloys as the ability of powders to avoid distortions, compositional changes and lack of fusion defects during the printing process, while Butscher *et al.* [109] defined the printability of $\beta$-tricalcium phosphate powders as the essential powder characteristics for binder jet printing, such as reactivity, flowability and wettability. In addition, depending on the AM technique used, other powder characteristics may influence the properties of the printed parts as well. For instance the wettability by the liquid binder of the powder in BJP, or the absorptance of the powder material in different wavelengths of the lase, in the case of SLS. In this section, we focus on the characteristics of powders for powder bed AM processes.

### *1.3.1. Particle size, particle size distribution and morphology*

The particle size and particle size distribution (PSD) influences the flowability of powders, and as consequence the packing of powders in the powder bed. This effect as repercussions in the density of the printed part and printing resolution. Sun *et al.* [110] studied the effect of the particle size gradation in the density and bending strength of parts printed with glass-ceramic powders. The authors found that a mixture of 80 wt.% of coarse particles and 20 wt.% of fine particles was the one where the tapped density reached the maximum. However, a powder mixture of 60 wt.% of particles with 45 – 100 μm and 40 wt.% of particles with 0 – 25 μm has good density (1,60 g/cm$^3$) and satisfactory bending strength for biomedical applications. Another conclusion in this work, regarding the particle size, is that a fine powder, in this case 100 wt.% of 0 – 25 μm, which has a bad flowability, jeopardizes homogenous layers in the BJP process, leading to a harder process and shifting of printed layers, as shown in Figure 1.22, due to roller action.

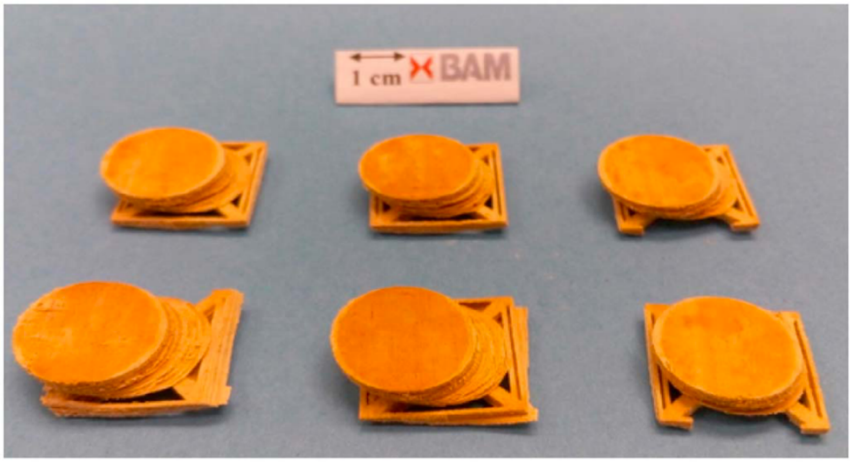


**Figure 1.22:** Example of layers shifting in a print with fine glass-ceramic powders. [110]

Butscher *et al.* [109] reported a complete study on the printability of calcium phosphate scaffolds in BJP. For that, the authors used six calcium phosphate powders with different particles sizes, ranging from the small sized powder with D90 of 14 μm to the coarse one with D90 of 75 μm. The first observation was that a peak in the density of the deposited powder occurred for an intermedium particle size (D90 of 39 μm). With fine particles the flowability is jeopardize due to inter particle forces, while for coarse particles, although they have better flowability, the void space between particles will increase and the powder bed density decreases. Regarding the printability, i.e., the ability to produce defect free parts, both fine and coarse powders lead to defective parts, as the intermediate particle size (D90 = 54 μm) lead to better printability. Zhou *et al.* [111] studied the printability of calcium phosphate powders in BJP, by using mixtures of powders with different particle size and PSD. The authors found that the use of coarse particles (D90 = 94 μm) leads to a higher powder packing in the powder bed (38 %) than with powders with fine particles (D90 = 3,5 μm) with a powder bed packing of 25 %. The authors also found that the use of fine particles jeopardizes the drop penetration time, increasing from 0,75 s with coarse particles up to 4,80 s with fine particles. Finally, the authors also found that the use of fine particles decreases the wettability of the powder by the liquid binder, decreasing from 1,05 % of wettability for coarse particles to 0,45 % for fine particles. PSD of lithium alumino-silicate powders for BJP was also studied by Zocca *et al.* [93], founding that printed parts with larger PSD (D90 = 368 μm) could be used with wider range of parameters, due to its better flowability, although parts printed with finer particles (D90 = 157 μm) would allow better dimensional precision and higher green density. Miyanaji *et al.* [112] used two metallic powders to study the wettability of the powder bed by the liquid binder: a 420 SS powder with a monomodal distribution peaking at 35 μm and a Ti-6Al-4V powder with bimodal

distribution peaking at 6 μm and 32 μm. The differences of the PSD have an impact in the packing density of the powder bed, reaching 55 % for the 420 SS powder and 66 % for the Ti-6Al-4V one. In addition, the 420 SS powder has a contact angle with the liquid binder drop of 25 °, while the Ti-6Al-4V powder has 40 °, which leads to higher saturation of the powder bed by the 420 SS powders.

The morphology of particles is also important in powder bed AM techniques influencing the powder flowability, the powder packing in the bed, the density of the printed and the contact between particles. The shape from commercial powders for BJP have been improved regarding the morphology. While the morphology of particles will depend in the type, brand and model of the printer, due to the powder feeding system, the particle size will be similar for all the powders. Miyajima *et al.* [113], in a study using 25 different powders of glass, mullite and silica with different shapes, sizes and densities. In this broad study, the authors conclude that spherical particles improve either the flowability of the powder and, as consequence, the compaction in the powder bed. In the study of Suwanprateeb *et al.* [114], the group used two different powders of hydroxyapatite: spray dried (spherical) and milled (irregular). The group found that the spray dried powder had better tap density, however the parts produced with milled powder showed a 32 % higher densification after sintering. Irregular shaped particles have worse flowability but provides higher green mechanical strength to the part due to higher inter particle contact area than the spherical ones. The use of spherical particles increases the flowability and the powder bed density, however, these particles leads to green parts with lower green strength.

The particle size distribution is one of the parameters that influences the most the green density of parts, and as consequence, the final density. In this sense, it is common to use a bimodal particle size distribution in order to reach higher densities due to better packing in the powder bed. Finer PSDs leads to an increase in the density; however these powders have more reactivity promoting agglomeration, leading to heterogeneous powder distribution in the printing bed. Coarser PSDs increase the flowability of the powder and leads to homogenous parts, however, the density of these parts decreases, when compared with finer powders. In the case of morphology, the spherical shape is preferred to reach better flowability, however, it hinders the mechanical strength of the green parts.

### 1.3.2. Hausner ratio and flowability

The flowability of powders is the property of powders to flow under certain circumstances [115], such as humidity, flowing area and temperature, among others. But also depends in the characteristics of powders such as morphology and particle size distribution. Several techniques are used to characterize the flowability of powders. One of them, the Hausner Ratio, is one of the most used in characterization of powders for AM.

Hausner ratio (HR), named by Grey and Beddow [116] gives information regarding the flowability and packing of powders [117] and it is defined as the following equation (Eq. 1.2),

$$\mathrm{HR} = \frac{\rho_{\mathrm{tapped}}}{\rho_{\mathrm{free\ settled}}} \qquad \text{(Eq. 1.2)}$$

where $\rho_{tapped}$ is the density of the powder after tapping and $\rho_{free\ settled}$ is the density of the powder after being freely settled in the bed. By this equation, as HR closer to 1 as better flowability a powder has.

As a matter of fact, this coefficient is being used for AM techniques, in order to evaluate the flowability of powders for AM. Abdullah *et al.* [118] used fluid cracking catalyst and aluminum trihydroxide fire retardant filler to produce different powder mixtures. The authors showed that a powder with HR < 1,25 has good flowability and a powder with HR > 1,40 has bad flowability. Butscher *et al.* [109] found promising results for calcium phosphate powders with a HR, called compaction rate in this work, between 1,30 and 1,40, using powders with different PSD. In the same work, the authors conclude that the use of plasma treatment in the surface of the particles may improve the flowability of powders. Zocca *et al.* [119] also used HR to evaluate the flowability of powders, finding, in accordance with previous work, that coarser powders (63 – 125 μm) have better flowability than fine powders (17 μm). Moghadasi *et al.* [120] assessed the effect of the particle size on the feedstock powder characteristics and the properties of the final parts. For that, the authors used the commercial ceramic powder TP80 (Microjet Technologies Co.), with a composition of 50 % quartz, 25 % of potassium feldspar and 25 % of kaolinite, sieved with three different particle size ranges: < 53 μm (fine), 53 - 90 μm (medium) and 90 - 150 μm (coarse), and printed using a water based commercial liquid binder (TB-31 N). The main results regarding the HR highlights the decrease of HR from 2,7 to 1,3 with the increase in the particle size from fine to coarse, supporting that coarser powders have higher flowability than the fine ones. In

addition, the bulk density of printed and sintered parts at a maximum temperature of 1250 °C for 30 min, exhibits a maximum for the medium particle size. The authors attribute the decrease in the bulk density for fine particles to the worse flowability of the powders and for coarse particles due to the decrease in the sinterability of coarse powders, i.e., appearance of larger porous between the ceramic particles, even though the flowability of coarse powders is higher than for medium and fine ones. In conclusion, the authors relate the particle size of the ceramic powders with the bulk density by firstly increase from fine to medium particle size powders, due to improvement in the flowability of the feedstock, and then decreasing from medium to coarse particles due to the reduction in the sinterability of the powders. The flowability of the powders 316L powders in SLM was studied by Chen *et al.* [121] by numerical modelling and experimental validation. The authors found that Van der Waals forces rise for particles with a radius < 21, 8 μm, jeopardizing the flowability of the powder. Finally, moisture and humidity can affect the flowability of the powders in two opposite ways: decrease the flowability by creating bridges between particles or acting as lubricant, reducing the inter-particle forces and improving the flowability [122][123]. The binder jet printing of porcelain powders studies found in the literature, typically refer to dental porcelain such as in the works of Miyanaji *et al.* [94][124] and Zhang *et al.* [125]. The three works focused on the BJP process parameters such as liquid binder amount, drying time, powder amount and powder spread speed, and the sintering schedule of the printed parts. One of the main information in the three works concerns in the fact that the use of irregular shaped particles jeopardizes the spread of powder and fumed silica is used in order to improve the spread of powder.

Although the HR is an important measurement to understand the flowability of a powder, in our opinion is not enough to characterize the packing of the powders. The reason is that coarse powders have usually low HR, which means it has better flowability. However, in this case more void space will be formed between the particles decreasing the sinterability of the powders and, as consequence, the density of the final parts. On the other hand, fine particles have usually worse HR, translating in poor flowability, but may reach higher density in the powder bed by reducing the void space between particles and improving the packing. In this sense, the value of free settled density ($\rho_{free\ settled}$) is also an important characteristic to assess, once $\rho_{free\ settled}$ of a powder is closest to the density of the powder in the powder bed. The powder characteristics effect in the printability of the feedstock is not addressed and in the case of industrial porcelain powders for tableware parts production there is a lack of reported works in the literature under our scope.

### *1.3.3. Reuse of powders*

From the industrial point of view, the reuse of exceeding powders from powder bed AM technologies is crucial for its implementation at industrial scale, as it decreases the cost of the process and maximizes the material use in these technologies. According to Bourell *et al.* [126] only 10 to 20 % of the powder is used in the part and the recycling of powder is common in SLS after the depowdering of parts and overflow chambers and the recovery of these powders. Kruth *et al.* [127] reports that mixing the polyamide reused powder with new powder in a ratio of 30/70 % decreases the surface of the parts have higher roughness for parts processed in SLS. Also, the thermal degradation of the material and the increase of melt flow index (MFI) leads to worse mechanical properties. Shahzad *et al.* [128], even without studying it, refers that the non-melted powder (zirconia with polypropylene as binder) was sieved and reused in indirect SLS in order to reduce the impact of agglomerates formed during SLS process.

The use of powders in powder bed technologies rise challenges in the powder segregation and the homogeneity of particle size through the process, especially in powder feedstocks with broad range of particle size. The segregation of powders occurs in several steps of the processing and affects the PSD in each layer of the printing process, and as consequence, the printed parts may have different characteristics in its different sections. According to Mostafaei *et al.* [129] in a recent review paper, the most common segregation mechanisms in powder bed AM processes are: trajectory segregation, where the segregation occurs when the particles are in movement and body forces and air drag act in the particles and predominantly body forces act in coarse particles and air drag act in fine particles, leading to different trajectories of the particles; sieving segregation, where the fine particles of the feedstock move downwards in the void space between large particles due gravity forces; percolation segregation, where the fine particles move in the void space between stationary large particles, and comparing to sieving segregation, which occurs mainly during printing process, the percolation segregation occurs when the feedstock is stored; push-away segregation, where heavier particles push lighter ones aside due to gravitational forces and is especially important in feedstock mixtures of powders with different densities (for instance, in feedstock for powder bed AM technologies with *in-bed* binders); and finally agglomeration, which occurs especially for fine particles which have inter particles forces leading to agglomeration [130][131]. Material related factors, such as particle size and shape, particle size distribution and material density, operational factors such as powder

feeding system and spread of layer, and handling and feeding the feedstock to the 3D printer, are some of the most important factors for powder segregation [129][131]. One example reported in the literature by Strondl *et al.* [132], where the authors study the reuse of a nickel alloy powder, founding that in the case of SLS, properties are almost comparable with parts printed with new powder. However, an increase in the flowability of the powders was observed, in accordance with the decrease of finer particles, due to powder manipulation. This difference leads to a slightly higher porosity in the printed parts. Although this work was done with metallic powders, the same behavior is expected in the case of polymers and ceramics, since it is a common appearance during powder manipulation.

As conclusion, even if the reused powders can affect the properties of printed parts, especially in SLS which requires the use of temperature for the process, however this can be controlled with the addition of virgin powder. At an industrial scale, the powder manipulation, such as handling, feeding the 3D printer and storage, is expected to have a higher effect in the properties of printed parts due to its effect in the PSD of the feedstock, and the processing features both in SLS and BJP, which may lead to powder segregation during the process.

## 1.4. Binder selection

As discussed previously, the use of powder bed AM technologies can be used in an indirect way, where *in-bed* binders are used as sacrificial binders, forming a binder skeleton to bond the ceramic particles in order to provide enough mechanical resistance to the green printed parts for handling in post conformation processing. Usually, the *in-bed* binder is then removed. This approach is especially important for materials for which particles are not bonded by the deposition of the liquid binder, in the case of BJP, or by the laser, in the case of SLS.

In BJP process two different agents are used to bond ceramic particles in the powder bed using this approach: the liquid binder deposited by the printhead and the *in-bed* binder mixed with ceramic powder. As the most common liquid binders are water-based, one of the requirements for the *in-bed* binder is to be water soluble. In the case of SLS the binder must sinter or melt when interact with the laser beam and has absorptance in the wavelength of the laser type used, as discussed previously.

In the case of the *in-bed* binder two main approaches are reported in the literature for both BJP and SLS technologies: (1) composite form, where dry binder powder mixed with the ceramic powder and (2) coating form, where the binder is used as coating for the ceramic particles [133]. In our work, we aim at *in-bed* binders that can be removed thermally, without leaving any residue, and which can provide enough mechanical resistance to green printed parts for further handling. In addition, from the industrial point of view, an *in-bed* binder that can be used in powder form and dry mixed with the ceramic powder is preferable over the use of *in-bed* binder as coatings, due to its easier application at industrial scale.

In this section we present and discuss the use of different types of *in-bed* binders for BJP and SLS processes.

### *1.4.1. Binders in Binder Jet Printing*

The core process of BJP is the use of binders to effectively bind the powders. Consequently, the success of rendering a 3D object by BJP depends not only on the printing process, but also on the ideal formulation of the feedstock and binder. Both the physical and chemical properties of binders have a substantial effect on the quality of the ceramic printed parts [133]. Feedstock and binders together with the process details for printing and post-processing, all play a major role in defining the mechanical response of the printed parts. The ideal feedstock depends directly on the interaction between the binder jet and powder particles; turning the effective selection of the binder system and binding method the key to the accomplishment.

There are different ways for choosing an appropriate binder, being the most common the binding location. The binding location can be divide into two different methods: *in-liquid* binding and *in-bed* binding [134]. The *in-liquid* binding uses only liquid binder that contains all the necessary components for binding the powders. However, its use with solutions containing several chemicals may lead to clog printheads and being chemically aggressive to the feeding system. The *in-bed* binding uses typically a solid binder mixed with the powder to be printed, which interacts with a liquid binder to promote the bond of particles and provides enough mechanical strength to the green part [133] [134].

Liquid binders are dispensed during the printing process as the powder bed is formed and as described above. There are two different types of liquid binders: i) trigger powder reactive

and ii) self-adhesive, classified according to the way that they interact to the powder and provide mechanical strength [133]. The interaction between the powder to be printed and the liquid binder needs to be optimal, i.e., the liquid must interact with and bind the powder to reach a successful printing. Accordingly, the most relevant parameters of liquid binders include: the viscosity and surface tension [135]. If the viscosity is too high the ability to spread is delayed and even jeopardized; while if it is too low the stability of the powder bed becomes questionable. If the surface tension is too high, the liquid binder does not wet the powder surface an acceptable system is not formed jeopardizing the printing, albeit both individually, powder and binder, fulfill the requirements to be printed. The liquid binder should spread ideally over the powder, not absorbing too much and resulting in a rough surface texture. The interactions between powders and liquid binders, as formation mechanism of binder droplets and droplet-infiltration kinetics, have been frequently addressed in the literature and comprehensive reviews of the binding methods and formulation can be found in references [133] and [134]. The use of self-adhesive of liquid binders has been reported with organic liquid binders that harden after UV or heat curing for materials systems such as lithium alumino-silicate (LAS) [93], alumina [136], aluminum nitride (AlN) [137] and tungsten carbide (WC) [138]. In recent developments, ceramic suspensions were used as liquid binders and in this way increasing the relative density of the printed parts, even after sintering and reducing the linear shrinkage [139]. In this work, Zhao *et al.* [139] prepared a nanozirconia suspension of 20 wt.% of zirconia nanoparticles in ethyl alcohol and Polyvinylpyrrolidone (PVP) medium and produced CaO parts by BJP.

On the contrary, solid binders or *in-bed* binders, are added to (mixed with) the powder to be printed during the feedstock preparation. An ideal *in-bed* binder should interact with the liquid binder used in the printing, dissolving and penetrating the powder bed. The *in-bed* binder must provide enough mechanical strength to the green part in order to be manipulated when being removed from the powder bed and in post-conformation steps as well. In addition, ideally the binder should be able to be removed thermally without leaving residues [134]. There are two main types of *in-bed* binders [133]: in composite form and in coating form. The first type, designated as *in-bed* binder pre-mixing, implies that the solid binder particles are mixed with ceramic powders. The powder feedstocks become a mixture of ceramic powders and solid (*in-bed*) binder particles [140][141][142]. The second type, designated as the binder pre-coating, involves the dispersion of ceramic powders and solid binder particles in water, followed by spray-drying [143] or drying, milling and sieving [144]–[147]. Ceramic powders with a surface coated with solid binder can then be obtained. Once

the liquid binder is deposited, a binding reaction between the solid binder and the ceramic powders is triggered, strengthening the green body. Comparatively, the latter type (coating form) may be more expensive and difficult to implement at an industrial scale, raising the interest in the use of the *in-bed* binders by dry mixing of powders. Indeed, while for commercial powders for BJP, usually plaster based ones, the liquid binder is enough to give mechanical resistance to the green printed parts, for the majority of ceramic materials extra binding action might be needed to provide enough mechanical strength to the *as*-printed part to be handled in the post conformation processes [133]. On the other hand, if a common commercial printer is to be used to print ceramic feedstocks using only water based liquid binders, this may require the modification of the liquid binder feeding system of the printer (tubes and printheads), as Inzana *et al.* [148] reported for the use of acidic binder solutions, or even the binder system itself. In this context, the use of an *in-bed* binder, which reacts with the water based liquid binder to better bond the ceramic particles, providing the needed mechanical behavior for the green parts, is currently the most used approach for binder jet printing of ceramic powders, especially for industrial scale applications.

Usually, and more related with the sustainability of the industrial processes, commercial liquid binders are water-based; furthermore, water-soluble binders have been the most used in BJP of technical ceramics. To be considered as well is that the use of an *in-bed* binder requires its removal, which leads to porosity creation in the final parts. While this is quite suitable for applications as in biomaterials [149][150], or applications such as cooling systems, filtration or refractory applications [151], for which porosity is a key parameter, in the case of dense ceramics, as tableware, porosity is a limiting parameter. How the removal of the *in-bed* binder affects the properties of printed porcelain is for example currently not known.

Several studies have been conducted to optimize BJP of ceramic powders, to get best strength and optimized performance for the printed parts. In this sense several *in-bed* binders and liquid binders combinations and *in-liquid* binders were used in the BJP of different ceramic systems, as presented in Table 1.IV. This is the case of dextrin, used by Fu *et al.* [140] to print SiSiC lattice structures by binder jet printing. A fraction of 18 vol.% in the dry powder blend of Si/SiC/dextrin composites was used and printed with water-based liquid binder and to produce as-printed parts with 55-60 % of porosity and the whole binder was eliminated. Melcher *et al.* [145] used dextrin as *in-bed* binder with alumina powders. In this case the dextrin was used as coating for the alumina powders with 6 wt.%, and then

printed using a layer thickness of 100 µm and a binder saturation of 200 %. Although the green density of the printed parts is not disclosed, the authors were able to reach 64 % of densification, after sintering at 1600 °C for 4 h. Maltodextrin is usually employed as a pre coating of ceramic particles; as an example maltodextrin coated hydroxyapatite (HA) exhibit 50-60 % of porosity [114] in the printed parts and 60-65 % of density after sintering [114][143]. Maltodextrin was also used as solid *in-bed* binder for BJP of porcelain [152], using a fraction of 16,7 wt.%, with the addition of sugar powder also in 16,7 wt.%, mixed in 66,7 wt.% of dry clay powder. The ceramics were sintered at 1316 °C for 2 h, producing sintered ceramics with a minimum of porosity of 58 %. In addition, maltodextrin was also used as solid *in-bed* binder by Suwanprateeb *et al.* [153]. The authors found that changing the mixtures of polystyrene, as main material, and maltodextrin, as solid *in-bed* binder, is possible to control the porous structure of printed parts, for example, designing a macroporous feature changing the particle size of polystyrene and maltodextrin, composition of the mixture and processing temperature. Polyvinyl Alcohol (PVA) was also reported as *in-bed* binder for binder jet printing of HA powders [154] with average particle size of 3.5 ± 0.4 µm and 70.9 ± 12.7 for PVA and HA powders, respectively. In this case, only mixtures with 50 wt.% of PVA were mechanically suitable for post conformation steps, producing sintered printed parts with a total porosity of ~55 %. PVA was used as *in-bed* binder for BJP of spray dried alumina powders, in 10 wt.% amount, using a mixture of water and alcohol as liquid binder, as well [155]. Printed green parts with relative density 20-25 % and sintered parts with relative density of 35-40 % were achieved [155]. Basalah *et al.* [156] used PVA as *in-bed* binder, mixed with titanium powders in 3, 5 and 10 wt.% ratios. The authors used a jar milling to produce the powder formulations reaching a minimum of porosity of 31 %. The same organic binder was used by Shanjani *et al.* [157] with CaP powders. In this study both powders were mixed trough jar milling process and tested with commercial liquid binder ZB58 (ZCorporation, USA), a water based binder. The authors found that parts produced by BJP will have better mechanical properties, when compared with the conventional route to fabricate porous structures of CaP. Sodium alginate, a water-soluble organic, was used in ink-jet printing of alumina slurries providing good mechanical resistance to the green parts even used in small amount (0,3 wt.%) [158]. Cellulose-based *in-bed* binders have also been used for BJP of calcium phosphate (CaP) based materials, as reported by Vorndran *et al.* [149].

**Table 1.IV:** Classification of binders for BJP and the most typical *in-bed* binders and liquid binders currently in use. (adapted from [133])

| Binders | | Additives | System | Obs. |
|---|---|---|---|---|
| Liquid binders | Water based | Methanol, Ethanol, Polyethylene glycol, Glycerol, Glycerin, Citric Acid, Polyvinyl Alcohol | $TiC\text{-}TiO_2$ [141][142]<br>Porcelain [152]<br>CaP-based [92][114][143][149][154][159]<br>SiSiC [140]<br>$Al_2O_3$ [145][146][155]<br>TiC [144]<br>HA-Bioactive Glass [147] | Trigger powder reactive |
| | Phosphoric acid | Isopropanol | CaP-based [109][148][149]<br>$\beta$-TCP-Bioactive Glass [150] | |
| | Citric acid | | CaP-based [149] | |
| | Commercial | | LAS [93]<br>$Al_2O_3$ [136]<br>AlN [137]<br>WC [138] | Self-adhesive |
| | Nanoparticle suspension | Polyvinylpyrrolidone | CaO [139] | |
| Solid binders (*in-bed*) | Polyvinyl alcohol (PVA) | | $Al_2O_3$ [155]<br>CaP-based [92][154][157] | Requires the use of a liquid binder |
| | Dextrin / Maltodextrin | | $TiC\text{-}TiO_2$ [141][142]<br>Porcelain [152]<br>CaP-based [114][143][159]<br>SiSiC [140]<br>TiC [144]<br>$Al_2O_3$ [145][146]<br>HA-Bioactive Glass [147] | |
| | Cellulose-based | | CaP-based [149] | |

In spite the interactions between powders and liquid binders are thoroughly described in the literature [133][134], the same in not valid for the systematic information on the role of *in-bed* binders. In addition, although recently, several reports have demonstrated the potential of BJP for AM of ceramics using solid *in-bed* binders, nearly all of these reports are related

with technical ceramics and almost none with traditional ceramics with added value, as the porcelain and possible industrialization.

### *1.4.2. Binders in Selective Laser Sintering*

As described previously, the use of *in-bed* binders for SLS of ceramics allows the indirect SLS approach, where a sacrificial binder is used during SLS process and removed from the ceramic body in post-conformation steps. In this way, thermal gradients in the printed part and defects formed based on them may be avoided. In Table 1.V the most used *in-bed* binders and the ceramic materials used are presented. An overall overview highlights the use of organic materials, such as thermosets and thermoplastic organic materials.

A complete study in the indirect SLS of ceramics was reported by Deckers *et al.* [160], where the authors discuss the use of different in-bed binders for SLS of alumina parts, such as polyamide (PA), polystyrene (PS), polypropylene (PP) and wax, and different ways to produce the feedstock, such as ball milling, dispersion polymerization and thermally induced phase separation (TIPS). The authors found that the powder deposition during SLS, was classified as excellent for the TIPS produced powders, while the feedstock produced by dispersion polymerization was good and for the ball milling feedstock it was poor due to the irregular shaped agglomerates. Concerning the relative density of the green bodies, as consequence of poor powder deposition, the ball milled powders only reached 37 %, while a maximum of 66 % was reached for dispersion polymerization powders and TIPS powders. Comparing the different binders, the feedstock prepared using PA lead to green parts with 55 % of relative density, while a minimum of 51 % was observed with PP as binder and a maximum of 66 % was reached using wax as binder. After solid state sintering the parts produced with ball milled feedstock exhibit a relative density varying between 83 - 93 %, while for the other processes the relative density varied between 48 - 83 %. As conclusion, the feedstocks using PA as *in-bed* binder reached higher relative densities than the ones with PP, PS and Wax. Bai *et al.* [161] used PMMA/wax as binder for $Al_2O_3/ZrO_2/TiC$ powders. The authors mixed the ceramic powders with the liquid binder, followed by dry and crush, until reach powder with 56 μm maximal particle size. Mechanical properties comparable to parts produced by conventional methods were obtained. Using ceramic particles coated with polymeric binder was also studied by Shahzad *et al.* [162]. The authors used high pure alumina and coated it with PA 12 (DuraForm PA, 3D Systems, USA) and used the phase inversion technique to produce microspheres of alumina coated with 50 and

60 vol.% of PA. The results showed a maximum relative density of 50% after sintering, due to the intersphere space formed during SLS process. Another interesting result was the higher green and sintered density of parts produced with lower content of ceramic powders when compared with the feedstock with higher amount. The group conclude that, despite the fact of the other formulation has 10 vol.% more of ceramics, the plastic flow of the binder during SLS, increase the interparticle contact area, leading to higher density in parts. A similar experiment using polypropylene [163] instead of polyamide was also reported. In this study the authors reached only 34 % of densification, however, after some post processing steps, 89 % of densification was reached. Cardon *et al.* [164] also used alumina powders for indirect SLS. In this work, polystyrene was used as coating (30 and 39 wt.%) on the ceramic particles, trough dispersion polymerization, showing that is suitable for indirect SLS. Another technique used to coat particles for indirect SLS is chemical vapor deposition (CVD) [165], which Davydova *et al.* used to coat $B_4C$ particles with a 2 μm layer of cobalt. The result is a metallic matrix with ceramic particles inclusions. However, due to the high porosity (37 %), the printed parts were not suitable for the targeted application of the group: cutting tools. From the point of view of industry, a ball milling process to produce feedstock is more economically viable than producing ceramic particles coated with the binder, as previously discussed. This process was used by Deckers *et al.* [166] to produce alumina powders feedstock with polyamide as binder (22 wt.%) reaching 85 – 92 % of relative density.

**Table 1.V:** Classification and the most used *in-bed* binders for SLS of ceramics. (adapt. from [167])

| Binder | | | System |
|---|---|---|---|
| Inorganic | | $HBO_2$ | $Al_2O_3$ [168]<br>$Al_2O_3$ glass-ceramic [169] |
| | | Cobalt | $B_4C$ [165] |
| Organic | Acid | Stearic acid | $ZrB_2$ [170] |
| | Wax | Carnauba wax | $Al_2O_3$ [160][171] |
| | Thermoset | Phenolic resin | SiC [172] |
| | | Epoxy resin | Porcelain [173] |
| | Thermoplast | Polyamide (PA) | $Al_2O_3$ [162][166][174][160] |
| | | Polypropylene (PP) | $Y_2O_3$–$ZrO_2$ [128]<br>$Al_2O_3$ [163][160] |
| | | Polystyrene (PS) | $Al_2O_3$ [164][175][160] |
| | | PMMA | $Al_2O_3$ [176]<br>$Al_2O_3$–TiC–$ZrO_2$ [161] |
| | | Acrylic | Apatite-mullite glass-ceramic [177] |

Summarizing, the use of organic *in-bed* binders, especially in the thermoplastic class is a viable option to produce ceramic parts through indirect SLS. However, reaching full densification is not reported in the literature and often post-conformation processing is required to improve relative density of the ceramic bodies.

## 1.5. Post-conformation processing

Due to the nature of powder bed AM techniques, the green parts produced through these techniques have high porosity. In some cases, as materials for bioapplications, this remaining porosity is an advantage, but for the general ceramic materials, applications require high densification. Furthermore, post-conformation processing is required in order to reach near full or full densification in printed parts. A variety of processes are reported in literature as enhancement for the relative density of ceramic printed parts by BJP and SLS,

as exhibited in Table 1.VI. A general overview of the table highlights that furnace sintering, i.e., thermal processing, is the most one used, as it is also used in ceramic parts produced through conventional routes. Although the furnace sintering can be the only post conformation processing step [143] or in combination with a debinding step [92][110][162], it is often used in combination with processes as isostatic pressing and infiltration.

Both in BJP and SLS, the use of binder is a limitation regarding reaching the maximum density of ceramic parts. Furthermore, a complete removal of binder during debinding is a crucial step in the processing of AM parts. In this sense, thermal processing is the most common way for binder removal and densification of the ceramic body. Shahzad *et al.* [162] showed that a lower heating rate (0,1 °C/min) during debinding process is better to reach fully removal of binder and avoid crack and distortions in printed parts by SLS, using alumina powders with polyamide as *in-bed* binder. Sun *et al.* [110] produced glass ceramic parts by BJP and performed a thermal cycle comprising a debinding stage from room temperature up to 400 °C with a heating rate of 5 °C/min, followed by a heating rate of 10 °C/min up to 720 °C with a dwell time of 1 h and a final heating up to 1050 °C, with a heating rate of 15 °C/min and a dwell time of 1 h. The authors were able to produce parts with a minimum of 47 % of porosity.

**Table 1.VI:** Materials, binders and post conformation steps of ceramic parts produced through powder bed AM techniques, with highlight for the main results concerning porosity.

| Material | Binder | Technique | Post processing | Porosity (%) | | Ref. |
|---|---|---|---|---|---|---|
| | | | | Green | Sintered | |
| Calcium Polyphosphate | PVA (n.d.) | BJP | DEB, FS | n.d. | 35 | [92] |
| Glass-ceramic | Commercial | BJP | FS | n.d. | 47 | [110] |
| SiC/Si | Commercial | BJP | PI, DEB, LSI | n.d. | 0,5 | [140] |
| Hydroxya-patite | Maltodextrin | BJP | FS | n.d. | 65 | [143] |
| $Ti_3SiC_2$ | Dextrin | BJP | FS, LSI | n.d. | 2,4 | [144] |
| $Al_2O_3$ | Polyvinyl Alcohol | BJP | DEB, VI, FS | 63 | 14 | [155] |
| $Al_2O_3$ | n.d. | BJP | FS | 73 | 45 | [178] |
| $ZrO_2$ | Polypropylene | SLS | PI, WIP, DEB, FS | 64 | 8 | [128] |
| $Al_2O_3$ | Polyamide | SLS | DEB, FS | 45 | 50 | [162] |
| $Al_2O_3$ | Polypropylene | SLS | PI, WIP, DEB, FS | 66 | 11 | [163] |
| $Al_2O_3$ | Polyamide | SLS | CIP, DEB, FS | 76 | 5,9 | [166] |
| $K_2O$-$Al_2O_3$-$SiO_2$ | Epoxy resin E-12 | SLS | CIP, DEB, FS | 63 | n.d. | [173] |
| $Al_2O_3$ | Polyamide | SLS | DEB, FS, PI, PLI, WIP | n.d. | 29 | [174] |
| $Al_2O_3$ | PVA + Epoxy resin | SLS | CIP, DEB, FS | 66 | 8 | [179] |

***Note:*** ***DEB*** *– Debinding;* ***FS*** *– Furnace Sintering;* ***PI*** *– Pressure Infiltration;* ***PLI*** *– Pressureless Infiltration;* ***VI*** *– Vacuum Infiltration;* ***WIP*** *– Warm Isostatic Pressing;* ***CIP*** *– Cold Isostatic Pressing;* ***LSI*** *- Liquid Silicon Infiltration;* ***n.d.*** *– non-defined*

Deckers *et al.* [174] reported a complete study in post conformation processing to improve the density of alumina parts produced by SLS. The authors used a debinding cycle with 0,1 °C/min, with a dwell of 2 h at 600 °C. However, the authors found later the need of another thermal cycle (5 °C/min, 2 h, 1050 °C) in order to reach enough strength of the part to be able of post processing steps. The authors also used WIP (Warm Isostatic Pressing), which is similar to CIP (Cold Isostatic Pressing) but temperature is applied at the same time as pressure is. In this case, the temperature used is 110 °C, which is above the Tg of the *in-bed* binder used (polyamide). The main advantage found by the authors using WIP over CIP, is that with the temperature, the polymer fraction increases its ductility and promotes the elimination of porosity between the particles. The authors found an increase in the relative density of the final sintered parts from 48 % (without any processing) to 64 %. Finally, the authors studied the process of pressureless infiltration, using a submicrometric alumina dispersed in ethanol in green parts and after the debinding step, concluding that the infiltration performed in the green parts reduce the shrinkage during furnace sintering but do not increase the density of the final parts, while the infiltration performed after the debinding step does not reduce the shrinkage of the part but increase the density of the final part without crack formation.

Isostatic pressing was also used as cold isostatic pressing (CIP) [166], hot isostatic pressing (HIP) and as combination with infiltration. As a matter of fact, Shahzad *et al.* [163] studied pressure infiltration (PI), warm isostatic pressing (WIP) and WIP/PI combination as different routes after SLS process with alumina powders. The results show a 53% densification of pressure infiltrated parts and 93% for warm isostatically pressed parts, as green density. After sintering, parts present 64 and 89% of densification for PI and WIP, respectively. Liu *et al.* [179] reached 92 % of densification after CIP and sintering, of $Al_2O_3$ and resin epoxy composite parts produced by SLS.

Maleksaeedi *et al.* [155] used vacuum infiltration in 3D printed alumina parts. The authors reached an increase from 37 to 86 % of densification after sintering, using a slurry with 50 vol. % of infiltrant solid loading. They also conclude that slurries with higher content of solid (> 40 vol. %) will lead to an incomplete infiltration, while with slurries with lower content of solids, the infiltration is complete, but the densification behavior is not as good as for parts impregnated with slurries with higher amount of solids content. The mechanical behavior was studied as well, with an increase up to 15 times for slurries with lower content of solids (< 40 vol. %). In the work of Nan *et al.* [144] $Ti_3SiC_2$-based ceramics were produced

by BJP and liquid silicon infiltration (LSI). The authors were able to reach 2,4 % of open porosity after infiltration at 1700 °C. The results also show an increase of more than 240 MPa in the bending strength, after infiltration. Preceramic materials were also used in infiltration of printed parts. Fu *et al.* [140] used polymethylphenylhydrogensilsesquioxane, a preceramic resin, as infiltrant agent in SiSiC structures. Combined with infiltration with liquid silicon, the group was able to reach a dense microstructure with 70 vol.% of Si.

Higher retractions after sintering of printed parts is one of the limitations of parts produced through powder bed AM techniques. It is even more crucial in a product driven company as *Porcelanas da Costa Verde*, where all the product designs are made. Deckers *et al.* [174] found that infiltration of green parts can reduce the linear shrinkage from 29-30 % to 24-25 %. The retraction is also high after isostatic pressing, as shown by Liu *et al.* [173] reaching a 57 % shrinkage in glass-ceramic for dental applications. The fact that the parts are produced in a layer-by-layer process, usually leads to anisotropic shrinkage of the parts. This fact was observed by Shanjani *et al.* [92] using calcium phosphate powders in 3D printing. The group observed higher shrinkage (17 %) in the directions parallel to the layers and 12 % in directions perpendicular to the layers. Yao *et al.* [178] were able to produce alumina parts with near no retraction. The group used alumina powders (< 25 μm) to produce alumina parts with macroporous after sintering. The oxidation process performed before high temperature sintering allowed the parts to reach high bonding between particles and near zero retraction.

As conclusion, the post conformation steps to improve the density of the final parts is required for objects produced through powder bed AM techniques. From the industrial point of view, the thermal processing, isostatic pressing and infiltration are the most interesting due to its ease of application at industrial scale. In addition, it is not reported, in the literature under our scope, the use of post conformation processing for parts produced through powder bed AM techniques regarding traditional ceramics, such as porcelain, and a comparison between the parts produced through the different ways.

## 1.6. References


[1] ASTM, “C 242 - 01 - Standard Terminology of Ceramic Whitewares and Related Products.” pp. 1–11, 2001.

[2] H. Boussak, H. Chemani, and A. Serier, “Characterization of porcelain tableware formulation containing bentonite clay,” *Int. J. Phys. Sci.*, vol. 10, no. 1, pp. 38–45, 2015.

[3] C. Barry Carter and M. Grant Norton, *Ceramic materials: Science and engineering*. 2007.

[4] W. M. Cam and U. Senapati, “Porcelain-Raw Materials, Processing, Phase Evolution, and Mechanical Behavior,” *J. Am. Ceram. Sociaty*, vol. 81, no. 1, pp. 3–20, 1998.

[5] D. W. Richerson, *Modern Ceramic Engineering*, Seond Edit. 2001.

[6] ASTM International, “F2792-12a - Standard Terminology for Additive Manufacturing Technologies.” ASTM International, 2012.

[7] ASTM International and ISO, “ISO/ASTM 52900 - Additive manufacturing - General principles - Terminology.” ISO / ASTM International, 2015.

[8] K. G. Swift and J. D. Booker, *Manufacturing Process Selection Handbook*. Butterworth-Heinemann, Elsevier, 2013.

[9] T. Campbell, C. Williams, O. Ivanova, and B. Garrett, “Could 3D Printing Change the World? Technologies, Potential, and Implications of Additive Manufacturing,” 2011.

[10] Hideo Kodama, “Automatic method for fabricating a three- dimensional plastic model with photo- hardening polymer,” *Rev. Sci. Instrum.*, vol. 52, no. 11, pp. 1770–1773, 1981.

[11] C. W. Hull, “Apparatus for production of three-dimensional objects by stereolithography,” US Patent 4575330, 1986.

[12] T. Wohlers and T. Gornet, “History of additive manufacturing,” *Wohlers Report 2016*. 2016.

[13] S. S. Crump, “Apparatus and Method for Creating Three-Dimensional Objects,” US Patent 5121329, 1992.

[14] E. M. Sachs, S. H. Haggerty, J. C. Michael, and P. A. Williams, “Three-dimensional printing techniques,” US Patent 5204055, 1993.

[15] C. R. Deckard, J. J. Beaman, and J. F. Darrah, “Method for selective laser sintering with layerwise cross-scanning,” US Patent 5155324, 1992.

[16] L. Dowling, J. Kennedy, S. O’Shaughnessy, and D. Trimble, “A review of critical

repeatability and reproducibility issues in powder bed fusion," *Mater. Des.*, vol. 186, p. 108346, 2020.

[17] B. Redwood, F. Schöffer, and B. Garret, "The 3D Printing Handbook," *3D Hubs*, p. 304, 2017.

[18] G. A. Appuhamillage, N. Chartrain, V. Meenakshisundaram, K. D. Feller, C. B. Williams, and T. E. Long, "110th Anniversary: Vat Photopolymerization-Based Additive Manufacturing: Current Trends and Future Directions in Materials Design," *Ind. Eng. Chem. Res.*, vol. 58, pp. 15109–15118, 2019.

[19] Z. Chen *et al.*, "3D printing of ceramics: A review," *J. Eur. Ceram. Soc.*, vol. 39, no. 4, pp. 661–687, 2019.

[20] J. W. Halloran, "Ceramic Stereolithography: Additive Manufacturing for Ceramics by Photopolymerization," *Annu. Rev. Mater. Res*, vol. 46, 2016.

[21] V. Tomeckova and J. W. Halloran, "Flow behavior of polymerizable ceramic suspensions as function of ceramic volume fraction and temperature," *J. E*, vol. 31, pp. 2535–2545, 2011.

[22] M. L. Griffith and J. W. Halloran, "Freeform fabrication of ceramics via stereolithography," *J. Am. Ceram. Soc.*, vol. 79, no. 10, pp. 2601–2608, 1996.

[23] W. Harrer, M. Schwentenwein, T. Lube, and R. Danzer, "Fractography of zirconia-specimens made using additive manufacturing (LCM) technology," *J. Eur. Ceram. Soc.*, vol. 37, no. 14, pp. 4331–4338, 2017.

[24] J. C. Wang and H. Dommati, "Fabrication of zirconia ceramic parts by using solvent-based slurry stereolithography and sintering," *Int. J. Adv. Manuf. Technol.*, vol. 98, no. 5–8, pp. 1537–1546, 2018.

[25] M. Schwentenwein and J. Homa, "Additive manufacturing of dense alumina ceramics," *Int. J. Appl. Ceram. Technol.*, vol. 12, no. 1, pp. 1–7, 2014.

[26] A. Goswami, K. Ankit, N. Balashanmugam, A. M. Umarji, and G. Madras, "Optimization of rheological properties of photopolymerizable alumina suspensions for ceramic microstereolithography," *Ceram. Int.*, vol. 40, no. 2, pp. 3655–3665, 2014.

[27] T. Chartier *et al.*, "Influence of irradiation parameters on the polymerization of ceramic reactive suspensions for stereolithography," *J. Eur. Ceram. Soc.*, vol. 37, no. 15, pp. 4431–4436, 2017.

[28] M. Zhou *et al.*, "Preparation of a defect-free alumina cutting tool via additive manufacturing based on stereolithography – Optimization of the drying and debinding processes," *Ceram. Int.*, vol. 42, no. 10, pp. 11598–11602, 2016.

[29] Y. de Hazan and D. Penner, "SiC and SiOC ceramic articles produced by

stereolithography of acrylate modified polycarbosilane systems," *J. Eur. Ceram. Soc.*, vol. 37, no. 16, pp. 5205–5212, 2017.

[30] Y. Yang *et al.*, "Three dimensional printing of high dielectric capacitor using projection based stereolithography method," *Nano Energy*, vol. 22, pp. 414–421, 2016.

[31] R. Gmeiner, G. Mitteramskogler, J. Stampfl, and A. R. Boccaccini, "Stereolithographic ceramic manufacturing of high strength bioactive glass," *Int. J. Appl. Ceram. Technol.*, vol. 12, no. 1, pp. 38–45, 2015.

[32] F. Scalera, C. Esposito Corcione, F. Montagna, A. Sannino, and A. Maffezzoli, "Development and characterization of UV curable epoxy/hydroxyapatite suspensions for stereolithography applied to bone tissue engineering," *Ceram. Int.*, vol. 40, no. 10, pp. 15455–15462, 2014.

[33] M. Dehurtevent, L. Robberecht, J. C. Hornez, A. Thuault, E. Deveaux, and P. Behin, "Stereolithography: A new method for processing dental ceramics by additive computer-aided manufacturing," *Dent. Mater.*, vol. 33, no. 5, pp. 477–485, 2017.

[34] B. G. Mekonnen, G. Bright, and A. Walker, "A Study on State of the Art Technology of Laminated Object Manufacturing ( LOM )," in *CAD/CAM Robotics and Factories of the Future*, 2016, pp. 207–216.

[35] H. Zhong *et al.*, "Preparation of SiC Ceramics by Laminated Object Manufacturing and Pressureless Sintering," *J. Ceram. Sci. Technol.*, vol. 6, no. 2, pp. 133–140, 2015.

[36] Y. Zhang, X. He, S. Du, and J. Zhang, "$Al_2O_3$ Ceramics Preparation by LOM (Laminated Object Manufacturing)," *Int. J. Adv. Manuf. Technol.*, vol. 17, no. 7, pp. 531–534, 2001.

[37] X. Tian, D. Li, and J. G. Heinrich, "Rapid prototyping of porcelain products by layer-wise slurry deposition (LSD) and direct laser sintering," *Rapid Prototyp. J.*, vol. 18, pp. 362–373, 2012.

[38] P. Lima, A. Zocca, W. Acchar, and J. Günster, "3D printing of porcelain by layerwise slurry deposition," *J. Eur. Ceram. Soc.*, vol. 38, no. 9, pp. 3395–3400, 2018.

[39] J. N. Stuecker, J. Cesarano, and D. A. Hirschfeld, "Control of the viscous behavior of highly concentrated mullite suspensions for robocasting," *J. Mater. Process. Technol.*, vol. 142, no. 2, pp. 318–325, 2003.

[40] E. Feilden, E. G. T. Blanca, F. Giuliani, E. Saiz, and L. Vandeperre, "Robocasting of structural ceramic parts with hydrogel inks," *J. Eur. Ceram. Soc.*, vol. 36, no. 10, pp. 2525–2533, 2016.

[41] T. Schlordt, S. Schwanke, F. Keppner, T. Fey, N. Travitzky, and P. Greil,

"Robocasting of alumina hollow filament lattice structures," *J. Eur. Ceram. Soc.*, vol. 33, no. 15–16, pp. 3243–3248, 2013.

[42] Z. Fu, M. Freihart, L. Wahl, T. Fey, P. Greil, and N. Travitzky, "Micro- and macroscopic design of alumina ceramics by robocasting," *J. Eur. Ceram. Soc.*, vol. 37, no. 9, pp. 3115–3124, 2017.

[43] A. Ghazanfari, W. Li, M. C. Leu, J. L. Watts, and G. E. Hilmas, "Additive manufacturing and mechanical characterization of high density fully stabilized zirconia," *Ceram. Int.*, vol. 43, no. 8, pp. 6082–6088, 2017.

[44] U. Scheithauer, T. Slawik, E. Schwarzer, H. Richter, T. Moritz, and A. Michaelis, "Additive Manufacturing of Metal-Ceramic-Composites by Thermoplastic 3D-Printing (3DTP)," *J. Ceram. Sci. Technol.*, vol. 6, no. 2, pp. 125–132, 2015.

[45] H. Shao, D. Zhao, T. Lin, J. He, and J. Wu, "3D gel-printing of zirconia ceramic parts," *Ceram. Int.*, vol. 43, no. 16, pp. 13938–13942, 2017.

[46] P. Miranda, E. Saiz, K. Gryn, and A. P. Tomsia, "Sintering and robocasting of β-tricalcium phosphate scaffolds for orthopaedic applications," *Acta Biomater.*, vol. 2, no. 4, pp. 457–466, 2006.

[47] S. Eqtesadi, A. Motealleh, P. Miranda, A. Pajares, A. Lemos, and J. M. F. Ferreira, "Robocasting of 45S5 bioactive glass scaffolds for bone tissue engineering," *J. Eur. Ceram. Soc.*, vol. 34, no. 1, pp. 107–118, 2014.

[48] Y. Maazouz *et al.*, "Robocasting of biomimetic hydroxyapatite scaffolds using self-setting inks," *J. Mater. Chem. B*, vol. 2, no. 33, pp. 5378–5386, 2014.

[49] B. Román-Manso *et al.*, "Electrically functional 3D-architectured graphene/SiC composites," *Carbon N. Y.*, vol. 100, pp. 318–328, 2016.

[50] X. Zhang, Z. Guo, C. Chen, and W. Yang, "Additive manufacturing of WC-20Co components by 3D gel-printing," *Int. J. Refract. Met. Hard Mater.*, vol. 70, pp. 215–223, 2017.

[51] S. Eqtesadi *et al.*, "Fabricating geometrically-complex $B_4C$ ceramic components by robocasting and pressureless spark plasma sintering," *Scr. Mater.*, vol. 145, pp. 14–18, 2018.

[52] E. Peng, D. Zhang, and J. Ding, "Ceramic Robocasting: Recent Achievements, Potential, and Future Developments," *Adv. Mater.*, vol. 30, no. 47, pp. 1–14, 2018.

[53] K. Rane and M. Strano, "A comprehensive review of extrusion-based additive manufacturing processes for rapid production of metallic and ceramic parts," *Adv. Manuf.*, vol. 7, no. 2, pp. 155–173, 2019.

[54] A. Dass and A. Moridi, "State of the Art in Directed Energy Deposition : From Additive

Manufacturing to Materials Design," *Coatings*, vol. 9, p. 418, 2019.

[55] Y. Li, Y. Hu, W. Cong, L. Zhi, and Z. Guo, "Additive manufacturing of alumina using laser engineered net shaping: Effects of deposition variables," *Ceram. Int.*, vol. 43, no. 10, pp. 7768–7775, 2017.

[56] F. Y. Niu, D. J. Wu, S. Yan, G. Y. Ma, and B. Zhang, "Process Optimization for Suppressing Cracks in Laser Engineered Net Shaping of Al2O3 Ceramics," *Jom*, vol. 69, no. 3, pp. 557–562, 2017.

[57] D. Wu *et al.*, "$Al_2O_3$-YAG eutectic ceramic prepared by laser additive manufacturing with water-cooled substrate," *Ceram. Int.*, vol. 45, no. 3, pp. 4119–4122, 2019.

[58] S. Yan, D. Wu, G. Ma, F. Niu, R. Kang, and D. Guo, "Formation mechanism and process optimization of nano $Al_2O_3$-$ZrO_2$ eutectic ceramic via laser engineered net shaping (LENS)," *Ceram. Int.*, vol. 43, no. 17, pp. 14742–14747, 2017.

[59] Y. Hu, F. Ning, W. Cong, Y. Li, X. Wang, and H. Wang, "Ultrasonic vibration-assisted laser engineering net shaping of ZrO2-Al2O3 bulk parts: Effects on crack suppression, microstructure, and mechanical properties," *Ceram. Int.*, vol. 44, no. 3, pp. 2752–2760, 2018.

[60] D. Ke, A. A. Vu, A. Bandyopadhyay, and S. Bose, "Compositionally graded doped hydroxyapatite coating on titanium using laser and plasma spray deposition for bone implants," *Acta Biomater.*, vol. 84, pp. 414–423, 2019.

[61] S. A. Bernard, V. K. Balla, S. Bose, and A. Bandyopadhyay, "Direct laser processing of bulk lead zirconate titanate ceramics," *Mater. Sci. Eng. B Solid-State Mater. Adv. Technol.*, vol. 172, no. 1, pp. 85–88, 2010.

[62] K. K. B. Hon, L. Li, and I. M. Hutchings, "Direct writing technology-Advances and developments," *CIRP Ann. - Manuf. Technol.*, vol. 57, no. 2, pp. 601–620, 2008.

[63] M. Vaezi, H. Seitz, and S. Yang, "A review on 3D micro-additive manufacturing technologies," *Int. J. Adv. Manuf. Technol.*, vol. 67, no. 5–8, pp. 1721–1754, 2013.

[64] C. Ainsley, N. Reis, and B. Derby, "Freeform fabrication by controlled droplet deposition of powder filled melts," *J. Mater. Sci.*, vol. 37, no. 15, pp. 3155–3161, 2002.

[65] K. A. M. Seerden, N. Reis, J. R. G. Evans, P. S. Grant, J. W. Halloran, and B. Derby, "Ink-Jet Printing of Wax-Based Alumina Suspensions," *J. Am. Ceram. Soc.*, vol. 84, no. 11, pp. 2514–2520, 2001.

[66] P. Gingter, A. M. Wätjen, M. Kramer, and R. Telle, "Functionally graded ceramic structures by direct thermal inkjet printing," *J. Ceram. Sci. Technol.*, vol. 6, no. 2, pp. 119–124, 2015.

[67] U. Scheithauer *et al.*, “Investigation of Droplet Deposition for Suspensions Usable for Thermoplastic 3D Printing (T3DP),” *J. Mater. Eng. Perform.*, vol. 27, no. 1, pp. 44–51, 2017.

[68] R. Noguera, M. Lejeune, and T. Chartier, “3D fine scale ceramic components formed by ink-jet prototyping process,” *J. Eur. Ceram. Soc.*, vol. 25, no. 12, pp. 2055–2059, Jan. 2005.

[69] S. A. M. Tofail, E. P. Koumoulos, A. Bandyopadhyay, S. Bose, L. O’Donoghue, and C. Charitidis, “Additive manufacturing: Scientific and technological challenges, market uptake and opportunities,” *Mater. Today*, vol. 00, no. 00, pp. 1–16, 2017.

[70] E. Castro e Costa, J. P. Duarte, and P. Bártolo, “A review of additive manufacturing for ceramic production,” *Rapid Prototyp. J.*, vol. 23, no. 5, pp. 954–963, 2017.

[71] T. T. Wohlers, “Wohlers Report 2019 - Additive Manufacturing and 3D Printing State of the Industry,” Colorado, USA, 2019.

[72] T. D. Ngo, A. Kashani, G. Imbalzano, K. T. Q. Nguyen, and D. Hui, “Additive manufacturing (3D printing): A review of materials, methods, applications and challenges,” *Compos. Part B Eng.*, vol. 143, no. December 2017, pp. 172–196, 2018.

[73] S. Singh, S. Ramakrishna, and R. Singh, “Material issues in additive manufacturing: A review,” *J. Manuf. Process.*, vol. 25, pp. 185–200, 2017.

[74] D. Bourell *et al.*, “Materials for additive manufacturing,” *CIRP Ann. - Manuf. Technol.*, vol. 66, no. 2, pp. 659–681, 2017.

[75] S. Bose, D. Ke, H. Sahasrabudhe, and A. Bandyopadhyay, “Additive manufacturing of biomaterials,” *Prog. Mater. Sci.*, vol. 93, pp. 45–111, 2018.

[76] J. S. Hyatt and J. W. Hyatt, “Improvement in Process and Apparatus for Manufacturing Pyroxyline,” US 133229, 1872.

[77] J. Torr, “A Short History of Injection Moulding.” AV Plastics Injection Moulding, 2010.

[78] S. J. Hu, “Evolving paradigms of manufacturing: From mass production to mass customization and personalization,” *Procedia CIRP*, vol. 7, pp. 3–8, 2013.

[79] W. Oropallo and L. A. Piegl, “Ten challenges in 3D printing,” *Eng. Comput.*, vol. 32, no. 1, pp. 135–148, 2015.

[80] Z. Simkin and A. Wang, “Wohlers Report 2015 - Cost-Benefit Analyses,” 2015.

[81] S. Tibbits, “4D printing: Multi-material shape change,” *Archit. Des.*, vol. 84, no. 1, pp. 116–121, 2014.

[82] J. J. Wu, L. M. Huang, Q. Zhao, and T. Xie, “4D Printing: History and Recent Progress,” *Chinese J. Polym. Sci. (English Ed.)*, vol. 36, no. 5, pp. 563–575, 2018.

[83] M. Singh and S. Jonnalagadda, “Advances in bioprinting using additive

manufacturing," *Eur. J. Pharm. Sci.*, vol. 143, no. August 2019, p. 105167, 2020.

[84] A. Bandyopadhyay and B. Heer, "Additive manufacturing of multi-material structures," *Mater. Sci. Eng. R Reports*, vol. 129, no. March, pp. 1–16, 2018.

[85] Y. Li *et al.*, "A Review on Functionally Graded Materials and Structures via Additive Manufacturing: From Multi-Scale Design to Versatile Functional Properties," *Adv. Mater. Technol.*, vol. 5, no. 6, 2020.

[86] X. Gong, T. Anderson, and K. Chou, "Review on powder-based electron beam additive manufacturing technology," *Manuf. Rev.*, vol. 1, no. 2, pp. 1–12, 2014.

[87] F. Niu, D. Wu, S. Zhou, and G. Ma, "Power prediction for laser engineered net shaping of $Al_2O_3$ ceramic parts," *J. Eur. Ceram. Soc.*, vol. 34, no. 15, pp. 3811–3817, 2014.

[88] H. Miyanaji, M. Orth, J. M. Akbar, and L. Yang, "Process development for green part printing using binder jetting additive manufacturing," *Front. Mech. Eng.*, vol. 13, no. 4, pp. 504–512, 2018.

[89] M. Castilho, B. Gouveia, I. Pires, J. Rodrigues, and M. Pereira, "The role of shell/core saturation level on the accuracy and mechanical characteristics of porous calcium phosphate models produced by 3Dprinting," *Rapid Prototyp. J.*, vol. 21, no. 1, pp. 43–55, 2015.

[90] A. Farzadi, M. Solati-Hashjin, M. Asadi-Eydivand, and N. A. A. Osman, "Effect of layer thickness and printing orientation on mechanical properties and dimensional accuracy of 3D printed porous samples for bone tissue engineering," *PLoS One*, vol. 9, no. 9, pp. 1–14, 2014.

[91] M. Vaezi and C. K. Chua, "Effects of layer thickness and binder saturation level parameters on 3D printing process," *Int. J. Adv. Manuf. Technol.*, vol. 53, no. 1–4, pp. 275–284, 2011.

[92] Y. Shanjani, Y. Hu, R. M. Pilliar, and E. Toyserkani, "Mechanical characteristics of solid-freeform-fabricated porous calcium polyphosphate structures with oriented stacked layers," *Acta Biomater.*, vol. 7, no. 4, pp. 1788–1796, Apr. 2011.

[93] A. Zocca, C. M. Gomes, E. Bernardo, R. Müller, J. Günster, and P. Colombo, "LAS glass–ceramic scaffolds by three-dimensional printing," *J. Eur. Ceram. Soc.*, vol. 33, no. 9, pp. 1525–1533, Aug. 2013.

[94] H. Miyanaji, S. Zhang, A. Lassell, A. A. Zandinejad, and L. Yang, "Optimal Process Parameters for 3D Printing of Porcelain Structures," *Procedia Manuf.*, vol. 5, pp. 870–887, 2016.

[95] X. Tian, J. Günster, J. Melcher, D. Li, and J. G. Heinrich, "Process parameters

analysis of direct laser sintering and post treatment of porcelain components using Taguchi's method," *J. Eur. Ceram. Soc.*, vol. 29, pp. 1903–1915, 2009.

[96] N. K. Tolochko, T. Laoui, Y. V. Khlopkov, S. E. Mozzharov, V. I. Titov, and M. B. Ignatiev, "Absorptance of powder materials suitable for laser sintering," *Rapid Prototyp. J.*, vol. 6, no. 3, pp. 155–160, 2000.

[97] J. Zhang *et al.*, "Influence of Particle Size on Laser Absorption and Scanning Track Formation Mechanisms of Pure Tungsten Powder During Selective Laser Melting," *Engineering*, vol. 5, no. 4, pp. 736–745, 2019.

[98] H. Lee, C. H. J. Lim, M. J. Low, N. Tham, V. M. Murukeshan, and Y. J. Kim, "Lasers in additive manufacturing: A review," *Int. J. Precis. Eng. Manuf. - Green Technol.*, vol. 4, no. 3, pp. 307–322, 2017.

[99] M. Schmid, A. Amado, and K. Wegener, "Polymer powders for selective laser sintering (SLS)," *AIP Conf. Proc.*, vol. 1664, no. 160009, 2015.

[100] I. Shishkovsky, I. Yadroitsev, P. Bertrand, and I. Smurov, "Alumina-zirconium ceramics synthesis by selective laser sintering/melting," *Appl. Surf. Sci.*, vol. 254, no. 4, pp. 966–970, 2007.

[101] Q. Liu, B. Song, and H. Liao, "Microstructure study on selective laser melting yttria stabilized zirconia ceramic with near IR fiber laser," *Rapid Prototyp. J.*, vol. 20, no. 5, pp. 346–354, 2014.

[102] H. Yves-Christian, W. Jan, M. Wilhelm, W. Konrad, and P. Reinhart, "Net shaped high performance oxide ceramic parts by Selective Laser Melting," *Phys. Procedia*, vol. 5, pp. 587–594, 2010.

[103] J. Wilkes, Y.-C. Hagedorn, W. Meiners, and W. Konrad, "Additive manufacturing of $ZrO_2$-$Al_2O_3$ ceramic components by selective laser melting," *Rapid Prototyp. J.*, vol. 19, no. 1, pp. 51–57, 2013.

[104] Q. Liu, Y. Danlos, B. Song, B. Zhang, S. Yin, and H. Liao, "Effect of high-temperature preheating on the selective laser melting of yttria-stabilized zirconia ceramic," *J. Mater. Process. Technol.*, vol. 222, pp. 61–74, 2015.

[105] J. Deckers, S. Meyers, J. P. Kruth, and J. Vleugels, "Direct selective laser sintering / melting of high density alumina powder layers at elevated temperatures," *Phys. Procedia*, vol. 56, pp. 117–124, 2014.

[106] A. Danezan *et al.*, "Selective laser sintering of porcelain," *J. Eur. Ceram. Soc.*, vol. 38, no. 2, pp. 769–775, 2018.

[107] J. Christian Nelson, N. K. Vail, J. W. Barlow, J. J. Beaman, D. L. Bourell, and H. L. Marcus, "Selective Laser Sintering of Polymer-Coated Silicon Carbide Powders," *Ind.*

*Eng. Chem. Res.*, vol. 34, no. 5, pp. 1641–1651, 1995.

[108] T. Mukherjee, J. S. Zuback, A. De, and T. DebRoy, “Printability of alloys for additive manufacturing,” *Sci. Rep.*, vol. 6, pp. 1–8, 2016.

[109] A. Butscher *et al.*, “Printability of calcium phosphate powders for three-dimensional printing of tissue engineering scaffolds,” *Acta Biomater.*, vol. 8, no. 1, pp. 373–385, Jan. 2012.

[110] C. Sun *et al.*, “Effect of particle size gradation on the performance of glass-ceramic 3D printing process,” *Ceram. Int.*, vol. 43, no. 1, pp. 578–584, 2017.

[111] Z. Zhou, F. Buchanan, C. Mitchell, and N. Dunne, “Printability of calcium phosphate: Calcium sulfate powders for the application of tissue engineered bone scaffolds using the 3D printing technique,” *Mater. Sci. Eng. C*, vol. 38, no. 1, pp. 1–10, 2014.

[112] H. Miyanaji, S. Zhang, and L. Yang, “A new physics-based model for equilibrium saturation determination in binder jetting additive manufacturing process,” *Int. J. Mach. Tools Manuf.*, vol. 124, no. April 2017, pp. 1–11, 2018.

[113] T. Miyajima, K.-I. Yamamoto, and M. Sugimoto, “Effect of particle properties during tapping,” *Adv. Part. Technol.*, vol. 12, no. 1, pp. 117–134, 2001.

[114] J. Suwanprateeb, R. Sanngam, and T. Panyathanmaporn, “Influence of raw powder preparation routes on properties of hydroxyapatite fabricated by 3D printing technique,” *Mater. Sci. Eng. C*, vol. 30, no. 4, pp. 610–617, May 2010.

[115] A. Santomaso, P. Lazzaro, and P. Canu, “Powder flowability and density ratios: the impact of granules packing,” *Chem. Eng. Sci.*, vol. 58, no. 13, pp. 2857–2874, 2003.

[116] R. O. Grey and J. K. Beddow, “On the Hausner Ratio and its relationship to some properties of metal powders,” *Powder Technol.*, vol. 2, no. 6, pp. 323–326, 1969.

[117] H. H. Hausner, “Friction conditions in a mass of metal powder,” *Int. J. Powder Metall.*, vol. 3, pp. 7–13, 1967.

[118] E. Abdullah and D. Geldart, “The use of bulk density measurments as a flowability indicators,” *Powder Technol.*, vol. 102, pp. 151–165, 1999.

[119] A. Zocca, C. M. Gomes, T. Muhler, and J. Gunster, “Powder-bed stabilization for powder-based additive manufacturing,” *Adv. Mech. Eng.*, vol. 6, pp. 1–6, 2014.

[120] M. Moghadasi, W. Du, M. Li, Z. Pei, and C. Ma, “Ceramic binder jetting additive manufacturing: Effects of particle size on feedstock powder and final part properties,” *Ceram. Int.*, vol. 46, no. 10, pp. 16966–16972, 2020.

[121] H. Chen, Q. Wei, S. Wen, Z. Li, and Y. Shi, “Flow behavior of powder particles in layering process of selective laser melting: Numerical modeling and experimental verification based on discrete element method,” *Int. J. Mach. Tools Manuf.*, vol. 123,

no. July, pp. 146–159, 2017.

[122] C. Hirschberg, C. C. Sun, J. Risbo, and J. Rantanen, “Effects of Water on Powder Flowability of Diverse Powders Assessed by Complimentary Techniques,” *J. Pharm. Sci.*, vol. 108, no. 8, pp. 2613–2620, 2019.

[123] A. M. N. Faqih, A. Mehrotra, S. V. Hammond, and F. J. Muzzio, “Effect of moisture and magnesium stearate concentration on flow properties of cohesive granular materials,” *Int. J. Pharm.*, vol. 336, no. 2, pp. 338–345, 2007.

[124] H. Miyanaji, S. Zhang, A. Lassell, A. Zandinejad, and L. Yang, “Process Development of Porcelain Ceramic Material with Binder Jetting Process for Dental Applications,” *Jom*, vol. 68, no. 3, pp. 831–841, 2016.

[125] S. Zhang, H. Miyanaji, L. Yang, A. A. Zandinejad, J. J. S. Dilip, and B. Stucker, “An experimental study of ceramic dental porcelain materials using a 3D print (3DP) process,” *25th Annu. Int. Solid Free. Fabr. Symp. &#65533; An Addit. Manuf. Conf. SFF 2014*, pp. 991–1011, 2014.

[126] D. L. Bourell, T. J. Watt, D. K. Leigh, and B. Fulcher, “Performance limitations in polymer laser sintering,” *Phys. Procedia*, vol. 56, pp. 147–156, 2014.

[127] J. P. Kruth, G. Levy, F. Klocke, and T. H. C. Childs, “Consolidation phenomena in laser and powder-bed based layered manufacturing,” *CIRP Ann. - Manuf. Technol.*, vol. 56, no. 2, pp. 730–759, 2007.

[128] K. Shahzad, J. Deckers, Z. Zhang, J.-P. Kruth, and J. Vleugels, “Additive manufacturing of zirconia parts by indirect selective laser sintering,” *J. Eur. Ceram. Soc.*, vol. 34, no. 1, pp. 81–89, Jan. 2014.

[129] A. Mostafaei, A. M. Elliott, J. E. Barnes, C. L. Cramer, P. Nandwana, and M. Chmielus, “Binder jet 3D printing – process parameters, materials, properties, and challenges,” *Prog. Mater. Sci.*, p. 100684, 2020.

[130] J. C. Williams, “The segregation of particulate materials. A review,” *Powder Technol.*, vol. 15, no. 2, pp. 245–251, 1976.

[131] P. Tang and V. M. Puri, “Methods for minimizing segregation: A review,” *Part. Sci. Technol.*, vol. 22, no. 4, pp. 321–337, 2004.

[132] A. Strondl, O. Lyckfeldt, H. Brodin, and U. Ackelid, “Characterization and Control of Powder Properties for Additive Manufacturing,” *J. Miner. Met. Mater. Soc.*, vol. 67, no. 3, pp. 549–554, 2015.

[133] X. Lv, F. Ye, L. Cheng, S. Fan, and Y. Liu, “Binder jetting of ceramics: Powders, binders, printing parameters, equipment, and post-treatment,” *Ceram. Int.*, vol. 45, no. 10, pp. 12609–12624, 2019.

[134] B. Utela, D. Storti, R. Anderson, and M. Ganter, “A review of process development steps for new material systems in three dimensional printing (3DP),” *J. Manuf. Process.*, vol. 10, no. 2, pp. 96–104, Jul. 2008.

[135] J. Moon, J. E. Grau, V. Knezevic, M. J. Cima, and E. M. Sachs, “Ink-jet printing of binders for ceramic components,” *J. Am. Ceram. Soc.*, vol. 85, no. 4, pp. 755–762, 2002.

[136] J. A. Gonzalez, J. Mireles, Y. Lin, and R. B. Wicker, “Characterization of ceramic components fabricated using binder jetting additive manufacturing technology,” *Ceram. Int.*, vol. 42, no. 9, pp. 10559–10564, 2016.

[137] C. A. Díaz-Moreno *et al.*, “Binder jetting additive manufacturing of aluminum nitride components,” *Ceram. Int.*, vol. 45, no. 11, pp. 13620–13627, 2019.

[138] R. K. Enneti, K. C. Prough, T. A. Wolfe, A. Klein, N. Studley, and J. L. Trasorras, “Sintering of WC-12%Co processed by binder jet 3D printing (BJ3DP) technology,” *Int. J. Refract. Met. Hard Mater.*, vol. 71, no. October 2017, pp. 28–35, 2017.

[139] H. Zhao, C. Ye, Z. Fan, and C. Wang, “3D printing of CaO-based ceramic core using nanozirconia suspension as a binder,” *J. Eur. Ceram. Soc.*, vol. 37, no. 15, pp. 5119–5125, 2017.

[140] Z. Fu, L. Schlier, N. Travitzky, and P. Greil, “Three-dimensional printing of SiSiC lattice truss structures,” *Mater. Sci. Eng. A*, vol. 560, pp. 851–856, 2013.

[141] X. Yin, N. Travitzky, and P. Greil, “Near-Net-Shape Fabrication of Ti3AlC2-Based Composites,” *Int. J. Appl. Ceram. Technol.*, vol. 4, no. 2, pp. 184–190, 2007.

[142] X. Yin, N. Travitzky, and P. Greil, “Three-dimensional printing of nanolaminated Ti3AlC2 toughened TiAl3-Al2O3 composites,” *J. Am. Ceram. Soc.*, vol. 90, no. 7, pp. 2128–2134, 2007.

[143] R. Chumnanklang, T. Panyathanmaporn, K. Sitthiseripratip, and J. Suwanprateeb, “3D printing of hydroxyapatite: Effect of binder concentration in pre-coated particle on part strength,” *Mater. Sci. Eng. C*, vol. 27, pp. 914–921, May 2007.

[144] B. Nan, X. Yin, L. Zhang, and L. Cheng, “Three-Dimensional Printing of $Ti_3SiC_2$-Based Ceramics,” *J. Am. Ceram. Soc.*, vol. 94, no. 4, pp. 969–972, Apr. 2011.

[145] R. Melcher, S. Martins, N. Travitzky, and P. Greil, “Fabrication of Al2O3-based composites by indirect 3D-printing,” *Mater. Lett.*, vol. 60, no. 4, pp. 572–575, 2006.

[146] R. Melcher, N. Travitzky, C. Zollfrank, and P. Greil, “3D printing of Al2O3/Cu-O interpenetrating phase composite,” *J. Mater. Sci.*, vol. 46, no. 5, pp. 1203–1210, 2011.

[147] A. Winkel *et al.*, “Sintering of 3D-printed glass/HAp composites,” *J. Am. Ceram. Soc.*,

vol. 95, no. 11, pp. 3387–3393, 2012.

[148] J. a Inzana *et al.*, “3D printing of composite calcium phosphate and collagen scaffolds for bone regeneration.,” *Biomaterials*, vol. 35, no. 13, pp. 4026–34, Apr. 2014.

[149] B. E. Vorndran *et al.*, “3D Powder Printing of B-Tricalcium Phosphate Ceramics Using Different Strategies,” *Adv. Eng. Mater.*, vol. 10, no. 12, pp. 67–71, 2008.

[150] C. Bergmann *et al.*, “3D printing of bone substitute implants using calcium phosphate and bioactive glasses,” *J. Eur. Ceram. Soc.*, vol. 30, no. 12, pp. 2563–2567, 2010.

[151] L. Rabinskiy, A. Ripetsky, S. Sitnikov, Y. Solyaev, and R. Kahramanov, “Fabrication of porous silicon nitride ceramics using binder jetting technology,” *IOP Conf. Ser. Mater. Sci. Eng.*, vol. 140, no. 1, 2016.

[152] G. Marchelli, M. Ganter, and D. Storti, “New material systems for 3D ceramic printing,” in *Solid Freeform Fabrication Symposium*, 2009, pp. 477–487.

[153] J. Suwanprateeb and R. Chumnanklang, “Three-dimensional printing of porous polyethylene structure using water-based binders,” *J. Biomed. Mater. Res. - Part B Appl. Biomater.*, vol. 78B, no. 1, pp. 138–145, 2006.

[154] S. C. Cox, J. A. Thornby, G. J. Gibbons, M. A. Williams, and K. K. Mallick, “3D printing of porous hydroxyapatite scaffolds intended for use in bone tissue engineering applications,” *Mater. Sci. Eng. C*, vol. 47, pp. 237–247, 2015.

[155] S. Maleksaeedi, H. Eng, F. E. Wiria, T. M. H. Ha, and Z. He, “Property enhancement of 3D-printed alumina ceramics using vacuum infiltration,” *J. Mater. Process. Technol.*, vol. 214, no. 7, pp. 1301–1306, 2014.

[156] A. Basalah, Y. Shanjani, S. Esmaeili, and E. Toyserkani, “Characterizations of additive manufactured porous titanium implants,” *J. Biomed. Mater. Res. - Part B Appl. Biomater.*, vol. 100 B, no. 7, pp. 1970–1979, 2012.

[157] Y. Shanjani, J. N. Amritha De Croos, R. M. Pilliar, R. A. Kandel, and E. Toyserkani, “Solid freeform fabrication and characterization of porous calcium polyphosphate structures for tissue engineering purposes,” *J. Biomed. Mater. Res. - Part B Appl. Biomater.*, vol. 93, no. 2, pp. 510–519, 2010.

[158] A. Zocca, P. Lima, and J. Günster, “LSD-based 3D printing of alumina ceramics,” *J. Ceram. Sci. Technol.*, vol. 8, no. 1, pp. 141–148, 2017.

[159] J. Suwanprateeb, R. Sanngam, W. Suvannapruk, and T. Panyathanmaporn, “Mechanical and in vitro performance of apatite-wollastonite glass ceramic reinforced hydroxyapatite composite fabricated by 3D-printing,” *J. Mater. Sci. Mater. Med.*, vol. 20, no. 6, pp. 1281–1289, 2009.

[160] J. Deckers, K. Shahzad, P. L. Cardon, M. Rombouts, J. Vleugels, and J. P. Kruth,

"Shaping ceramics through indirect Selective Laser Sintering," *Rapid Prototyp. J.*, vol. 20, no. 4, 2016.

[161] P. Bai and Y. Li, "Study on High Temperature Sintering Processes of Selective Laser Sintered $Al_2O_3/ZrO_2$/TiC Ceramics," *Sci. Sinter.*, vol. 41, no. 1, pp. 35–41, 2009.

[162] K. Shahzad, J. Deckers, S. Boury, B. Neirinck, J.-P. Kruth, and J. Vleugels, "Preparation and indirect selective laser sintering of alumina/PA microspheres," *Ceram. Int.*, vol. 38, no. 2, pp. 1241–1247, Mar. 2012.

[163] K. Shahzad, J. Deckers, J. P. Kruth, and J. Vleugels, "Additive manufacturing of alumina parts by indirect selective laser sintering and post processing," *J. Mater. Process. Technol.*, vol. 213, no. 9, pp. 1484–1494, 2013.

[164] L. Cardon *et al.*, "Polystyrene-Coated Alumina Powder via Dispersion Polymerization for Indirect Selective Laser Sintering Applications," *J. Appl. Polym. Sci.*, pp. 2121–2128, 2013.

[165] A. Davydova *et al.*, "Selective laser melting of boron carbide particles coated by a cobalt-based metal layer," *J. Mater. Process. Technol.*, vol. 229, pp. 361–366, 2016.

[166] J. Deckers, K. Shahzad, J. Vleugels, and J. P. Kruth, "Isostatic pressing assisted indirect selective laser sintering of alumina components," *Rapid Prototyp. J.*, vol. 18, no. 5, pp. 409–419, 2012.

[167] J. Deckers, J. Vleugels, and J. Kruth, "Additive Manufacturing of Ceramics : A Review," *J. Ceram. Sci. Technol.*, vol. 5, no. 4, pp. 245–260, 2014.

[168] I. Lee, "Influence of heat treatment upon SLS processed composites fabricated with alumina and monoclinic $HBO_2$," *J. Mater. Sci. Lett.*, vol. 21, no. 3, pp. 209–212, 2002.

[169] I. Lee, "Rapid full densification of alumina-glass composites fabricated by a Selective Laser Sintering process," *J. Mater. Sci. Lett.*, vol. 17, pp. 1907–1911, 1998.

[170] M. C. Leu, S. Pattnaik, and G. E. Hilmas, "Investigation of laser sintering for freeform fabrication of zirconium diboride parts," *Virtual Phys. Prototyp.*, vol. 7, no. 1, pp. 25–36, 2012.

[171] M. Rombouts, J. Deckers, I. Thijs, J. Deckx, and J.-P. Kruth, "Wax based binder for indirect selective laser sintering of alumina," *Proc. 5th Int. PMI Conf.*, no. Figure 1, pp. 184–188, 2012.

[172] B. Stevinson, D. L. Bourell, and J. J. Beaman, "Dimensional stability during post-processing of selective laser sintered ceramic preforms," *Virtual Phys. Prototyp.*, vol. 1, no. 4, pp. 209–216, 2006.

[173] J. Liu, B. Zhang, C. Yan, and Y. Shi, "The effect of processing parameters on characteristics of selective laser sintering dental glass-ceramic powder," *Rapid*

*Prototyp. J.*, vol. 16, no. 2, pp. 138–145, 2010.

[174] J. Deckers, J. Kruth, K. Shahzad, and J. Vleugels, “Density improvement of alumina parts produced through selective laser sintering of alumina-polyamide composite powder,” *CIRP Ann. - Manuf. Technol.*, vol. 61, no. 1, pp. 211–214, 2012.

[175] J. Deckers, J.-P. Kruth, L. Cardon, K. Shahzad, and J. Vleugels, “Densification and Geometrical Assessments of Alumina Parts Produced Through Indirect Selective Laser Sintering of Alumina-Polystyrene Composite Powder,” *Stroj. Vestnik-Journal Mech. Eng.*, vol. 59, no. 11, pp. 646–661, 2013.

[176] K. Subramanian, N. Vail, J. Barlow, and H. Marcus, “Selective laser sintering of alumina with polymer binders,” *Rapid Prototyp. J.*, vol. 1, no. 2, pp. 24–35, 1995.

[177] R. D. Goodridge, D. J. Wood, C. Ohtsuki, and K. W. Dalgarno, “Biological evaluation of an apatite-mullite glass-ceramic produced via selective laser sintering,” *Acta Biomater.*, vol. 3, no. 2, pp. 221–231, 2007.

[178] D. Yao, C. M. Gomes, Y. P. Zeng, D. Jiang, J. Gunster, and J. G. Heinrich, “Near zero shrinkage porous $Al_2O_3$ prepared via 3D-printing and reaction bonding,” *Mater. Lett.*, vol. 147, pp. 116–118, 2015.

[179] K. Liu, Y. Shi, C. Li, L. Hao, J. Liu, and Q. Wei, “Indirect selective laser sintering of epoxy resin-$Al_2O_3$ ceramic powders combined with cold isostatic pressing,” *Ceram. Int.*, vol. 40, no. 5, pp. 7099–7106, 2014.

[180] M. Alger, *Polymer science dictionary*, 3rd Editio., vol. 38, no. 3. Springer, 2003.

[181] ASTM International, “C373-14a - Standard Test Method for Water Absorption, Bulk Density, Apparent Porosity, and Apparent Specific Gravity of Fired Whiteware Products, Ceramic Tiles, and Glass Tiles.” ASTM International, USA, 2014.

[182] D. de Britto and O. B. G. Assis, “Thermal degradation of carboxymethylcellulose in different salty forms,” *Thermochim. Acta*, vol. 494, no. 1–2, pp. 115–122, 2009.

[183] T. Sugama and T. Pyatina, “Effect of sodium carboxymethyl celluloses on water-catalyzed self-degradation of 200 °c-heated alkali-activated cement,” *Cem. Concr. Compos.*, vol. 55, pp. 281–289, 2015.

[184] J. P. Soares, J. E. Santos, G. O. Chierice, and E. T. G. Cavalheiro, “Thermal behavior of alginic acid and its sodium salt,” *Eclet. Quim.*, vol. 29, no. 2, pp. 57–63, 2004.

[185] Z. Peng and L. Xue, “A thermal degradation mechanism of polyvinyl alcohol / silica nanocomposites,” vol. 92, 2007.

[186] L. Co, J. Kim, and H. Lee, “Thermal and Carbothermic Decomposition of Na 2 CO 3 and,” vol. 32, no. February, pp. 17–24, 2001.

[187] 3D Systems, “ZP131 Safety Data Sheet.” 3D Systems, Inc, Rock Hill, South Carolina,

USA, pp. 1–5, 2014.

[188] I. 3D Systems, “ZP140 Safety Data Sheet.” Z Corporation, pp. 1–6, 2007.

[189] 3D Systems, “VisiJet PXL Core Safety Data Sheet.” 3D Systems, Inc, Rock Hill, South Carolina, USA, pp. 1–4, 2013.

[190] G. Nichols *et al.*, “A review of the terms agglomerate and aggregate with a recommendation for nomenclature used in powder and particle characterization,” *J. Pharm. Sci.*, vol. 91, no. 10, pp. 2103–2109, 2002.

[191] G. W. Brindley and M. Nakahira, “The kaolinite-mullite reaction series: I, a survey of outstanding problems,” *J. Am. Ceram. Soc.*, vol. 42, no. 7, pp. 23–71, 1959.

[192] H. B. Johnson and F. Kessler, “Kaolinite Dehydroxylation Kinetics,” *J. Am. Ceram. Soc.*, vol. 52, no. 4, pp. 199–203, 1969.

[193] K. Okada, N. ŌTsuka, and J. Ossaka, “Characterization of Spinel Phase Formed in the Kaolin-Mullite Thermal Sequence,” *J. Am. Ceram. Soc.*, vol. 69, no. 10, p. C-251-C-253, 1986.

[194] B. Sonuparlak, M. Sarikaya, and I. A. Aksay, “Spinel Phase Formation During the 980°C Exothermic Reaction in the Kaolinite-to-Mullite Reaction Series,” *J. Am. Ceram. Soc.*, vol. 70, no. 11, pp. 837–842, 1987.

[195] O. D. Neikov and N. A. Yefimov, *Powder Characterization and Testing*, 2nd ed. Elsevier Ltd., 2019.

[196] M. Schmid, A. Amado, and K. Wegener, “Polymer powders for Selective Laser Sintering,” in *30th International Conference of the Polymer Processing Society*, 2014, pp. 1–5.

[197] K. Wudy and D. Drummer, “Aging effects of polyamide 12 in selective laser sintering: Molecular weight distribution and thermal properties,” *Addit. Manuf.*, vol. 25, pp. 1–9, 2019.

[198] A. Rashid, *Additive Manufacturing Technologies*. 2019.

[199] JaaYoo, “Thingiverse, Thing: 1094870,” 2015. [Online]. Available: https://www.thingiverse.com/thing:1094870. [Accessed: 25-Nov-2018].

[200] E. Rauch, M. Unterhofer, and P. Dallasega, “Industry sector analysis for the application of additive manufacturing in smart and distributed manufacturing systems,” *Manuf. Lett.*, vol. 15, pp. 126–131, 2018.

[201] C. Klahn, B. Leutenecker, and M. Meboldt, “Design strategies for the process of additive manufacturing,” *Procedia CIRP*, vol. 36, pp. 230–235, 2015.

[202] P. Stavropoulos, P. Foteinopoulos, A. Papacharalampopoulos, and H. Bikas, “Addressing the challenges for the industrial application of additive manufacturing:

Towards a hybrid solution," *Int. J. Light. Mater. Manuf.*, vol. 1, no. 3, pp. 157–168, 2018.

[203] H. Levi, "Changing the way we manufacture – AM in technical ceramics," *Met. Powder Rep.*, vol. 73, no. 6, pp. 314–315, 2018.

[204] D. Santos, A. C. Maurício, V. Sencadas, J. D. Santos, M. H. Fernandes, and P. S. Gomes, "Spray Drying: An Overview," *Biomater. - Phys. Chem. - New Ed.*, 2018.

[205] BerlinRockz, "Thingiverse, Thing: 1692007," 2016. [Online]. Available: https://www.thingiverse.com/thing:1692007. [Accessed: 25-Nov-2018].

[206] S. J. Lukasiewicz, "Spray-Drying Ceramic Powders," *J. Am. Ceram. Soc.*, vol. 72, no. 4, pp. 617–624, 1989.

[207] V. One and A. S. Mujumdar, *Spray Drying Technology*. .

[208] L. C. Ardila *et al.*, "Effect of IN718 recycled powder reuse on properties of parts manufactured by means of Selective Laser Melting," *Phys. Procedia*, vol. 56, no. C, pp. 99–107, 2014.

[209] H. Asgari, C. Baxter, K. Hosseinkhani, and M. Mohammadi, "On microstructure and mechanical properties of additively manufactured AlSi10Mg_200C using recycled powder," *Mater. Sci. Eng. A*, vol. 707, no. September, pp. 148–158, 2017.

[210] W. Gao *et al.*, "The status, challenges, and future of additive manufacturing in engineering," *Comput. Des.*, 2015.

[211] Y. Bai and C. B. Williams, "Binder jetting additive manufacturing with a particle-free metal ink as a binder precursor," *Mater. Des.*, vol. 147, no. 2017, pp. 146–156, 2018.

[212] Y. Bai and C. B. Williams, "The effect of inkjetted nanoparticles on metal part properties in binder jetting additive manufacturing," *Nanotechnology*, 2018.

[213] H. Zhao, C. Ye, S. Xiong, Z. Fan, and L. Zhao, "Fabricating an effective calcium zirconate layer over the calcia grains via binder-jet 3D-printing for improving the properties of calcia ceramic cores," *Addit. Manuf.*, vol. 32, no. June 2019, 2020.

# *Chapter 2: Experimental*

**Abstract**

In this chapter we present materials and methods details that are common to the several chapters of practical work. Porcelain powders production, powder materials and feedstocks characterization, such as Hausner Ratio, free settled density and morphology, and printed parts characterization such as relative density and variation of dimensions to virtual designs are common to several chapters and are here presented. The main characterization at the different stages of the process is schematically represented in Figure 2.1. The chapters will refer to this one for the methods here described in detail. However, specific materials, such as feedstock composition, or methods of the chapters are presented in the respective experimental chapter section.

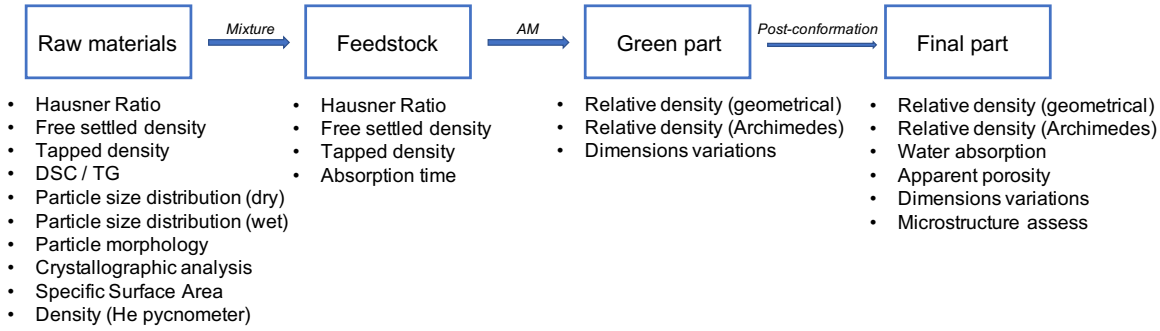


**Figure 2.1:** Characterization flowchart of the materials and the parts at the different stages of processing.

## 2.1. Materials

### *2.1.1. Porcelain powders production*

The powders used in this work, here after defined as porcelain powders, were produced by industrial spray drying using a ceramic suspension, with 50 % of kaolin and clay, 25 % of quartz and 25 % of feldspar in water medium. The spray drying was performed in a mixed flow spray dryer with 0,9 mm of hydraulic nozzles diameter, 10 bar of porcelain suspension feeding pressure and 147 Pa of the cyclone depression. The porcelain suspension was prepared with 1580 g/L of density and without the use of any additives.

Some of these powders were heat treated, in the industrial continuous furnace, with a maximum temperature of 1000 ºC, for 15 h 30 min, under oxidant atmosphere. Here after, the porcelain powders before the heat treatment will be designated as raw porcelain

powders and the ones after the heat treatment will be designated as heat-treated porcelain powders.

The industrial porcelain powders, both raw and heat-treated, were sieved at 80 µm in order to be used in BJP. For the case of porcelain powders for SLS, the powders were sieved at 150 µm.

### *2.1.2. Feedstock preparation*

The term feedstock used in this work refers to the mixture used in powder bed AM technologies, which comprises the porcelain powders mixed with the *in-bed* binders. In the case of BJP, the *in-bed* binders used are: Polyvinyl Alcohol $(C_2H_4O)_n$ (Zschimmer & Schwarz) here after designated as PVA, Maltodextrin $(C_6H_{10}O_5)_n$ (Fagron), here after designated as Malto, Sodium Alginate $(C_6H_7O_6Na)_n$ (PanReac AppliChem), here after designated as Algin, and Carboxymethylcellulose $(C_8H_{11}O_7Na)_n$ (Zschimmer & Schwarz), here after designated as CMC. Polyamide 12 (PA 650, Advanced Laser Materials, USA) was used as in-bed binder in the feedstock for SLS.

The feedstocks were prepared by dry rotational mixing for 24 h at 55 rpm. In the case of BJP, the feedstocks were prepared in 4 kg batches and for the case of SLS the feedstocks were prepared in 15 kg batches.

The feedstocks and the *in-bed* binders used are described in the materials and methods section of the respective chapter, once different feedstocks were prepared for the different subjects assessed in this thesis.

### *2.1.3. Rheological characterization*

Powders and feedstocks were characterized regarding their rheological behavior, focusing in Hausner Ratio (HR) gives information of the flowability and packing of powders [1], of utmost relevance for the printing process. HR, as per Eq. 2.1 [2], is determined by the ratio between tapped and free settled powder densities. Free settled density ($\rho_{free\ settled}$) was determined by measuring the free settled volume ($V_{free\ settled}$) of a known mass of powder ($m_{powder}$) in a graduated cylinder beaker (Eq. 2.2). After 250 taps, in a manual homemade

device, the volume of the compact powder ($V_{tapped}$) was measured and the tapped density ($\rho_{tapped}$) was calculated (Eq. 2.3).

$$HR = \frac{\rho_{tapped}}{\rho_{free\ settled}} \quad \text{(Eq. 2.1)}$$

$$\rho_{free\ settled} = \frac{m_{powder}}{V_{free\ settled}} \quad [g/cm^3] \quad \text{(Eq. 2.2)}$$

$$\rho_{tapped} = \frac{m_{powder}}{V_{tapped}} \quad [g/cm^3] \quad \text{(Eq. 2.3)}$$

To assess these properties, the process described in Figure 2.2 was performed in a self-made equipment. The first step is the free deposition of a known mass of powder, between 50 g and 80 g, Figure 2.2 (A), and the respective measurement of the free settled volume, Figure 2.2 (B). Then the powder is compacted (tapped), using the process shown in Figure 2.2 (C) for 250 taps (rotations). The tapped volume is then assessed, Figure 2.**2** (D), and the tapped density is calculated.

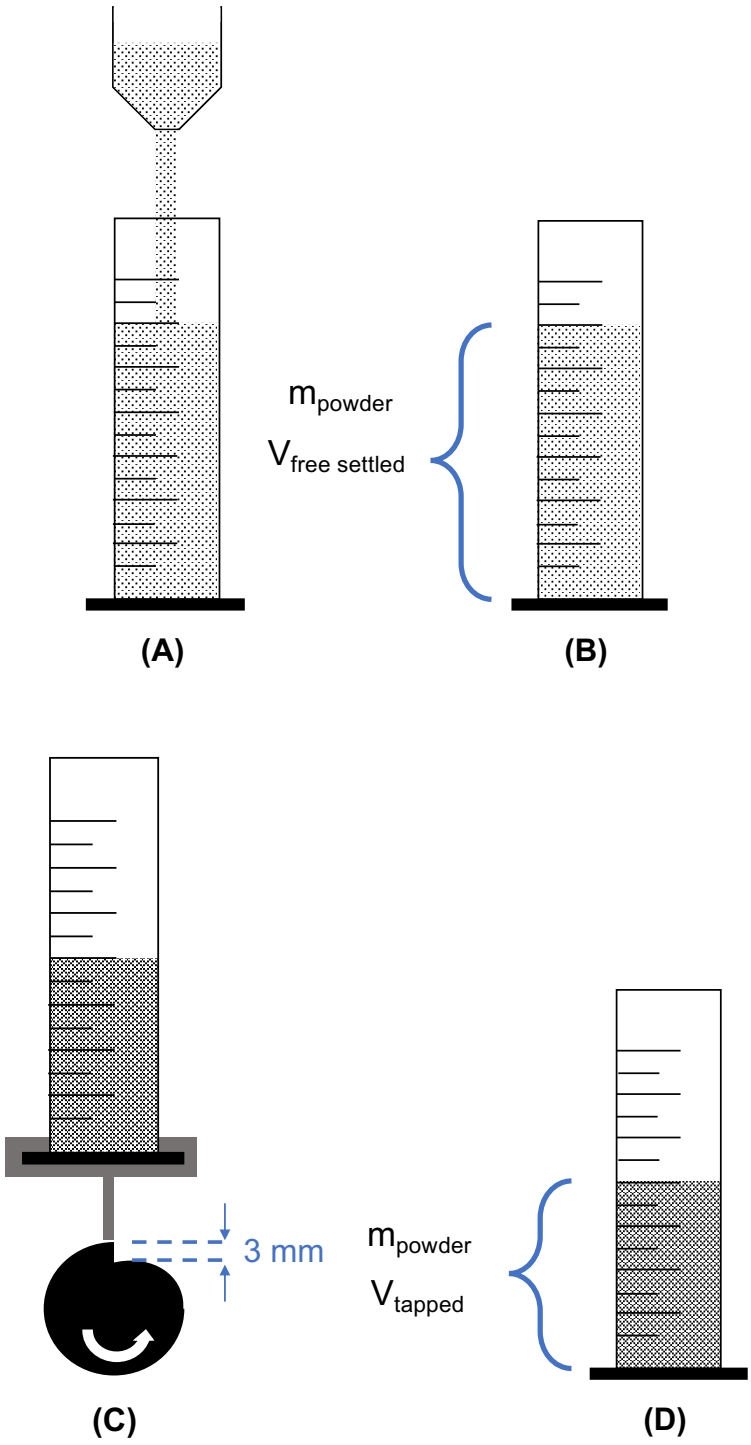


**Figure 2.2:** Steps to assess the free settled density and the Hausner Ratio of powders and feedstocks: (A) free deposition of powder, (B) assessment of free settled density, (C) 250 taps and (D) assessment of tapped density.

### 2.1.4. Morphological characterization

The particle size distribution of the dried porcelain and binders powders, was assessed in dry state, by Aero Mode Mastersizer 3000 (Malvern) using air pressure and obscuration values of 0,5 bar and 4 %, respectively. In the same analysis the Dv10, Dv50 and Dv90 were determined for each powder, representing respectively 10%, 50% and 90% of the powder amount (in vol.%) under the measured values in micrometers (μm).

The same equipment was used to measure the particle size distribution in water of the raw and heat-treated porcelain powders in the Chapter IV.

The morphology of the dried powders was assessed by Scanning Electron Microscopy (SEM) using a Hitachi S4100 microscope, at 25 keV. The samples for observation were prepared by free deposition of powders in a carbon tape, followed by coating the powders with carbon using a carbon evaporator.

### 2.1.5. Thermal characterization

The thermal behavior of the *in-bed* binders powders was analyzed by a Simultaneous Thermal Analyzer, STA 449F5 Jupiter (Netzsch) with a heating rate of 10 ºC/min, from room temperature up to 1000 ºC, under air atmosphere. The analysis comprise the thermogravimetric loss (TG) and the differential scanning calorimetry (DSC) and its derivatives.

In the case of the *in-bed* binder for SLS, polyamide 12, the DSC analysis was performed using a DSC-60 (Shimadzu) from 30 to 250 °C, with heating and cooling rates of 10 °C/min.

Raw and heat-treated porcelain powders were also characterized regarding its thermal behavior, using a STA 449F5 Jupiter (Netzsch) with a heating rate of 10 ºC/min, from room temperature up to 1200 ºC, under air atmosphere, and TG and DSC and their respective derivatives were obtained.

### 2.1.6. Physical characterization

For each *in-bed* binder powders for BJP, the density was measured by Helium Pycnometer analysis using a Quantachrome Multi Pycnometer (Anton Paar, Austria), using Helium as gas medium and a sample size between 2,2 g and 2,5 g of dry *in-bed* binders powders.

The specific surface area (SSA) of the porcelain powders, was assessed based on Brunauer, Emmet Teller (BET) isotherm method, using a Micromeritics Instrument Corp., with the software Gemini V2.0, at 10 relative pressure points. The gas used was $N_2$ at 100 °C.

### 2.1.7. Crystallographic characterization

The crystallographic phases of the porcelain powders were assessed using an XRD Panalytical - X'pert-PRO equipment, at room temperature, equipped with a copper target X-ray source. The wavelength of the radiation K$\alpha$1 is 1.54060 and of K$\alpha$2 is 1.54443 $A$. The scan range was from 2θ = 10.0021 ˚ until 2θ = 79,9681 ˚, with a step size of 0.0260 ˚, with a scanning step time of ~96.4 s.

### 2.1.8. Absorption time

A Kino Optical Contact Angle Meter & Interfacial Tensiometer SL200HT (USA Kino Industry Co., Ltd), combined with the software Drop Shape Analysis System, CAST® 3.0, was used to assess the time absorption of the liquid binder by the 0HT and 100HT feedstock formulations for BJP, by recording the absorption of the drops with a high resolution video camera. A schematic representation of the system is shown in Figure 2.3. The liquid used was the commercial liquid binder VisiJet PXL Clear (3D Systems), with 2 µL drops. The feedstock formulations were freely deposited in a Petri dish and a ruler was used to remove the excess of powder and turn the surface of the feedstock flat, to mimic the powder bed surface during the BJP process.

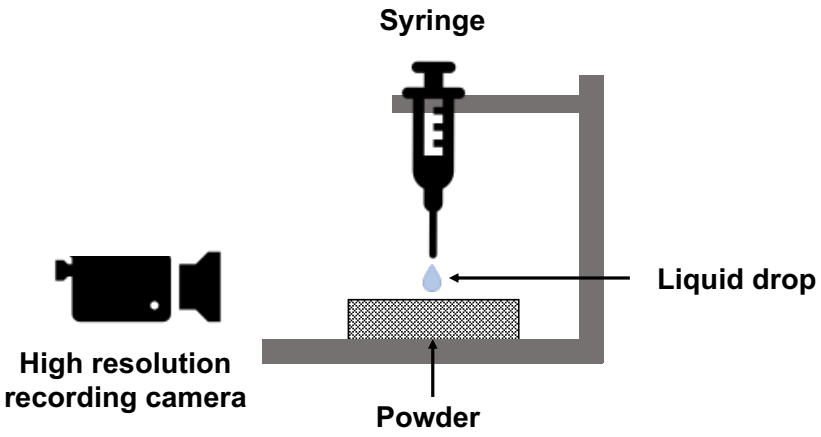


**Figure 2.3:** Scheme of the setup to assess the absorption time of the liquid binder by the powder formulation.

## 2.2. Additive manufacturing process

### *2.2.1. Binder Jet Printing*

The printing tests were performed in a ZPrinter 650 (ZCorporation, USA). The prints were done using a layer thickness of 0,1 mm and binder saturation of 180%, programmed using the 3DPrint Software, version 1.03.8 (3D Systems, USA). The liquid binder used during the printing was the commercial binder VisiJet PXL Clear (3D Systems, USA). In the case of Chapter VI, different set of layer thickness and binder saturation were used and are presented in the Materials and Methods section of the chapter.

The layer thickness corresponds to the height of each layer used in the process and the binder saturation corresponds to the ratio of the liquid binder volume deposited and the volume of void space between the powder particles in the powder bed [3]. As discussed in Chapter 1 (Figure 1.15), the printed parts are divided in two sections: core and shell. The core correspond to the inner section of the printed part and the shell corresponds to the outer section of the printed parts in the three directions (x, y and z). The shell thickness used for all the printed parts is 2 mm and the binder saturation of 180 % corresponds to 0,21 in the core section and 0,43 in the shell section of the part.

### 2.2.2. Selective Laser Sintering

Green parts were produced by indirect SLS using a Sinterstation HiQ+HiS (3D Systems), equipped with a $CO_2$ laser. The feed beds were heated at 140 °C and the part bed was heated at 170 °C. The layer thickness, laser power and hatching space were kept constant for all tests at 100 µm, 32 W and 300 µm, respectively.

The virtual designs of the printed parts and the post-conformation steps of the printed parts, such as industrial sintering, are described in the Materials and Methods section of each chapter.

## 2.3. Part characterization

### 2.3.1. Dimension variation

Cylinders were produced in the different chapters to control the dimension variations to the virtual design ones (diameter and length) of the green and sintered parts. A caliper was used to measure the diameter and the length of the parts. 10 measurements were taken for each sample. The diameter variation was calculated using Eq. 2.4 and for the length variation Eq. 2.5 was used.

$$\Delta D = \frac{D_f - D_i}{D_i} \times 100 \qquad [\%] \qquad \text{(Eq. 2.4)}$$

$$\Delta L = \frac{L_f - L_i}{L_i} \times 100 \qquad [\%] \qquad \text{(Eq. 2.5)}$$

where $\Delta D$ and $\Delta L$ are the diameter variation and the length variation, $D_f$ and $L_f$ are the diameter and the length of the part and $D_i$ and $L_i$ are the diameter and the length of the virtual design.

### 2.3.2. Physical characterization

The geometric density, $\rho_{geom}$, of the green and sintered parts was calculated using Eq. 2.6,

$$\rho_{geom} = \frac{m}{\pi \times r^2 \times l} \quad [g/cm^3] \quad \text{(Eq. 2.6)}$$

where $m$ is the mass of the part in the dry state and $r$ and $l$ are the radius and the length of the cylinder, respectively.

The relative geometric density ($\%\rho_{geom}$) of the green printed cylinders was calculated using Eq. 2.7 and for the sintered parts the Eq. 2.8 was used,

$$\%\rho_{geom} = \frac{\rho_{geom}}{\rho_c} \times 100 \quad [\%] \quad \text{(Eq. 2.7)}$$

$$\%\rho_{geom} = \frac{\rho_{geom}}{\rho_p} \times 100 \quad [\%] \quad \text{(Eq. 2.8)}$$

where $\rho_{geom}$ is the geometric density, $\rho_p$ is the reference density of Costa Verde porcelain (2,44 g/cm$^3$) and $\rho_c$ is the reference density of the composite feedstock powders with the different types and contents of *in-bed* binders, calculated using the Rule of Mixtures [5], defined by the Eq. 2.9,

$$\rho_c = \rho_p V_p + \rho_b V_b \quad \text{(Eq. 2.9)}$$

where $\rho_p$ and $V_p$ are the density and the volume of the porcelain fraction, respectively, and $\rho_b$ and $V_b$ are the density and the volume of the *in-bed* binder fraction. In each chapter the reference density of the different feedstocks is presented.

The sintered parts were characterized regarding their density, $\rho_{Arc}$, (Eq. 2.10), water absorption, WA, (Eq. 2.11), and apparent porosity, AP, (Eq. 2.12), by Archimedes method according with ASTM C373-14a [5], using an AND GR200 analytical balance with AD-1653 Archimedes setup (A&D Company) and the following equations. The parts weighted in dry state, $m_{dry}$, were then soaked with water after 5 h in boiling water and 24 h in cold water,

using a wet paper towel to remove the excess of water on the surface of the sample, and weighted, $m_{soak}$, and the weight immersed in water, $m_{imp}$, at room temperature (25 °C). The liquid medium used for Archimedes method was water ($\rho_0$ = 1,001 g/cm$^3$).

$$\rho_{Arc} = \frac{m_{dry}}{m_{soak} - m_{imp}} \times \rho_0 \qquad [g/cm^3] \qquad \text{(Eq. 2.10)}$$

$$WA = \frac{m_{soak} - m_{dry}}{m_{dry}} \times 100 \qquad [\%] \qquad \text{(Eq. 2.11)}$$

$$AP = \frac{m_{soak} - m_{dry}}{m_{soak} - m_{imp}} \times 100 \qquad [\%] \qquad \text{(Eq. 2.12)}$$

The relative density assessed by Archimedes method, $\%\rho_{Arc}$, was calculated using Eq. 2.13,

$$\%\rho_{Arc} = \frac{\rho_{Arc}}{\rho_p} \times 100 \qquad [\%] \qquad \text{(Eq. 2.13)}$$

where $\rho_{Arc}$ is the density measured by Archimedes density and $\rho_p$ is the reference density of porcelain (2,44 g/cm$^3$) from *Porcelanas da Costa Verde*.

### *2.3.3. Microstructural characterization*

The microstructure of the sintered parts was assessed by Scanning Electron Microscopy (SEM) using a Hitachi S4100 microscope, at 25 keV. The parts for observation were broken and polished using SiC grind paper, followed by polishing using diamond paste. The samples were glue to the sample holder using carbon cement and the surface was coated with carbon using a carbon evaporator. In addition, the fresh fracture zone, before the polishing was also observed.

## 2.4. Standard deviation

The standard deviation, $\sigma$, was calculate, Eq. 2.14, and the standard error, $\sigma_{\bar{x}}$ , Eq. 2.15, was assessed for the different measurements, using a sample size, $n$, of 10, where $\bar{x}$ is the mean of the measurements.

$$\sigma = \sqrt{\frac{\sum_{i=1}^{n}(x_i - \bar{x})^2}{(n-1)}} \quad \text{(Eq. 2.14)}$$

$$\sigma_{\bar{x}} = \frac{\sigma}{\sqrt{n}} \quad \text{(Eq. 2.15)}$$

## 2.5. References


[1] H. H. Hausner, “Friction conditions in a mass of metal powder,” *Int. J. Powder Metall.*, vol. 3, pp. 7–13, 1967.

[2] R. O. Grey and J. K. Beddow, “On the Hausner Ratio and its relationship to some properties of metal powders,” *Powder Technol.*, vol. 2, no. 6, pp. 323–326, 1969.

[3] H. Miyanaji, M. Orth, J. M. Akbar, and L. Yang, “Process development for green part printing using binder jetting additive manufacturing,” *Front. Mech. Eng.*, vol. 13, no. 4, pp. 504–512, 2018.

[4] M. Alger, *Polymer science dictionary*, 3rd Edition, vol. 38, no. 3. Springer, 2003.

[5] ASTM International, “C373-14a - Standard Test Method for Water Absorption, Bulk Density, Apparent Porosity, and Apparent Specific Gravity of Fired Whiteware Products, Ceramic Tiles, and Glass Tiles.” ASTM International, USA, 2014.

# *Chapter 3: The role of in-bed binders in the printability of porcelain powders feedstock in Binder Jet Printing*

**Abstract**

The additive manufacturing of ceramic powders by binder jet printing requires the use of a liquid binder and, in some cases, *in-bed* binders in the feedstock, to guarantee the needed mechanical strength for the next processing steps. Although known for technical ceramics, much remains to be understood for industrial porcelain powders. In this work a systematic study of different *in-bed* binders is used to elucidate its role in binder jet printing of industrial porcelain powders. Differences are demonstrated between polyvinyl alcohol (PVA), carboxymethylcellulose (CMC), Sodium alginate and Maltodextrin. PVA is a suitable and industrial viable *in-bed* binder for the production of porcelain parts by binder jet printing, allowing to produce near defect free porcelain parts after industrial sintering. CMC due to its fiber-type particles jeopardizes the printing process. The thermal degradation behavior of sodium alginate leads to the fracture of the printed porcelain parts during the sintering. Maltodextrin allows to produce printed parts without major defects both as green and sintered parts, although its price might be a relevant limitation from an industrial point of view. This work adds understanding on additive manufacturing of ceramics and demonstrates the potential to industrialize the binder jet printing of porcelain powders.

**Keywords**: Binders, *In-bed* Binders, Binder Jet Printing, Additive Manufacturing, Porcelain, Industrialization

## 3.1. Introduction

As discussed in Chapter 1, the use of *in-bed* binders is required for a successful BJP process of ceramics and a list of liquid and *in-bed* binders was presented in Table 1.IV. The most common *in-bed* binders used in BJP of ceramics are water-based and can be thermally removed.

A fundamental understanding of the *in-bed* binders role for industrial production of porcelain parts by BJP and its effect on the printability of the feedstocks with industrial porcelain powders and properties of the final parts is not known and is critical to this disruptive technology and its industrialization.

In the present chapter we systematically study different organic, water-soluble and thermally removed *in-bed* powder binders for the production of porcelain parts by BJP and its effect on the printability of the feedstocks and properties of the final parts. The *in-bed* binders

chosen for this study are polyvinyl alcohol (PVA), carboxymethylcellulose (CMC), Sodium alginate and Maltodextrin. This selection choice is also related, among other factors above mentioned, to the fact that some of these binders are already utilized in different steps of conventional production of porcelain.

## 3.2. Materials and methods

Spray dried industrial porcelain powders were produced and provided by *Porcelanas da Costa Verde, Portugal* using the conditions described in Chapter 2. In this chapter industrial raw porcelain powders were used and the *in-bed* binders used were PVA, maltodextrin, sodium alginate and CMC, as presented in Chapter 2.

The feedstocks of porcelain and *in-bed* binder powders were prepared as described in Chapter 2 and its composition is presented in Table 3.I.

**Table 3.I:** Feedstock formulation of industrial porcelain and *in-bed* binder powders for binder jet printing, with *in-bed* binder and porcelain weight content specifications.

| **Feedstock designation** | **Porcelain wt.%** | ***In-bed* binder wt.%** | | | |
|---|---|---|---|---|---|
| | | **PVA** $(C_2H_4O)_n$ | **Maltodextrin** $(C_6H_{10}O_5)_n$ | **Sodium Alginate** $(C_6H_7O_6Na)_n$ | **CMC** $(C_8H_{11}O_7Na)_n$ |
| PP-5PVA | 95,0 | 5 | | | |
| PP-5Malto | | | 5 | | |
| PP-5Algin | | | | 5 | |
| PP-5CMC | | | | | 5 |
| PP-7PVA | 92,5 | 7,5 | | | |
| PP-10PVA | 90,0 | 10,0 | | | |
| PP-12PVA | 87,5 | 12,5 | | | |
| PP-15PVA | 85,0 | 15,0 | | | |
| PP-17PVA | 82,5 | 17,5 | | | |
| PP-20PVA | 80,0 | 20,0 | | | |

The individual materials and the feedstocks were characterized regarding its particle size distribution, Hausner Ratio, free settled density and tapped density. The thermal behavior of the *in-bed* binders was analyzed by STA. The analysis conditions are presented in Chapter 2.

Printing was performed in a ZPrinter 650 (ZCorp) as described in Chapter 2, and cylindrical parts (Figure 3.1 A) were produced to evaluate the density and shrinkage of the green and sintered printed parts. To assess printability and to evaluate designs limitation, rectangular parts with different thicknesses of walls (Figure 3.1 B) and parts with overhangs with different angles (Figure 3.1 C) were also printed and processed. The diameter variation ($\Delta D$), the geometric density ($\rho_{geom}$) and relative geometric density ($\%\rho_{geom}$) were assessed using the procedure described in chapter 2.

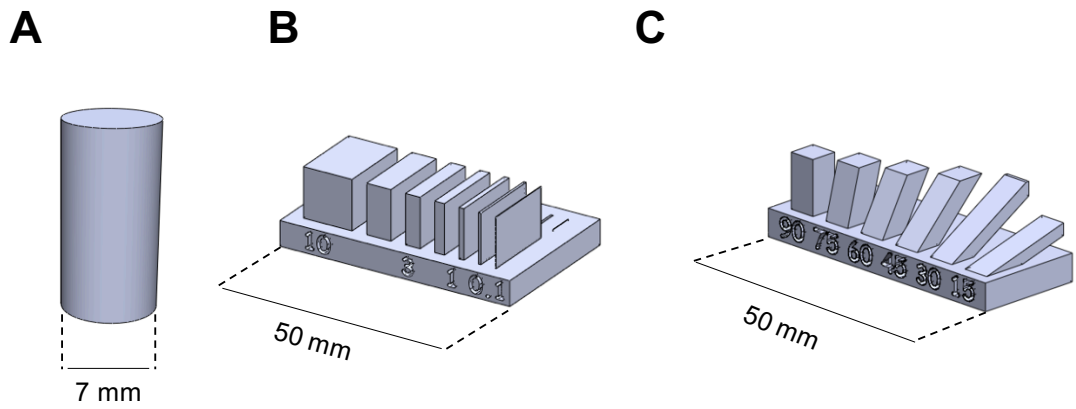


**Figure 3.1:** Schematic representation of the virtual design of the (A) cylinders and the parts to be printed with: (B) different wall thicknesses: 10 , 5 , 3 , 2 , 1 , 0,5 and 0,1 mm (from left to right, respectively) and (C) different overhang angles: 90 °, 75 °, 60 °, 45 °, 30 ° and 15 ° (from left to right, respectively).

The printed parts were sintered in an industrial continuous kiln of Costa Verde, Portugal, using a maximum temperature of 1345 ºC, measured with process temperature control rings, PTCR-STH (Ferro Corporation), for a total time cycle of 5 h 30 min. The sintered cylinders were characterized regarding its geometrical relative density ($\%\rho_{geom}$), water absorption (WA), apparent porosity (AP) and relative density using the Archimedes method ($\%\rho_{Arc}$), using the procedure described in Chapter 2. The microstructure of the printed parts was analyzed by SEM as described in Chapter 2, as well.

For the calculation of the green part reference density ($\rho_c$), the density of porcelain powders designated as $\rho_p$ is 2,44 g/cm$^3$, and for each *in-bed* binder powders the density was measured by helium pycnometer, as presented in Chapter 2. The calculations and values used are presented in Table 3.II.

**Table 3.II:** Reference density for the powder feedstocks for each *in-bed* binder and porcelain composition and calculated according Eq. 2.9.

| Feedstock | Reference density $\rho_c$ (g/cm$^3$) | Porcelain density $\rho_p$ (g/cm$^3$) | Porcelain volume fraction $V_p$ | *In-bed* binder density $\rho_b$ (g/cm$^3$) | *In-bed* binder volume fraction $V_b$ |
|---|---|---|---|---|---|
| PP-5PVA | 2,32 | 2,44 | 0,905 | 1,22 ± 0,02 | 0,095 |
| PP-5Malto | 2,31 | | 0,903 | 1,19 ± 0,01 | 0,097 |
| PP-5Algin | 2,37 | | 0,927 | 1,62 ± 0,01 | 0,073 |
| PP-5CMC | 2,37 | | 0,926 | 1,60 ± 0,02 | 0,074 |
| PP-7PVA | 2,27 | | 0,860 | 1,22 ± 0,02 | 0,140 |
| PP-10PVA | 2,22 | | 0,821 | | 0,179 |
| PP-12PVA | 2,17 | | 0,782 | | 0,218 |
| PP-15PVA | 2,13 | | 0,745 | | 0,255 |
| PP-17PVA | 2,09 | | 0,710 | | 0,290 |
| PP-20PVA | 2,04 | | 0,676 | | 0,324 |

## 3.3. Results and discussion

To understand *in-bed* binders role and printability of porcelain in binder jet printing, the porcelain and *in-bed* binder powders were systematically characterized.

The porcelain powders sieved at 80 µm are composed of both irregular and spherical shaped particles (Figure 3.2, A) and their particle size distribution is bimodal with a major peak at 48 µm, with a shoulder in the fine side of the PSD and a smaller peak at 2 µm (Figure 3.2, B), with Dv10, Dv50 and Dv90 values of 10 µm, 38 µm and 74 µm, respectively. These powders exhibit a HR of 1,40 ± 0,02 and a free settled density of 0,90 ± 0,01 g/cm$^3$.

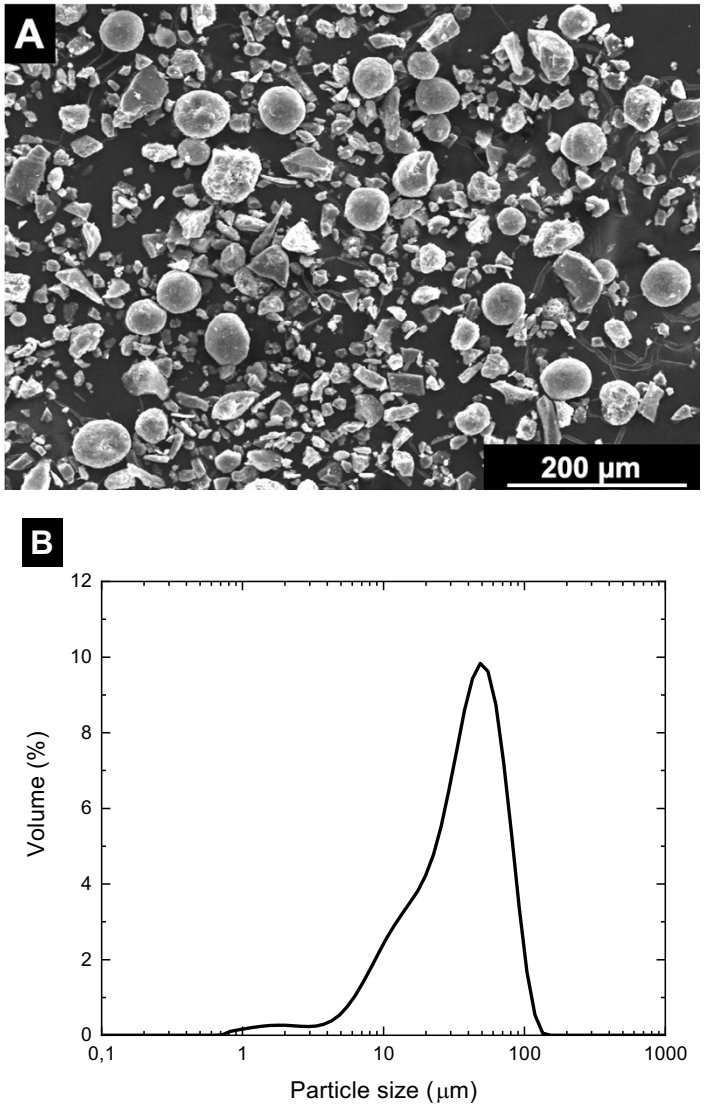


**Figure 3.2:** Morphology of porcelain powders: (A) SEM micrograph of porcelain particles sieved at 80 µm, composed of both irregular and spherical shaped particles, and (B) Particle size distribution of porcelain powders, as bimodal distribution with a major peak at 48 µm.

In terms of dry particle size distribution (PSD) the *in-bed* binders powders used in this work present mainly monomodal similar distributions (Figure 3.3), with peaks between 40 and 65 µm and the respective Dv10, Dv50 and Dv90 values presented in Table 3.III. The narrower PSD curve is exhibited by PVA and Maltodextrin has the wider one. The curve of PVA peaks at 62 µm, with Dv50 and Dv90 values of 51 and 94 µm, respectively. The curves of Algin and CMC peak both at 55 µm, but they are broader than the one of PVA, with an increase in the finer particles for the case of Algin, as a Dv50 of 43 µm suggests, and an increase in the coarser particles for CMC, with a Dv90 value of 124 µm. On the other hand,

Maltodextrin exhibits a broader monomodal PSD that peaks at 48 µm, with a shoulder type on the side of the finer particles and values of Dv50 and Dv90 of 31 and 84 µm, respectively. The curves of Malto, Algin and CMC seem to present a second peak in the range 0,3 – 0,8 µm, however the vol.% of these particles is < 0,1 % through this range, which may be considered a continuous vol.% of particles < 1 µm.

Comparing with the PSD of porcelain powders (Figure 3.2, B), PVA, Algin and CMC present values of Dv10, Dv50 and Dv90 higher than the ones for porcelain, while the maltodextrin powders have Dv10 and Dv50 smaller which may lead to a better packing of the powders due to possible better filling of space between porcelain particles by maltodextrin ones, when compared with PVA, sodium alginate and CMC powders.

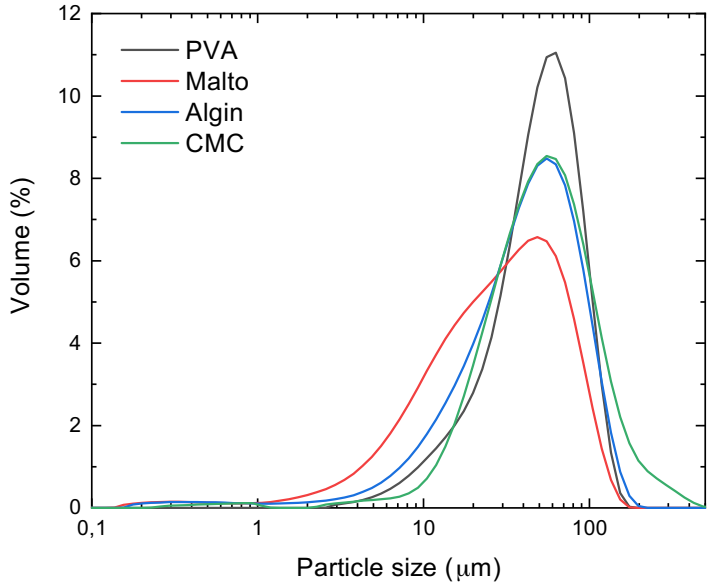


**Figure 3.3:** Particle size distribution of dry powders of PVA, Malto, Algin and CMC powders after sieving at 80 µm. The in-bed binders present mainly monomodal distributions with peaks between 40 and 65 µm.

**Table 3.III:** Dv10, Dv50 and Dv90 values from the particle size distribution curves of PVA, Maltodextrin, Sodium Alginate and CMC powders, measured in dry state.

| | PVA | Malto | Algin | CMC |
|---|---|---|---|---|
| Dv10 (μm) | 18 | 7 | 12 | 19 |
| Dv50 (μm) | 51 | 31 | 43 | 52 |
| Dv90 (μm) | 94 | 84 | 95 | 124 |

In terms of particle morphology (Figure 3.4) PVA, maltodextrin and Algin have irregular shaped particles, while CMC has both irregular shaped and fiber type shaped particles. To aid the discussion, we provide illustrations of these types of particles with different aspect ratio, with indication of the minimum dimension, $D_{min}$, and maximum dimension, $D_{max}$, in Figure 3.4 E and F.

Although the dry sieving of the *in-bed* binder and porcelain powders is performed at 80 μm, some particles larger than 80 μm still pass through the mesh of the sieve. Here we advocate that these observations are related with the irregular morphology of the powders; if the equivalent minimum dimension ($D_{min}$) of these irregular particles is lower than the mesh aperture of the sieve (< 80 μm), the particles can align along with $D_{min}$ and pass through the sieve, even though they have one dimension ($D_{max}$) bigger than the sieve mesh (Figure 3.4 E and F). These evidences are maximized for the fiber type particles of CMC, leading to a PSD with the highest Dv90 of 124 μm and minimized for the porcelain powders that revealed a more nuanced effect. Another contribution for this error may be related with the dry PSD analysis, where some agglomeration of the *in-bed* binder powders can occur during measuring, however the agglomeration is not noticeable in SEM micrographs (Figure 3.4) furthermore, its contribution may be residual. Even though this effect can be attribute to the dry sieving of the powders, the wet sieving and analysis is not possible because the *in-bed* binders are soluble in water and the porcelain powders processing in water leads to deagglomeration of powders.

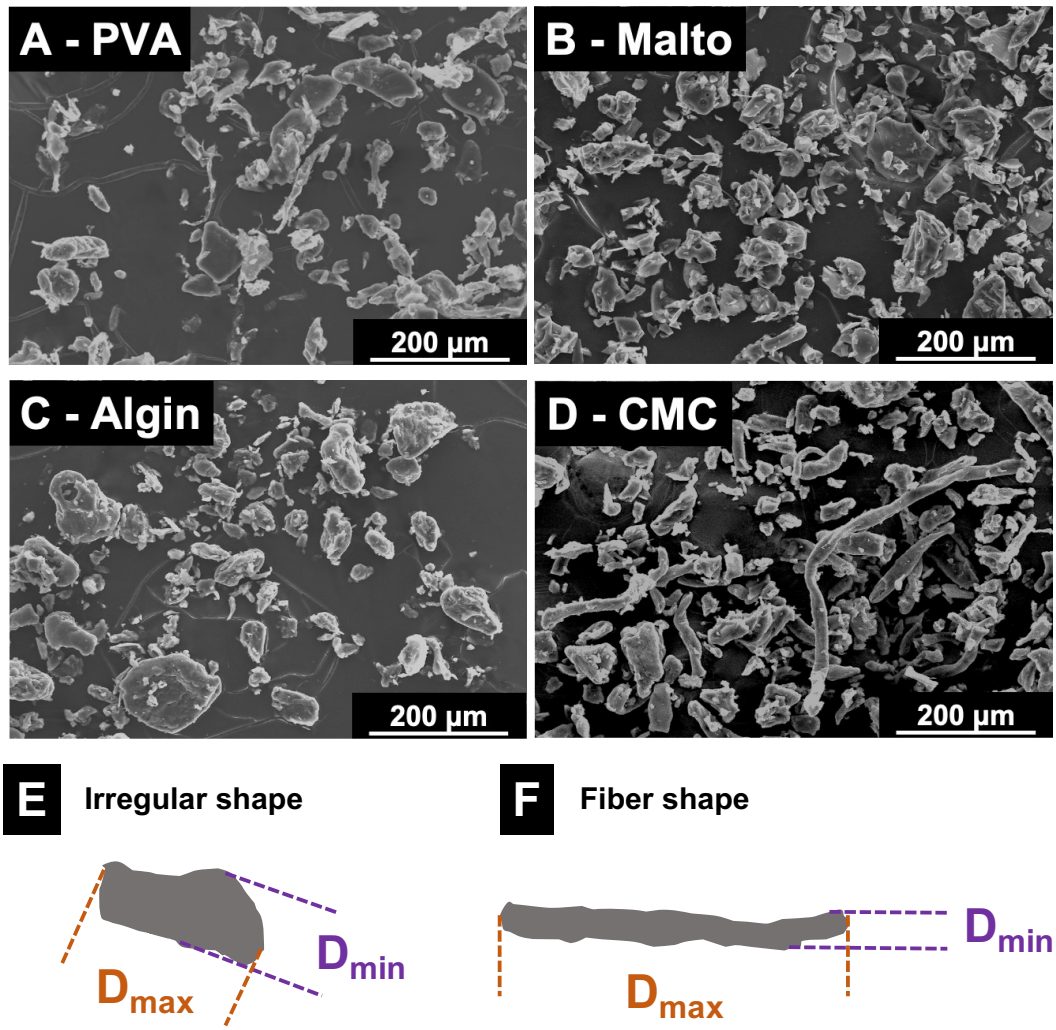


**Figure 3.4:** SEM micrographs of the in-bed binders used in this work: (A) PVA, (B) Malto, (C) Algin and (D) CMC powders, after sieving (< 80 µm), highlighting the irregular shaped particles of PVA, Maltodextrin and Algin, and the mixture of irregular and fiber type shaped particles of CMC. Schematic representation of (E) irregular and (F) fiber shaped particles of the in-bed binders used in this work. $D_{max}$ represents the maximum dimension and $D_{min}$ represents the minimum dimension of both particles.

As mentioned above, the use of *in-bed* binders requires their removal prior to the final densification what may lead to open porosity which jeopardizes the mechanical resistance of the printed parts. Knowing their burning behavior is hence fundamental. Figure 3.5 presents the thermogravimetry analysis of each *in-bed* binder for a thermal cycle up to 1000 °C, at a heating rate of 10 °C/min, under atmospheric air. The thermogravimetric

weight loss (TG) and its derivative (DTG), also known as burning rate, are presented as a function of temperature, in which the nuanced alterations of the TG curve are highlighted.

CMC TG curve is characterized by a major mass loss of 36 wt.% between 270 and 300 °C, with a maximum burning rate of 57 %/min at 290 °C. On further temperature increasing, a second mass loss of 3 wt.% with a peak at 657 °C, at a burning rate of 9 %/min, appeared. At 1000 °C, the total mass loss of CMC is 87 wt.%. Algin presents the first major mass loss of 30 wt.% between 230 and 260 °C, with a maximum burning rate of 22 %/min at 245 °C, followed by other mass loss of 15 wt.% between 340 and 355 °C, with a maximum burning rate of 85 %/min at 346 °C. On further increasing of temperature two other mass loss of 1 wt.% at 535 and 570 °C appear, both with a burning rate of 8 %/min. At 1000 °C, the total mass loss of sodium alginate is 87 wt.%. Malto presents a major mass loss of 50 wt.% between 290 and 330 °C, with a maximum burning rate of 20 %/min, followed by a continuous elimination of 35 wt.% until 560 °C, which is the temperature that maltodextrin is completely eliminated. In what concerns PVA, the thermogravimetry presents a continuous elimination of 85 wt.% between 300 and 520 °C, with a maximum burning rate of 10 %/min between 300 and 320 °C, being completely eliminated at 520 °C.

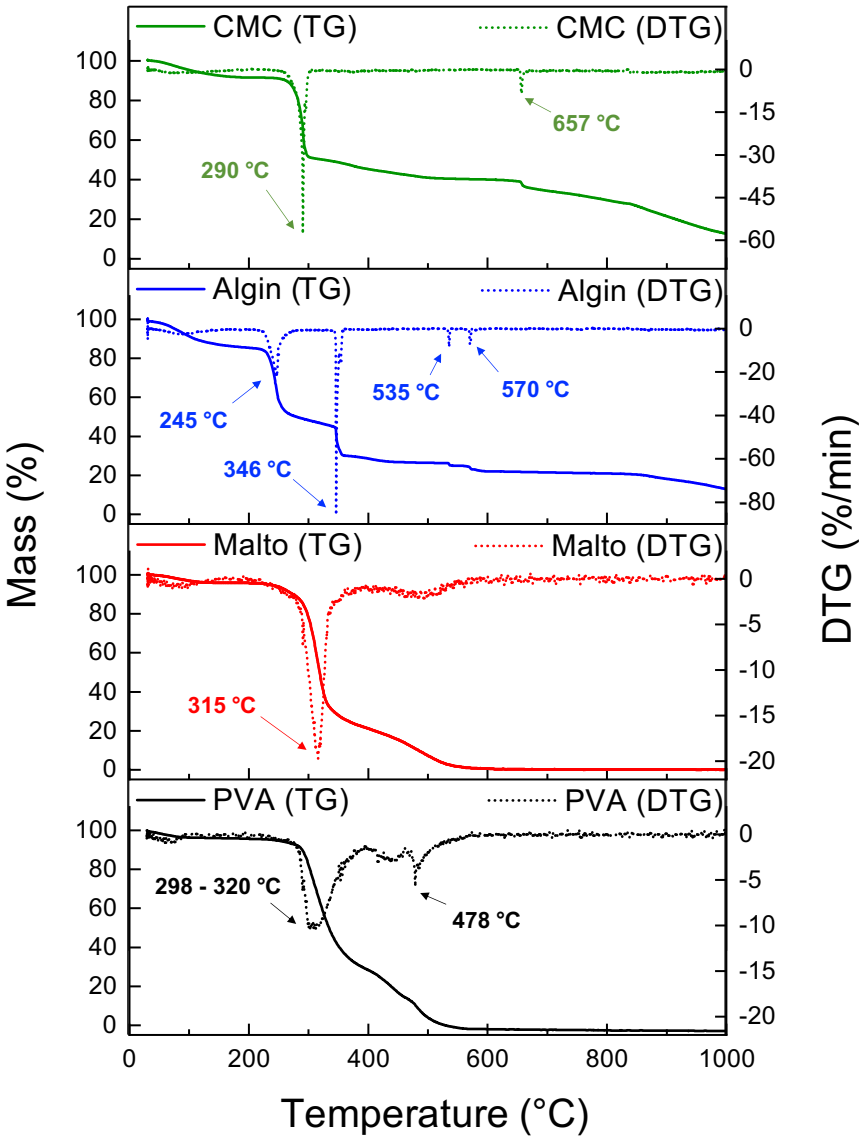


**Figure 3.5:** Thermogravimetry analysis of each in-bed binder. Thermogravimetric weight loss (TG) and its derivate (DTG) of PVA, Malto, Algin and CMC as a function of temperature. The temperatures of DTG peaks are identified for each in-bed binder.

If we compare the TG behavior of all the *in-bed* binders, as represented in Figure 3.6 A, although all the major loss weight occurs between 200 and 600 °C, PVA (at 520 °C) and maltodextrin (at 560 °C) are completely eliminated before reaching 600 °C, while both sodium alginate and CMC still have a mass fraction around 13 wt.% at 1000 °C. In addition, the burning process of sodium alginate and CMC occurs abruptly with accelerated kinetics, with 85 %/min at 346 °C and 59 %/min at 290 °C burning rates, respectively, as presented in Figure 3.6 B.

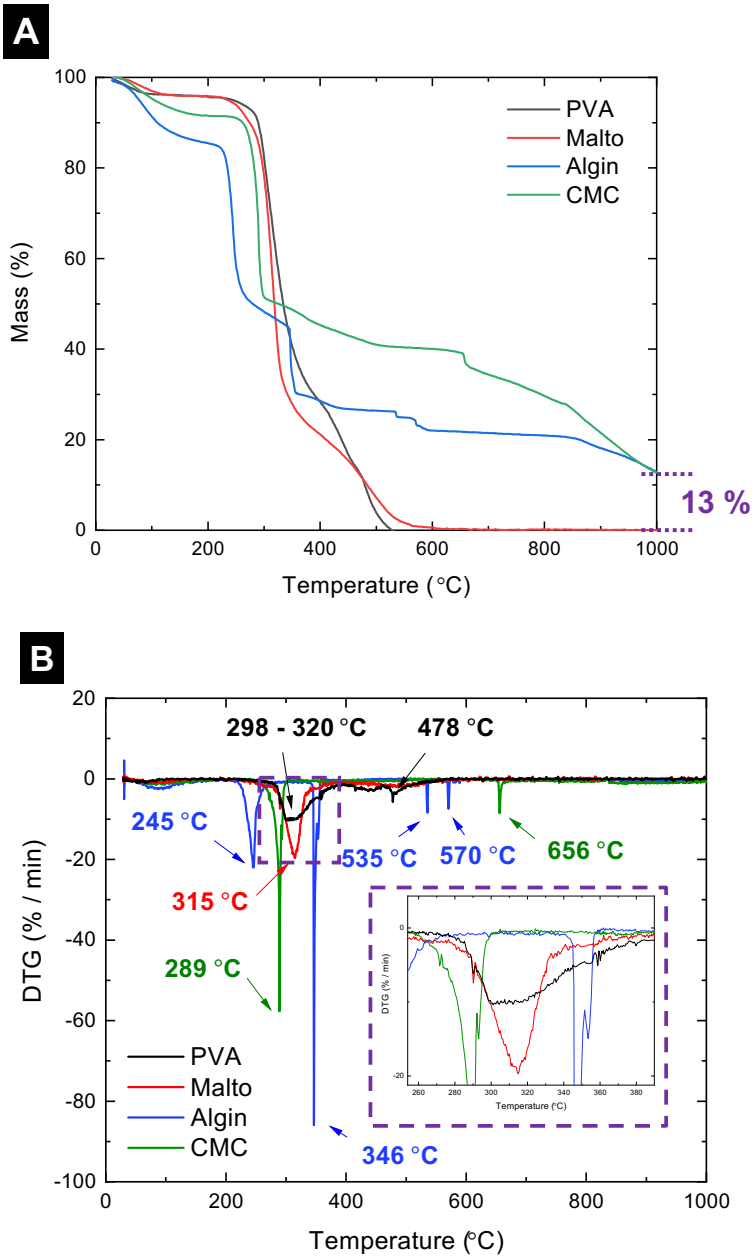


**Figure 3.6:** Comparison of the thermogravimetric behavior of the in-bed binders in air atmosphere up to 1000 °C, with a heating rate of 10 °C/min. (A) Weight loss and (B) burning rate, i.e. the derivative of the thermogravimetric curve. At 1000 °C, Algin and CMC present an incomplete mass loss, with 13 wt.% remaining, presenting also the highest burning rates.

These studies were further corroborated and complemented by differential scanning calorimetry (DSC) analysis of each *in-bed* binder (Figure 3.7). CMC presents initially two

exothermic peaks related with the onset of the thermal decomposition of CMC [1][2]; the first one identified as (1) in Figure 3.7, peaks at 293 °C, and corresponds to the peak at 290 °C, observed in the DTG curve (Figure 3.5), followed by a small one at 373 °C, identified as (2) (Figure 3.7). A third exothermic peak appears at 656 °C, identified as (3), which corresponds to the peak at 657 °C (Figure 3.5) and is related with the second stage of its thermal decomposition [2]. As per sodium alginate four peaks are clearly visible in the DSC chart up to 600 °C. The two first exothermic peaks, identified as (4) and (5) in Figure 3**.7**, occur at 249 °C and 356 °C, respectively and correspond to the two major peaks registered in the DTG curve (Figure 3.5), at 245 °C and 346 °C respectively, and are related with the thermal decomposition of sodium alginate. The two other exothermic peaks found at 548 °C and 575 °C (identified as 6 and 7 in Figure 3.7) are related with $Na_2CO_3$ formation, as previously reported [3], and are associated with the peaks at 535 °C and 570 °C in the DTG curve. Maltodextrin presents an exothermic broaden peak that extends in the temperature range from 300 to 600 °C (identified as 8), related to its thermal decomposition and matches with the broader DTG peak previously registered (Figure 3.5). While PVA presents a major exothermic peak starting at a temperature around 350 °C, reaching a maximum at 485 °C (identified as 9 in Figure 3.7), corresponding to the two step thermal degradation of PVA [4]. The typical endothermic peaks of organic compounds as glass transition temperature (Tg) and melting temperature (Tm) were not identified due to the smaller intensity of the peaks comparing with the exothermic ones. In this sense, a sensitive DSC equipment in low temperatures should be used in further studies to find these temperatures.

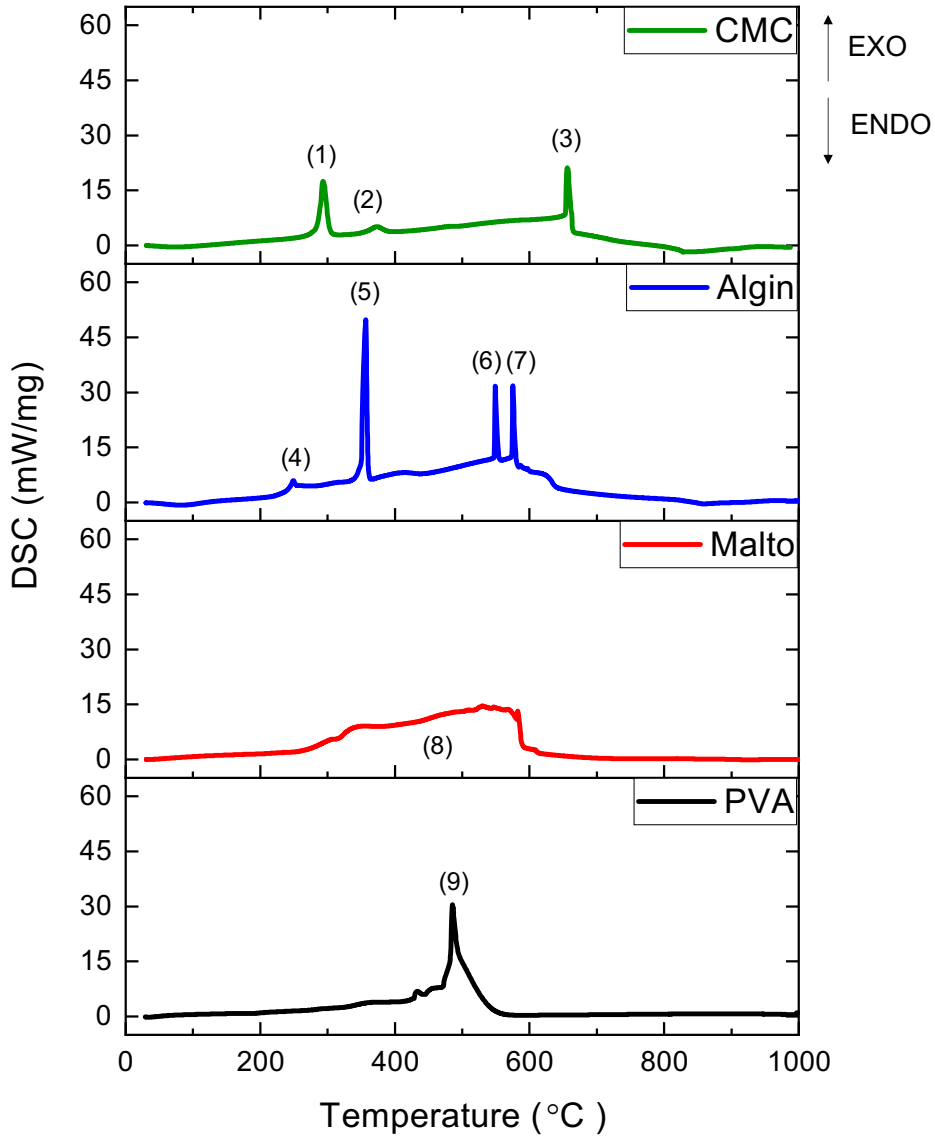


**Figure 3.7:** DSC analysis of PVA, maltodextrin, Sodium Alginate and CMC binders, with identification of points of interest.

The examination of the thermal behavior of the *in-bed* binders of this study have highlighted the main thermal differences among them. CMC and sodium alginate are not fully decomposed at 1000 °C with a mass fraction of 13 wt.%, in the case of Algin related with the incomplete decomposition of $Na_2CO_3$ [5]. Also, the kinetics of the low temperature decomposition is abrupt and at lower temperatures when compared with PVA and maltodextrin, which present lower rates of decomposition and are completely decomposed before the cycle reaches 600 °C. Indeed, from the industrial point of view and related with the sintering cycle of porcelain it is of the utmost importance the additives to be fully

decomposed before the final densification step and not abruptly, in order to avoid internal mechanical fragilities that may lead to the cracking of parts at a further stage of the processing. Under this perspective PVA and maltodextrin are good *in-bed* binder choices for the binder jet printing of porcelain powders.

The other relevant aspect for a successful binder jet printing is related with the powder bed which implies the knowledge about the rheology of powder materials (*in-bed* binder and industrial porcelain) and feedstocks. HR, determined by the ratio between tapped and free settled powder densities, is an adequate tool to characterize powder flowability and packing behavior. To further explore the *in-bed* binders behavior and their implications for porcelain binder jet printing, the rheology of the materials (Table 3.IV) and feedstocks (Table 3.V) was assessed.

The bulk density of the *in-bed* binders powders was assessed by He pycnometer analysis and PVA and Malto present lower values (1,22 and 1,19 g/cm$^3$, respectively) than Algin and CMC (1,62 and 1,60 g/cm$^3$, respectively). In terms of free settled density, the same trend was observed, with similar values between PVA and maltodextrin with 0,39 and 0,40 g/cm$^3$, respectively, and comparable densities between sodium alginate and CMC with 0,47 and 0,48 g/cm$^3$, respectively. The free settled density of each material depends will depend on the particle morphology, PSD and density of the material. Considering the particle shape of particles, CMC powders should have presented the lowest free settled density among the *in-bed* binders studied, once its particles shape is composed by both irregular and fiber type particles, as presented in Figure 3.4 D, which typically leads to more void space between particles, and as consequence, should decrease the packing density. However, this was not observed, and CMC presents the highest value of free settled density. On the other hand, the broader PSD curve of Malto (Figure 3.3) was expected to lead to the highest free settled density, once the fine particles will fill the void space between the coarse ones and promoting higher packing and free settled density than the *in-bed* binders with narrower PSD, but his was not observed as well and maltodextrin one of the lowest free settled density. In this sense, considering the *in-bed* binder characteristics studied in this work, the bulk density has the highest impact in the free settled density of the *in-bed* binder powders, once the ones with the highest free settled density, Algin and CMC, have also the highest bulk density (~1,60 g/cm$^3$), while PVA and Malto, which present the lowest and similar free settled density, have also similar values of bulk density (~1,20 g/cm$^3$). Other properties such

as surface energy, functionalization, among others, may also influence the free settled density, however they were not subject of study in this work.

As per HR, the lowest value was obtained for Malto and the highest for Algin. Since the HR is the ratio between the tapped density and the free settled density, this means that as close to 1 the HR is, the tapped and free settled densities have the same value and less variation in the density is observed after the tapping. In this sense, free settled Malto powders present better packing than the other in-bed binders and, based on the previous characterization of PSD, this fact regards in the broader PSD which supports the previous explanation that fine particles fill the void space among coarse particles.

**Table 3.IV:** Rheological characteristics of *in-bed* binders studied in this work.

| | **PVA** | **Malto** | **Algin** | **CMC** |
|---|---|---|---|---|
| Density $\rho_b$ (g/cm$^3$) | 1,22 ± 0,02 | 1,19 ± 0,01 | 1,62 ± 0,01 | 1,60 ± 0,02 |
| Free settled density $\rho_{free\ settled}$ (g/cm$^3$) | 0,39 ± 0,01 | 0,40 ± 0,01 | 0,47 ± 0,01 | 0,48 ± 0,01 |
| Tapped density $\rho_{tapped}$ (g/cm$^3$) | 0,53 ± 0,01 | 0,50 ± 0,01 | 0,66 ± 0,01 | 0,62 ± 0,01 |
| HR | 1,36 ± 0,02 | 1,25 ± 0,01 | 1,41 ± 0,01 | 1,30 ± 0,01 |

In Table 3.V the rheological characteristics of the feedstocks prepared using different *in-bed* binders are presented. The free settled density of the PP-5PVA, PP-5Malto and PP-5Algin exhibits values between 0,61 and 0,63 g/cm$^3$, while PP-5CMC feedstock presents the lowest value (0,56 g/cm$^3$), not following the trend described above for each individual *in-bed* binder. We advocate here that the particle shape of the *in-bed* binders plays a key role in the settling of the powders, i.e. for the case of the feedstock with CMC powders, due to the fiber type shape particles (Figure 3.4 D), when the particles freely settled the packing will be determined by the orientation of the individual particles and expectably the occupied volume will be higher and the free settled density of the feedstock decreases. In the case of the PP-5PVA, PP-5Malto and PP-5Algin, the *in-bed* binders are composed by irregular

shaped particles and the variation among them is residual. However, the PP-5Malto feedstock exhibits the highest free settled density value and this fact is attributed to the broader PSD (Figure 3.3) when compared with the Algin and PVA ones.

Regarding the HR of the feedstock, as opposed to the observations for the *in-bed* binders as individual materials, there is not significative differences among the different feedstock, varying between 1,38 and 1,42. This fact is explained by the amount of porcelain in the feedstock (95 wt.%) and its value of HR (1,40). This is even more preeminent in the case of PP-5Malto, once the Malto has the lowest HR as *in-bed* binder (Table 3.IV) but similar HR to the other feedstock prepared. The PP-5CMC feedstock has the highest HR registered, meaning a poorer flowability when compared to the other ones, and, as detailed above, this fact may be attributed to the fiber type shape particles of CMC.

**Table 3.V:** Rheological and density characteristics of the feedstock (5 wt.% of *in-bed* binder and 95 wt.% of porcelain powders), presented in Table 3.I.

| | **PP-5PVA** | **PP-5Malto** | **PP-5Algin** | **PP-5CMC** |
|---|---|---|---|---|
| Free settled density $\rho_{free\ settled}$ (g/cm$^3$) | 0,62 ± 0,01 | 0,63 ± 0,01 | 0,61 ± 0,01 | 0,56 ± 0,01 |
| Tapped density $\rho_{tapped}$ (g/cm$^3$) | 0,86 ± 0,01 | 0,89 ± 0,01 | 0,84 ± 0,01 | 0,80 ± 0,03 |
| HR | 1,39 ± 0,02 | 1,41 ± 0,01 | 1,38 ± 0,02 | 1,42 ± 0,03 |

As discussed, and detailed above, the particle shape of the *in-bed* binders has an impact in the rheological behavior of the feedstock for BJP, supported by the lower free settled density and higher HR of PP-5CMC, which has fiber type shaped CMC particles. In the case of the feedstock prepared with PVA, Malto and Algin, all of them composed by irregular shaped particles, there was not significative differences and we advocate that the reason is explained by the high amount of porcelain powders (95 wt.%) in the mixture and, as consequence, higher impact in the feedstock characteristics than the *in-bed* binder powders.

With the rheological characteristics of the different feedstocks analyzed, it is now important to observe their behavior during the binder jet printing process. In Figure 3.8 the powder bed of (A) PP-5PVA, (B) PP-5Malto, (C) PP-5Algin and (D) PP-5CMC feedstocks, after the deposition of the liquid binder during the printing process are presented. No significative differences can be observed in the powder bed of (A) PP-5PVA, (B) PP-5Malto and (C) PP-5Algin feedstocks. However, in the case of (D) PP-5CMC feedstock, two different defects can be observed: (a) lack of binder deposition and (b) accumulation of the liquid binder drops in the powder bed. As highlighted in Figure 3.8 D (a), during the printing process a deposition lack of liquid binder was observed due to obstruction of the printhead with particles from the powder bed (Figure 3.9). Due to this obstruction, the liquid binder which is not deposited in the powder bed starts accumulating in the printhead forming drops, which fall from the printhead to the powder bed, originating the defect observed in detail in Figure 3.8 D (b). The obstruction of the printhead with particles from the powder bed was only observed during the printing process of PP-5CMC feedstock.

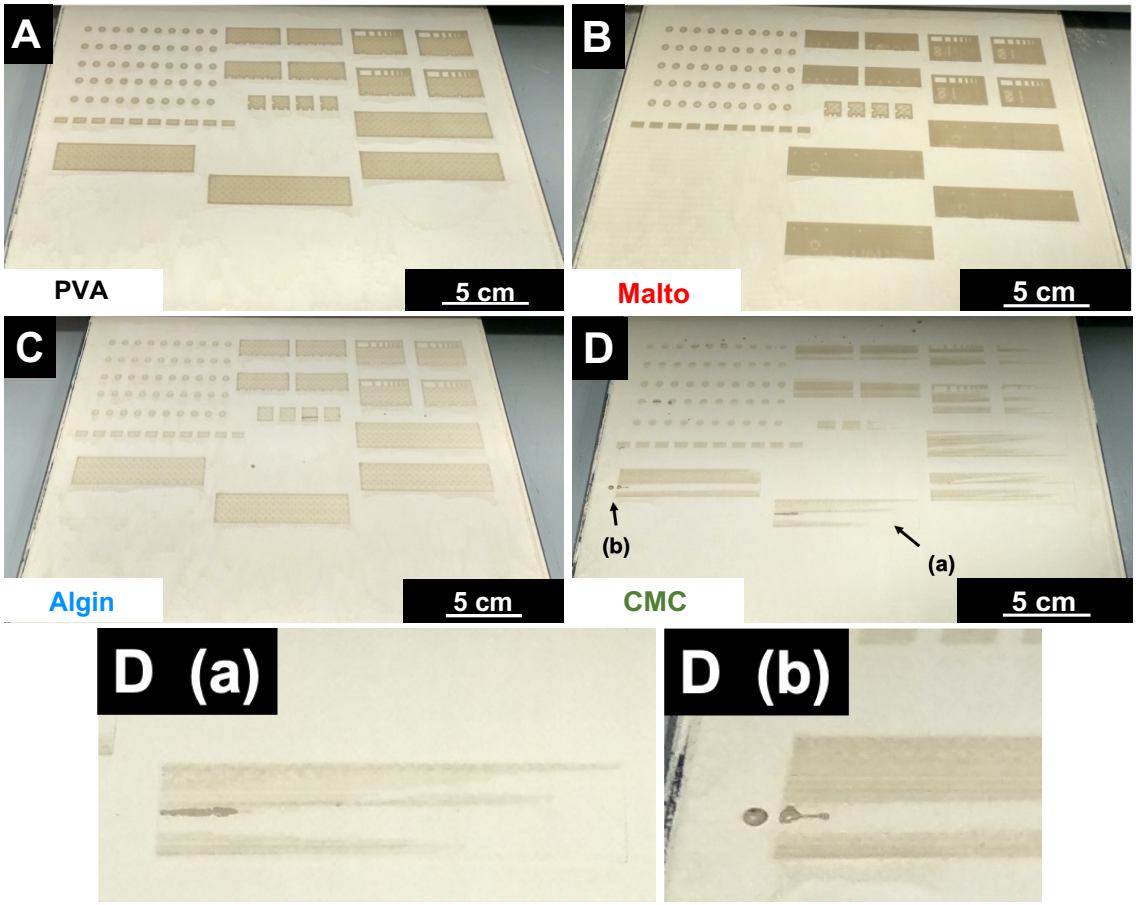


**Figure 3.8:** Images of the powder bed images of (A) PP-5PVA, (B) PP-5Malto, (C) PP-5Algin and (D) PP-5CMC feedstocks, after the deposition of the liquid binder, during the printing process. While for the powder bed of PP-5PVA, PP-5Malto and PP-5Algin the deposition is defect free, in the case of PP-5CMC, two types of defects were found: (a) lack of binder deposition and (b) accumulation of liquid binder drops. In detail, the defects found are illustrated in images D (a) and D (b).


**Figure 3.9:** Obstructed printhead after binder jet printing of the PP-5CMC feedstock.

The indicated defaults in the powder bed are only observed for the feedstock with CMC as *in-bed* binder. Here we advocate that the obstruction of the printhead (Figure 3.9) might be related to the fiber type shaped particles of CMC and its bigger size than the other in-bed binders, as indicated by its PSD curve (Figure 3.3 and Table 3.III). Because the printing process was performed using a layer thickness of 100 µm, the contact between the coarser and fiber type particles of CMC and the printhead is favored leading to the obstruction of the printhead. This does not rule out any particle surface effect that might be associated with the feedstock particles.

After observing the behavior of the feedstock prepared with different in-bed binders (Table 3.**I**), cylindrical parts (Figure 3.1 A) were printed, in the case of PP-5CMC, the printing process was paused in order to clean the printhead every time that the deposition of the liquid binder was defective, allowing the production of samples for further characterization, to assess the geometric relative density and the diameter variation to the virtual design. Due to the industrial interest for the production of porcelain parts by BJP, the variation of the dimensions of the green and sintered object to the dimensions of the virtual design is crucial for industrial implementation of the process. Although both diameter and length dimension variation are important, during the printing process with all the formulations tested, a layer shifting from the initial layers was observed. Due to the high impact as error that this defect would have in the length variation, only the diameter variation is presented.

The geometric relative density and diameter variation of the green printed parts is presented in Table 3.VI. The green density of the printed parts is in general quite small, varying between 32 % for PP-5CMC formulation to the highest geometric relative density of 41 % for PP-5Malto. The green density of printed parts is influenced, among others, by the free settled density, HR and PSD of the powders. In the case of the feedstock used in this work, PP-5CMC has the lowest free settled density (Table 3.V) and as consequence, the green printed part presents the lowest geometric relative density. The free settled density of PP-5PVA, PP-5MAlto and PP-5Algin are similar (Table 3.V) and do not explain the highest relative density of PP-5Malto green printed part, however, as discussed above, the PSD of Malto (Figure 3.3) is broader than the ones of PVA and Algin, promoting a better packing of particles and increase of the green printed part. The diameter variation measured for all the feedstocks has negative values, i.e., the diameter of the green printed part is lower than the diameter of the virtual design. This is explained by the deposition of the liquid binder which dissolves the *in-bed* binders and deagglomerate the porcelain particles, which leads to an

approximation of the particles in the green printed part. Bigger variation for PP-5Algin and PP-5CMC feedstocks (~ - 6 %) than for PP-5PVA and PP-5Malto (~ -3 %) was observed. Additionally, during the measuring process, it was observed that green printed parts with PP-5Algin and PP-5CMC loose powder from the surface due to the handling of the parts. This effect directly affects the diameter of the cylinders, reducing it and, as consequence, increasing the diameter variation to the virtual design. The loose of powder suggest poor mechanical resistance and poor bond of the particles. Although the lower *in-bed* binder volume fraction for PP-5Algin and PP-5CMC (0,073 and 0,074, respectively) than for PP-5PVA and PP-5Malto (0,095 and 0,097, respectively) could imply worse bond of particles, the difference is around 2 vol.% and should not have this impact. Additionally, the free settled density may also directly influence the mechanical strength of the green parts, however similar values of free settled density were observed for PP-5PVA, PP-5Malto and PP-5Algin (Table 3.V), and only for PP-5Algin this effect was observed. In this sense, other factors not subject of study in this work, such as *in-bed* binder wettability, solubility of *in-bed* binder in the liquid binder and liquid binder penetration, might play an important role in the bond of particles and, as consequence, in the mechanical strength and green density of printed parts.

**Table 3.VI:** Relative density and diameter variation of the green cylinders printed with the different feedstock.

| | **PP-5PVA** | **PP-5Malto** | **PP-5Algin** | **PP-5CMC** |
|---|---|---|---|---|
| Geometric relative density $\%\rho_{geom}$ (%) | 35,9 ± 0,4 | 41,3 ± 0,2 | 33,0 ± 0,2 | 32,1 ± 0,3 |
| Diameter variation $\Delta D$ (%) | - 3,5 ± 0,1 | - 3,4 ± 0,1 | - 6,7 ± 0,1 | - 6,1 ± 0,3 |

The cylindrical parts were then sintered with a maximum temperature of 1345 ºC for 15 h 30 min under industrial conditions of Costa Verde. The values of density, diameter variation to virtual design, water absorption and apparent porosity are presented in Table 3.VII. A general overview permits to conclude that the relative density values measured by Archimedes method are 13 - 17 % higher than the geometric relative density for the same parts, because using Archimedes method, possible geometric inconsistencies do not affect

its measure, while for geometric measurement, there is an assumption that the parts are perfect cylinders.

The PP-5CMC sintered printed parts exhibit the highest relative density, both measured by geometrical (62 %) and Archimedes (77 %) methods. This was not expected as PP-5CMC presented the lowest relative density of green parts, however this fact might be explained by deformation of the parts and fissures formed during the sintering process, which are not considered in the geometric and in Archimedes method. This is supported by the highest error registered (± 1,8 %), which suggest that the 10 sintered parts used for this measurement have higher differences among them, than the ones for the other feedstocks. The variation among the parts produced with the same PP-5CMC feedstock is related with the defects observed during the binder jet printing process (Figure 3.8). The values of water absorption (13 %) and apparent porosity (24 %) were also the lowest among the different feedstock used. As described above the fissures and fractures in the sintered parts, are big enough to not retain water inside as a porous does during the Archimedes method. In this way, fissures and fractures are measured as porous and the water absorption and apparent porosity is reduced.

Regarding the relative density PP-5PVA, PP-5Malto and PP-5Algin there was not significative differences among them, varying between 57 and 62 %, when measured by geometric method, and varying between 72 and 75 % when measured by Archimedes method. As the density of the green parts usually influences the density of a ceramic sintered body, it was expected that the sintered printed parts produced with PP-5Malto feedstock presented significantly higher relative density than the ones from PP-5PVA and PP-5Algin, once the green parts have the highest relative density (Table 3.VI). The explanation for the similar values of the sintered parts with the different feedstock regards in the high amount of porcelain powders (95 wt.%) in the feedstock, which leads to printed parts with similar relative density values after the thermal removal of the *in-bed* binders. Both water absorption and apparent porosity of the sintered parts also do not present significative variance, once the first varies between 15 and 16 % and the latter varies between 25 and 28 %.

In the case of diameter variation to the virtual design, the same trend observed for the green parts (Table 3.VI) was observed as well for the sintered parts (Table 3.VII). The PP-5PVA

and PP-5Malto sintered parts exhibit similar values (~ -22 %), while for PP-5Algin and PP-5CMC present also similar values (~ -27 %).

**Table 3.VII:** Relative density, diameter variation, water absorption and apparent porosity of the industrially sintered cylinders printed with the different feedstock.

| | **PP-5PVA** | **PP-5Malto** | **PP-5Algin** | **PP-5CMC** |
|---|---|---|---|---|
| Geometric relative density $\%\rho_{geom}$ (%) | 58,2 ± 0,7 | 60,8 ± 0,3 | 57,6 ± 0,5 | 62,0 ± 0,5 |
| Diameter variation $\Delta D$ (%) | - 22,4 ± 0,1 | - 21,9 ± 0,1 | - 26,7 ± 0,2 | - 26,9 ± 0,1 |
| Relative density $\%\rho_{Arc}$ (%) | 72,0 ± 0,7 | 73,3 ± 0,4 | 74,5 ± 0,5 | 77,4 ± 1,8 |
| Water absorption WA (%) | 15,3 ± 0,6 | 16,2 ± 0,3 | 15,2 ± 0,4 | 13,2 ± 1,0 |
| Apparent porosity AP (%) | 25,3 ± 0,8 | 28,5 ± 0,4 | 27,2 ± 0,5 | 24,4 ± 1,1 |

In Figure 3.10 the polished fracture zone microstructures of the industrially sintered parts, produced with the different feedstock are presented. A general overview of all the images permits to conclude that no significative differences are noticeable among them. In addition, the porous microstructures observed are in accordance with the relative densities measured (72 - 77 %), as presented in Table 3.VII. The similarity among the microstructures is explained again by the high amount of porcelain powders used in the feedstock (95 wt.%).

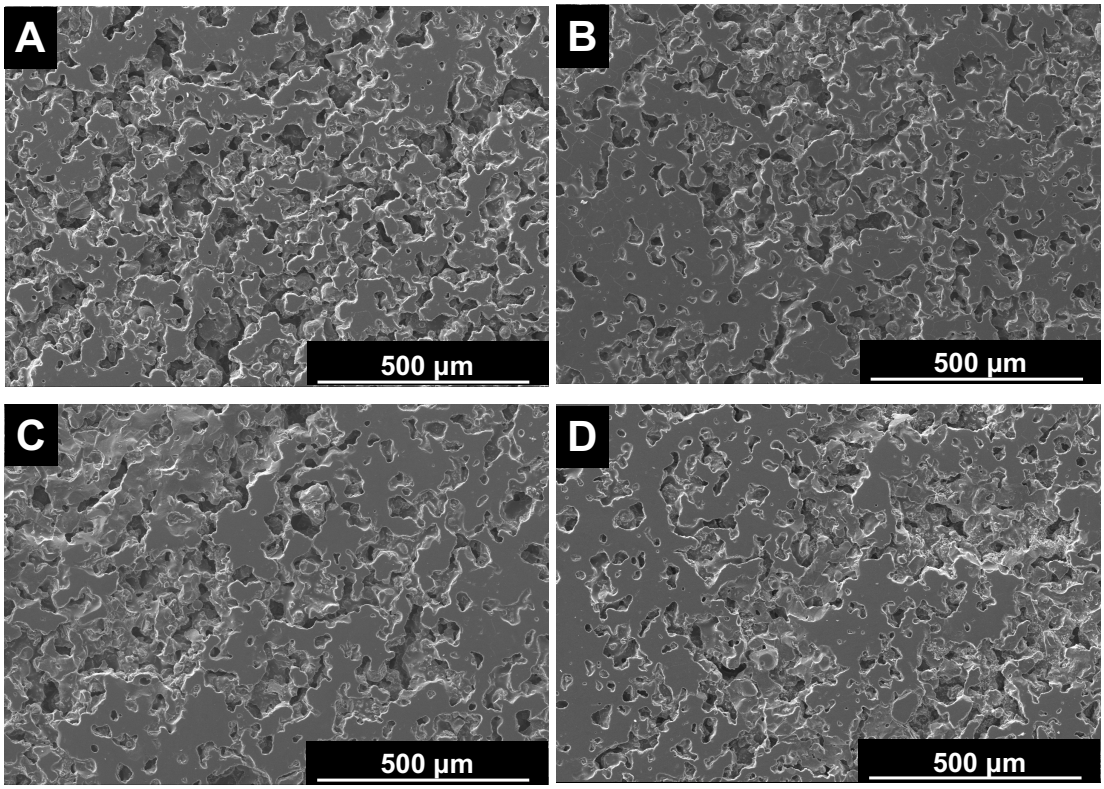


**Figure 3.10:** SEM micrographs of polished fracture zone, after industrial sintering at 1345 °C, of porcelain parts printed with (A) PP-5PVA, (B) PP-5Malto, (C) PP-5Algin and (D) PP-5CMC feedstock formulations. The images illustrate porous microstructures for all the feedstock and are in accordance with the measurements of relative density.

As general overview of the properties of the sintered printed parts with the feedstock using PVA, Malto, Algin and CMC as *in-bed* binders, concludes that no significative differences among them are noticeable. This is especially relevant when for porcelain parts conventionally produced the desired relative density is > 99,5 %, while for the industrially sintered printed parts of this work, the maximum relative densities are far from this value. However, it is important to refer that the conventionally porcelain parts production of Costa Verde uses two sintering steps, and the parts studied in this work were produced using only one, since the first sintering step of Costa Verde occurs at temperatures which does not allow the production of printed parts with enough mechanical strength to be handled. Furthermore, a debinding step or a first sintering step may be important for the thermal processing of porcelain parts produced by binder jet printing at industrial scale in order to reach porcelain parts with comparable densities to the ones produced via conventional routes.

After recognizing that the role of the *in-bed* binders, due to the small amount in which they are used, does not affect markedly the post sintering characteristics of the printed parts, understand the effect of the different *in-bed* binders in the parts design limitations is crucial. The part design limitation in this work, concerns in the study of design features, such as wall thickness, and what is the minimum thickness that can be printed and processed without deformation. The same rational is used for the minimum overhang able to be printed and processed. In this sense, parts with different wall thicknesses (Figure 3.1 B) and parts with different overhangs (Figure 3.1 C) were printed using the different feedstocks with different *in-bed* binders and industrially sintered. The parts in green state and after sintering are presented in Figure 3.11, for wall thickness, and in Figure 3.12, for overhangs.

As general observation of the parts with different wall thicknesses in green and sintered stage, printed with the different feedstocks, the walls with thicknesses of 10 mm, 5 mm, 3 mm and 2 mm were able to be printed and sintered without major problems (Figure 3.11). The minimum thickness able to be printed and removed from the powder bed was the 1 mm wall in the parts printed using PP-5PVA (Figure 3.11 A) and PP-5Malto (Figure 3.11 C) feedstock, while in the case of PP-5Algin (Figure 3.11 E) and PP-5CMC (Figure 3.11 G) the minimum wall thickness in the green part is the 2 mm wall. After industrial sintering, 1 mm walls present in the green parts broke for both PP-5PVA (Figure 3.11 B) and PP-5Malto (Figure 3.11 D) formulations, and the minimum thickness wall observed for sintered parts was 2 mm, as for PP-5Algin (Figure 3.11 F) and PP-5CMC (Figure 3.11 H) the minimum wall thickness of 2 mm was also observed. The minimum thickness able to be printed relates with the green density of the parts (Table 3.VI) which was higher for PP-5PVA and PP-5Malto than for PP-5Algin and PP-5CMC. In addition, the 1 mm wall of the PP-5Malto green part (Figure 3.11 C) is defect free, while the one of PP-5PVA (Figure 3.11 A) has a small defect on the top. Based on our results, this small difference may be related with the broader PSD of Malto (Figure 3.3) than the one of PVA, which leads to better packing of particles and, as consequence, the printing of a thinner wall. In the case of sintered parts, even for PP-5PVA and PP-5Malto, the 1 mm wall was not possible to print, due to the thermal removal of the *in-bed* binder followed to retraction of the wall, which is ~ 22 % after sintering (Table 3.VII), leading to an extremely thin wall which deforms and breaks during sintering.

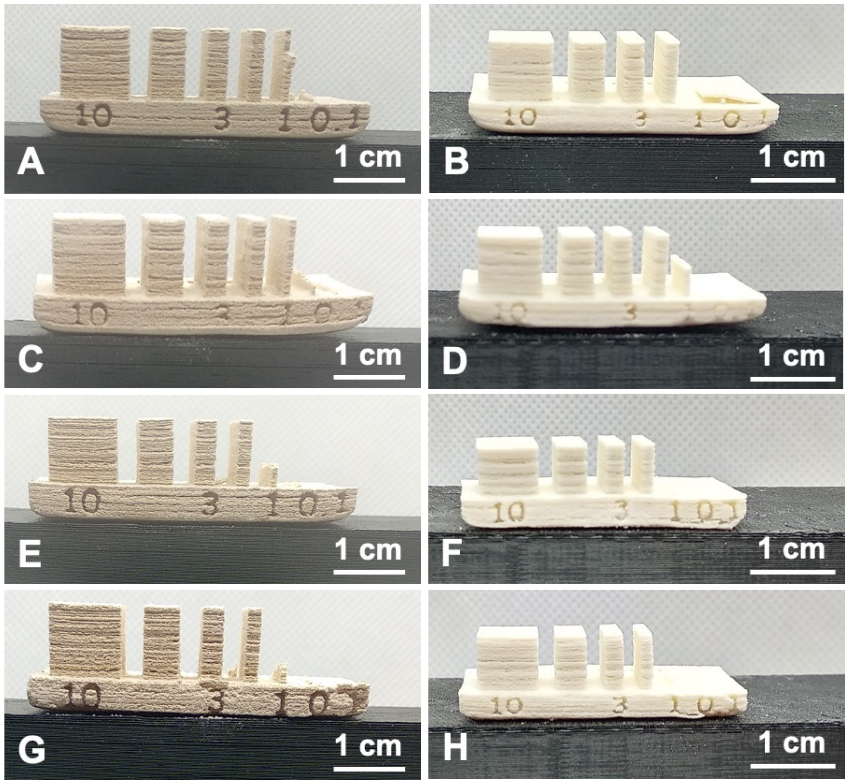


**Figure 3.11:** Printed parts to assess wall thickness as green part (A, C, E and G) and sintered part (B, D, F and H) at 1345 °C in an industrial kiln, produced with feedstock formulation (95 wt.% of porcelain + 5 wt.% of *in-bed* binder), using the following in-bed binders: (A, B) PVA, (C, D) Maltodextrin, (E, F) Sodium Alginate and (G, H) CMC.

As green parts, the overhangs were printed in all angles with all the feedstocks, without any noticeable difference among them (Figure 3.12). However, after industrial sintering, a small deformation was observed for the 30 ° and 15 ° overhang using PP-5PVA formulation (Figure 3.12 B), while in the case of the formulation PP-5Malto any major deformation was observed (Figure 3.12 D). In the case of PP-5Algin and PP-5CMC formulations, the parts present broken overhangs for the angles of 45 °, 30 ° and 15 °, as is possible to observe in Figure 3.12 F and Figure 3.12 H, respectively. During the industrial sintering, the lower angle overhangs break due to gravity forces associated with the lack of supports for the PP-5PVA. In addition, the lower green density of PP-5PVA contributes as well for the deformation, as opposed to the higher green density of PP-5Malto parts, which did not have any major defect. In the case of PP-5Algin and PP-5CMC the lower angles completely break during industrial sintering. Based on our results of this work, we advocate that are two major contributions for this effect: i) the lower green density of the parts, as presented in Table 3**.VI** and ii) the thermal degradation of Algin and CMC as *in-bed* binders. The low green density means that particles have more space among them and, as consequence,

jeopardizes the matter diffusion and the densification of the body. And the thermal degradation of Algin and Malto, as discussed above (Figure 3.5), occurs in multi steps and abruptly, with high burning rates, as opposed to PVA and Malto, for which the fractures of sintered parts were not observed after sintering. As discussed above, other factors may contribute to this effect, namely the liquid binder penetration, the wettability of *in-bed* binders and the solubility of *in-bed* binders in the liquid binder, however, these characteristics were not subject of study in this work and further investigation should be done in this sense.

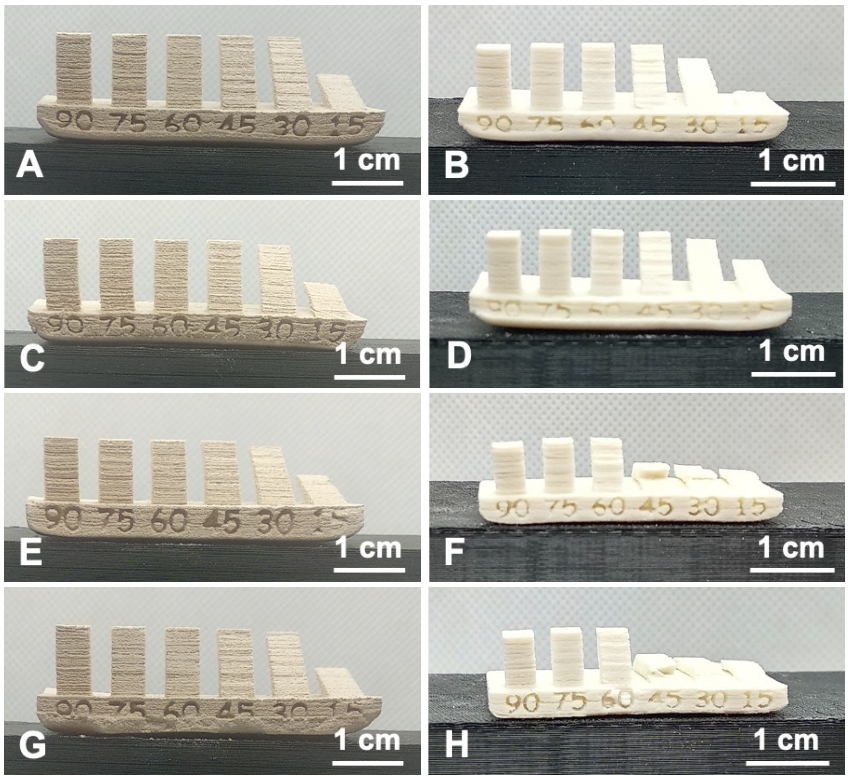


**Figure 3.12:** Printed parts to assess overhang angles as green part (A, C, E and G) and sintered part (B, D, F and H) at 1345 °C in an industrial kiln, produced with feedstock formulation (95 wt.% of porcelain + 5 wt.% of *in-bed* binder), using the following in-bed binders: (A, B) PVA, (C, D) Maltodextrin, (E, F) Sodium Alginate and (G, H) CMC.

The relative density achieved with maltodextrin (73 %) is higher than found in the literature, where Suwanprateeb *et al.* [6] reached a maximum of 49 % of relative density with sintered parts of hydroxyapatite, while Marchelli *et al.* [7] reached a maximum of 60 % of apparent density of porcelain bodies with maltodextrin as binder. The apparent porosity reached in this work is also lower than the reported in the literature by Chumnanklang *et al.* [8], reaching a minimum value of apparent porosity of 59 %, with hydroxyapatite powders and maltodextrin as binder coating the particles. Also with hydroxyapatite and using PVA as

binder, the reported values of relative density by Cox *et al.* [9], with average values of 45 % of relative density, are lower than we found with porcelain. Although these works regards on hydroxyapatite, a biomaterial where the porosity may be interesting, with alumina powders [10] the sintered parts also presented values of relative density (< 40 %) lower than we reached in this work. Alginate was also used as binder for AM production of alumina parts, however with slurry based techniques, reaching almost 100 % of relative density [11], but we need to emphasize that slurry based processes, typically, leads to denser parts.

Summarizing, we were able to compare PVA, maltodextrin, sodium alginate and CMC used as *in-bed* binders in the production of porcelain parts by binder jet printing. The first consideration regards on CMC, which has fiber type particles, a shape of particles that jeopardizes the printing process of porcelain powders, due to defects in the deposition of the liquid binder, resulted from the obstruction of the printhead (Figure 3.9). In the case of sodium alginate, even though it does not affect the printing process, it leads to fracture of parts after industrial sintering, especially low angle overhangs, and the presented results lead us to advocate the reason is its thermal degradation behavior (Figure 3.5) associated with the lower green density (Table 3.VI). Both PVA and maltodextrin allowed the printing of porcelain parts without major defects and its sintering as well. However, due to its costs and availability at industrial scale in porcelain parts production, the PVA as *in-bed* binder appears as the most suitable option for industrial implementation of by binder jet printing for porcelain parts production. Nevertheless, both binders exhibit a limitation in the printing of parts with details, especially in the printing of thinner walls (Figure 3.11 B and D), an important feature for product design driven companies, such as Costa Verde is. Hence, further investigation, regarding the amount of binder is needed, in order to improve the printability of detailed parts.

As stated, there are limitations in the design features possible to print with PP-5PVA formulation, especially thinner walls. In this sense, the amount of PVA was increased in steps of 2,5 wt.%, from 5 up to 20 wt.% (Table 3.I). We need to emphasize that without any *in-bed* binder added and with 2,5 wt.% of PVA, it was not possible to print porcelain objects by binder jet printing, due to the lack of bond among the porcelain particles, leading to loose powder in the powder bed and the impossibility to remove and handle parts. In further images these formulations will be identified as a non printable area.

The free settled density of the feedstock formulation is presented in Figure 3.13, starting with the value for porcelain powder without any addition of *in-bed* binder (0,90 ± 0,01 g/cm$^3$). With the addition of 5,0, 7,5 and 10,0 wt.% of PVA, the value decrease to 0,62 ± 0,01 g/cm$^3$ for the three formulations. PP-12PVA and PP-15PVA formulations exhibit values of 0,64 ± 0,01 g/cm$^3$ and 0,65 ± 0,01 g/cm$^3$, respectively. With further increase of the wt.% amount of PVA, the free settled density decreases to 0,56 ± 0,01 g/cm$^3$ and 0,55 ± 0,01 g/cm$^3$ for PP-17PVA and PP-20PVA formulations, respectively. The HR of the different formulations is presented in Figure 3.14, starting with the porcelain powder (1,40 ± 0,02) and decreasing with the addition of PVA, reaching a minimum of 1,37 ± 0,01 for PP-12PVA formulation. With the further addition of PVA an increase is observed for PP-15PVA formulation, with a value of 1,38 ± 0,01 and even more noticeable for PP-17PVA and PP-20PVA formulations with values of 1,42 ± 0,03 and 1,43 ± 0,04, respectively.

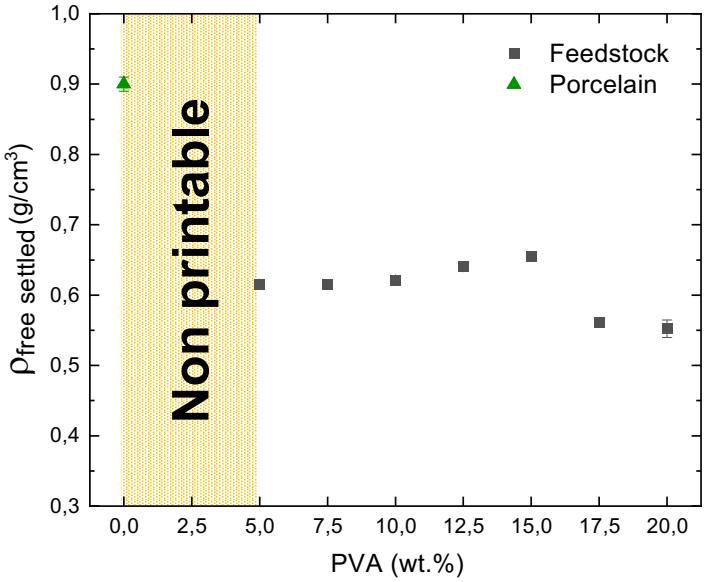


**Figure 3.13:** Free settled density of porcelain powders (▲) and of the feedstock formulation with variation of the amount of *in-bed* binder PVA (■). Highlight for the non printable formulations (< 5,0 wt.% of PVA).

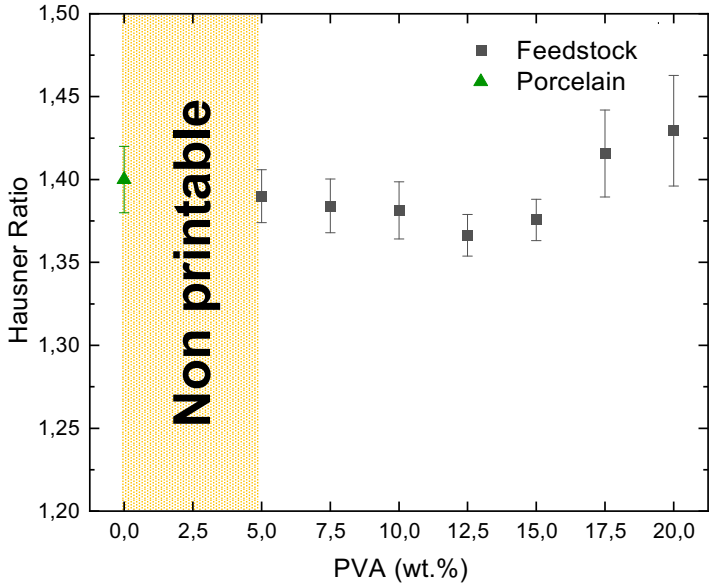


**Figure 3.14:** Hausner Ratio of porcelain powders (▲) and of the feedstock formulation with variation of the amount of *in-bed* binder PVA (■). Highlight for the non printable formulations (< 5,0 wt.% of PVA).

Regarding HR, the addition of PVA appears to not have a significative impact in the feedstock formulation, especially up to values of 15 wt.% and considering the errors associated with each feedstock formulation. This lower change in the values is explained by the similar HR values of porcelain (1,40 ± 0,02) and PVA (1,36 ± 0,02, Table 3.IV). However, for higher amounts of PVA, the HR and its associated error increases, showing higher variation of feedstock characteristics. The cause for this effect may be related with the heterogeneity in the feedstock mixture, due to difficulties in proper dry mixing, caused by the high amounts of PVA, corresponding to 0,290 (29 %) and 0,324 (32 %) volume fraction ($V_b$) of PVA for PP-17PVA and PP-20PVA feedstocks, respectively (Table 3.II). The free settled density trend matches the HR one, where higher free settled densities are reached for lower HR values, due to better powder packing, however there is no significative differences for feedstock formulations with equal or less than 15 wt.% of PVA., while for PP-17PVA and PP-20PVA the impact is higher, decreasing its values of free settled density. In all the studied feedstock formulations, as opposed to HR, the free settled density decreases when compared with the starting porcelain powders, due to lower density of PVA (Table 3.**II**).

As for the comparison of *in-bed* binders, cylindrical parts (Figure 3.1 A) were printed using the feedstocks with different amounts of PVA and its geometric relative density are

presented in Figure 3.15. The green parts exhibit an increase in the relative density with the increase of PVA amount, from 35,9 ± 0,3 % to 43,7 ± 0,7 %, corresponding to PP-5PVA and PP-20PVA feedstock. In the case of sintered parts, although having higher relative density when compared with its green part, present a decrease in relative density with the increase of PVA amount from 58,3 ± 0,1 % to 49,6 ± 0,4 %, for PP-5PVA and PP-20PVA feedstock, respectively (Figure 3.15). In Figure 3.16 the diameter variation of the cylinders to the virtual design with the variation of PVA content is presented and is possible to observe a negative variation for all the feedstock formulations while it increases for higher amounts of PVA, from - 3,5 ± 0,1 % for PP-5PVA to - 6,9 ± 0,2 % for PP-20PVA. The same trend in the diameter variation to virtual design is observed after industrial sintering process, however the is an increase in the values of variation to - 22,4 ± 0,1 % and - 24,2 ± 0,1 % for sintered parts of PP-5PVA and PP-20PVA, respectively.

Although the free settled density of the different feedstock did no show significative differences (Figure 3.13), the diameter variation of the cylinders is higher, i.e. the diameter of the green cylinders is smaller, with the increase of PVA content (Figure 3.16), leading to an increase in the geometric relative density of the green parts. This happens with liquid binder deposition, as it dissolves the PVA particles leading to higher compaction between porcelain particle. As the PVA amount increases, the space between particles is better filled by the PVA solution (PVA powder + liquid binder), reducing the diameter of the green sample and increasing its relative density. After the industrial sintering of parts, although the same trend in diameter variation was observed, with higher variations for higher contents of PVA (Figure 3.16), an opposite variation was observed in the geometric relative density (Figure 3.15) with lower values for higher amounts of PVA. This fact is explained by the thermal degradation of PVA, which leaves open porosity in the parts, and has higher impact as higher amount of PVA is used.

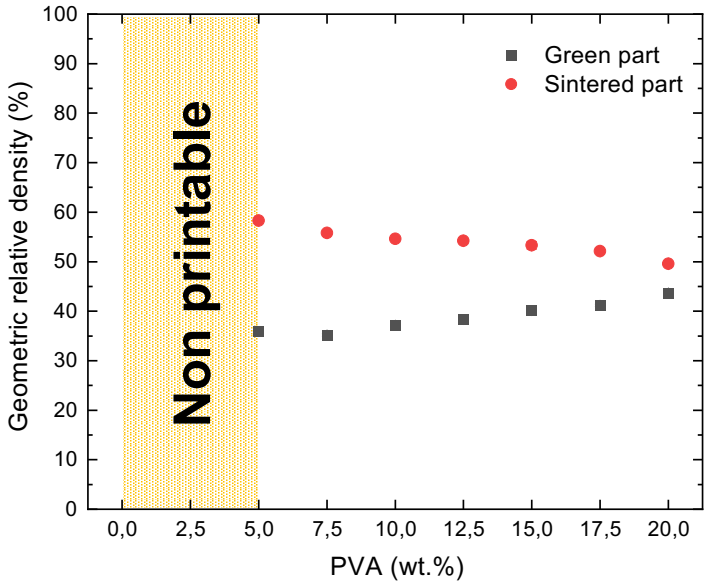


**Figure 3.15:** Geometric relative density of printed parts with feedstock formulation prepared with different amounts of *in-bed* binder PVA in the green state (■) and after industrial sintering at 1345 °C (●). Highlight for the non printable formulations (< 5,0 wt.% of PVA).

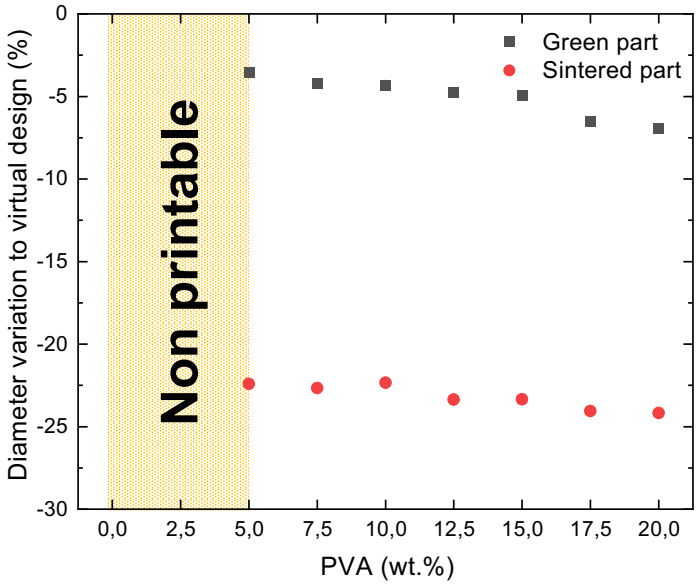


**Figure 3.16:** Diameter variation to virtual design of printed parts with feedstock formulation prepared with different amounts of *in-bed* binder PVA in the green state (■) and after industrial sintering at 1345 °C (●). Highlight for the non printable formulations (< 5,0 wt.% of PVA).

The relative density measured by Archimedes method presented the same trend as the geometric relative density after industrial sintering, decreasing from 72,0 ± 0,7 % with

PP-5PVA to 58,4 ± 0,5 % for PP-20PVA (Figure 3.17). The water absorption and the apparent porosity increased with the increase in the PVA amount from 15,3 ± 0,6 % (PP-5PVA) to 26,1 ± 0,5 % (PP-20PVA) and from 25,3 ± 0,8 % (PP-5PVA) to 37,2 ± 0,4 % (PP-20PVA), respectively. Any significative difference was observed for feedstocks using less than 15 wt.% of PVA as *in-bed* binder. However, for the case of PP-17PVA and PP-20PVA the difference is noticeable. As discussed above, the reason of this fact is related with the dry mixing of the feedstock which is jeopardized by the high amount of PVA in the mixture. Also, as the amount of PVA increases, the relative density of sintered parts decreases due to the thermal removal of the *in-bed* binder.

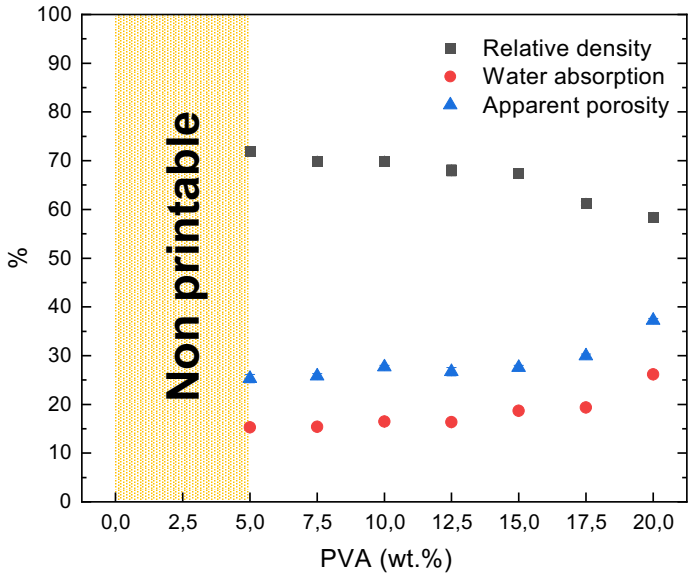


**Figure 3.17:** Relative density (■), water absorption (●) and apparent porosity (▲), measured by Archimedes Method, of parts produced with feedstock formulation with different amounts of in-bed binder PVA, after industrial sintering at 1345 °C.

As the results exhibit higher relative density for parts produced using PP-5PVA than for the other feedstocks, the difference for amounts up to 15 wt.% is not significative and the objective of increasing the amount of PVA is to understand its impact in design features of printed parts, as discussed previously. In that sense the parts with different wall thicknesses (Figure 3.1 B) and different overhang angles (Figure 3.1 C).

The use of wall thicknesses higher than 2 mm in the part design, do not show any challenge using PVA as *in-bed* binder from 5 wt.% to 20 wt.%, as is possible to see that both in green state and after industrial sintering the parts have this wall (Figure 3.18). While the 1 mm

wall was printed for all the used formulations, in the case of PP-5PVA (Figure 3.18 A) and PP-7PVA (Figure 3.18 C) formulations, it breaks during removal from powder bed and depowdering process. After industrial sintering only parts printed with PP-10PVA (Figure 3.18 F), PP-12PVA (Figure 3.18 H) and PP-15PVA (Figure 3.18 J) have it. However, it is possible to observe a slight deformation in these walls. In the case of overhang angles there was not a significative difference among the different formulations used, with all of them presenting green parts with all overhangs and, after sintering, small deformation was observed in 30 ° and 15 ° overhangs (Figure 3.19).

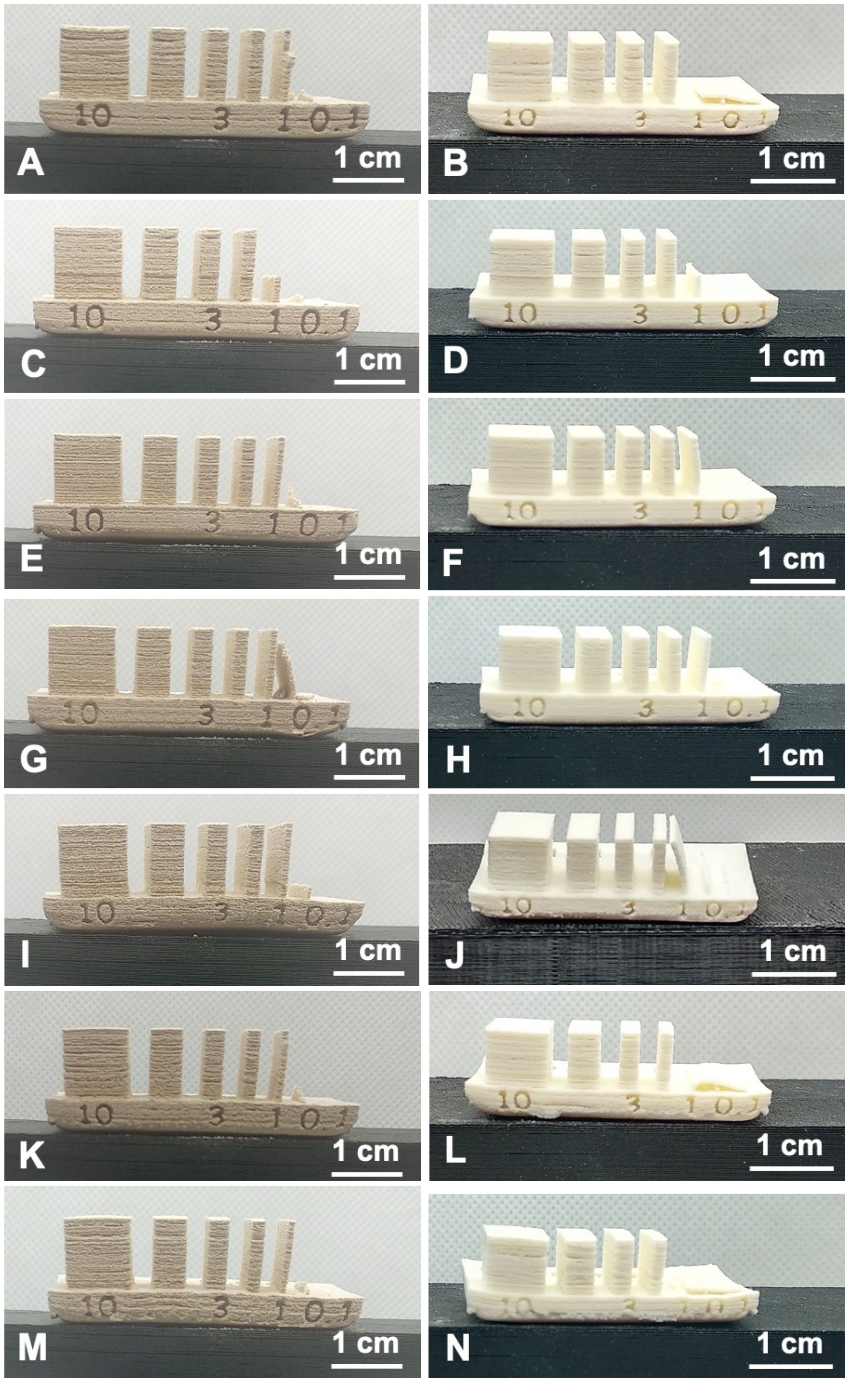


**Figure 3.18:** Printed parts to assess wall thickness as green part (A, C, E, G, I, K and M) and sintered part (B, D, F, H, J, L and N) at 1345 °C in an industrial kiln, produced with the following feedstock formulation: (A, B) PP-5PVA, (C, D) PP-7PVA, (E, F) PP-10PVA, (G, H) PP-12PVA, (I, J) PP-15PVA, (K, L) PP-17PVA and (M, N) PP-20PVA.

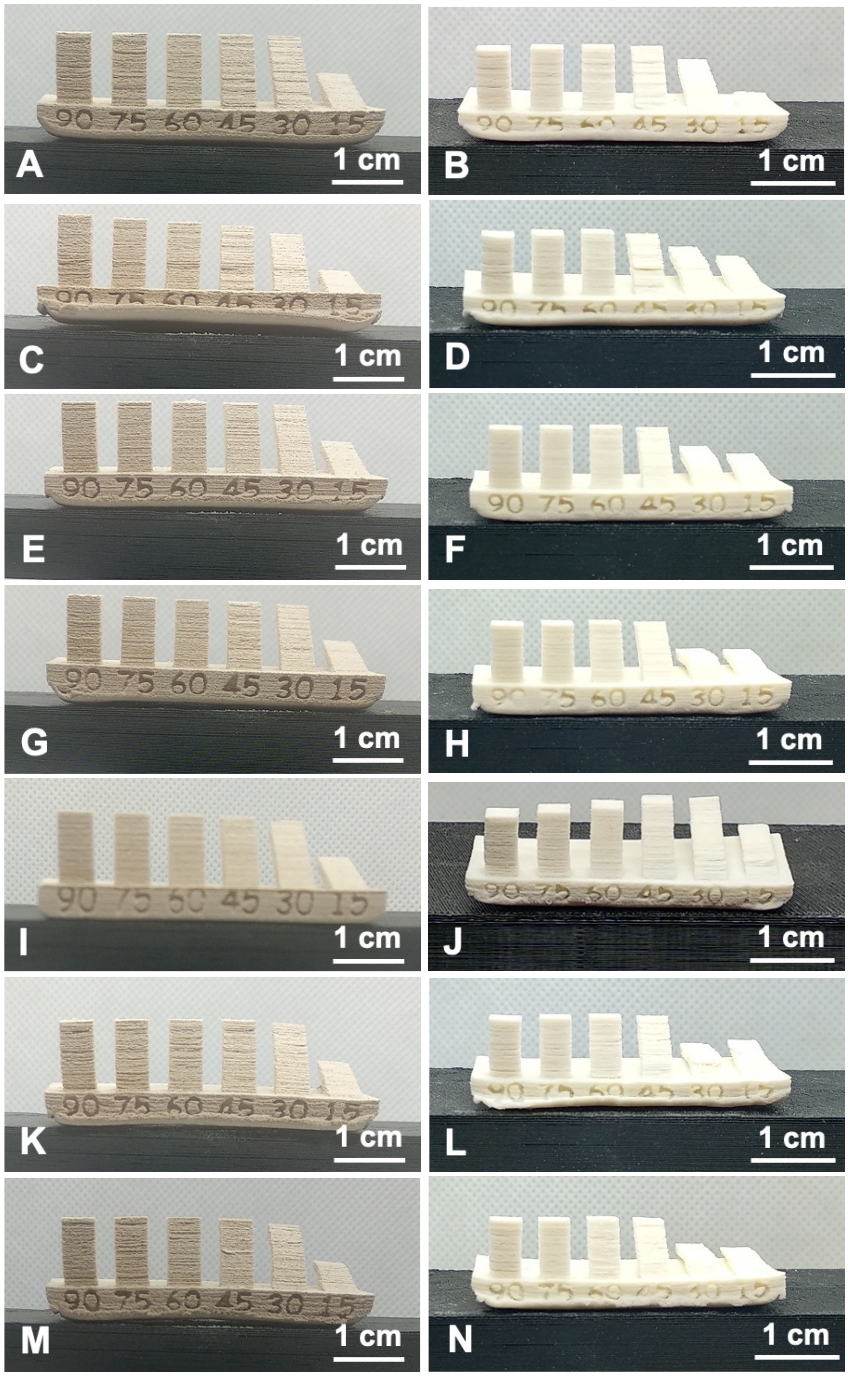


**Figure 3.19:** Printed parts to assess overhang angles as green part (A, C, E, G, I, K and M) and sintered part (B, D, F, H, J, L and N) at 1345 °C in an industrial kiln, produced with the following feedstock formulation: (A, B) PP-5PVA, (C, D) PP-7PVA, (E, F) PP-10PVA, (G, H) PP-12PVA, (I, J) PP-15PVA, (K, L) PP-17PVA and (M, N) PP-20PVA.

As per Figure 3.19 the variation of the amount of PVA did not present a significative difference regarding the overhang angles able to be produced, this is not the case of the wall thickness (Figure 3.18) where a minimum wall thickness of 1 mm was produced using

PP-10PVA, PP-12PVA and PP-15PVA formulations, which were the same formulations with slight higher free settled density (Figure 3.13) and lower HR (Figure 3.14). The 1 mm wall broke in the green part for PP-5PVA and PP-7PVA formulations and in during sintering for PP-17PVA and PP-20PVA formulations. In this sense, we can group the feedstock formulations in three groups due to its similar behavior: low amount of binder (PP-5PVA and PP-7PVA), adequate amount of binder (PP-10PVA, PP-12PVA and PP-15PVA) and high amount of binder (PP-17PVA and PP-20PVA).

In the low amount of binder group, as presented above, although it was possible to print 1 mm walls, the same presented low mechanical resistance and broke during removal from powder bed or during depowdering process. The low amount of binder, as schematically represented in Figure 3.20, does not fill the space between porcelain particles in the green parts, leading to walls without enough mechanical resistance to be removed from the powder bed and handled. As is possible to observe Figure 3.18 A, the top of the 1 mm wall has a small defect and in Figure 3.18 C the 1 mm wall broke.

In the high amount of binder group, the binder content leads to the fracture of thinner walls during the sintering process, as schematically represented in Figure 3.21, due to the high porosity between porcelain particles as result from the thermal removal of the in-bed binder, promoting the fracture of thinner walls. Another cause for the defect may be related with the liquid binder deposition and the incomplete solution of PVA particles due to the high content of PVA which may hinder the full penetration in the liquid binder drops.

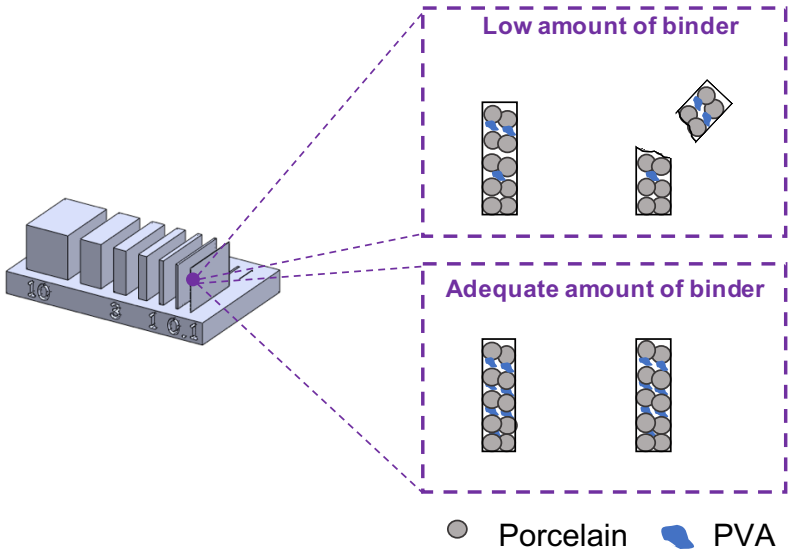


**Figure 3.20:** Defects observed in thinner walls (< 1mm) of the green parts with low (5,0 wt.% and 7,5 wt.%) amount of PVA as opposed to the parts with adequate (10,0, 12,5 and 15,0 wt.%) amount of PVA. The illustration highlights that with reduced amount of PVA the thinner walls do not have enough bond among particles and break.

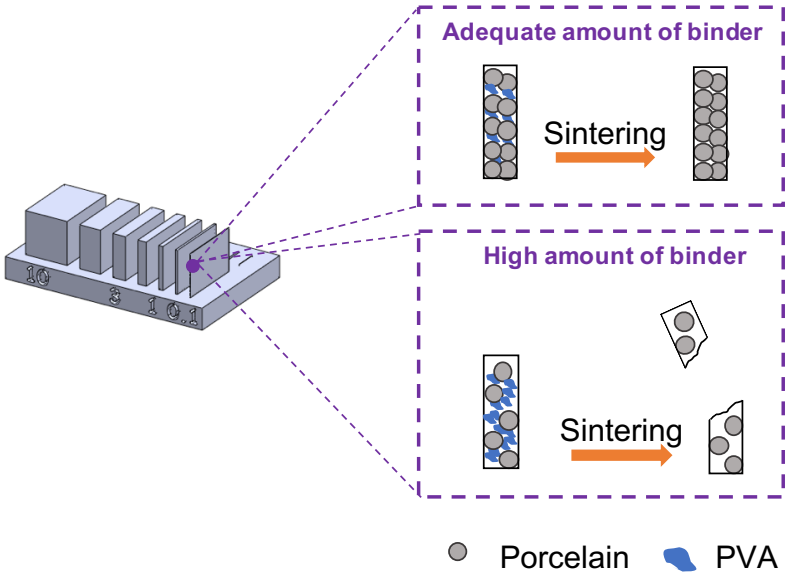


**Figure 3.21:** Defects observed in thinner walls (< 1mm) of the sintered parts with high (17,5 and 20,0 wt.%) amount of PVA as opposed to the parts with adequate (10,0, 12,5 and 15,0 wt.%) amount of PVA. The illustration highlights the effect of high amount of PVA, which after thermal removal leads high porosity which leads to fracture of the thinner walls.

Maleksaeedi *et al.* [10] were able to produce alumina parts using 10 wt.% of PVA mixed with the spray dried alumina powder. The group produced green parts with 20 – 25 % of relative density and sintered parts with 35 – 40 % of relative density. They found that the majority of the porosity resulted either from the removal of the PVA or the porosity created due to the poor packing of particles in the powder bed. Comparing with our work, especially the formulation with 10 wt.% of PVA, we were able to reach 37 % of relative geometrical density in the green part and 55 % of relative geometrical density in the sintered part, corresponding to 70 % of relative density measured by Archimedes method. One of the reasons is related with the particle size which was < 100 μm in the work of Maleksaeedi *et al.* [10], and < 80 μm in our work. As explained by the authors, one of the sources of porosity is the low packing of the powders in the powder bed, which increases when we decrease the particle size.

Shanjani *et al.* [12] showed a retraction, after sintering, in the planar direction of 17 %, in the binder jet printing of calcium polyphosphate with 10 wt.% of PVA. The retraction measured by the group used the dimensions of the green part as reference, while in our work we presented the retraction using the CAD file dimensions. If we use the same reference and the same amount of binder, we observe that we reached the same value of linear retraction (17 %) in the planar (diameter) direction.

Although this work shown to be possible to produce porcelain parts by BJP using PVA as *in-bed* binder, defects were observed for all the formulations tested in this work, for the initial layers of the binder jet printing process. These defects, as presented in Figure 3.22, lead to layer shifting by action of the roller. The defect was observed only in the initial layers of each print and it is the reason that the length variation of the printed cylinders was not evaluated in this work, because it would be mainly affected by this defect. In this sense, further investigation should be done in order to improve the printability, i.e., produce defect free porcelain parts, of porcelain powder feedstock with PVA as *in-bed* binder in binder jet printing process.

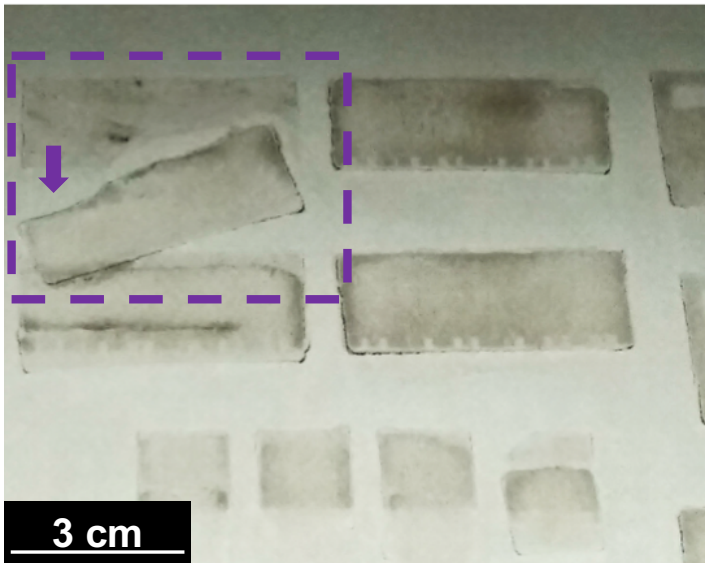


**Figure 3.22:** Layer shifting in binder jet printing of porcelain powders formulation. Occurring during the initial layers of each printing test.

## 3.4. Conclusions

In this work we studied the use of the *in-bed* binder for the production of porcelain parts by binder jet printing at industrial scale. To achieved so, we studied four different water soluble *in-bed* binders: PVA, maltodextrin, sodium alginate and CMC. Although it was possible to produce porcelain printed parts with all the *in-bed* binders, the fiber type shaped particles of CMC jeopardize the printing process, leading to the obstruction of the printheads, and as consequence, defective parts due to the lack of deposition of the liquid binder. Also, broken design features were observed after industrial sintering, such as low angle overhangs, and it was attributed to two main reasons: i) low green relative density of printed parts with PP-5Algin and PP-5CMC feedstock and ii) multistep thermal degradation associated with high burning rates of sodium alginate and CMC as *in-bed* binders. In this sense, PVA and maltodextrin are the most suitable *in-bed* binders for porcelain parts production due to comparable densification and thermal behavior, leading to almost defect free sintered parts. However, due to the industrial application of this work, allied to the fact that PVA binders are already used for porcelain conventional production, PVA was chosen as *in-bed* binder for porcelain powder formulations, to study the possibility to print parts with design features such as overhangs and wall thicknesses.

The defects observed for parts produced with high amount of PVA were attributed to the poor dry mixing of porcelain and PVA powders, and to the excessive porosity in the sintered

parts. While the low amount of PVA lead to green parts with mechanical strength. In this sense, with intermediate amounts of PVA (10 - 15 wt.%) it was possible to print parts with lower wall thickness (1 mm), while low angle overhangs (< 30 °) showed to have deformation during sintering for all the formulations studied. However, the 90 wt.% of porcelain with 10 wt.% of PVA shown to have the best combination of design features and relative density of sintered parts, among the several formulations studied.

## 3.5. References

[1] D. de Britto and O. B. G. Assis, “Thermal degradation of carboxymethylcellulose in different salty forms,” *Thermochim. Acta*, vol. 494, no. 1–2, pp. 115–122, 2009.

[2] T. Sugama and T. Pyatina, “Effect of sodium carboxymethyl celluloses on water-catalyzed self-degradation of 200 °c-heated alkali-activated cement,” *Cem. Concr. Compos.*, vol. 55, pp. 281–289, 2015.

[3] J. P. Soares, J. E. Santos, G. O. Chierice, and E. T. G. Cavalheiro, “Thermal behavior of alginic acid and its sodium salt,” *Eclet. Quim.*, vol. 29, no. 2, pp. 57–63, 2004.

[4] Z. Peng and L. Xue, “A thermal degradation mechanism of polyvinyl alcohol / silica nanocomposites,” vol. 92, 2007.

[5] L. Co, J. Kim, and H. Lee, “Thermal and Carbothermic Decomposition of Na 2 CO 3 and,” vol. 32, no. February, pp. 17–24, 2001.

[6] J. Suwanprateeb, R. Sanngam, and T. Panyathanmaporn, “Influence of raw powder preparation routes on properties of hydroxyapatite fabricated by 3D printing technique,” *Mater. Sci. Eng. C*, vol. 30, no. 4, pp. 610–617, May 2010.

[7] G. Marchelli, M. Ganter, and D. Storti, “New material systems for 3D ceramic printing,” in *Solid Freeform Fabrication Symposium*, 2009, pp. 477–487.

[8] R. Chumnanklang, T. Panyathanmaporn, K. Sitthiseripratip, and J. Suwanprateeb, “3D printing of hydroxyapatite: Effect of binder concentration in pre-coated particle on part strength,” *Mater. Sci. Eng. C*, vol. 27, pp. 914–921, May 2007.

[9] S. C. Cox, J. A. Thornby, G. J. Gibbons, M. A. Williams, and K. K. Mallick, “3D printing of porous hydroxyapatite scaffolds intended for use in bone tissue engineering applications,” *Mater. Sci. Eng. C*, vol. 47, pp. 237–247, 2015.

[10] S. Maleksaeedi, H. Eng, F. E. Wiria, T. M. H. Ha, and Z. He, “Property enhancement of 3D-printed alumina ceramics using vacuum infiltration,” *J. Mater. Process. Technol.*, vol. 214, no. 7, pp. 1301–1306, 2014.

[11] A. Zocca, P. Lima, and J. Günster, “LSD-based 3D printing of alumina ceramics,” *J.*

*Ceram. Sci. Technol.*, vol. 8, no. 1, pp. 141–148, 2017.

[12] Y. Shanjani, Y. Hu, R. M. Pilliar, and E. Toyserkani, “Mechanical characteristics of solid-freeform-fabricated porous calcium polyphosphate structures with oriented stacked layers,” *Acta Biomater.*, vol. 7, no. 4, pp. 1788–1796, Apr. 2011.

# *Chapter 4: Printability of porcelain powders in Binder Jet Printing*

**Abstract of the chapter**

In the previous chapter the role of the in-bed binders was assessed and PVA was identified, among the binders studied, as the in-bed binder to use in the binder jet printing of industrial porcelain parts. However, the printed porcelain parts were not defect free and further studies are needed in order to improve the printability of porcelain powders feedstock, i.e., produce defect free parts. In this sense, this chapter focus on the influence of the particle size of the feedstock as well as the role of heat treatment to the feedstock powders. Our observations reveal that large particles of the in-bed binder (100-150 μm) leads to clog of the printhead, jeopardizing the liquid binder deposition and as consequence, defective parts. We also found that large porcelain particles, which tend to be spherical, have higher flowability than the fine ones, promoting layer shifting during the printing process, and as consequence, lead to defective parts as well. On the other hand, the beneficial of the heat-treated porcelain powders use in the feedstock was clearly observed to eliminate design defects in the final parts. The heat treatment of porcelain powders transforms the porcelain agglomerates into aggregates, preventing its deagglomeration during the liquid binder deposition. This fact improves the printability of porcelain powders feedstock leading to defect free industrial porcelain parts produced by binder jet printing.

**Keywords of the chapter**

Printability, industrial porcelain powders, binder jet printing, additive manufacturing, ceramics

## 4.1. Introduction

Powders for AM techniques should fulfill requirements regarding properties such as particle size distribution, morphology and flowability, as described in Chapter 1. These properties are described in the literature as the ones more impactful both in the process itself and in the properties of green and final parts, such as porosity, density, mechanical behavior and dimensional stability. In addition, printability of powders was defined as the ability to produce design defect free objects by AM. As described in the previous chapter, the parts produced by BJP using raw porcelain powders lead to parts with defects due to layer shifting.

In this chapter we study the printability of feedstock with industrial porcelain powders, i.e., the ability to produce defect free printed parts, namely addressing the effect of the powder feedstock characteristics, as particle size distribution and heat treatment of the powders on the HR and free settled density of the powders formulations, and on the relative density of the green and sintered defect free porcelain parts.

## 4.2. Materials and methods

Spray dried industrial porcelain powders were produced and provided by *Porcelanas da Costa Verde, Portugal* using the conditions described in Chapter 2. In this chapter industrial raw porcelain powders and heat-treated porcelain powders were used and, based on the results of the previous chapter, 15 wt.% of Polyvinyl Alcohol (Zschimmer & Schwarz), PVA, was used as the *in-bed* binder in all feedstock formulations, prepared according to the procedure described in Chapter 2. Both raw and heat-treated porcelain powders were characterized regarding their thermal behavior, specific surface area, particle size distribution and crystallographic phases using the procedura described in Chapter 2.

For comparison purposes, ZP131 (3D Systems, USA) [1], ZP140 (ZCorporation, USA) [2] and VisiJet PXL Core (3D Systems, USA) [3] commercial powders for BJP were also characterized and used as reference powders. These powders are plaster based powders and are used by *Porcelanas da Costa Verde, Portugal*, for prototyping parts, using the BJP printer ZPrinter 650 (ZCorporation, USA).

The Taguchi method was used to study the influence of the particle size distribution of the components of the feedstock formulation for binder jet printing. In this sense, raw porcelain powders, heat-treated porcelain powders and PVA powders were individually dry sieved using 100 - 150 μm (defined as coarse), 100 - 80 μm (defined as medium) and Base - 80 μm (defined as fine) granulometric intervals, as presented in Figure 4.1. The feedstocks were prepared as described in Chapter 2, using 42,5 wt.% of raw porcelain powders, 42,5 wt.% of heat-treated porcelain powders and 15 wt.% of PVA, using the array of combination presented in Table 4.I.

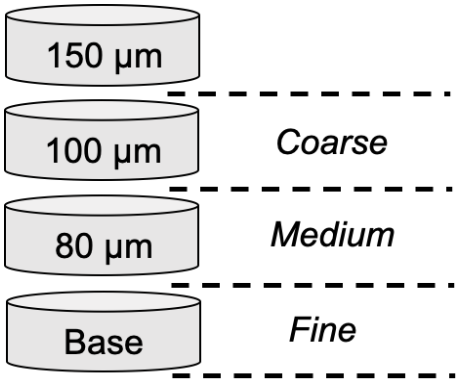


**Figure 4.1:** Granulometric cuts, 100 - 150 µm (coarse), 100 - 80 µm (medium) and base - 80 µm (fine), of raw porcelain powders, heat-treated porcelain powders and PVA powders, for the Taguchi study.

**Table 4.I:** Array of combination of three different powders (raw, heat-treated and PVA) with three different granulometric cuts (fine, medium, coarse), used for the Taguchi method. The powders were dry mixed using the following amounts: 42,5 wt.% of raw porcelain powders, 42,5 wt.% of heat-treated porcelain powders and 15 wt.% of PVA powders.

| Feedstock | Raw | Heat-treated | PVA |
|---|---|---|---|
| T1 | Fine | Fine | Fine |
| T2 | Fine | Medium | Medium |
| T3 | Fine | Coarse | Coarse |
| T4 | Medium | Fine | Medium |
| T5 | Medium | Medium | Coarse |
| T6 | Medium | Coarse | Fine |
| T7 | Coarse | Fine | Coarse |
| T8 | Coarse | Medium | Fine |
| T9 | Coarse | Coarse | Medium |

The individual materials after the granulometric cut were characterized regarding its Hausner Ratio, free settled density, particle size distribution and shape, using the procedure described in Chapter 2. In addition, the Hausner Ratio of the prepared feedstocks was also assessed using the procedure described.

Fine powders (0 - 80 μm) of raw porcelain, heat-treated porcelain and PVA, were used to study the influence of heat-treated powders in the printability if porcelain. The feedstocks were prepared using the procedure described in Chapter 2 producing the feedstock formulations presented in the Table 4.II. The *in-bed* binder (PVA) amount was 15 wt.% for all the formulations.

**Table 4.II:** Feedstock formulations prepared for the study of the heat-treated (HT) porcelain powders effect, using fine (0 - 80 μm) powders of raw porcelain, heat-treated porcelain and PVA.

| **Feedstock formulation** | **Porcelain (total: 85 wt.%)** | |
|---|---|---|
| | **HT (%)** | **Raw (%)** |
| 100HT | 100 | 0 |
| 75HT | 75 | 25 |
| 50HT | 50 | 50 |
| 25HT | 25 | 75 |
| 0HT | 0 | 100 |
| | **PVA (total: 15 wt.%)** | |

The Hausner Ratio and free settled density of the feedstocks were analysed using the procedure described in Chapter 2. In addition, the time absorption of the liquid binder by the 0HT and 100HT feedstocks was assessed using the procedure described as well in the Chapter 2.

Printing was performed in a ZPrinter 650 (ZCorp) as described in Chapter 2, and cylindrical parts (Figure 4.2 A) were produced to evaluate the density and shrinkage of the green and sintered printed parts. To assess printability and to evaluate designs limitation, a cube (Figure 4.2 B) and parts with different length bridges (Figure 4.2 C) were also printed and processed. The diameter variation ($\Delta D$), the geometric density ($\rho_{geom}$) and relative geometric density ($\%\rho_{geom}$) were assessed using the procedure described in chapter 2.

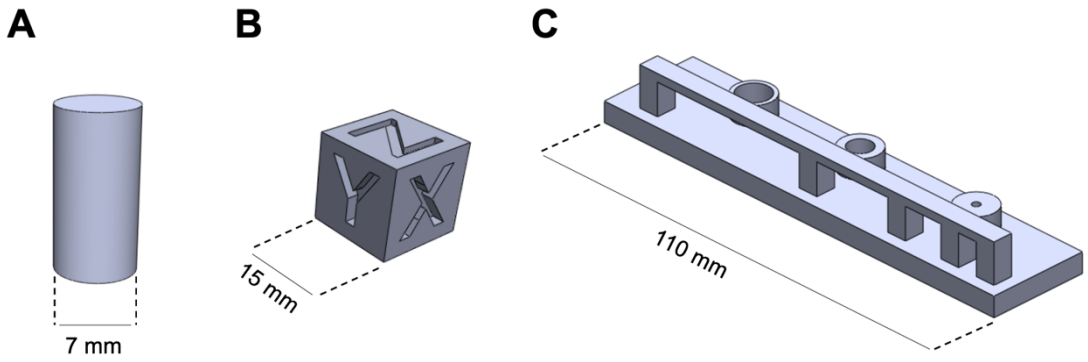


**Figure 4.2:** Representative image of the virtual design of (A) cylinders, (B) a cube with 15x15x15 mm dimensions and (C) a part with different bridges lengths: 40 mm, 20 mm, 10 mm and 5 mm, from left to right, respectively. These designs were used to evaluate relative density, dimension variations and evaluate the printability of the feedstocks.

The printed parts were sintered in an industrial continuous kiln of Costa Verde, Portugal, using a maximum temperature of 1345 ºC, measured with process temperature control rings, PTCR-STH (Ferro Corporation), for a total time cycle of 5 h 30 min. The sintered cylinders were characterized regarding its geometrical relative density ($\%\rho_{geom}$), water absorption (WA), apparent porosity (AP) and relative density using the Archimedes method ($\%\rho_{Arc}$), using the procedure described in Chapter 2. The microstructure of the printed parts was analysed by SEM as described in Chapter 2, as well.

## 4.3. Results and discussion

The microstructure of the particles of raw and heat-treated porcelain powders are presented in Figure 4.3. Both powders are similar and show spherical and irregular shaped particles. In terms of particle size distribution (PSD) both raw and heat-treated porcelain powders present a similar curve, as exhibit in Figure 4.4. Both powders have mainly a monomodal PSD peaking at 118 μm. There is however a minor peak, observable for the PSD curve of raw powders, peaking at 13 μm, clearly pointing the presence of a finer particles fraction. This shoulder is not visible for the heat-treated powders curve. This absence is accompanied by an increase of the peak intensity at 118 μm from 9,9 % for the raw powders curve to 11,4 % for the heat-treated powders curve, and by a narrower curve for the heat-treated powders than the one of raw powders as the value of Dv10 increases from 50 μm (raw) to 57 μm (heat-treated) and the value of Dv90 decreases from 233 μm (raw) to 210 μm (heat-treated), as exhibited in Table 4.III. This is an indication that fine particles

of the raw porcelain powders have reacted and became aggregated during the heat treatment.

The differences in the PSD curves of the powders, mainly the reduction in the fraction of finer particles, have impact in the HR and free settled density of the powders, as heat-treated powders present a lower HR (1,22 ± 0,01) than the raw powders (1,26 ± 0,02), while the free settled density also decreases from 0,94 ± 0,01 g/cm$^3$ to 0,87 ± 0,01 g/cm$^3$. The SSA analysis showed values of 9,7 m$^2$/g for the raw porcelain powders and 6,6 m$^2$/g supporting the previous results.

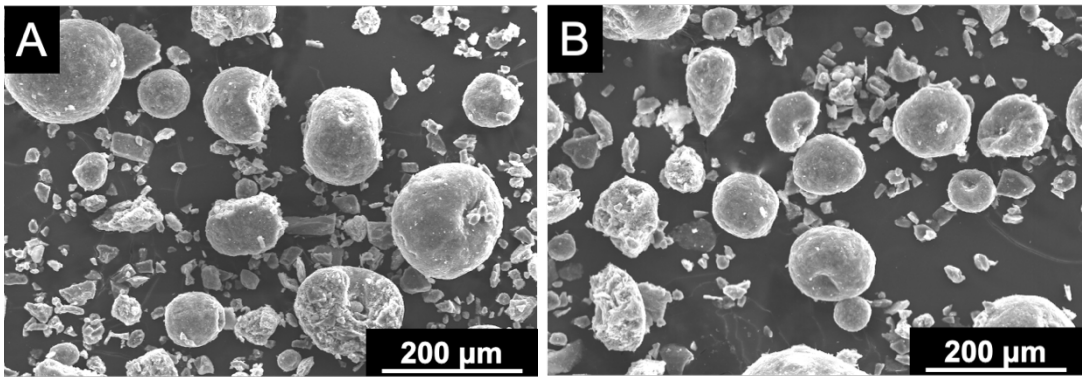


**Figure 4.3:** SEM micrograph of (A) raw and (B) heat-treated (B) porcelain powders, exhibiting both irregular and spherical shaped particles.

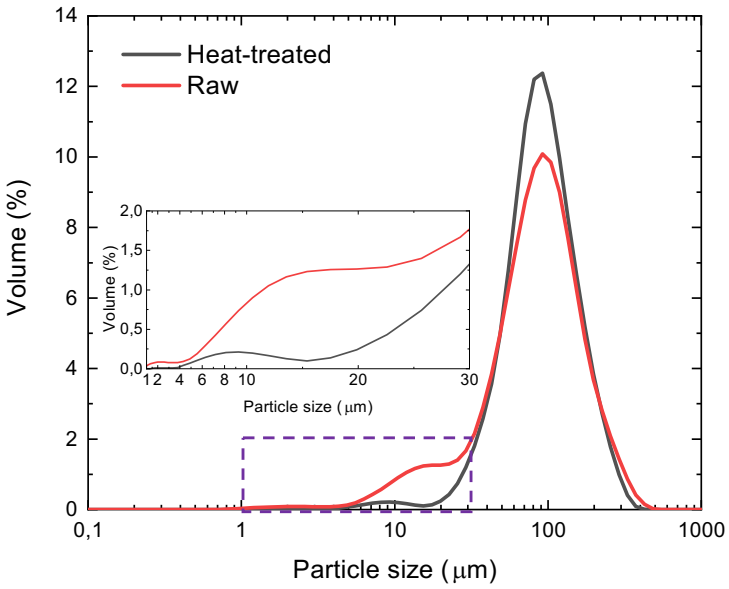


**Figure 4.4:** Particle size distribution of raw and heat-treated porcelain powders in dry state. The inset of the graph zooms the region between 1 and 30 μm.

**Table 4.III:** Dv10, Dv50 and Dv90 values from the particle size distribution curves of raw and heat-treated porcelain powders, measured in dry state.

| | **Raw** | **Heat-treated** |
|---|---|---|
| Dv10 (μm) | 51 | 57 |
| Dv50 (μm) | 110 | 112 |
| Dv90 (μm) | 233 | 210 |

With the heat treatment at high temperature, as 1000 °C, matter diffusion may occur within the initial porcelain powders agglomerates originating stronger bonds between the particles and the agglomerates originate aggregates, as schematically represented in Figure 4.5. The small particles and agglomerates of raw powders with high reactivity tend also to react among them, forming aggregates. As consequence, the ratio of small particles tends to decrease, as well seen in the PSD curve (Figure 4.4).

The main difference between agglomerates (raw porcelain powders) and aggregates (heat-treated porcelain powders) regards on bond strength between the particles inside each one, where the aggregates have stronger bonds among the particles as compared with the

agglomerates [4]. This is supported by the PSD analysis (Figure 4.6), where both powders were analyzed in dry state and in water medium. It is possible to observe that the raw powders deagglomerate once they are in water, while the heat-treated powders have similar PSD curves both as in dry and wet state.

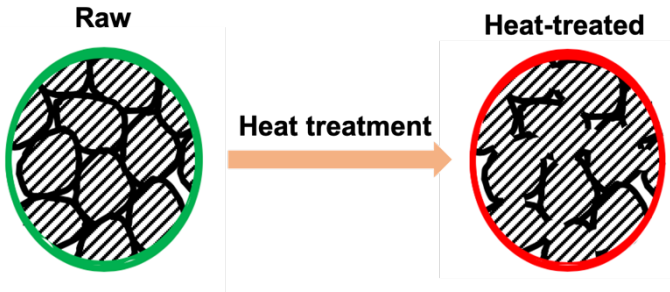


**Figure 4.5:** Schematic representation of changes inside the agglomerates of spray dried raw powders during heat treatment, with the formation of aggregates resulting from the matter diffusion and bond creation under the high temperature treatment. Simultaneously, the small individual particles or agglomerates react as well.

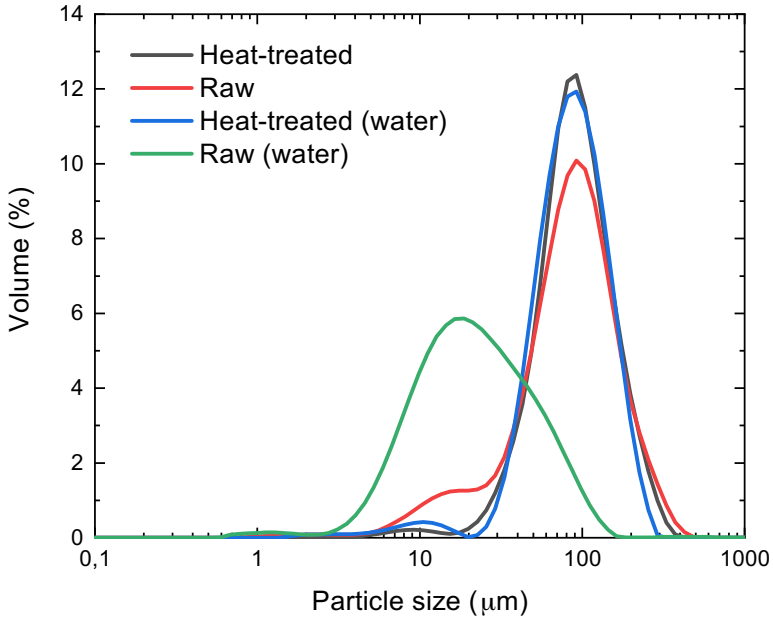


**Figure 4.6:** Particle size distribution of raw and heat-treated porcelain powders in dry state and in water medium. The main difference among the curves concerns in the raw porcelain powders measured in water medium, leading to deagglomeration and as consequence, increase the small particles fraction.

Figure 4.7 shows the diffractograms of raw and heat-treated porcelain powders. The difference between both powders resides mainly in the presence of the kaolinite phase in the raw powders. As expected, during the heat treatment of the powders, the kaolinite transforms into metakaolin, by dihydroxylation [5][6]. This transformation occurs around 550 °C, corresponding to the endothermic reaction illustrated in Figure 4.8. The thermogravimetric analysis (Figure 4.9) exhibits a mass loss of around 6 % in the same range of temperature, corresponding mainly to the loss of hydroxyl groups for the case of raw powders and an almost loss free curve for the case of the heat-treated ones, as expected. At 573 °C the $\alpha$- to $\beta$-quartz inversion occurs followed by the exothermic transformation around 990 °C and corresponds to the transformation of metakaolin to a spinel-type structure and free silica [7][8]. As the temperature further increase for temperatures higher than 1075 °C the spinel structures transforms into mullite [5] and above 1200 °C the quartz starts to transform into cristobalite and the prismatic crystals of mullite growth. The common transformation in both powders is the reversible inversion of quartz $\alpha$ in quartz $\beta$. The XRD pattern depicted in Figure 4.7 evidences the presence of $SiO_2$ in the heat-treated powder.

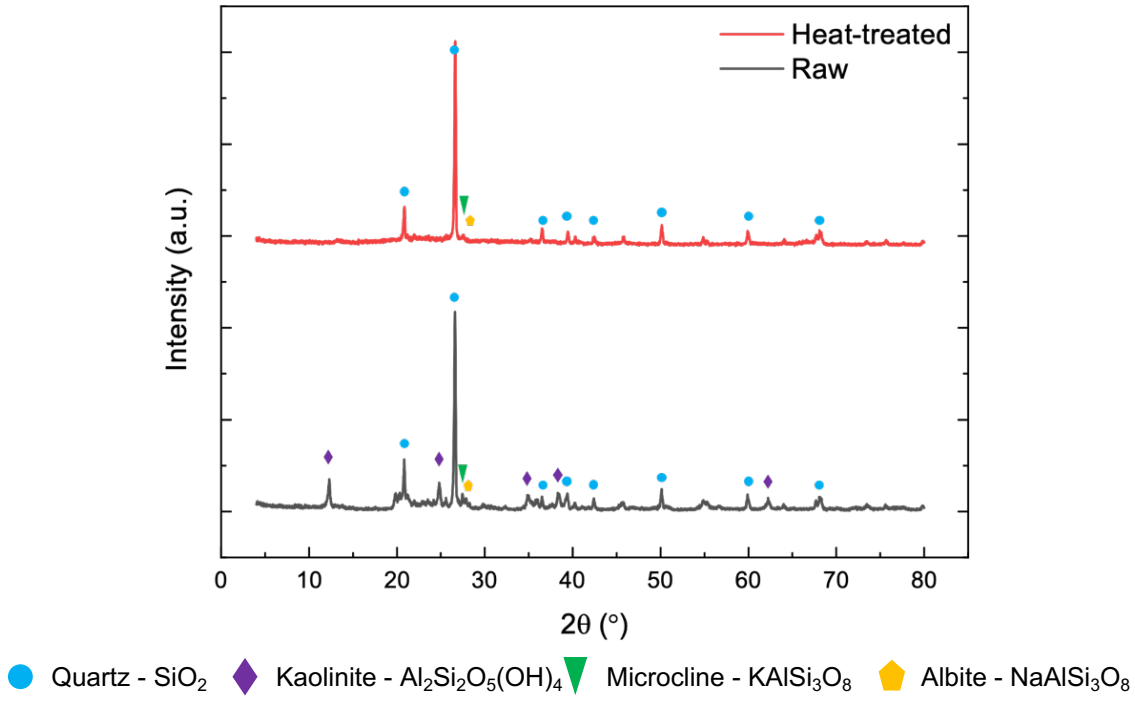


**Figure 4.7:** XRD patterns and phase identification of raw and heat-treated porcelain powders. The kaolinite phase was suppressed due to the heat treatment performed in the raw porcelain powders.

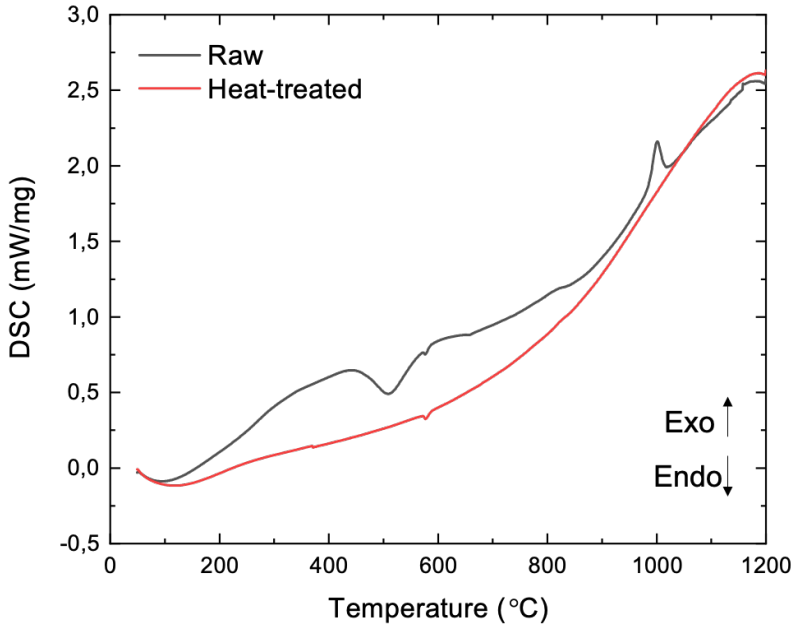


**Figure 4.8:** DSC analysis of raw (black) and heat-treated (red) porcelain powders, where the main differences regards on the transformations at 550 °C and at 990 °C for the raw powders, which were not visible for the heat-treated porcelain powders.

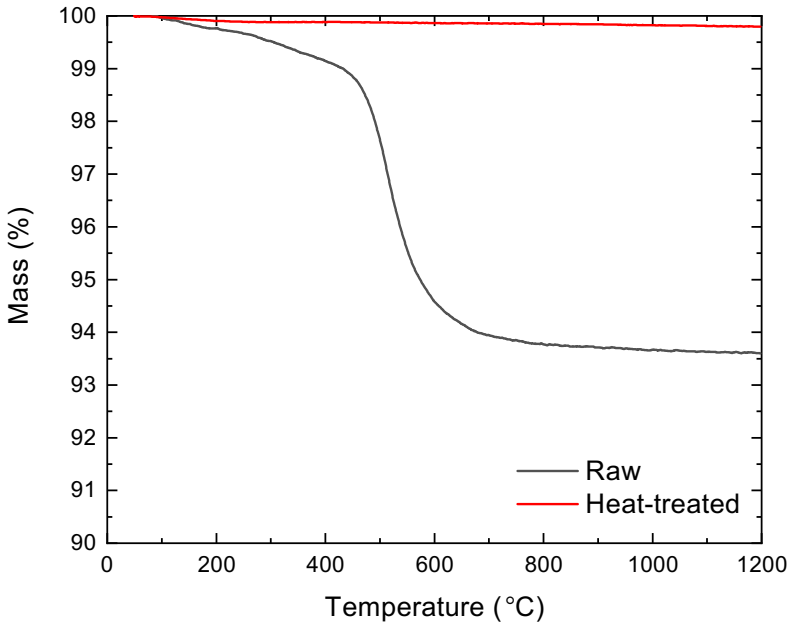


**Figure 4.9:** Thermogravimetric analysis of raw and heat-treated porcelain powders. The heat-treated powders (red curve) present near zero mass loss.

While the heat treatment performed in the raw porcelain agglomerates, turning into aggregates, do not change the morphology of the powders (Figure 4.3), it has an impact in

the PSD of the powders (Figure 4.4), with a decrease in the smaller particles fraction. As consequence, the HR and free settled density of powders also decrease and may have an impact in the printing process of these powders. In this sense, the commercial powders ZP131, ZP140 and VisiJet PXL were analyzed for comparison with both raw and heat-treated porcelain powders.

In Figure 4.10 SEM micrographs of the commercial powders for binder jet printing are presented. The three powders exhibit irregular shaped particles, however, in the case of Visijet PXL powder (Figure 4.10, C) small spherical particles are visible. In the case of the HR (Table 4.IV), the three powders present similar values varying from 1,20 ± 0,01 (ZP140) to 1,25 ± 0,01 (ZP131). Regarding the PSD of the commercial powders, depicted in Figure 4**.11**, the curves have a major peak at 48 µm (Visijet PXL), 55 µm (ZP131) and 71 µm (ZP140), accompanied by a shoulder for smaller particles (< 20 µm). For the three commercial powders studied the Dv10 value varied between 10 and 17 µm, while the Dv50 varied between 41 and 58 µm. In the case of Dv90 the difference is variation is higher, where VisiJet PXL exhibits a value of 81,6 µm while ZP131 and ZP140 exhibit 119 µm and 124 µm, respectively.

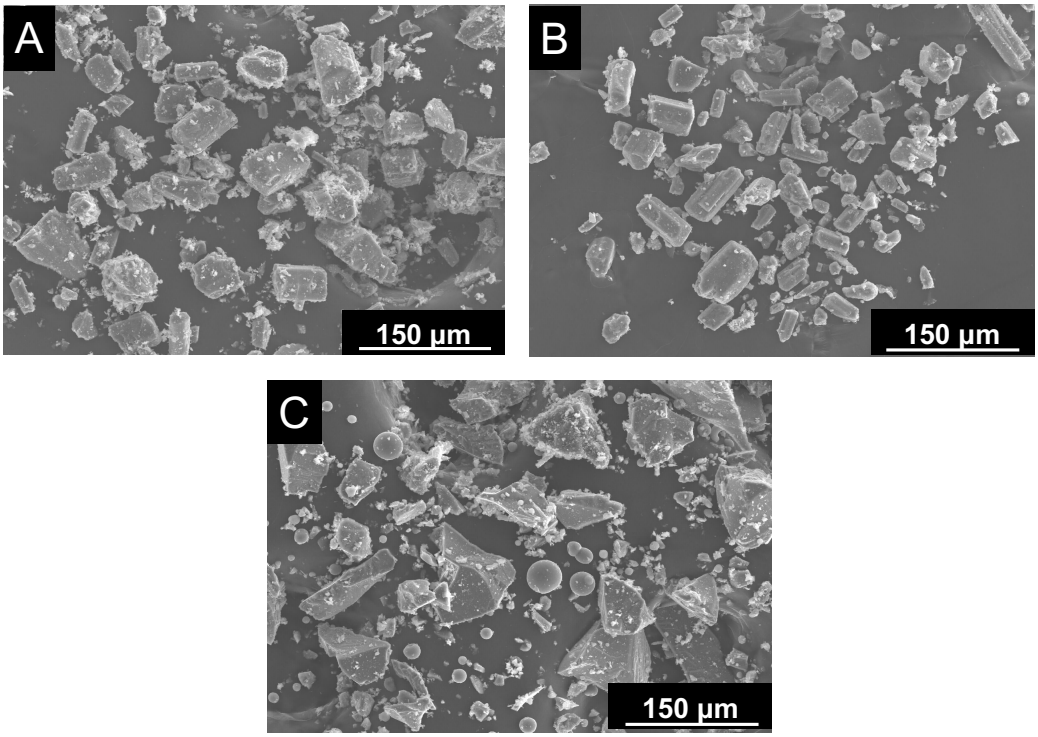


**Figure 4.10:** SEM micrographs of commercial powders for binder jet printing: (A) ZP140, (B) ZP131 and (C) Visijet PXL. The images present mostly irregular shaped particles for the commercial powders.

**Table 4.IV:** Hausner Ratio of commercial powders for binder jet printing.

| | **ZP140** | **ZP131** | **VisiJet PXL** |
|---|---|---|---|
| HR | 1,20 ± 0,01 | 1,25 ± 0,01 | 1,23 ± 0,01 |

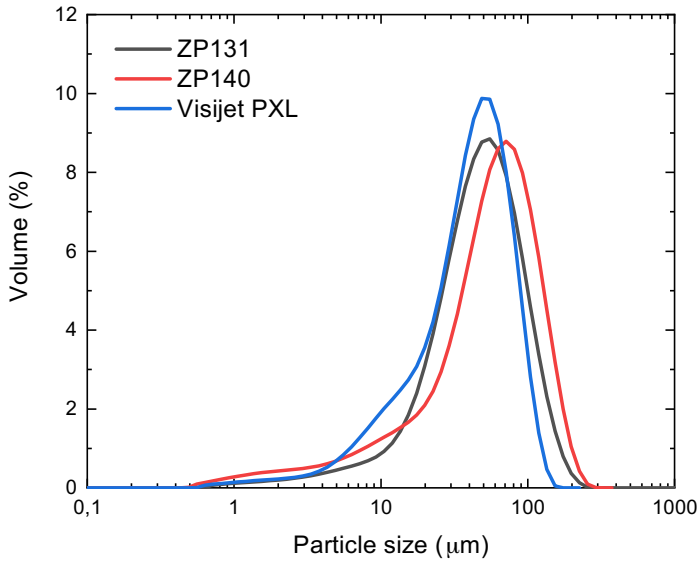


**Figure 4.11:** Particle size distribution, in the dry state, of the commercial powders for binder jet printing ZP131, ZP140 and Visijet PXL. The curves present mainly a monomodal distribution, with shoulders on the side of smaller particles.

**Table 4.V:** Dv10, Dv50 and Dv90 values from the particle size distribution curves of ZP131, ZP140 and Visijet PXL powders, measured in dry state.

| | **ZP140** | **ZP131** | **Visijet PXL** |
|---|---|---|---|
| Dv10 (μm) | 10 | 16 | 11 |
| Dv50 (μm) | 57 | 49 | 41 |
| Dv90 (μm) | 124 | 119 | 82 |

Comparing the morphology of the commercial powders for BJP (Figure 4.10) with the raw and porcelain powders (Figure 4.3) the main difference regards on the fact that both porcelain powders have spherical and irregular shaped particles, while the commercial powders have mostly irregular shaped particles. Concerning the HR, the porcelain powders exhibit values between 1,22 and 1,26, while the commercial powders have similar values, varying between 1,20 and 1,25.

The PSD is the main difference between the porcelain powders (Figure 4.4) and the commercial powders (Figure 4.11). As a general overview, both raw and heat-treated porcelain powders present powders with bigger particles than the ones of commercial

powders. The PSD curves of the porcelain powders peak at 118 µm, while the commercial powders exhibit the major peak at 48 µm (Visijet PXL), 55 µm (ZP131) and 71 µm (ZP140). The same trend is observed when comparing the Dv10 values lower than 20 µm for commercial powders (Table 4.V), while for porcelain powders the Dv10 values reach 50,6 µm (raw) and 56,9 µm (heat-treated). The Dv90 values for porcelain powders are higher than 210 µm, while for commercial powders are compressed between 80 µm and 125 µm.

Considering this discussion, the PSD of raw and heat-treated porcelain powders as produced may be not suitable for BJP, considering the PSD of commercial powders, and there is a need to sieve the powders in order to reach a PSD with finer particles.

### *4.3.1. Effect of particle size and particle size distribution*

With the objective to study the PSD effect in the printing process, the raw porcelain, heat-treated porcelain and PVA powders were sieved. The granulometric cuts were chosen considering the layer thickness used in the printing process, 100 µm, where the fine particles (< 80 µm) are lower than the layer thickness, the medium particles (80 - 100 µm) have a size similar to the layer thickness and the coarse particles (100 - 150 µm) have a size higher than the layer thickness.

Table 4.VI presents the HR and the $\rho_{free\ settled}$ of the different powders used in this part of the work. HR decreases with the increase of the particle size, in the three powders, while the $\rho_{free\ settled}$ does not have significant differences through the different particle sizes. Both raw and heat-treated porcelain powders present similar values for HR, decreasing from 1,38 to 1,10 and 1,34 to 1,10, respectively, with the increase of the particle size from fine to coarse powders. The raw porcelain powders (0,93 g/cm$^3$) and the heat-treated powders (0,90 g/cm$^3$) present similar values of free settled density. In the case of the PVA powders, the values are higher than the porcelain ones, presenting an HR of 1,44 for fine particles decreasing to 1,28 for coarse powders. The $\rho_{free\ settled}$ of the PVA powders are lower than the porcelain powders (< 0,76 g/cm$^3$). These differences in the HR are explained by the shape of the particles, as it is possible to observe in Figure 4.12. While the medium and coarse particles of the porcelain powders are spherical, in the case of PVA particles the shape is irregular, which decreases the flowability of the powder and the increase of the HR.

Raw and heat-treated porcelain powders present spherical particles of medium and coarse granulometric cuts (Figure 4.12), while the fine ones of both porcelain powders, present spherical and irregular shaped particles. In the case of PVA, powders have irregular shape for the three granulometric cuts. The PSD of the raw (Figure 4.13) present bi modal curve for medium and coarse powders, while the fine powders present a broader monomodal distribution with a shoulder on the side of smaller particles. The coarse powders have major peak at 104 μm and a minor one at 17 μm, while the medium powders have a major peak at 81 μm and a minor one at 15 μm. The fine powders peaks at 48 μm, presenting also a shoulder for particles < 20 μm. When compared with the PSD of the raw porcelain starting powders (Figure 4.4) it is noticeable the increase in the smaller particles, due to the suppression of coarse particles through sieving. The increase of smaller particles after the granulometric cuts, occurs in the range of 13 μm, which is the range of a minor peak visible in the starting raw porcelain powders (Figure 4.4). In the case of heat-treated porcelain powders, the PSD curves (Figure 4.14) the curve of coarse powder presents monomodal distributions peaking at 104 μm, while the medium and fine powders present a bi-modal distribution peaking at 71 μm and 48 μm, respectively, with a minor peak under 10 μm. The same type of PSD was observed for the starting heat-treated porcelain powders (Figure 4.4), however, with different peaks positions, due to the granulometric cut. PVA exhibits bi-modal PSD (Figure 4.15) for medium and coarse powders, with a major peak at 104 μm and minor one at 20 μm, in the case of medium powders, and a major peak at 134 μm and a minor one at 23 μm for the coarse powders. The fine powders present a monomodal distribution, peaking at 63 μm, with a small shoulder for particles < 20 μm. Comparing the PSD curves of PVA with the ones of both porcelain powders, it is noticeable that PVA present powders with bigger particles for the same granulometric cuts. The raw porcelain powders (Figure 4.13) and the PVA ones (Figure 4.15) exhibit minor peaks for smaller particles, in the case of medium and coarse powders, which should pass through the mesh of the sieve, suggesting that the dry sieving process is not efficient is not efficient for these powders.

**Table 4.VI:** Hausner Ratio and free settled density of raw porcelain, heat-treated porcelain and PVA powders, used in the Taguchi method.

| Powder | Hausner Ratio | $\rho_{free\ settled}$ (g/cm$^3$) |
|---|---|---|
| Raw porcelain fine (< 80 µm) | 1,35 ± 0,02 | 0,92 ± 0,02 |
| Raw porcelain medium (80 - 100 µm) | 1,12 ± 0,01 | 0,93 ± 0,01 |
| Raw porcelain coarse (100 - 150 µm) | 1,10 ± 0,02 | 0,93 ± 0,02 |
| Heat-treated porcelain fine (< 80 µm) | 1,34 ± 0,01 | 0,88 ± 0,02 |
| Heat-treated porcelain medium (80 - 100 µm) | 1,12 ± 0,01 | 0,90 ± 0,01 |
| Heat-treated porcelain coarse (100 - 150 µm) | 1,10 ± 0,01 | 0,90 ± 0,01 |
| PVA fine (< 80 µm) | 1,44 ± 0,03 | 0,73 ± 0,05 |
| PVA medium (80 - 100 µm) | 1,36 ± 0,06 | 0,75 ± 0,03 |
| PVA coarse (100 - 150 µm) | 1,28 ± 0,03 | 0,76 ± 0,04 |

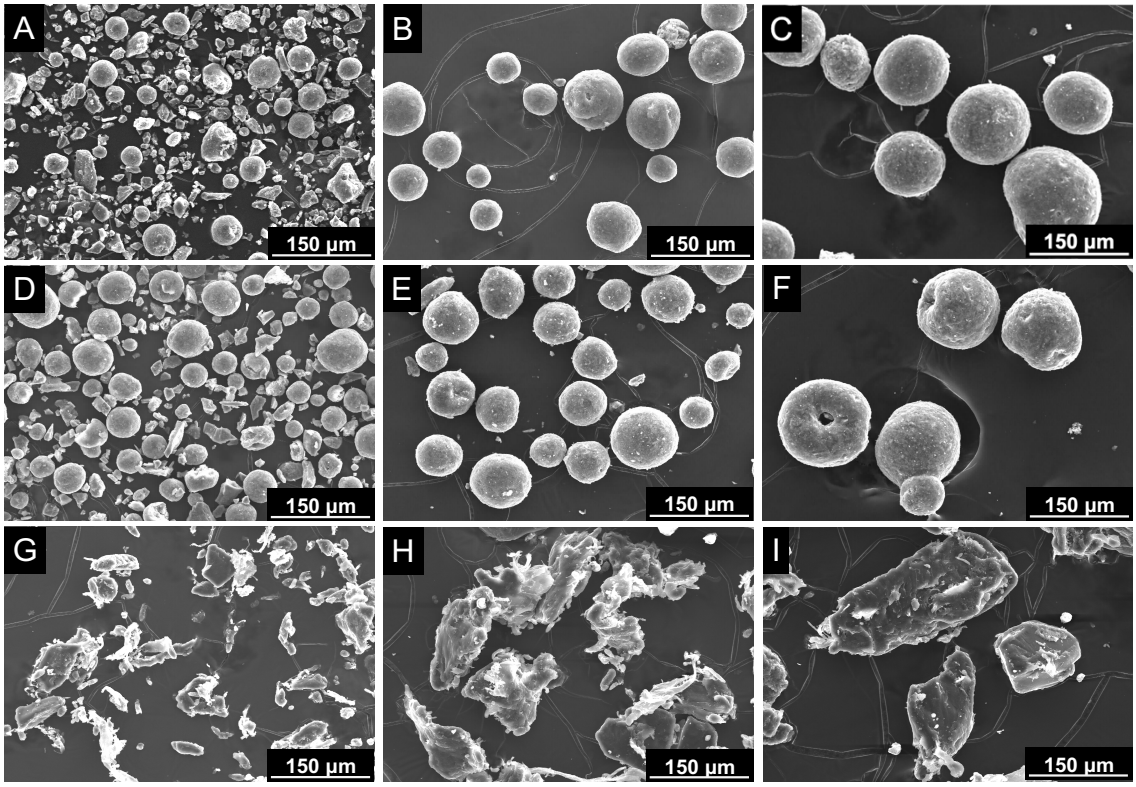


**Figure 4.12:** SEM micrograph of powders used in the Taguchi method: (A) Raw porcelain fine, (B) Raw porcelain medium, (C) Raw porcelain coarse, (D) Heat-treated porcelain fine, (E) Heat-treated porcelain medium, (F) Heat-treated porcelain coarse, (G) PVA fine,

(H) PVA medium and (I) PVA coarse. The porcelain powders present mostly spherical shaped particles for medium and coarse powders, while for finer particles there is both spherical and irregular particles. In the case of PVA, powders exhibit irregular shaped particles for the three granulometric cuts.

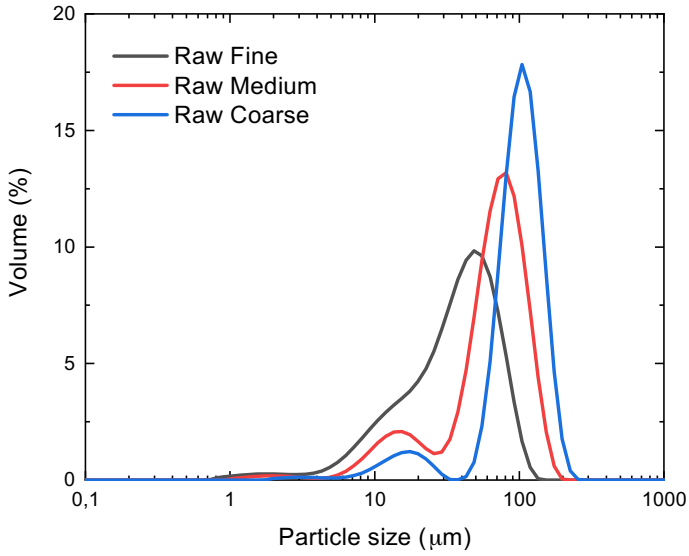


**Figure 4.13:** Particle size distribution, in the dry state, of raw porcelain powders for the Taguchi method. The coarse and medium powders present bi-modal distributions, while for fine powders the curve is monomodal with a shoulder in the smaller particles region.

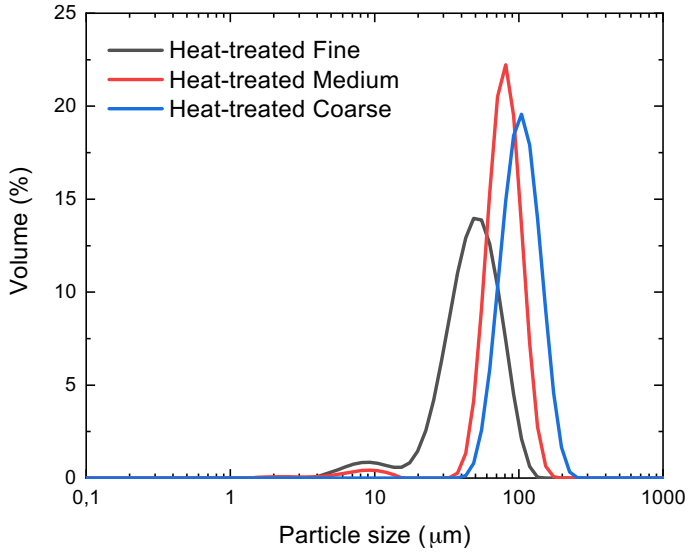


**Figure 4.14:** Particle size distribution, in the dry state, of heat-treated porcelain powders for the Taguchi method. The three granulometric cuts present a narrow monomodal distribution.

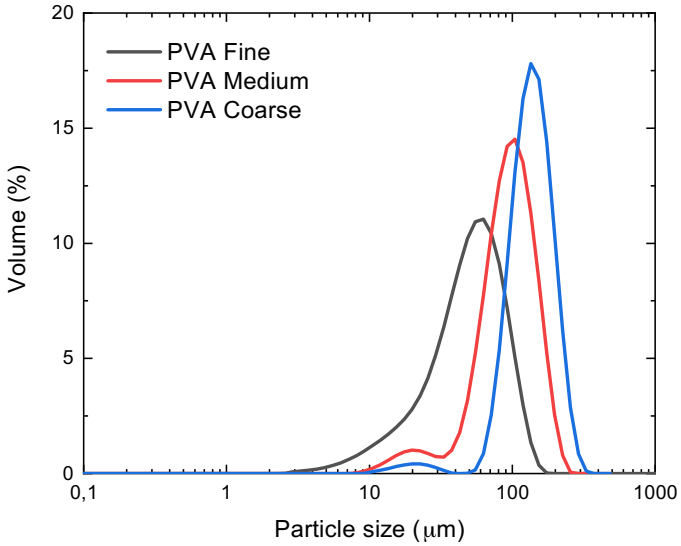


**Figure 4.15:** Particle size distribution, in the dry state, of PVA powders for the Taguchi method. The coarse and medium powders exhibit a bimodal distribution, while the fine powders exhibit a monomodal distribution with a broad peak.

Taguchi method was used to assess the effect of the PSD of raw porcelain, heat-treated porcelain and PVA powders in the HR of the feedstock for BJP. As presented before, fine,

medium and coarse particles, of each powder were dry mixed, using the composition of feedstock as described in Table 4.I. In Table 4.VII the HR values of the different formulations are presented. It is noticeable that the formulation T1, which has fine powders of the three components, has the higher HR (1,27), while the T9 formulation which has coarse powders of raw and heat-treated porcelain and medium powders of PVA presents the lowest HR (1,13). The rest of the formulations studied present HR between 1,16 and 1,19. In Figure 4.16 the effect of the particle size of each component (raw porcelain, heat-treated porcelain and PVA) in the HR of the porcelain powders formulations is presented. For each feedstock formulation of Table 4.VII, the respective granulometric cut (fine, medium and coarse) of each component (raw, heat-treated and PVA) was represented in the graph (Figure 4.16) and a linear influence was represented by lines. It is noticeable that with the increase of particle size, the trend is HR to decrease, for the three powders used. This is explained by the lower reactivity of bigger particles, leading to higher flowability and, as consequence, a decrease in the HR. It is also visible that heat-treated powders have higher influence in the HR, once the slope of the represented line (red) is higher than the one from raw and PVA powders.

**Table 4.VII:** HR measured for the feedstock formulations prepared according the Taguchi method, where fine (0 - 80 μm), medium (80 - 100 μm) and coarse (100 - 150 μm) granulometric cuts of raw porcelain, heat-treated porcelain and PVA powders were used.

| Sample | Raw (μm) | Heat-treated (μm) | PVA (μm) | Hausner Ratio |
|---|---|---|---|---|
| T1 | 0 - 80 | 0 - 80 | 0-80 | 1,27 |
| T2 | 0 - 80 | 80 - 100 | 80-100 | 1,19 |
| T3 | 0 - 80 | 100 - 150 | 100-150 | 1,17 |
| T4 | 80 - 100 | 0 - 80 | 80-100 | 1,19 |
| T5 | 80 - 100 | 80 - 100 | 100-150 | 1,16 |
| T6 | 80 - 100 | 100 - 150 | 0-80 | 1,19 |
| T7 | 100 - 150 | 0 - 80 | 100-150 | 1,19 |
| T8 | 100 - 150 | 80 - 100 | 0-80 | 1,19 |
| T9 | 100 - 150 | 100 - 150 | 80-100 | 1,13 |

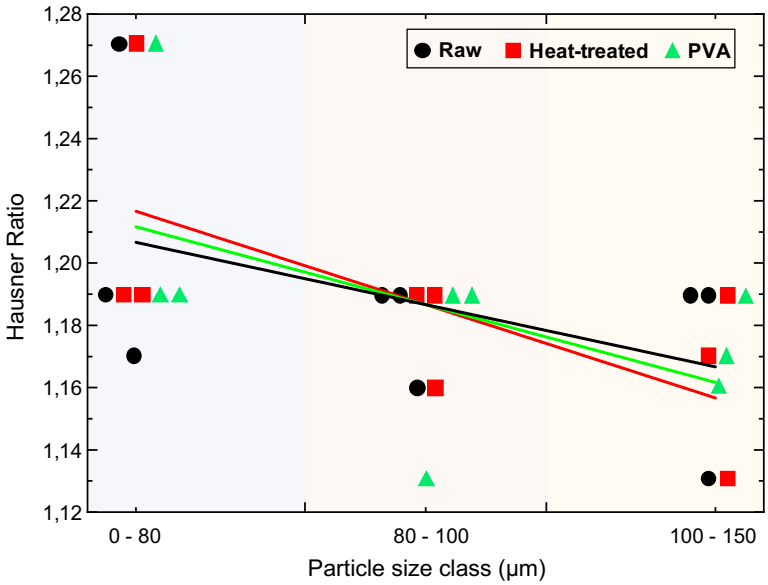


**Figure 4.16:** Effect of the particle size of each component in the Hausner Ratio of the porcelain powder formulation. For the three components, raw, heat-treated and PVA powders, with the increase of particle size class, the Hausner Ration tends to decrease.

Figure 4.17 presents the obtained part produced by binder jet printing, using T3, T5 and T7 feedstock formulations (Table 4.I) which have in common the use of coarse PVA powders. The object to be printed is a cube (Figure 4.2, B), however, as it is possible to observe, the part is highly damaged. This result is explained by the use of coarse PVA powders, with a size of 100 - 150 µm, while the layer thickness parameter used in the binder jet printing process is 100 µm. The fact that PVA particles are bigger than the layer thickness will promote the contact between these particles and the printhead of the binder jet printer, during the deposition of the liquid binder. The fact that PVA is water soluble and the printhead is depositing the liquid binder, leads to the clog of the printhead orifices jeopardizing the printing process. This effect is noticeable in Figure 4.18, where the printhead is presented before and after the printing process with T3, T5 and T7 formulations, and leads to defective liquid binder deposition, and as consequence, defective printed parts.

| Sample | Raw (µm) | Heat-treated (µm) | PVA (µm) | Hausner Ratio |
|---|---|---|---|---|
| T1 | 0-80 | 0-80 | 0-80 | 1,27 |
| T2 | 0-80 | 80-100 | 80-100 | 1,19 |
| T3 | 0-80 | 100-150 | 100-150 | 1,17 |
| T4 | 80-100 | 0-80 | 80-100 | 1,19 |
| T5 | 80-100 | 80-100 | 100-150 | 1,16 |
| T6 | 80-100 | 100-150 | 0-80 | 1,19 |
| T7 | 100-150 | 0-80 | 100-150 | 1,19 |
| T8 | 100-150 | 80-100 | 0-80 | 1,19 |
| T9 | 100-150 | 100-150 | 80-100 | 1,13 |

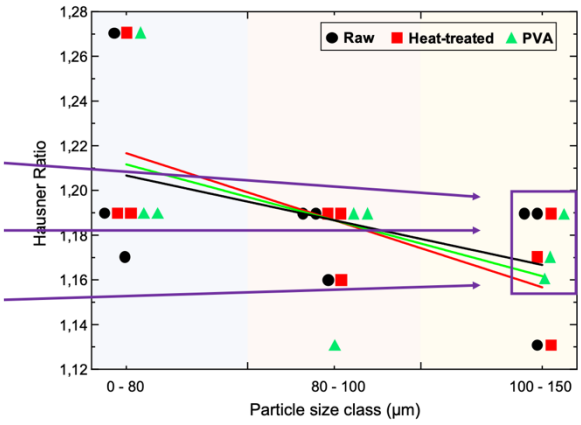


**Figure 4.17:** Printed part (cube) using T3, T5 and T7 formulations, which have in common the coarse particles of PVA powders.

**Figure 4.18:** Clean (left) and clogged (right) printhead during the binder jet printing of T3, T5 and T7 formulations, which have PVA coarse particles in their composition.

In Figure 4.19 a printed part, produced with T9 formulation is presented. The part exhibits a continuous defect due to layer shifting. As T9 formulations presents the lowest HR among the formulations prepared, it also means it has the highest flowability. In this case, the higher flowability of the powders, comparing with the other formulations, leads to layer shifting due to roller action, pushing the first layers forward, as schematically represented in Figure 4.20. Although this defect may happen during the whole printing process, it has higher impact in the initial layers. This is result of the lowest amount of powder in the bed, leading to lower resistance to movement by the printed part. Once the printing process continues and the number of printed layers increases, the higher amount of powders in front of the printed part prevents the part to keep moving by the roller action. This defect was also observed in the case of printing with T5 formulation, which presents a HR of 1,16, however in this case the defect was not as clear as for the printing with T9 formulation. Layer shifting was also observed by Sun *et al.* [9] with glass ceramics in BJP, but in this case the effect was only found for fine particles (< 25 μm).

| Sample | Raw (µm) | Heat-treated (µm) | PVA (µm) | Hausner Ratio |
|---|---|---|---|---|
| T1 | 0-80 | 0-80 | 0-80 | 1,27 |
| T2 | 0-80 | 80-100 | 80-100 | 1,19 |
| T3 | 0-80 | 100-150 | 100-150 | 1,17 |
| T4 | 80-100 | 0-80 | 80-100 | 1,19 |
| T5 | 80-100 | 80-100 | 100-150 | 1,16 |
| T6 | 80-100 | 100-150 | 0-80 | 1,19 |
| T7 | 100-150 | 0-80 | 100-150 | 1,19 |
| T8 | 100-150 | 80-100 | 0-80 | 1,19 |
| T9 | 100-150 | 100-150 | 80-100 | 1,13 |

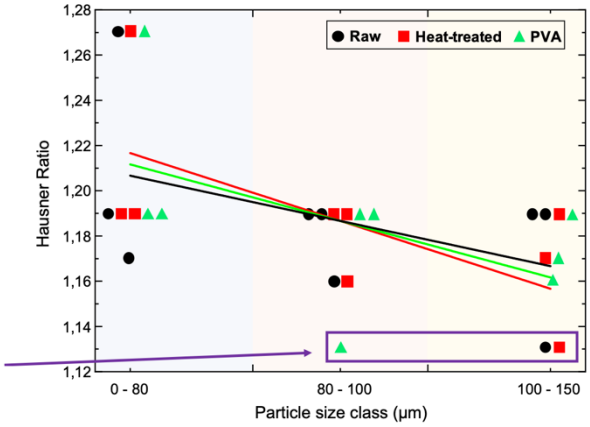


**Figure 4.19:** Printed part (cube) with T9 formulation, which exhibits the lowest Hausner Ratio and higher flowability.

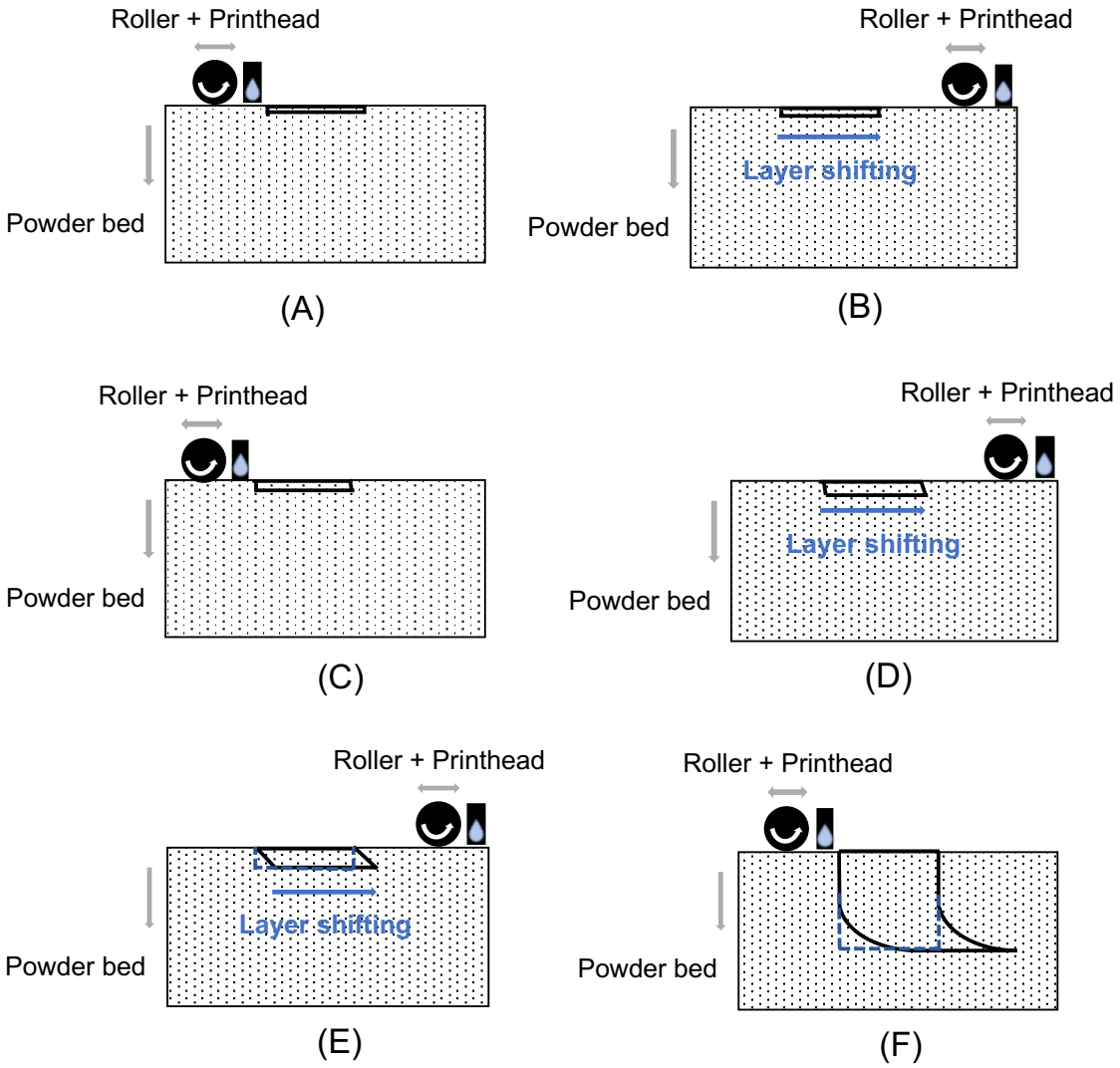


**Figure 4.20:** Schematic representation of layer shifting defect, formed during printing process, due to roller action and maximized by the higher flowability of powders.

With the T1 formulation, which is prepared using fine powders of raw and heat-treated porcelain and PVA, the printing process occurred without major defects in the printed part, as it is visible in Figure 4.21. As presented in Figure 4.12, the fine powders of raw and heat-treated porcelain have irregular shaped particles which prevent the spherical ones to move, as schematically represented in Figure 4.22. This fact leads to lower flowability, supported by the higher value of HR than with the other formulations, and eliminates the layer shifting defects observed in Figure 4.19.

| Sample | Raw (µm) | Heat-treated (µm) | PVA (µm) | Hausner Ratio |
|---|---|---|---|---|
| T1 | 0-80 | 0-80 | 0-80 | 1,27 |
| T2 | 0-80 | 80-100 | 80-100 | 1,19 |
| T3 | 0-80 | 100-150 | 100-150 | 1,17 |
| T4 | 80-100 | 0-80 | 80-100 | 1,19 |
| T5 | 80-100 | 80-100 | 100-150 | 1,16 |
| T6 | 80-100 | 100-150 | 0-80 | 1,19 |
| T7 | 100-150 | 0-80 | 100-150 | 1,19 |
| T8 | 100-150 | 80-100 | 0-80 | 1,19 |
| T9 | 100-150 | 100-150 | 80-100 | 1,13 |

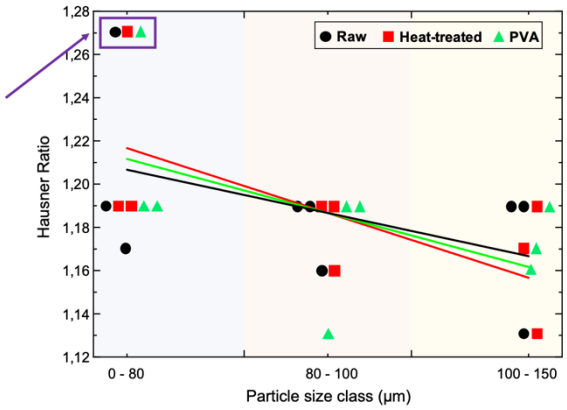


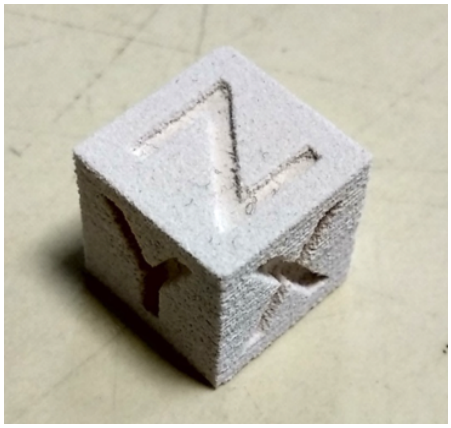

**Figure 4.21:** Printed part (cube) with the T1 formulation, presenting the highest Hausner Ratio.

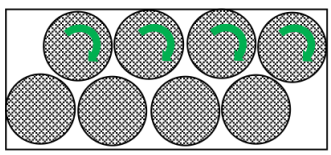

Powder bed with spherical particles

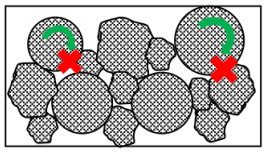

Powder bed with spherical and irregular particles

**Figure 4.22:** Schematic representation of the behavior of spherical and irregular shaped particles in the powder bed, where the irregular shaped particles prevent the spherical ones to roll, which leads to lower flowability of powders,

The use of finer particles lead to printed parts of porcelain without major defect, once it avoids the clog of the printhead as observed for feedstock formulations with coarse PVA particles (Figure 4.17), due to the fact that PVA particles are bigger than 100 µm, which is the layer thickness used and avoids the layer shifting defect as observed for feedstock formulations with low HR (Figure 4.19), due to the higher HR and worse flowability.

The printed parts with T2, T4, T6 and T8, which have medium size powders of raw porcelain, heat-treated porcelain and PVA showed low mechanical resistance to handling, breaking during the removal from powder bed of the printer. This fact may be attributed to the use of medium particles, as opposed in formulation T1, which was prepared using fine powders. As presented in Figure 4.12, the medium powders of raw and heat-treated porcelain exhibit mainly spherical particles. Spherical particles in a green part will have low initial surface contact area between particles, leading to lower mechanical resistance [10]. This is especially important in green parts produced by BJP which have lower density when compared with other production processes.

The printing test with T1 formulation, which was prepared with fine powders of raw porcelain, heat-treated porcelain and PVA, exhibited better results (Figure 4.21) than the tests printing with the other formulations (T2 - T9), since the printed part (cube) retained its shape as it should and did not break during the removal from the powder bed. In this sense, the use of fine (< 80 μm) particles is more suitable for the binder jet printing of porcelain powders than the use of formulations with medium (80 - 100 μm) and coarse (100 - 150 μm) powders.

Although the use of porcelain and PVA particles with the granulometric cut at 80 μm, proved to lead to defect free printed parts, it was observed in Chapter 3 that the use of only raw porcelain and PVA powders may lead to defective parts. The T1 formulation was prepared using 42,5 wt.% of raw porcelain powders, 42,5 wt.% of heat-treated porcelain powders and 15 wt.% PVA. However, it is not clear that a ratio of 50/50 of raw porcelain and heat-treated porcelain leads to the best results, and in this sense, there is a need to study the amount of raw and heat-treated porcelain powders in the feedstock formulations for industrial binder jet printing of porcelain.

### *4.3.2. Effect of heat-treated porcelain powders in the printability*

As presented in Table 4.II, feedstock formulations with different ratios of raw porcelain powders and heat-treated porcelain powders were prepared, after a granulometric cut at 80 μm. All the formulations were produced using 15 wt.% of PVA powders after the granulometric cut at 80 μm.

In Figure 4.23 and Figure 4.24 the free settled density and the HR of feedstock formulations with different amounts of heat-treated porcelain powders are presented. The free settled density varies from 0,66 ± 0,00 g/cm$^3$ for 0HT and 100HT feedstock formulations and reaches a maximum of 0,71 ± 0,00 g/cm$^3$ for 50HT feedstock formulation. In the case of HR the 0HT exhibits the maximum value (1,38 ± 0,01) and a minimum value was found for the 50HT formulation (1,32 ± 0,01).

The main observation regards in the 50HT which presents the lowest HR, and as consequence, the highest flowability of powders among the formulations presented. This fact leads to the highest free settled density observed in these results. Considering the error values for the formulations 50HT, 75HT and 100HT, the difference of the HR among them are not significative, however a relation with the increase of the heat-treated porcelain powders amount is visible, suggesting that the heat-treated powders may improve the flowability of the feedstock.

Among these three feedstock formulations (50HT, 75HT and 100HT) the highest free settled density is observed for the 50HT formulation, which is the one with the highest amount of raw porcelain powders. Although the 0HT formulation did not present the highest value of free settled density, the raw porcelain powder, with a granulometric cut at 80 µm, exhibits a slightly higher free settled density value (0,92 ± 0,02 g/cm$^3$) than the heat-treated porcelain powder with the same granulometric cut (0,88 ± 0,02 g/cm$^3$), as presented in Table 4.VI. This fact explains the higher free settled density of 50HT than the ones for 75HT and 100HT, due to the higher amount of raw porcelain powder.

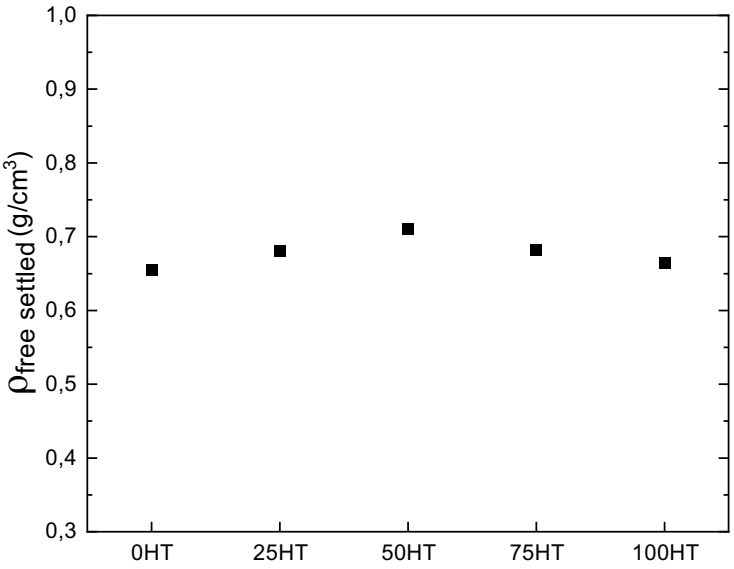


**Figure 4.23:** Free settled density of porcelain powders formulations with different amounts of raw and heat-treated porcelain powders. The graph exhibits a maximum for the 50HT formulation.

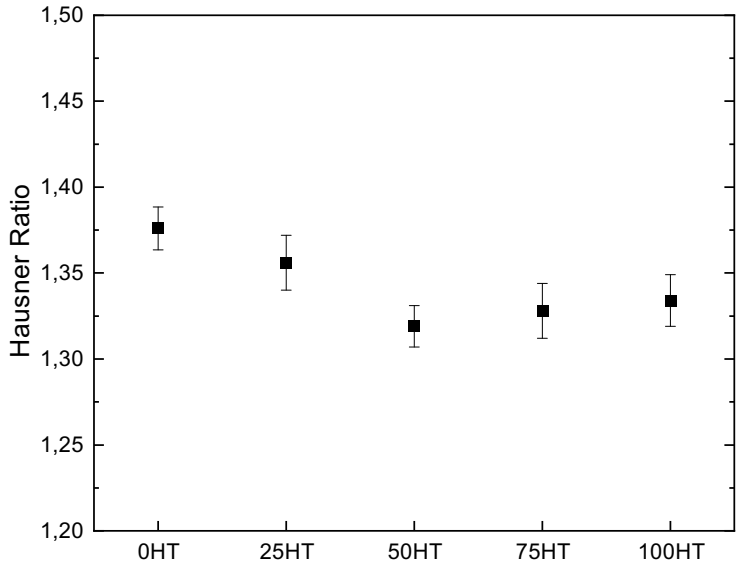


**Figure 4.24:** Hausner Ratio of porcelain powders formulations with different amounts of heat-treated and raw porcelain powders. The formulations exhibit a trend of lower HR for 50HT, 75HT and 100HT, which have higher amount of heat-treated porcelain powders.

During the binder jet printing process, an effect was observed in the 0HT formulation (high amount of raw porcelain powders). After the deposition of the liquid binder, the powder in

the powder bed, slightly raises above the powder bed surface, and by the roller action, the initial layers of the printed part are moved forward in the powder bed, as identified by the dash red circle (initial position) and the solid red circle (final position) in Figure 4.25. In the same figure are also identified green solid circles, which exhibit printed parts (in the case cylinders) for which this defect was not observed, suggesting that in these cases the powder did not raise above the powder bed surface enough to be moved by roller action.

This defect was assuaged in the case of the 25HT and eliminated in the case of 50HT, 75HT and 100HT formulations, as presented in Figure 4.26, where the part produced with 0HT formulation (Figure 4.26, A) exhibits the layer shifting in the bottom, while 25HT part (Figure 4.26, B) presents a slight curvature in the initial layers and 75HT (Figure 4.26,D) exhibits a small deformation after industrial sintering , while for the 50HT (Figure 4.26, C), and 100HT (Figure 4.26, E) the defect was eliminated.

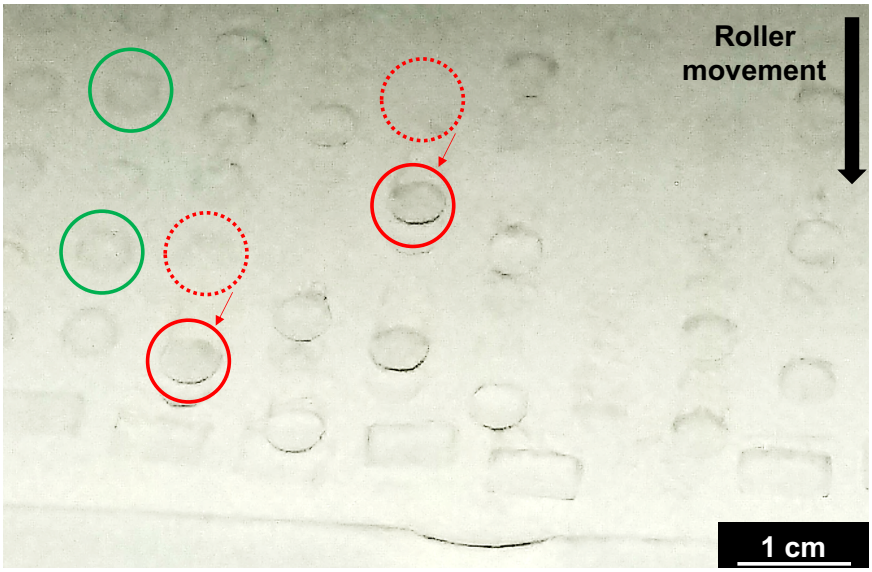


**Figure 4.25:** Movement of initial layers during the printing process with 0HT and 25HT formulations. The green circles highlight the parts which did not shift position, while the dash red circles indicate the initial position of layers which end up in solid red circle positions.

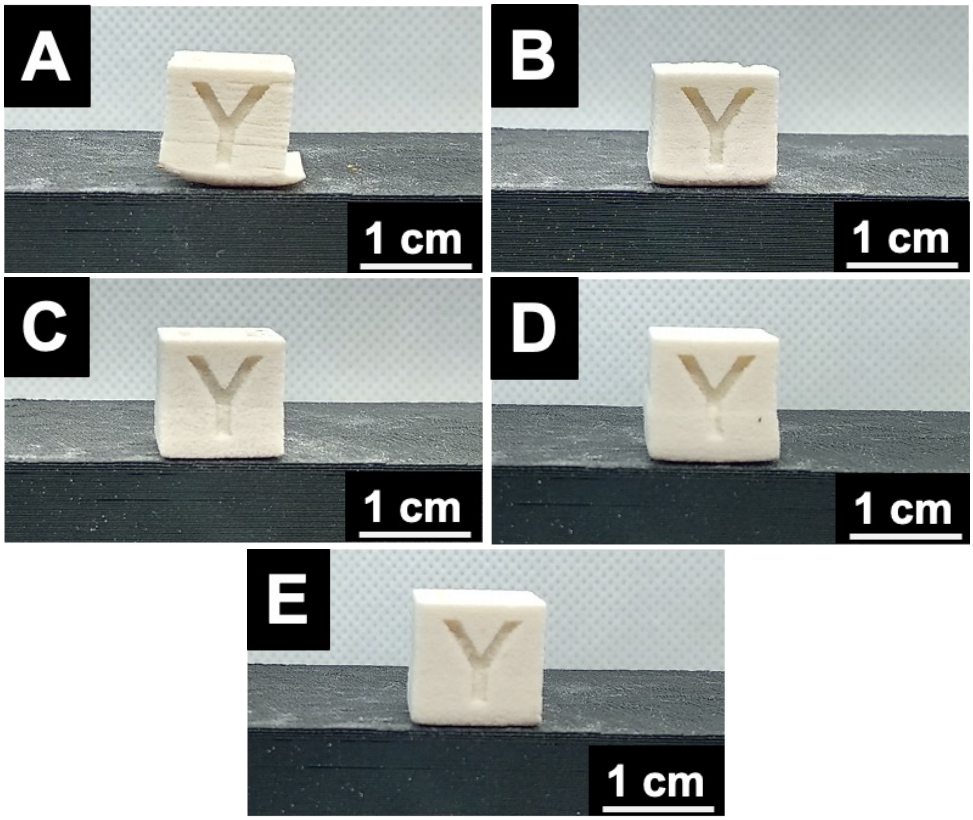


**Figure 4.26:** Printed parts with (A) 0HT, (B) 25HT, (C) 50HT, (D) 75HT and (E) 100HT feedstock formulations, after industrial sintering at 1345 °C. The images present the layer shifting defect in the bottom of the 0HT part (A), which was eliminated adding heat-treated powders to the feedstock formulations.

In order to understand the behavior observed with the different feedstock formulations, the interaction of the liquid binder with the powder bed was studied using the setup described in Chapter 2 and the absorption time of the commercial liquid binder VisiJet PXL was assessed. The interaction of the liquid binder with the 0HT and 100HT feedstock formulations is illustrated in Figure 4.27. The images A-D present the interaction of VisiJet PXL with the 0HT formulation, using two drops of binder, where the second liquid drop was deposited after the first one was totally absorbed. The first drop takes 4,41 s to be completely absorbed, while the second drop is never totally absorbed by the powder. The images E-H correspond to the interaction of the liquid binder with the 100HT formulation, where the first drop of liquid binder is absorbed in under 1 s, and the second drop is totally absorbed in less than 3 s.

Figure 4.28 schematically presents the interaction of the liquid binder, VisiJet PXL, with the 0HT and 100HT powder formulations. As explained before in this chapter, the raw porcelain powders are agglomerates, which deagglomerate when in interaction with the liquid binder, turning the powder bed into a paste-like form. This effect is what prevents the powder to absorb the second drop of liquid binder, as shown in Figure 4.27, D. In the case of 100HT formulation, which has heat-treated powders, after the deposition of the liquid binder, the particles retain their shape, as they are aggregates, and this fact allows the powder bed of 100HT to absorb the second liquid binder drop and absorb both drops faster than the 0HT formulation.

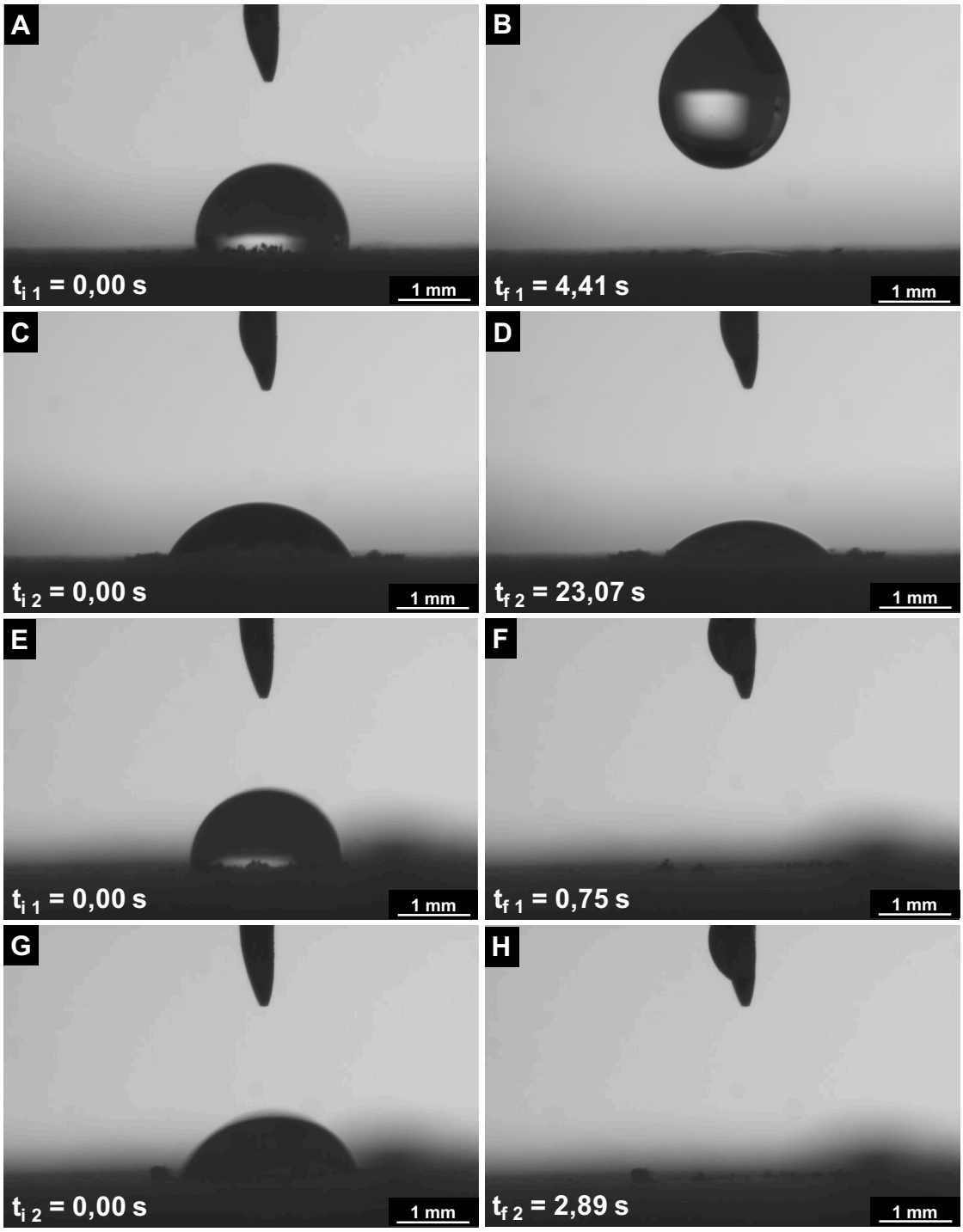


**Figure 4.27:** Absorption of the liquid binder (VisiJet PXL) by formulations 0HT (A-D) and 100HT (E-H) for one and two drops of binder. While the second drop of VisiJet PXL is never totally absorbed by the 0HT formulation, in the case of 100HT the absortion of both first and second drop of liquid binder is complete and faster than for 0HT formulation.

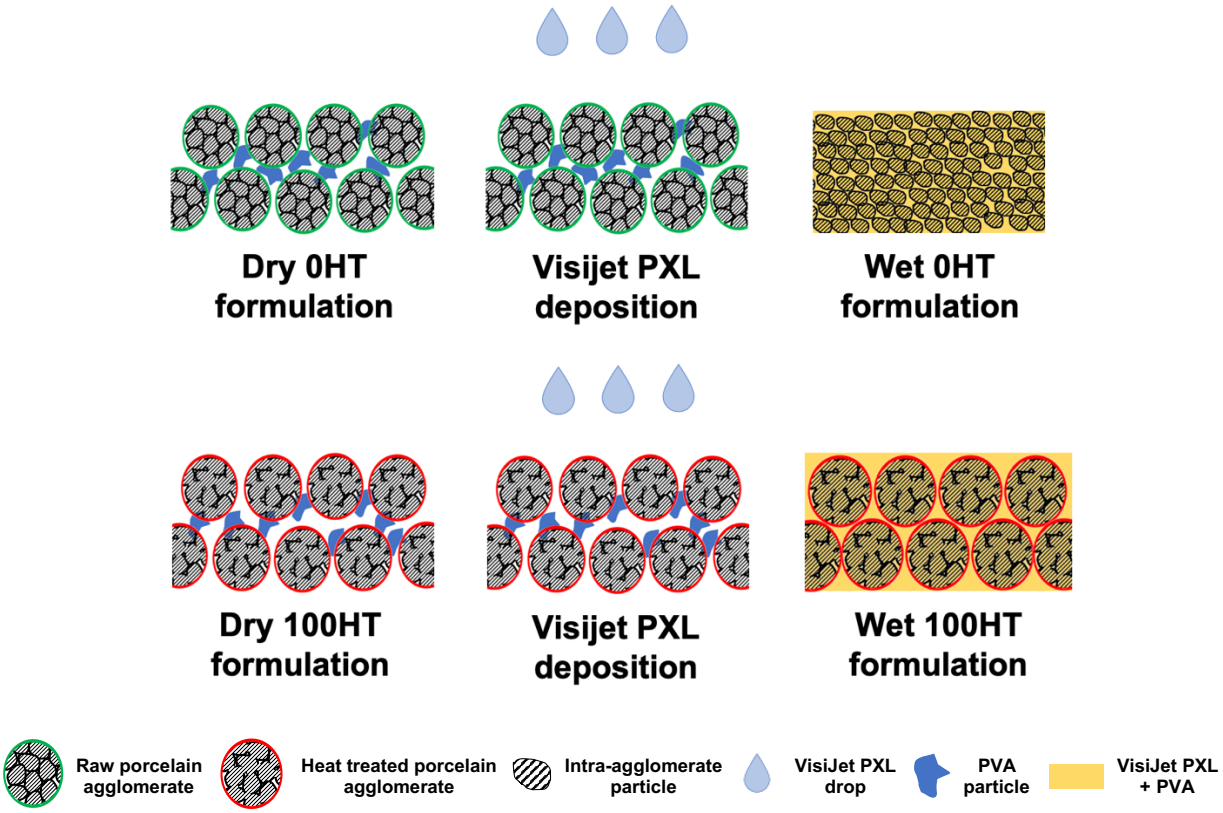


**Figure 4.28:** Schematic representation of 0HT and 100HT formulations behavior during the interaction with commercial liquid binder VisiJet PXL drops. In the case of 0HT formulations, the raw porcelain agglomerates deagglomerate after the deposition of the liquid binder, while for the 100HT the heat-treated porcelain aggregates retain its form after the deposition of the liquid binder.

The printing process of the 0HT formulation is schematically represented in Figure 4.29. After the deposition of the liquid binder, the raw porcelain powder deagglomerate in the powder bed, creating an impediment to the absorption of the following deposited liquid binder. During the deposition of the following layer of 0HT powder, the raw porcelain powders will be quickly saturated in liquid binder and deagglomerate as well, rising above the powder bed surface (Figure 4.29, B). Then, by the roller movement the layer is shifted forward in the powder bed (Figure 4.29, C).

This effect is not observed during the BJP with 100HT formulation, as represented in Figure 4**.30**. With the heat-treated powders, which do not deagglomerate with the liquid binder, there is a complete absorption of the liquid binder in every layer, Figure 4.30 (B), and the powders do not rise above the powder surface, keeping a smooth and flat surface. In this

case the movement of the roller do not move the initial layers forward in the printing bed, as represented in Figure 4.30 (C). The lack of this effect promotes better adhesion of the layer with the previous one, keeping the surface of the powder bed smooth and avoiding the layer shifting during the printing, leading to defect free printed parts.

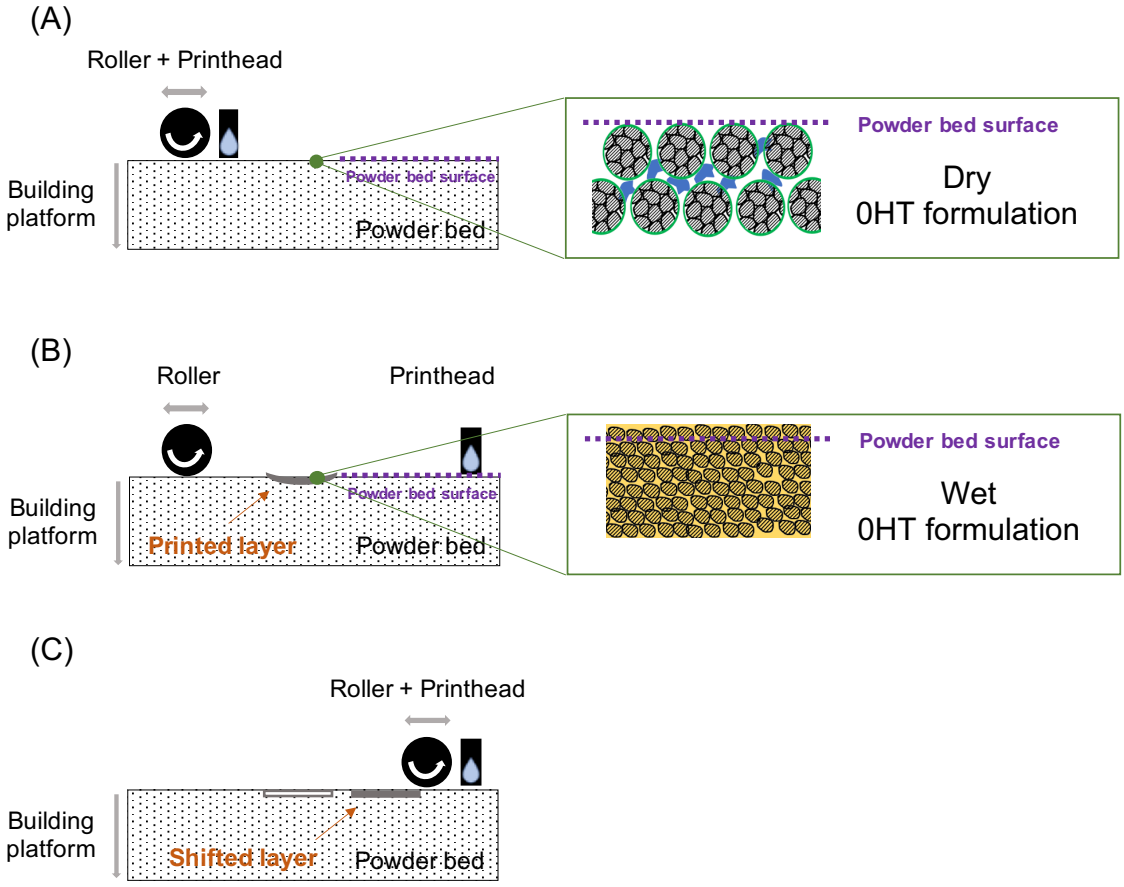


**Figure 4.29:** Schematic of the binder jet printing process of 0HT formulation (A). The detail illustrates the deagglomeration of powders and rise of powder above of powder bed surface, especially in the external limits of the part (B), promoting the shifting of the initial layers by roller movement (C).

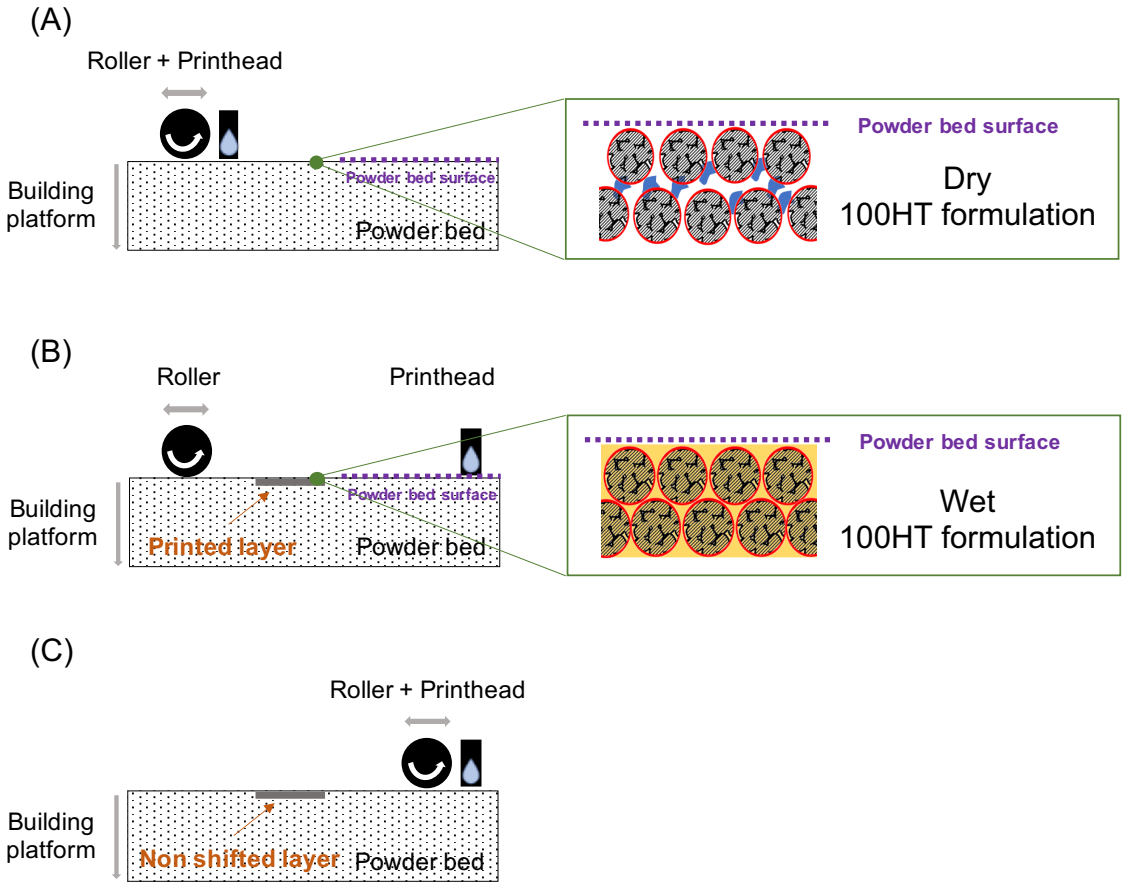


**Figure 4.30:** Schematic of the binder jet printing process of 100HT formulation (A). The detail illustrates the form retention by the aggregates, preventing the powders to rise above of powder bed surface (B) and leading to a proper initial layer (C).

This layer shifting defect is different from the one observed before, in the printing tests with medium size particles (spherical particles) and illustrated in Figure 4.19. In the first case (Figure 4.19) the layer shifting is continuous and occurs due to the higher flowability of the powders, while in the second one (Figure 4.26, A) the defect occurs by the deagglomeration of raw porcelain powders. This effect is attributed to the deposition of the liquid binder. In this work we used 180 % of binder saturation, corresponding to 0,22 in the core section and 0,43 in the shell section. It is expected that a reduction in the binder saturation in the shell section may reduce the observed defect, however, because the binder saturation in the shell and in the core sections of the printed part have a relation, we are not able to reduce the binder saturation only in the shell. Reducing the binder saturation for the whole part implies a reduction in the binder saturation of the core which leads to printed parts with poor

mechanical strength due to the lack of liquid binder to dissolve PVA particles, jeopardizing the post-conformation steps.

Regarding the printed parts with the different feedstock formulations, Figure 4.31 presents its relative geometrical density. As green part, the parts produced with 50HT formulation presented the highest relative density (42,8 ± 0,1 %), while for the other formulations the geometric relative density varied between 37 and 40 %. This result is directly associated with the higher free settled density of the 50HT formulation when compared with the 0HT, 25HT, 75HT and 100HT (Figure 4.23). In the case of the geometric relative density of the industrial sintered parts, the ones produced with 0HT formulation presented highest relative geometrical density (55,2 ± 0,8 %), closely followed by the ones prepared with 50HT formulation (54,1 ± 0,4 %), while the parts produced with 25HT, 75HT and 100HT exhibit values varying between 47 and 50 %. This result is explained by the use of raw porcelain powders in 0HT formulation, which deagglomerate during the binder jet printing process, which reduces the space between the intra-agglomerate particles and promotes the mass diffusion during the industrial sintering, and as consequence, increases the density of the final parts. In the case of 50HT formulation, the fact that 50HT formulation has higher free settled density in the powder bed then the 0HT one, compensate the fact that the heat-treated powders do not deagglomerate, and as consequence prevents the intra-agglomerate particles of raw powders to reduce the space among them, and leads to a close geometric relative density. On the other hand, the parts prepared with 75HT and 100HT, which are formulations with high fraction of heat-treated porcelain powders, have lower relative density after industrial sintering than the ones for 0HT, 25HT and 50HT, due to the same effect. In this case, the heat-treated porcelain aggregates, do not deagglomerate, increasing the space between particles, and as consequence, jeopardizes the mass diffusion and densification during the industrial sintering.

As expected, the relative density of all parts measured by Archimedes method (Figure 4.32) is higher than the relative density measured by geometric method, because it disregards open porosity and design deformations of the parts. However, it is still noticeable the same trend of lower relative density for parts produced with 75HT (58,3 ± 0,4 %) and 100HT (59,6 ± 0,4 %) formulations, than for 0HT (69,7 ± 0,1 %), 25HT (68,2 ± 0,5 %) and 50HT (68,6 ± 0,5 %). Regarding the microstructure of the parts, Figure 4.33 illustrates the microstructure of a fresh fracture zone of green parts and Figure 4.34 exhibits the polished microstructure of the industrial sintered parts, produced with the different formulations. No

significative differences are visible among the microstructure of the different parts, even though 75HT and 100HT parts have lower relative density than the ones of 0HT, 25HT and 50HT.

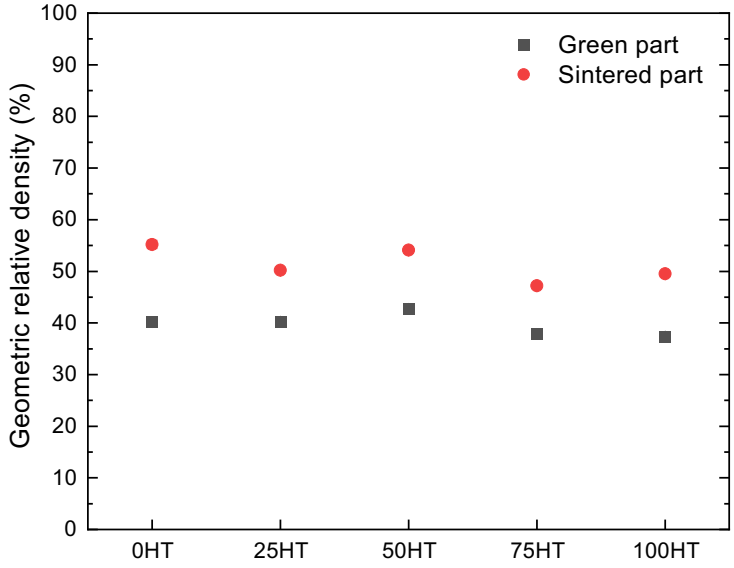


**Figure 4.31:** Geometric density of green and industrial sintered parts at 1345 °C, using formulations with different amounts of raw and heat-treated porcelain powders. The graph presents a maximum relative density in the green state for 50HT formulation and similar relative density of sintered parts for 0HT and 50HT formulations.

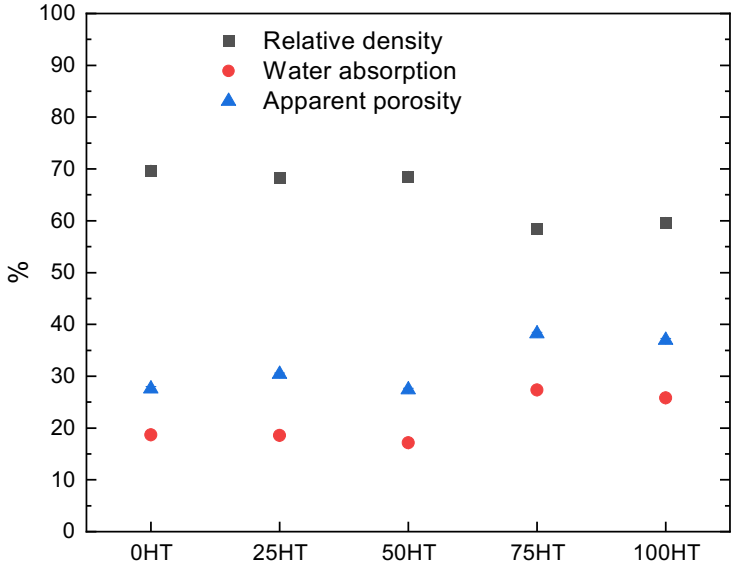


**Figure 4.32:** Relative density, water absorption and apparent porosity, measured by Archimedes method, of industrial sintered parts produced by binder jet printing with different amounts of raw and heat-treated porcelain powders. The relative density of parts

decreases with formulations with high amount of heat-treated porcelain powders (75HT and 100HT)

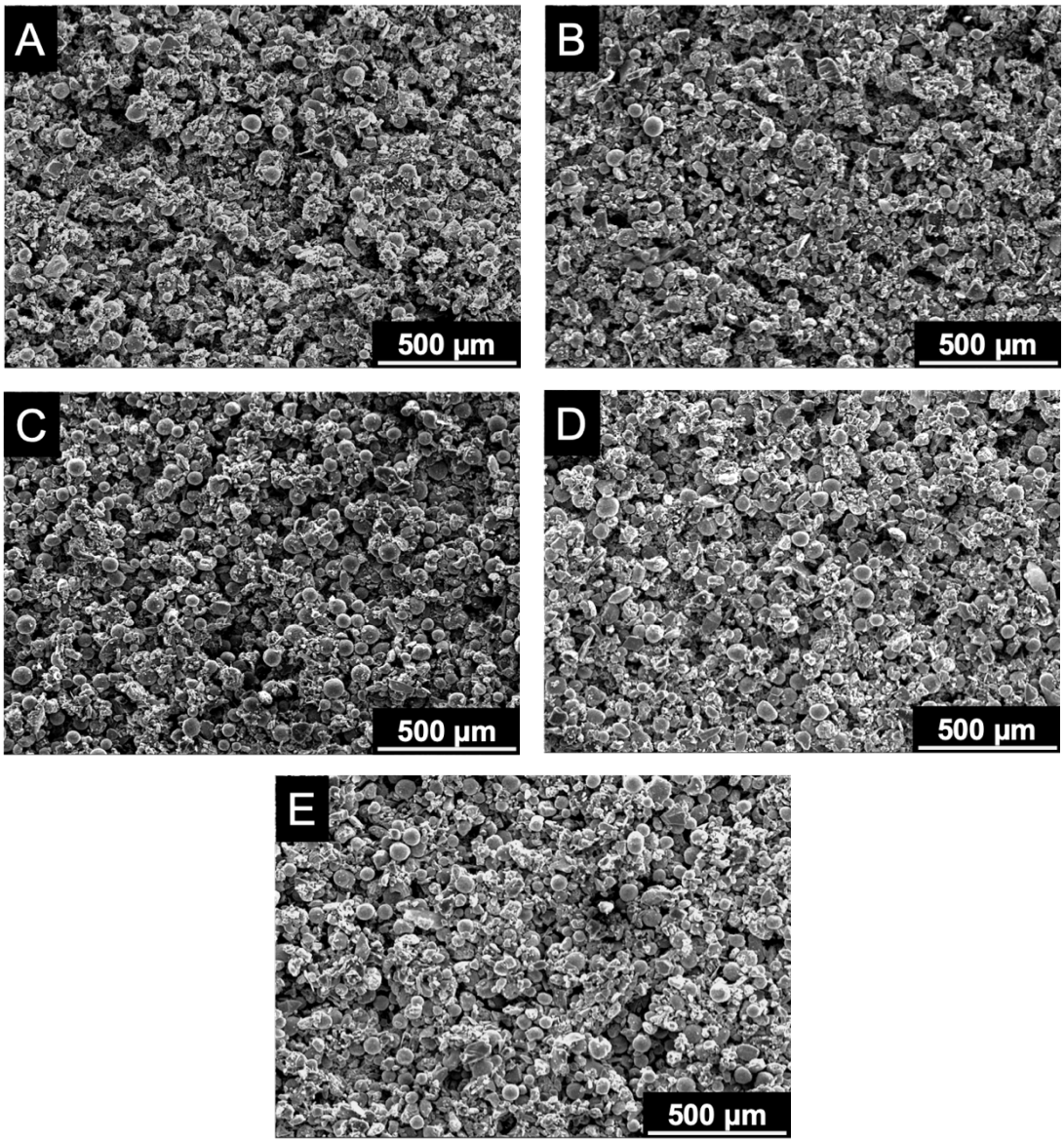


**Figure 4.33:** SEM micrographs of fresh fracture zone of green parts of (A) 0HT, (B) 25HT, (C) 50HT, (D) 75HT and (E) 100HT formulations. The images do not present significative differences among them.

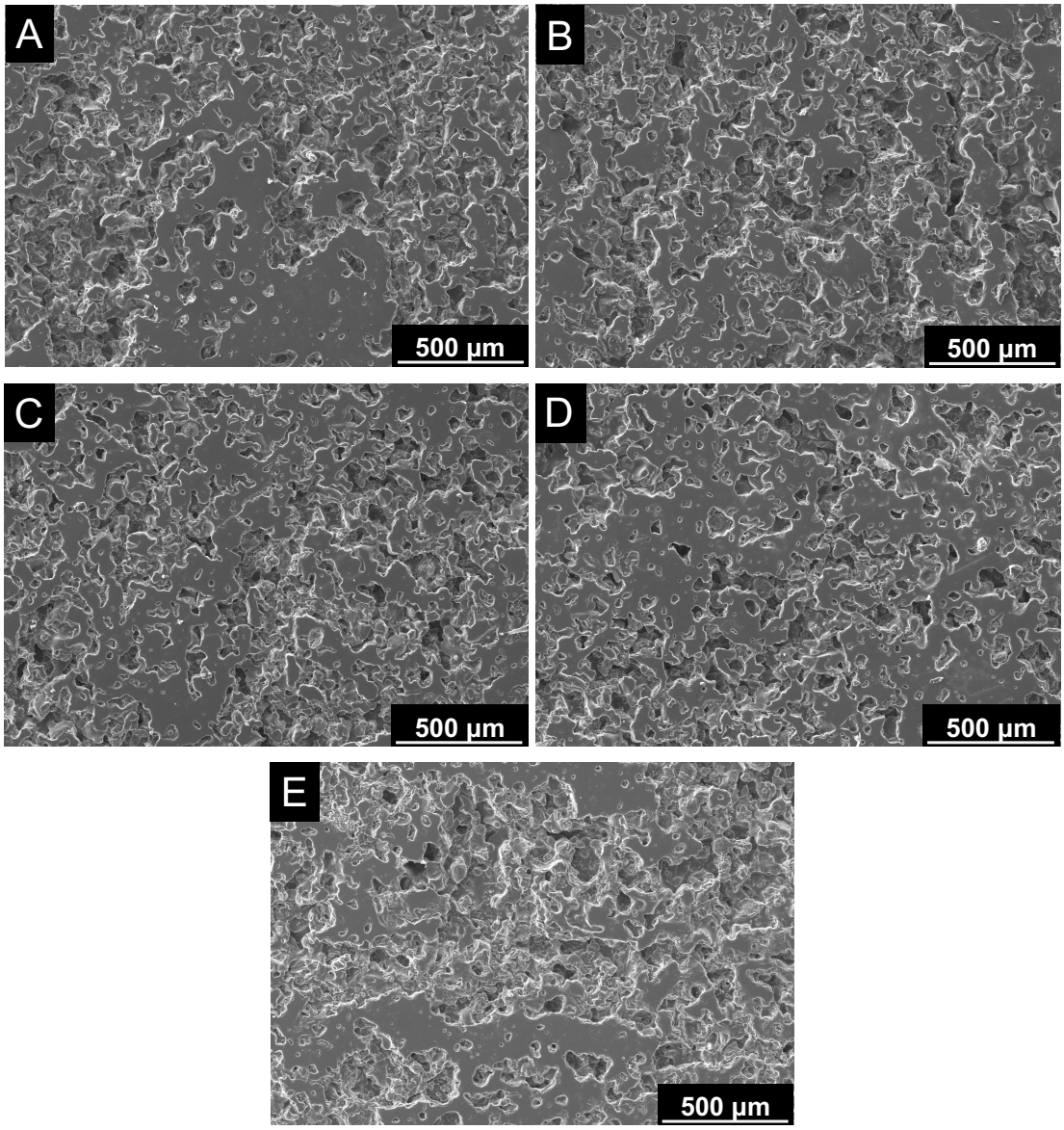


**Figure 4.34:** SEM micrographs of polished fracture zone of industrial sintered parts of (A) 0HT, (B) 25HT, (C) 50HT, (D) 75HT and (E) 100HT formulations. The images do not present significative differences among them.

Due to the industrial aim of this work, as a product design driven company, it is relevant for Costa Verde to know how the dimensions of a part evolve during the several steps of the production process. With this in mind, in Figure 4.35 the diameter variation of cylinders, relative to the virtual design dimensions (Figure 4.2, A) is presented for the formulations with different amounts of heat-treated porcelain powders. As general overview, the increase of the heat-treated porcelain powders fraction in the feedstock for binder jet printing, reduces the variation of the diameter from - 4,95 ± 0,13 % for 0HT formulation to - 1,15 ± 0,11 % for the 100HT one, in the green part, and from - 23,35 ± 0,22 % (0HT) to

- 20,69 ± 0,21 % (100HT), in the case of industrial sintered part. These results are in accordance with the ones observed for the relative density. On one hand, the raw powders present in 0HT formulation, deagglomerate during the deposition of the liquid binder, leading to a paste-like form in the powder bed and approximate the intra-agglomerate particles of raw powders. This fact leads to a higher variation in the diameter of the cylinder, than for feedstock with heat-treated porcelain powders. This is supported by the fact that the variation is negative, meaning a reduction in the diameter, when compared with the virtual design dimension. On the other hand, after the industrial sintering, the parts produced with high fraction of heat-treated porcelain, present the lowest variation (in absolute value), due to the fact that heat-treated aggregates have higher space among them, preventing the mass diffusion during sintering, and as consequence the densification of the part.

Industrial sintered complex shaped parts, with bridges with different lengths, are presented in Figure 4.36, for the different feedstock formulations used. While the bridges with low length (5 and 10 mm) did not deformed during the sintering process for all the formulations, in the case of the 20 mm bridge the deformation is more noticeable for 75HT (Figure 4.36, D) and 100HT (Figure 4.36, E). In the case of the longer bridge (40 mm), different behaviors were observed for the different formulations after the industrial sintering. In the case of 0HT, 25HT and 50HT, where the fraction of raw porcelain powders is higher or equal to the heat-treated one, the bridge presents a plastic deformation, while for 75HT and 100HT formulations, the bridge broke. This difference is once again explained by the higher distance among the heat-treated porcelain aggregates, preventing its densification and leading to fracture, then for the intra-agglomerate particles, which, resulting from the deagglomeration during the liquid binder deposition, have lower space among them promoting the densification of the body during industrial sintering, which avoids the type of fracture observed for parts produced with 75HT and 100HT formulations.

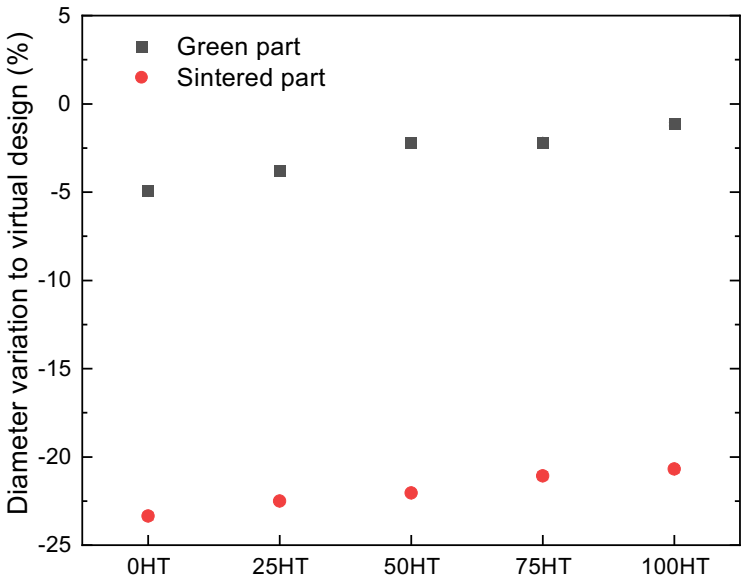


**Figure 4.35:** Diameter variation of green and industrial sintered parts (cylinders) to virtual design, prepared using the feedstock formulations with different amounts of raw and heat-treated porcelain powders. The increase in the amount of heat-treated porcelain powders reduces the diameter variation to the virtual design dimensions.

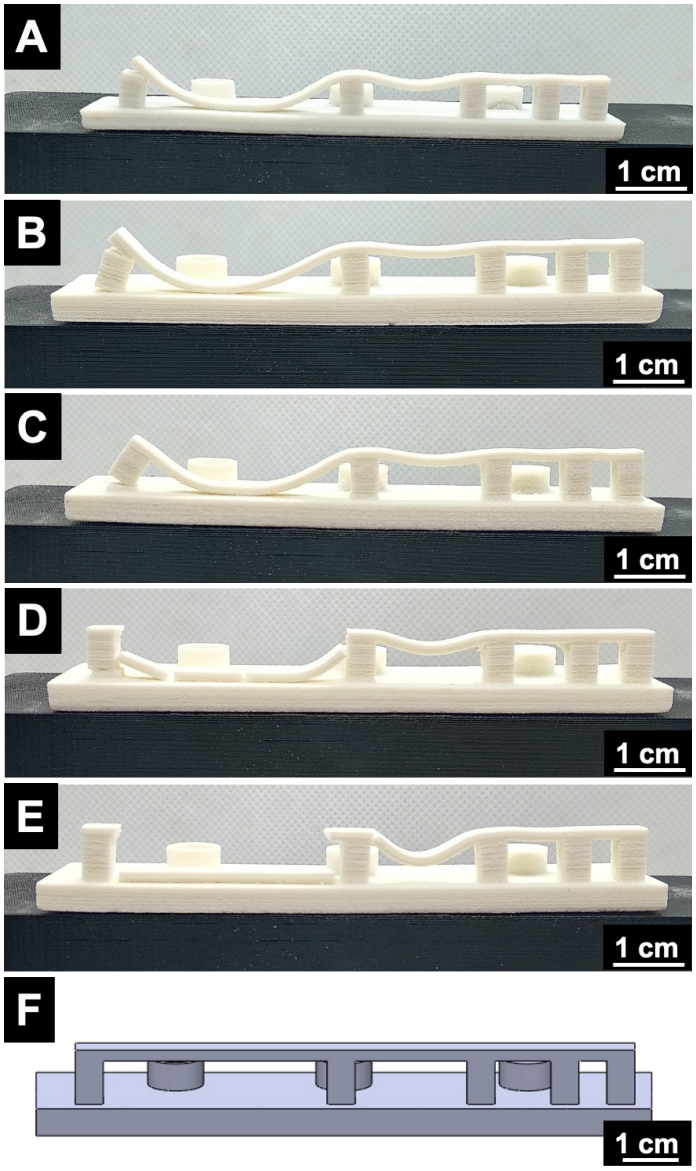


**Figure 4.36:** Complex shaped parts, after industrial sintering, with different length bridges, produced by binder jet printing with the (A) 0HT, (B) 25HT, (C) 50HT, (D) 75HT and (E) 100HT formulations. Image (F) represents the virtual design with the desired part. The longer bridge deforms for 0HT, 25HT and 50HT formulations, while it breaks in the extremes for the 75HT and 100HT formulations.

Considering the results of this chapter, we proved that the use of heat-treated porcelain powders improves the printability of porcelain powder feedstock, by leading to defect free final parts. However, its use compromises physical properties, such as relative density, of the industrial sintered parts. The use of 50HT formulation, which has the same amount of

raw porcelain powders and heat-treated ones, balances the elimination of defects in the final parts, while do not lead to low relative density parts.

## 4.4. Conclusions

The printability of industrial porcelain powder feedstock for binder jet printing was assessed by studying the effect of the particle size distribution and the heat treatment of porcelain powders in the elimination of defects in the porcelain parts.

The use of fine particles (< 80 μm) in the porcelain powder feedstock leads to defect free printed parts, due to the fact that has both irregular and spherical particles, as opposed to large particles (80-100 μm) and (100-150 μm), which have high flowability (HR < 1,20), leading to layer shifting defect in the printed parts. Additionally, the use of large in-bed binder particles (100-150 μm) promotes the clog of the printhead, jeopardizing the liquid binder deposition and leading to highly defective printed parts.

The use of heat-treated porcelain powders in the feedstock for binder jet printing, is not reported, and here we shown the advantages of its use. The addition of heat-treated porcelain powders improves the printability of powder feedstock by avoiding the defect free printed parts. This influence is attributed to the fact that the heat treatment transforms agglomerates into aggregates, preventing its deagglomeration during the deposition of liquid binder and avoiding the layer shifting by roller action. However, its use with high amount in the feedstock also leads to final parts with lower relative density, when compared with feedstock with lower amounts of heat-treated porcelain.

In this sense, we found that 0HT formulation (85 wt.% of raw porcelain and 15 wt.% of PVA) leads to parts with the highest relative density (70 %), and the 50HT formulation (42,5 wt.% of raw porcelain, 42,5 wt.% of heat-treated porcelain and 15 wt.% of PVA) leads to parts with almost the same relative density (68 %), but in the case of 0HT the final parts exhibit design defects due to layer shifting in the initial layers, while the parts produced with 100HT are defect free final parts.

Nevertheless, the highest value of relative density measure (70 % with 0HT formulation) is far from the desired for industrial porcelain bodies (> 99,5 %) and in this sense there is a need to improve the relative density of the bodies, using different post-conformation steps.

## 4.5. References


[1] 3D Systems, “ZP131 Safety Data Sheet.” 3D Systems, Inc, Rock Hill, South Carolina, USA, pp. 1–5, 2014.

[2] I. 3D Systems, “ZP140 Safety Data Sheet.” Z Corporation, pp. 1–6, 2007.

[3] 3D Systems, “VisiJet PXL Core Safety Data Sheet.” 3D Systems, Inc, Rock Hill, South Carolina, USA, pp. 1–4, 2013.

[4] G. Nichols *et al.*, “A review of the terms agglomerate and aggregate with a recommendation for nomenclature used in powder and particle characterization,” *J. Pharm. Sci.*, vol. 91, no. 10, pp. 2103–2109, 2002.

[5] G. W. Brindley and M. Nakahira, “The kaolinite-mullite reaction series: I, a survey of outstanding problems,” *J. Am. Ceram. Soc.*, vol. 42, no. 7, pp. 23–71, 1959.

[6] H. B. Johnson and F. Kessler, “Kaolinite Dehydroxylation Kinetics,” *J. Am. Ceram. Soc.*, vol. 52, no. 4, pp. 199–203, 1969.

[7] K. Okada, N. ŌTsuka, and J. Ossaka, “Characterization of Spinel Phase Formed in the Kaolin-Mullite Thermal Sequence,” *J. Am. Ceram. Soc.*, vol. 69, no. 10, p. C-251-C-253, 1986.

[8] B. Sonuparlak, M. Sarikaya, and I. A. Aksay, “Spinel Phase Formation During the 980°C Exothermic Reaction in the Kaolinite-to-Mullite Reaction Series,” *J. Am. Ceram. Soc.*, vol. 70, no. 11, pp. 837–842, 1987.

[9] C. Sun *et al.*, “Effect of particle size gradation on the performance of glass-ceramic 3D printing process,” *Ceram. Int.*, vol. 43, no. 1, pp. 578–584, 2017.

[10] O. D. Neikov and N. A. Yefimov, *Powder Characterization and Testing*, 2nd ed. Elsevier Ltd., 2019.

# *Chapter 5: Porcelain powder formulation for indirect selective laser sintering*

**Abstract**

The use of Selective Laser Sintering (SLS) with ceramic powders is limited by the processing challenges, mainly the sintering temperatures required for ceramic materials. In this sense, the use of a sacrificial binder, used for the SLS process and its removal from the final ceramic parts can be a solution for ceramic parts production through SLS, known as indirect SLS. In this work we approach the use of indirect SLS for the production of porcelain parts by using a polyamide as sacrificial powder binder. The obtained parts by indirect SLS followed by post-conformation steps were produced using heat treated porcelain powders, required in order to avoid printing defects in the powder bed. Polyamide powders in a weight ratio of 5:1, reach the highest relative density. The position of the parts in the powder bed showed to have influence in the design quality of the parts, while the reuse of powders exhibit promising results showing not significative differences in properties of the final parts.

**Keywords**

Additive manufacturing, porcelain, indirect SLS, ceramics

## 5.1. Introduction

As discussed in Chapter 1, the use of the direct SLS approach for ceramics may promote the crack formation and delamination of the ceramic bodies, due to thermal stresses formed during the process. In this sense, the indirect way, where a sacrificial *in-bed* binder is use during the SLS process and thermally removed in post-conformation processes.

This study aims the use of indirect SLS of industrial porcelain powders for porcelain parts production. In order to achieve it, the improvement of the printability of porcelain powders by the use of heat treatment and the study of the amount by weight of polyamide as *in-bed* binder are the main focus of this work. The printing direction and the reuse of powder are also within subject of study of this work. These results have implications for our fundamental understanding regarding the printability of industrial porcelain powders in SLS and avenues to accelerate the implementation of AM technologies in industrial production of ceramics area.

## 5.2. Materials and methods

Spray dried industrial porcelain powders were produced and provided by *Porcelanas da Costa Verde, Portugal* using the conditions described in Chapter 2. In this chapter industrial raw porcelain powders and heat-treated porcelain powders were used and the organic in-bed binder used in the present study is a polyamide 12 (PA 650, Advanced Laser Materials, USA), with a melt flow rate of 50 g/10 min, according to its technical data sheet. All feedstock formulations (Table 5.I), prepared according to the procedure described in Chapter 2. Both raw and heat-treated porcelain powders were characterized regarding their specific surface area, particle size distribution and morphology and the polyamide powder was characterized regarding its PSD, morphology and thermal behavior using the procedure described in Chapter 2.

**Table 5.I:** Porcelain powders formulations used in SLS.

| Formulation | Porcelain | Weight ratio (Porcelain:Polyamide 12) |
|---|---|---|
| P0 | Raw powders | 3:1 |
| P3 | Heat treated powders | 3:1 |
| P4 | Heat treated powders | 4:1 |
| P5 | Heat treated powders | 5:1 |
| R1 | Reuse from P3 | 3:1 |
| R2 | Reuse from R1 | 3:1 |

The SLS process was performed as described in Chapter 2 and cylinders with diameter of 6,35 mm and length of 12,7 mm, were printed as parts.

The printed parts were subject to post conformation steps. Cold isostatic pressing (CIP) performed during 60 s at a pressure of 196 MPa in oil bath was used. A rubber bag was employed to prevent the part to contact the oil. The parts were also submitted to sintering process using an industrial continuous kiln, with a maximum temperature of 1365 °C, for 6 h. A group of parts was subject to both processing steps, first with CIP followed by the industrial sintering.

The relative density and diameter and length variation of the green and sintered parts was assessed using the procedure described in Chapter 2. In addition, the microstructure of the sintered parts was analyed as described in Chapter 2.

The density of the porcelain used is 2,44 g/cm$^3$, and the density of the polyamide 12 is 1,02 g/cm$^3$, according to its technical data sheet. The reference density for P0, P3, R1 and R2 compositions, all with the porcelain/polyamide 12 weight ratio of 3/1, is 1,81 g/cm$^3$ and for P4 and P5 formulations are 1,91 g/cm$^3$ and 1,98 g/cm$^3$, respectively.

## 5.3. Results and discussion

Porcelain powders exhibit spherical and irregular shaped particles, both as raw (Figure 5.1, A) and as heat-treated powders (Figure 5.1, B). Raw porcelain powders exhibit a particle size distribution peaking at 62 μm, with a shoulder in the smaller particles side (< 20 μm), and a small peak for particles smaller than 2 μm, while the heat-treated porcelain powders exhibit a bi-modal distribution, with a major peak at 104 μm and smaller one at 17 μm, as presented in Figure 5.2. The specific surface area (SSA) analysis exhibit a decrease from 9,7 to 6,6 m$^2$/g after the heat treatment of the spray dried porcelain powders. The polyamide 12 powders, used as *in-bed* binder, exhibit irregular shaped particles and a narrow monomodal PSD, peaking at 55 μm (Figure 5.3). In Table 5.II characteristics of the particle size distribution of raw porcelain, heat-treated porcelain and polyamide 12 powders are presented. The Dv10 of raw porcelain powders is lower (11 μm) than the one for heat-treated porcelain powders (28 μm), while the Dv90 is also lower for raw powders (104 μm) than for heat-treated porcelain powders (118 μm). As polyamide 12 exhibit the narrower PSD curve, the Dv10 is the highest with 37 μm and the Dv90 is the lowest with 86 μm.

Both the morphology and the PSD curves of raw and heat-treated porcelain powders are in accordance with the results discussed in Chapter 4 of this thesis. The heat treatment performed in the spray dried powders did not change significantly the shape of the particles, however, there was a decrease in the fine particle fraction after the heat treatment, due to the aggregation of fine particles among them and with bigger particles, accompanying the increase in the fraction of coarse particles. The transformation of the raw porcelain agglomerates into heat-treated porcelain aggregates is also supported by the decrease in the SSA of the porcelain powders. Comparing the PSD curves of raw and heat-treated porcelain powders (Figure 5.2) with the one of polyamide 12 (Figure 5.3), and having in

consideration the values in Table 5.II, it is noticeable that the raw porcelain powders exhibit smaller particles than the ones of polyamide 12, while the heat-treated porcelain powders exhibit bigger particles than polyamide 12. These particles can be more suitable for the use of polyamide 12 as *in-bed* binder, which needs to fill the voids among the porcelain particles.

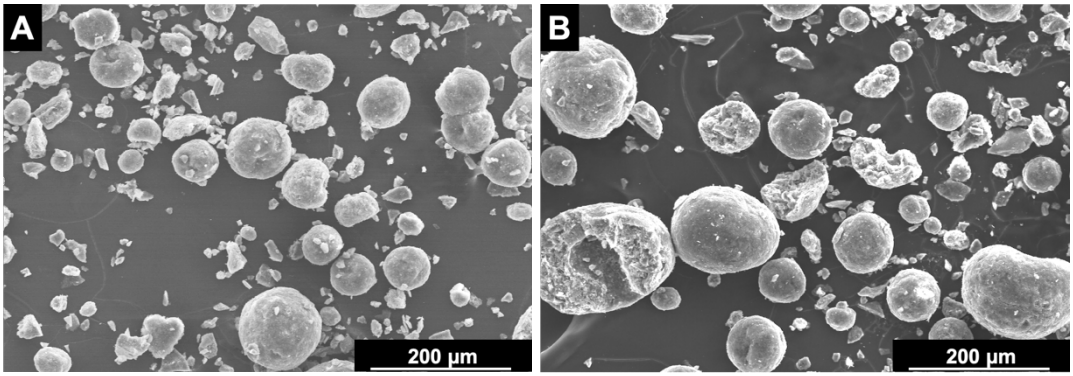


**Figure 5.1:** SEM micrographs of the porcelain powders used in this work: (A) Raw porcelain powders and (B) heat-treated porcelain powders. Both powders present spherical and irregular shaped particles.

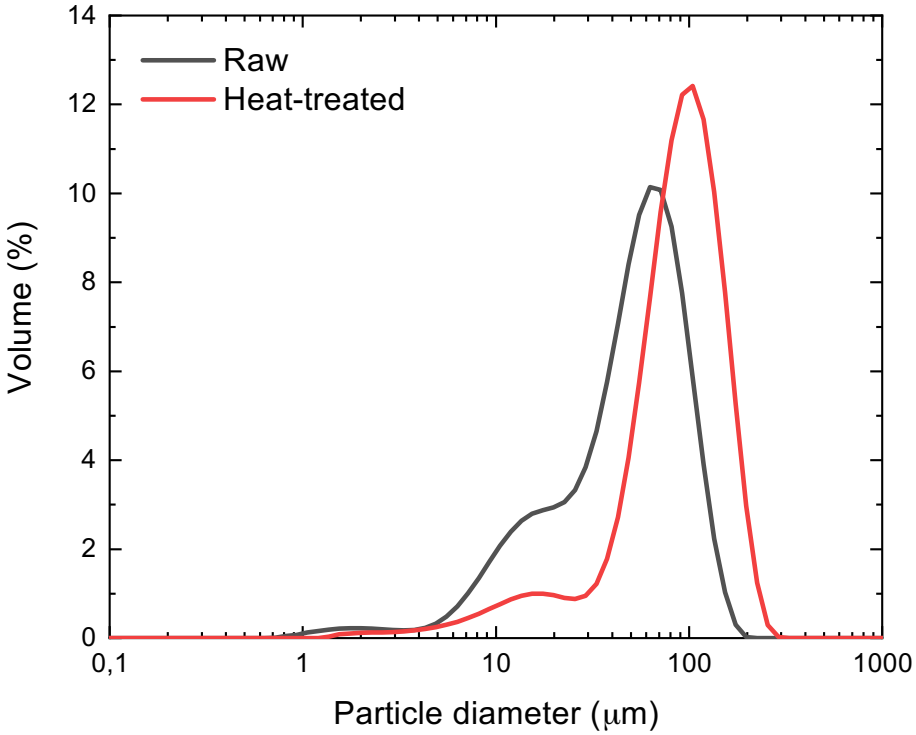


**Figure 5.2:** Particle size distribution of raw (black) and heat-treated (red) porcelain powders. The raw porcelain powders have a monomodal distribution with a shoulder in

the smaller particles side, peaking at 62 μm, and the heat-treated porcelain powders present a bi-modal distribution, peaking at 104 μm.

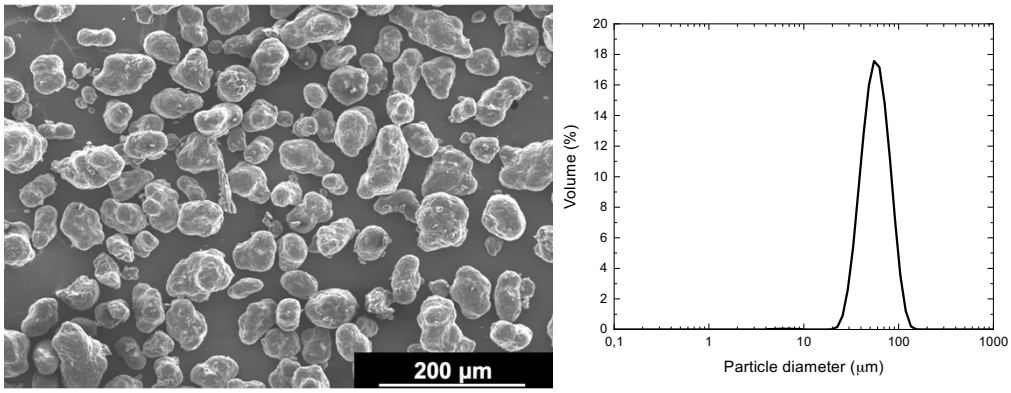


**Figure 5.3:** SEM micrograph (left) and particle size distribution (right) of polyamide 12 powders. The powders exhibit irregular shaped particles and a narrow monomodal particle size distribution, peaking at 55 μm.

**Table 5.II:** Characteristics of the particle size distribution of the porcelain and polyamide 12 powders used in this work.

| | Raw porcelain | Heat-treated porcelain | Polyamide 12 |
|---|---|---|---|
| Dv10 (μm) | 11 | 28 | 37 |
| Dv50 (μm) | 49 | 83 | 57 |
| Dv90 (μm) | 104 | 118 | 86 |

The initial tests of indirect SLS with porcelain powders were performed using raw porcelain powders with polyamide 12 (P0 formulation). However, several limitations were observed during the printing process, namely the bad spread of powder in the powder bed, as illustrated in Figure 5.4, where the red circles highlight the existence of holes in the powder bed (Figure 5.4, A) and the agglomeration of powder (Figure 5.4, B). In Figure 5.5 the powder bed surface during the printing with the P3 formulation is presented. The surface is homogenous, and the defects observed for the P0 formulation were not observed.

The ineffective spread of the powder with the P0 formulation leads to highly defective parts, and poor mechanical strength of the parts, as illustrated in Figure 5.6 A, where loose powder is seen around the printed part. Most of the printed parts with P0 are not possible to remove from the powder bed since they break as they are handled. On the other hand, the part printed with the P3 formulation, where heat-treated porcelain powders were used, presented in Figure 5.6 B, was produced without major defects, as result of the proper spread of powder observed for the P3 formulation.

The improvement in the spread of the formulations, and as consequence, in the defect free printed parts is clear when heat-treated porcelain powders are used as opposed to raw porcelain powders. Three main reasons may explain this effect: 1) the heat treatment performed in the porcelain powders may reduce the reactivity of the powders by turning the agglomerates into aggregates; 2) in addition, the heat-treated porcelain powders present larger particles than the raw powders (Figure 5.2), improving the spread of the powders; 3) the PSD of raw porcelain powders exhibit smaller particles than the ones of polyamide (Figure 5.3) and, in this sense, the molten polyamide after the laser scan, do not fill the voids between porcelain particles properly and does not provide enough mechanical resistance to the printed part. This is opposed to the heat-treated porcelain powders which have larger particles than the ones of polyamide 12, promoting a better filling of the voids between the porcelain particles by the molten polyamide after laser scan, improving mechanical resistance of the green printed part.

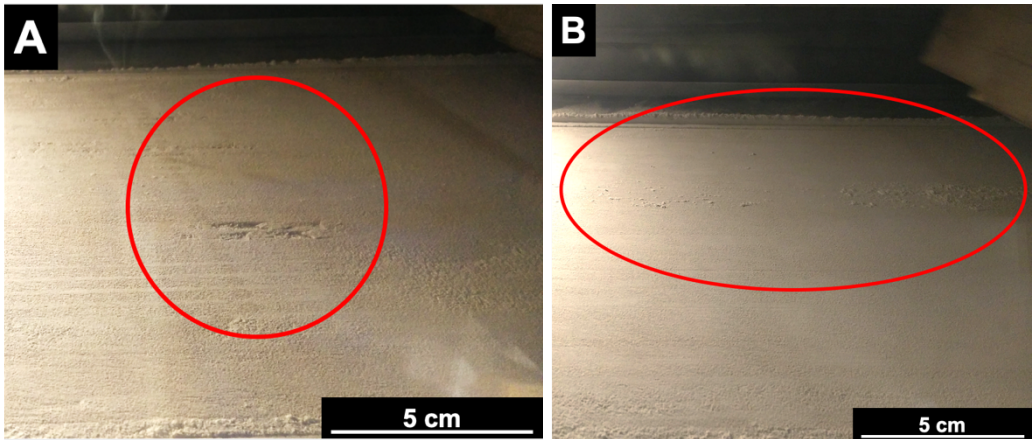


**Figure 5.4:** Defects created in the powder bed with P0 formulation (raw porcelain powders), with highlight for holes created (A) and agglomeration of powders (B).

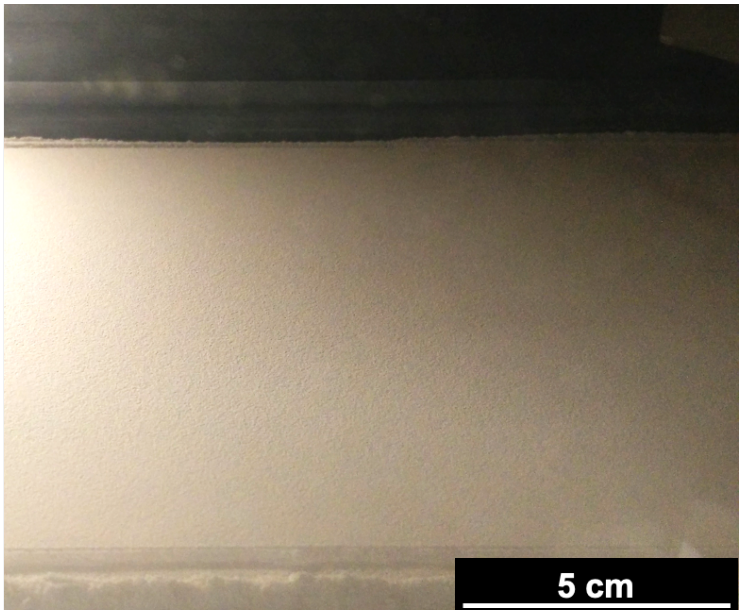


**Figure 5.5:** Part bed surface during the printing with P3 (heat-treated porcelain powders). The image shows a smooth and homogenous powder bed surface, without the defects observed for the P0 formulation.

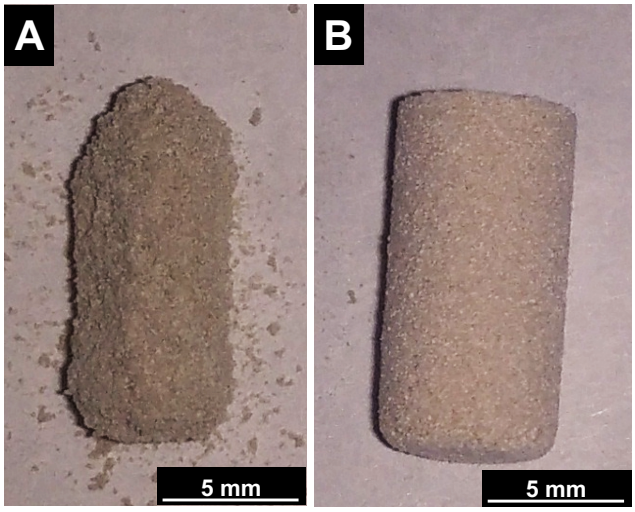


**Figure 5.6:** Cylinders printed with (A) P0 and (B) P3 formulations. It is clear the effect of heat-treated porcelain powders use in the P3 formulation, leading to a proper printed part (cylinder) as opposed to the use of raw porcelain powders in the P0 formulation.

The effect of the ceramic/binder ratio in the printability, relative density and dimensions variation to the virtual design was also analyzed. Three different weight ratios were used: 3:1 (P3), 4:1 (P4) and 5:1 (P5) (Table 5.I) and the green parts are depicted in Figure 5.7.

For the three compositions used, the green printed parts present a well-defined cylindrical shape and homogenous and smooth surface aspect. A careful analysis highlights a curling effect (underlined with the red circle) that appears at the bottom of the cylinder, i.e., the initial layers of the printed part. The defect is more perceptible in the parts printed with the formulation with higher amount of polyamide (P3 formulation, Figure 5.7 A), when compared with parts printed with lower content of polyamide. This defect is maximized for parts, for instance a cylinder, printed in the horizontal position (Figure 5.8), which have the circular section deformed. To understand what gives rise to this different behavior it is important to considerer the operation conditions of SLS, being one of the most important the part bed temperature.

The SLS window is defined as the SLS temperature work range, which is the difference between the onset of Tm (melting temperature) peak and the offset of Tc (crystallization temperature) peak of the powder to be printed, as shown in Figure 5.9 (vertical black line) [1]. The SLS process is more effective, producing parts with better properties, if the part bed temperature is kept in the onset of the Tm peak of the powder, and in the case of this work, of the *in-bed* binder. In the case of the polyamide 12 used, the temperature of the part bed should be settled for 170 °C. Keeping the temperature at this value will keep the material in the powder bed in a melt stage after the laser crossing. When the part bed temperature is too low, the material is not melted anymore and curling effects appear in the edges of the part [2].

However, due to the addition of the porcelain powder to the formulation, the Tm onset of the formulation is shifted to the right, i.e., for higher temperatures (Figure 5.9, vertical red lines), leading to the curling defects in the printed part. In the case of P3 formulation, the part bed temperature should be kept around 174 °C. Due to the high amount of polyamide in the P3 formulations, this defect is more perceptible in the parts printed with this formulation.

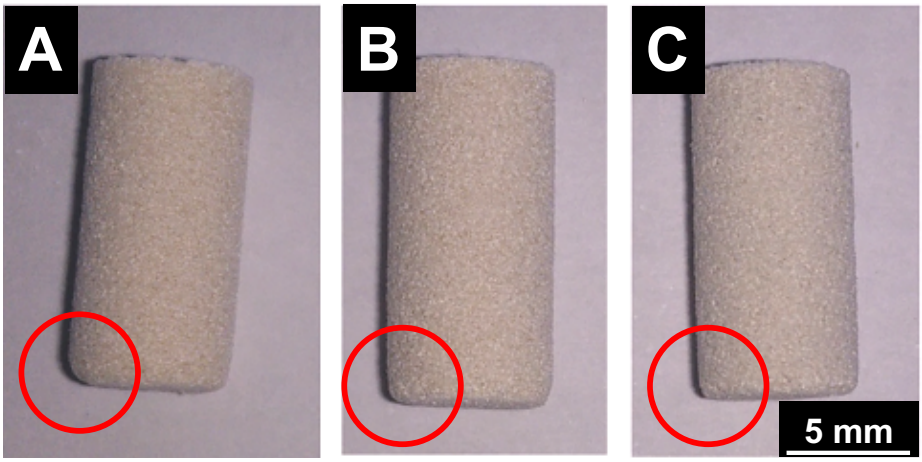


**Figure 5.7:** Green parts after SLS, printed with the formulations (A) P3, (B) P4 and (C) P5, with highlight for the curling effect at the bottom of the part. The part printed with P3 formulation, i.e., higher amount of polyamide, exhibits more curling.

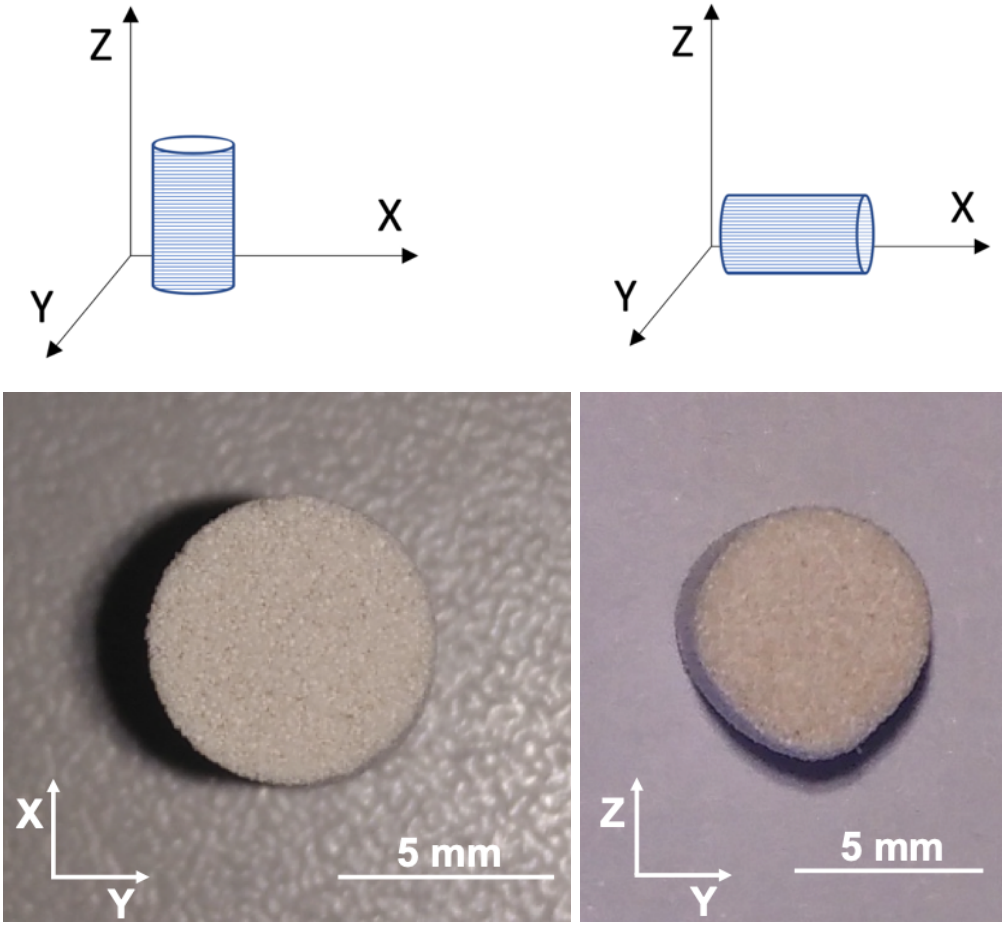


**Figure 5.8:** Parts printed by SLS in vertical position (left) and in horizontal position (right). On top the schematic representation of the parts position in the powder bed. In the case of the horizontal position it is noticeable that the cylinder does not have a circular section.

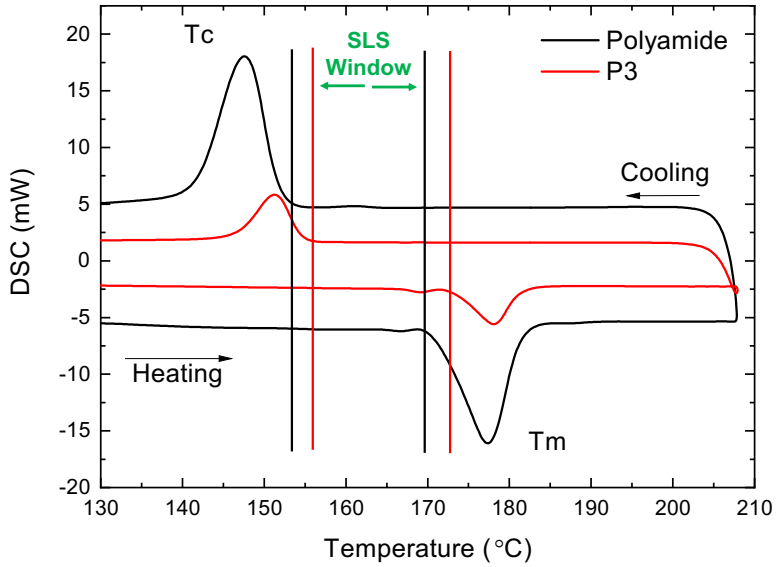


**Figure 5.9:** SLS window of the virgin polyamide 12 (black) and the formulation with porcelain powders (red).

Although our studies indicate that the part bed temperature parameter, during the SLS of porcelain powders with polyamide 12 as *in-bed* binder might solve the problem of curling, further research focused in the printing parameters needs to be done. Other parameters such as laser power, scan speed and roller speed might have an impact in the curling effect as well. This subject is particularly important for companies that are product design driven, as *Porcelanas da Costa Verde*, in order to avoid design deformations in the porcelain parts produced by SLS.

The relative density of parts printed using different amounts of polyamide is presented in Figure 5.10, after the different stages of processing. In the green state, parts produced with formulation with higher content of porcelain, P5, presents lower relative density (42 %), while P3 and P4 exhibit 55 % and 51 %, respectively. Based on our results, here we advocate that the relative density of the green parts is related with the ratio of porcelain/polyamide. In one hand, the porcelain powders have bigger particles (Dv90 of 118 μm) than the polyamide (Dv90 of 86 μm) and the increase in the amount of porcelain from P3 to P5 formulation leads to an increase in large particles and as consequence, higher void space among them and a decrease in the relative density. On the other hand, the reduction of polyamide content in the powder bed leads to less melted *in-bed* binder during the laser scan, and as consequence, less binder will fill the void space between porcelain

particles, which also contributes to the lower relative density of printed parts with P5 formulation than for P4 and P3 ones.

The relative density of printed parts processed by CIP and printed parts processed by industrial sintering is also presented in Figure 5.10. The same trend observed for green parts was also observed for parts after the CIP, where the highest relative density was measured for parts printed with P3 formulation (70 %) followed by the ones with P4 (67 %) and P5 (65 %). However, the increase in relative density for P5 parts is higher (21 %) than for P3 and P4 ones (15 %). This difference is explained by the lower relative density of P5 green parts than for P3 and P4 ones, i.e., more void space between particles for P5 formulation, which is reduced during CIP process. In the case of industrially sintered printed parts, which were not processed by CIP, the highest relative density was observed for parts printed with the P4 formulation, followed by the P3 ones (69 %), while industrially sintered P5 printed parts exhibit only 60 % of relative density. This result was not expected, as P5 formulation has the highest content of porcelain powders and should present the highest relative density of printed parts, after the *in-bed* binder is thermally removed during sintering. Based on our results, we can advocate that in this case the lower relative density of P5 green parts than the ones of P3 and P4 hinders the densification of the bodies during the sintering process, due to the higher void space between particles than for P3 and P4 parts.

For printed parts processed by CIP followed by industrial sintering, the highest relative density was obtained for P5 parts (80 %), while P4 and P3 ones presented 78 % and 77 %, respectively. In this result, the use of CIP combined with the industrial sintering, leads to similar values of relative density among printed parts with the different formulations, however for the P5 parts the increase in the relative density (38 %) is higher than the ones observed for P3 (22 %) and P4 (27 %) after CIP and industrial sintering combined. This result is in accordance with the higher amount of porcelain in P5 formulation and, even though its green part exhibit the lowest relative density, the use of CIP which approximates the porcelain particles, followed by the industrial sintering which removes the *in-bed* binder and promotes the matter diffusion between porcelain particles, leads to the highest relative density measured among all the printed parts.

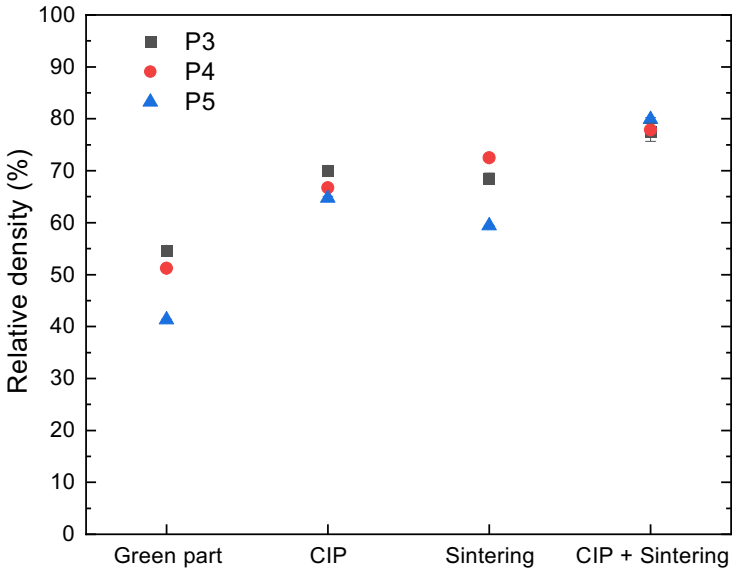


**Figure 5.10:** Relative density of printed parts using P3, P4 and P5 formulations, in the different steps of processing. The P5 formulation, the one with higher content of porcelain, has the highest relative density after CIP followed by industrial sintering.

The micrographs of fractures zone of parts produced with the different formulations are presented in Figure 5.11, after CIP and industrial sintering. It is possible to observe that the microstructures do not present significative differences among them, which is in accordance with the results discussed above for the relative density. The parts produced with the different formulations have relative densities varying between 78 and 80 %.

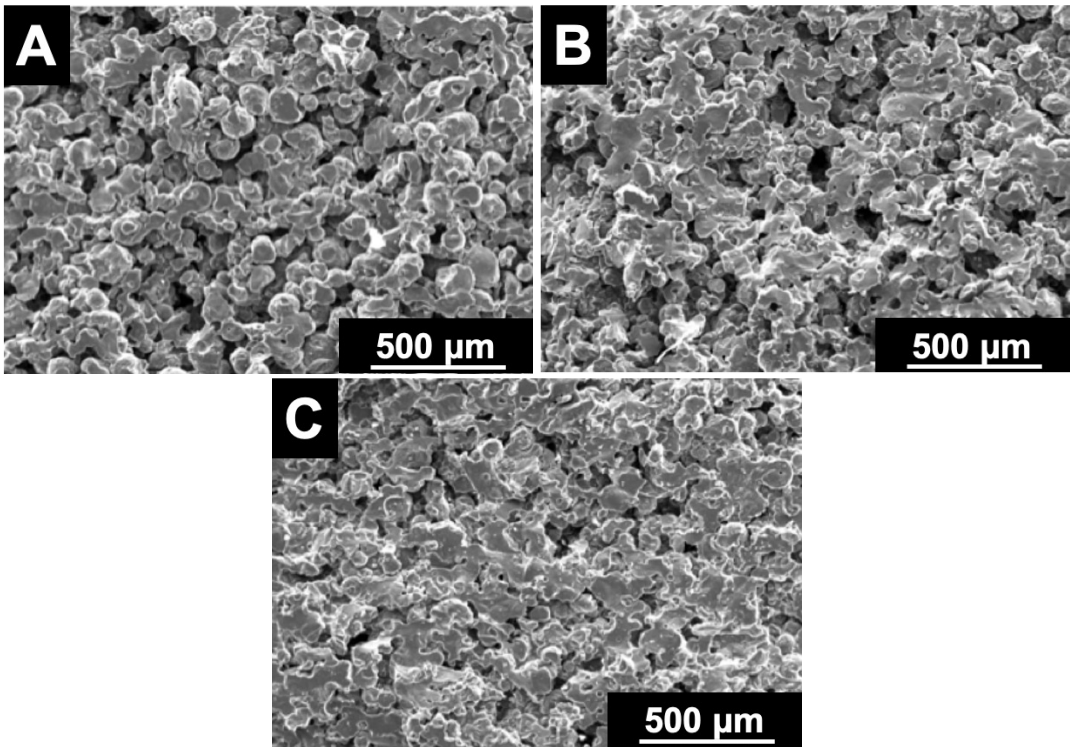


**Figure 5.11:** Micrographs of fracture zone of printed parts produced with (a) P3, (b) P4 and (c) P5, after CIP followed by industrial sintering processing. The microstructures do not have significative differences among them, in accordance with relative density results, which are similar and close to 80 %.

The results of relative density are close to the ones found in the literature with alumina parts using polyamide as sacrificial binder. Deckers *et al.* [3] reached 86 % of relative density after CIP and sintering, using 22 wt.% of polyamide. The green parts of the group have lower relative density (40 %) when compared with the parts with similar amount of polyamide in our work: 55 % for P3 (25 wt.%) and 51 % for P4 (20 wt.%). The same authors [4] only reached 34 % of relative density in green parts of alumina, using polypropylene as sacrificial binder. The group was able to reach 89 % of relative density, however they used warm isostatic pressing, which has a temperature slightly higher than the Tg of the binder, to improve the relative density of the green part.

The results of relative density showing similar values for the porcelain parts produced with formulations using different ratios of porcelain/polyamide, it is also important to assess the dimension variations of the produced parts and compared with the virtual design dimensions of the CAD design. This is a crucial property for a product design driven company as *Porcelanas da Costa Verde*.

In this sense, the length and diameter variation of printed parts to the virtual design are presented in Figure 5.12 for P3, P4 and P5 formulations, after each step of processing. As green parts, the length variation varies from 2,8 % for P5 parts to 3,6 % and 4,3 % for P4 and P3 parts, respectively. In the case of the diameter variation, the maximum values were observed for P3 green parts (4,1 %) and decreased for P4 (3,6 %) and P5 (3,2 %). These results exhibit a positive value, meaning that the diameter of the green part is higher than the diameter of the virtual design. The reason for this to happen is related with the commercial SLS and software which is prepared to work with only polyamide 12 powders, typically contracts during the laser sintering process. In this sense, the software automatically compensates this contraction scanning a larger section which will match the dimension of the virtual design after contracting. Once we are using a feedstock that has a bigger fraction of porcelain powders than the fraction of polyamide, the contraction during laser sintering is lower than the one of a feedstock using only polyamide. Thus, the printed parts with P3, P4 and P5 will have larger dimensions than the virtual design once they do not contract as much as a feedstock with only polyamide.

In the case of parts processed by CIP, while P3 and P4 presented close values of diameter variation (-6,3 % and -7,7 %, respectively) and length variation (-6,0 % and -6,7 %, respectively), the P5 parts exhibit a diameter and length variation of -11,4 %. This difference among the parts of different formulations regards on the relative density of the green parts, which is lower for P5 (42 %) than for P3 (55 %) and P4 (51 %), as presented in Figure 5.10, meaning that the P5 part has more void space between particles and retracts more during the CIP process than parts of P3 and P4 formulations. This result also supports the different values of relative density after CIP (Figure 5.10), discussed above, which exhibit a higher increase in relative density for P5 parts (21 %) than for P3 and P4 ones (15 %) after CIP, and was explained by their relative density of green parts. In the case of industrially sintered parts, P5 parts presented the highest diameter variation (-19,1 %) followed by P4 (-16,1 %) and P3 (-13,9 %) ones, and the same trend was observed for the length variation with P5 parts presenting a value of -17,0 %, followed by P4 (-15,1 %) and P3 (-13,9 %). Although the P5 parts presented the highest negative variation of diameter and length, i.e., the highest retraction, it did not translate in the highest relative density, as presented in Figure 5.10, and our results leads us to advocate that this fact is attributed to the lower relative density of the green part than the ones of P3 and P4 formulations.

The parts processed by CIP followed by industrial sintering, presented the highest variations, as illustrated in Figure 5.11. The diameter variation was higher for P5 parts (-26,7 %) than for P4 (-21,9 %) and P3 (-20,7 %), while the length variation followed the same trend, with values of -27,4 %, -23,1 % and -21,2 % for P5, P4 and P3 parts, respectively. The higher retraction of P5 parts than the ones of P4 and P3, are in accordance with the relative density values (Figure 5.10) which were similar after CIP followed by industrial sintering for the three formulations, meaning that P5 parts retracted more to reach similar values of relative density.

This range of retractions are typical from powder bed AM processes, as found by Deckers *et al.* [5] where the group found retractions between 22 and 24 % using warm isostatic pressing as densification step, followed by debinding and sintering processes, with alumina as ceramics and polystyrene as binder. However, the retractions measured by the authors used the green part dimensions as reference, while in our work we used the CAD file dimensions as reference. The same authors found retractions between 31 and 44 % in X/Y and Z directions, respectively, for parts with only debinding and sintering processes. In our work we found also anisotropy in the dimension variations of parts which were not processed by CIP and were directly sintered after SLS. However, the difference was between 1 and 3 %, with higher retraction in the X/Y direction of the parts printed with P5 formulation. In accordance with the work of Deckers, we also found that the isostatic pressing reduces the anisotropy of the linear retraction of the final sintered parts.

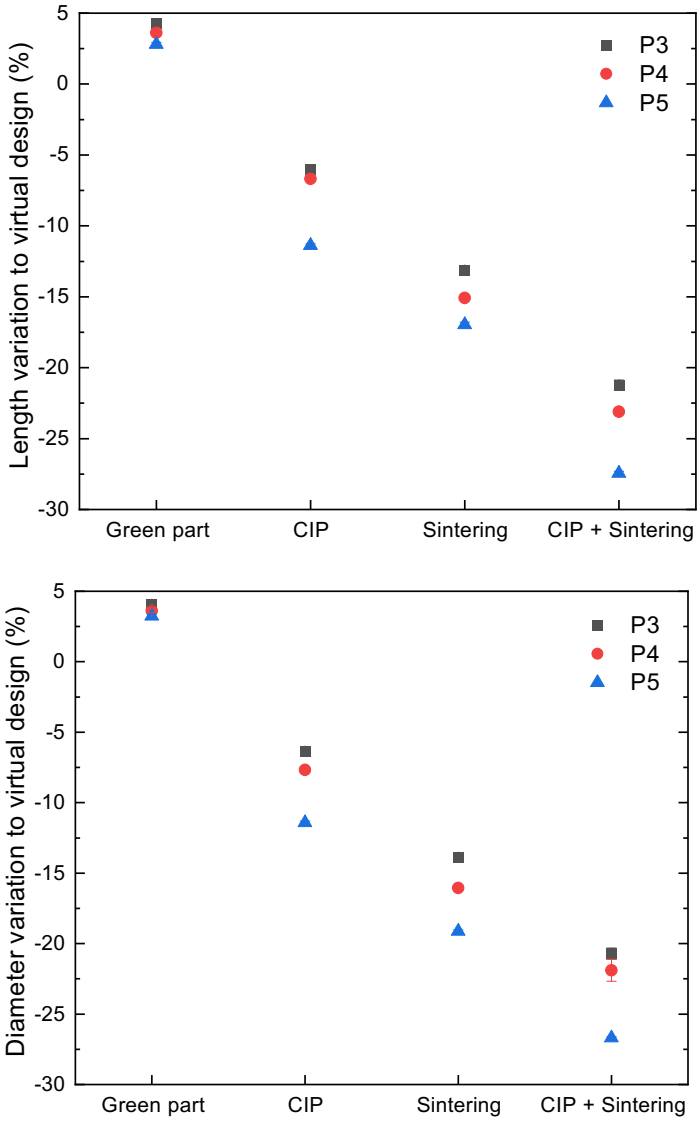


**Figure 5.12:** Length and diameter variation of the printed parts with different amounts of polyamide 12 as *in-bed* binder, after each processing step to the virtual design dimensions. The increase in the porcelain content leads to higher variations of both length and diameter of the printed cylinder.

Summarizing, the most relevant results regarding the relative density of the printed parts occur after the green parts are isostatically pressed and then sintered. In this case, the parts with the higher content of porcelain, P5, present slightly higher relative density (80 %) than the ones produced with P3 (77 %) and P4 (78 %) formulations. The relative density of the three parts produced with different amounts is similar, while the dimension variations of the P5 part is 5 % higher than the P4 and P3 formulations. We also observed that the use of CIP may reduce the anisotropy of the dimensional variations during the following industrial sintering.

### 5.3.1. Reuse of powder formulation

The amount of waste powders in SLS is quite high, as discussed in Chapter 1, and from the industrial application point of view, reusing the powders is relevant. Hence, due to the industrial interest of this work, the reuse of powder formulation was studied as well. The formulations R1 and R2 were used to perform this study. They were obtained as exceeding powders from previous SLS prints: the R1 after the P3 SLS print, and the R2 formulation after the R1 SLS print, as indicated in Table 5.I.

The relative density of the parts produced using reused powders is presented in Figure 5.13. As general overview, it is possible to observe that parts produced with R1 and R2 formulations have always lower relative density than the ones produced using the starting formulation P3. As green part, the relative density decreases from 55 % for P3 printed parts to 50 % for R1 and 46 % for R2 ones. The same trend was observed for parts processed by CIP, decreasing from 70 % for P3 to 67 % for R1 and 65 % for R2 and processed by industrial sintering, decreasing from 69 % for P3 to 65 % for R1 and 63 % for R2. The maximum of relative densities was obtained for printed parts processed by CIP followed by industrial sintering, reaching the maximum of 77 % for P3 parts, and decreasing to 74 % for R1 and 72 % for R2. Based on this result, we can advocate that the reuse of powders has an impact in the relative density of printed parts, leading to less dense parts with the reuse of powders. However, this difference is not significative once these relative densities are quite far from fully dense bodies, which is the goal for porcelain parts industrially produced.

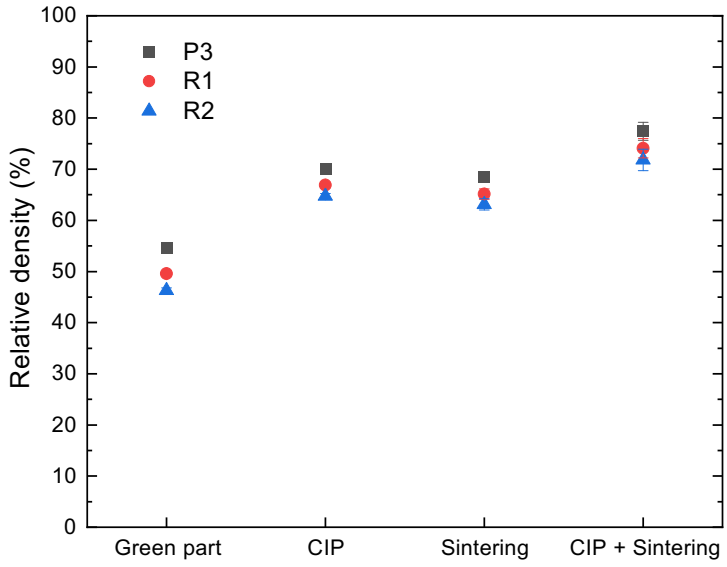


**Figure 5.13:** Relative density of printed parts with P3, R1 and R2 formulations, in the different steps of processing. The reuse of powders leads to a decrease in the relative density of parts, a trend observed at every stage of processing.

The diameter and length variations to the virtual design of the parts produced with reused powders are presented in Figure 5.14. A general overview leads to the conclusion that the parts produced with the reused formulations R1 and R2, have similar diameter and length variations as the starting formulation P3. In the green state, the diameter variation of P3 parts is 4,1 %, while for R1 and R2 parts is 3,9 %, while the length variation is 4,3 % for P3 parts and 3,9 % for R1 and 4,3 % for R2 respectively. After CIP, the diameter variation of P3 is -6,3 %, while for R1 and R2 are -6,5 % and -6,9 % respectively, while the length variation is -6,0 % for P3 and -6,5 % and -6,0 % for R1 and R2, respectively. The industrially sintered parts produced with P3 formulation presented a length and diameter variation of -13,8 % and -13,1 %, respectively, while the variation increased for R1 (-14,6 % and -13,9 %) and for R2 (-14,9 % and -14,1 %). The differences between the starting formulation and the reused powders reached a maximum for the parts processed by CIP and industrial sintering, as P3 exhibit diameter and length variations of -20,7 % and -21,2 %, respectively, while for R1 parts the values were -21,7 % and -22,1% and for -22,4 % and -23,0 %, for diameter and length variations respectively.

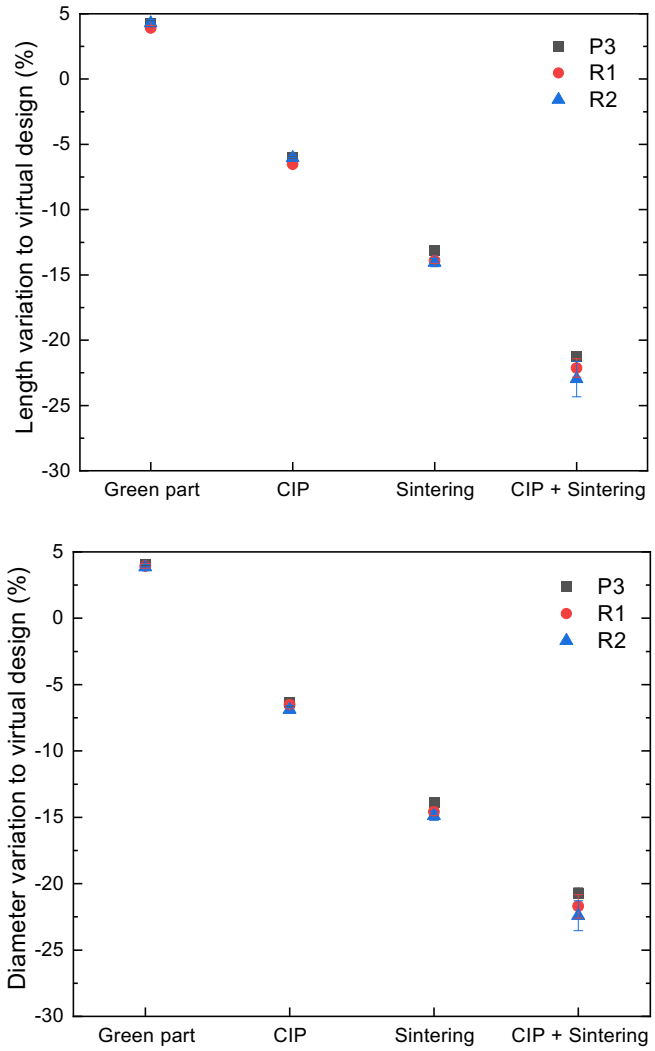


**Figure 5.14:** Length and diameter variation of the printed parts with P3, R1 and R2 formulations, after each processing step, to the virtual design dimensions. The reuse of powders does not have a significative impact in the dimension variations of the printed parts.

As for all powder formulations, 400 cylinders and cubes were printed, Figure 5.15 illustrates defective green printed parts produced with R1 and R2 formulations. These defective parts represent 4 and 8% of all printed parts for R1 and R2, respectively. The defects observed suggests a shift in position of parts during SLS process. It was possible to observe that some expansion of powder, rising above the powder bed surface occurs after the laser scan in the position of the parts to be printed. This expansion above the powder bed surface is enough for the roller to push the printed parts and move them out of position in the powder bed. Additionally, defect free parts were used for industrial sintering and some of these parts presented deformations and fractures after sintering, as illustrated in Figure 5.16.

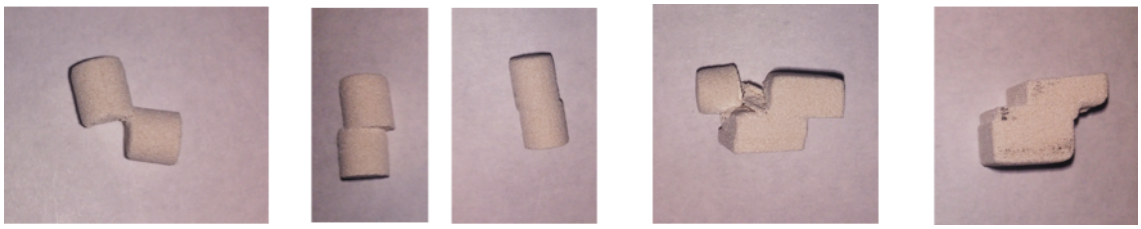

**Figure 5.15**: Examples of defective green parts printed with reused powder (R1 and R2). The parts present a shifting in position due to roller action during SLS.

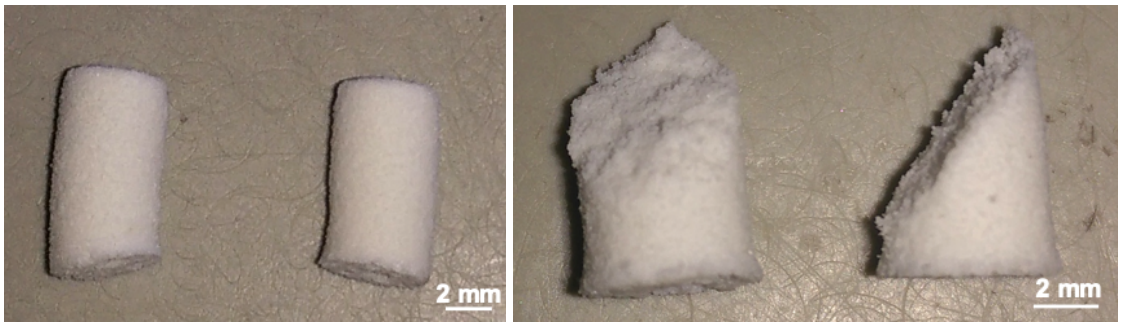


**Figure 5.16:** Examples of defective parts printed with reused powders (R1 and R2 formulations), after CIP followed by industrial sintering. The parts on the left exhibit a deformation while the parts on the right broke during sintering.

As for the first defect, observed for green parts (Figure 5.15), a hypothesis for this effect in the reused powders was attributed to the thermal processing of the polyamide, which is not used in any printed part but is subject to heating (up to 170 ºC) during the SLS process, as powder present in the part bed. Kruth *et al.* [6], found that the thermal deterioration of the polyamide leads to an increase in the molecular weight and its viscosity, promoting an inconstant consolidation and a shift in the melting point, which can result in coalescence of the particle size of the polyamide. This observation by Kruth is coherent with the effect of powder rising above the powder surface, observed in our work. However, further investigation is needed to understand the thermal deterioration of the polyamide 12 used in our work and its role in the development of the defects observed in the green parts.

The second set of defective porcelain printed parts, occurring after the industrial sintering, might be related with fine particle fraction reduction in the reused formulations (R1 and R2). In this sense, an analysis of cumulative PSD was done for P3, R1 and R2 formulations, and it is presented in Figure 5.17. It is possible to observe that the PSD cumulative curve presents a shift in position to the right, i.e., to the large particles side of the reused formulations (R1 and R2). Additionally, there is a decrease in the fraction of particles smaller

than 20 µm from 24 vol.% for P3 formulation to 19 vol.% for R1 and 12 vol.% for R2 powders. This reduction of fine particles fractions occurs during the setup of the printing process, where the powders are manually removed from the powder bed after the SLS process and deposited again in the feeding beds. This powder manipulation leads to a loss in fine particles fraction which remain suspended in the air rather than the larger particles [7].

The lack of these particles will leads to an increase of porosity in the printed part, as supported by the lower relative density of parts produced with R1 and R2 formulations than the ones of P3 formulation (Figure 5.13), leads to distortions (Figure 5.16, left) during the sintering or even the fracture of parts (Figure 5.16, right). This phenomenon was observed by Strondl *et al.* [8] with nickel alloy powders, where the lack of fine particles lead to distortions in the printed parts during sintering.

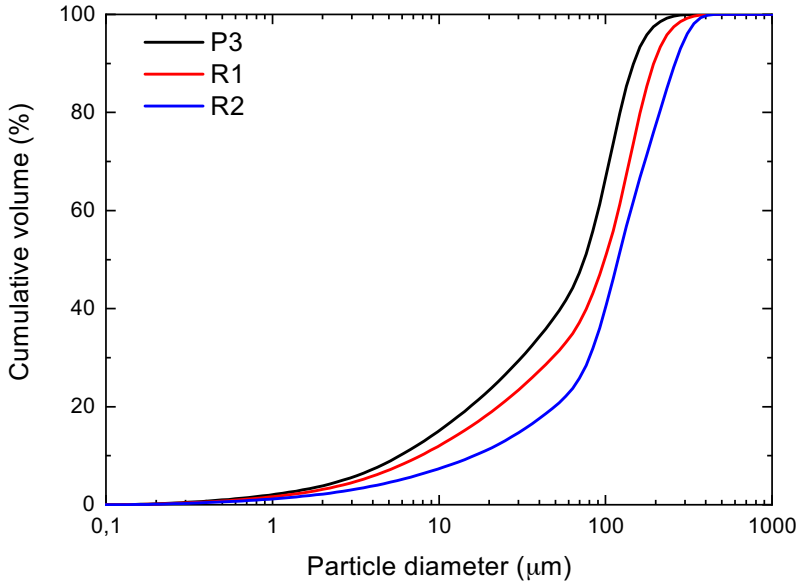


**Figure 5.17:** Cumulative particle undersize curves of P3, R1 and R2 formulations for SLS. The reused powders present a shift in the cumulative curve to the right, suggesting a decrease in the fine particles fraction.

Summarizing, the reuse of porcelain powders formulations with polyamide 12 as *in-bed* binder is possible and does not remarkably affect the relative density (Figure 5.13) and the part dimension variations (Figure 5.14). However, defective parts were obtained both in green state and after industrial sintering process, which may jeopardize the full reuse of powders in the SLS of porcelain parts. Further investigation is needed to understand how to avoid these defects, which may be done by mixing reused and new powders.

## 5.4. Conclusions

This work focused on the exploration of indirect selective laser sintering of porcelain powders for industrial production of porcelain objects. This paper shows that it is possible to produce porcelain parts by indirect SLS. However, due to the high reactivity of the spray dried porcelain powders there is a need of a heat treatment of the powders in order to make it printable. With the heat-treated porcelain powders, it was possible to obtain parts with 80 % densification, using a formulation with a porcelain/polyamide weight ratio of 5:1. The work also showed that formulations with higher amount of porcelain may produce green parts with lower densification, mainly due to the differences of the particle size of porcelain and the polyamide. However, the densification of the parts after CIP and sintering is slightly higher for the parts printed with higher amount of porcelain, followed with higher linear retractions (26 %). A curling effect was observed for the parts with higher amount of polyamide, especially for cylinders printed in the horizontal position, which leads to defective parts regarding its design.

Finally, due to the industrial application and interest, the reuse of powders in SLS was also studied, showing that the manipulation of the powders leads to the loss of finer particles, which reflects parts with lower densification and distortions after CIP and industrial sintering. However, the reuse of the powders is still possible, and the addition of virgin powders may avoid these defective parts.

At the end, this work show that the use of indirect selective laser sintering is possible to produce porcelain parts through AM. However, more post processing steps are required in order to reach higher density of final parts.

## 5.5. References

[1] M. Schmid, A. Amado, and K. Wegener, “Polymer powders for Selective Laser Sintering,” in *30th International Conference of the Polymer Processing Society*, 2014, pp. 1–5.

[2] K. Wudy and D. Drummer, “Aging effects of polyamide 12 in selective laser sintering: Molecular weight distribution and thermal properties,” *Addit. Manuf.*, vol. 25, pp. 1–9, 2019.

[3] J. Deckers, K. Shahzad, J. Vleugels, and J. P. Kruth, “Isostatic pressing assisted indirect selective laser sintering of alumina components,” *Rapid Prototyp. J.*, vol. 18,

no. 5, pp. 409–419, 2012.

[4] K. Shahzad, J. Deckers, J. P. Kruth, and J. Vleugels, “Additive manufacturing of alumina parts by indirect selective laser sintering and post processing,” *J. Mater. Process. Technol.*, vol. 213, no. 9, pp. 1484–1494, 2013.

[5] J. Deckers, J.-P. Kruth, L. Cardon, K. Shahzad, and J. Vleugels, “Densification and Geometrical Assessments of Alumina Parts Produced Through Indirect Selective Laser Sintering of Alumina-Polystyrene Composite Powder,” *Stroj. Vestnik-Journal Mech. Eng.*, vol. 59, no. 11, pp. 646–661, 2013.

[6] J. P. Kruth, G. Levy, F. Klocke, and T. H. C. Childs, “Consolidation phenomena in laser and powder-bed based layered manufacturing,” *CIRP Ann. - Manuf. Technol.*, vol. 56, no. 2, pp. 730–759, 2007.

[7] A. Rashid, *Additive Manufacturing Technologies*. 2019.

[8] A. Strondl, O. Lyckfeldt, H. Brodin, and U. Ackelid, “Characterization and Control of Powder Properties for Additive Manufacturing,” *J. Miner. Met. Mater. Soc.*, vol. 67, no. 3, pp. 549–554, 2015.

# *Chapter 6: Post-conformation processing of porcelain printed parts towards densification*

**Abstract**

In this chapter we discuss post-conformation steps aiming to increase the relative density of the porcelain printed parts obtained by powder bed AM techniques: binder jet printing (BJP) and selective laser sintering (SLS). Although several post-conformation processes have been reported in the literature to increase the density of the printed parts, there is a lack of comparison of processes suitable for industrial scale, especially for industrial porcelain parts. In this sense, a second goal is to compare BJP and SLS for the industrial production of porcelain parts, regarding the relative density of the parts at different stages of industrial processing. The porcelain printed parts used in the present study were selected as the ones exhibiting the best results in terms of printability and relative density in the previous studies. The porcelain bodies, produced with BJP and SLS, were processed through industrial thermal sintering cycles, cold isostatic pressing and pressureless infiltration with porcelain suspension. The cold isostatic pressing and the thermal cycles were, among the processes studied, the ones that increased more relative density of porcelain bodies. The infiltration process was found to be ineffective in the improvement of relative density of the final parts. The maximum relative density reached (97 %) was obtained for parts produced by BJP, while for the SLS parts the maximum relative density reached was 84 %, both after CIP and industrial sintering. The SLS ceramic bodies were less dense than the BJP parts, regardless the densification process, due to higher amount of *in-bed* binder used and the use of only heat-treated porcelain powders.

**Keywords**

Binder jet printing, industrialization, porcelain, additive manufacturing

## 6.1. Introduction

As discussed in Chapter 1, due to its working principle, powder bed AM techniques usually lead to fragile green parts and parts with high porosity and post-conformation steps are required in order to improve the density of the final parts. Thermal processing, isostatic pressing and infiltration are among the most used processes for densification of printed parts.

The main goal of this work is to explore post-conformation processes of printed parts by powder bed AM techniques using industrial porcelain powders by Costa Verde, such as industrial thermal processing, isostatic pressing and pressureless infiltration, in order to increase the relative density of the industrial porcelain parts. The thermal cycles and the pressureless infiltration were chosen due to its availability in the conventional production route, and CIP was chosen due to its impact in the increase of relative density of final parts, as discussed above. In addition, a second objective of this study is to compare porcelain parts produced though BJP and SLS regarding their relative density.

## 6.2. Materials and methods

### *6.2.1. Feedstock and printing conditions*

The feedstock and printing conditions used in this work were chosen based on the previous studies as the ones exhibiting the best results in terms of printability and relative density. Two different feedstocks formulations were used for BJP and are here identified as 0HT and 50HT. The 0HT formulation has 90 wt.% of spray dried porcelain powders and 10 wt.% of PVA as *in-bed* binder. The 50HT formulation has 45 wt.% of spray dried porcelain, 45 wt.% of heat-treated porcelain powder and 10 wt.% of PVA, as *in-bed* binder. A ZPrinter 650 (ZCorporation) was used to print both feedstocks using the printing parameters described in Chapter 2. The SLS parts, identified in this work as SLS, were produced in Sinterstation HiQ+HiS (3D Systems) using the conditions described in Chapter 2. The feedstock was composed of 84 wt.% of heat-treated porcelain powder mixed with 16 wt.% of polyamide 12 (PA 650, Advanced Laser Materials, USA), used as *in-bed* binder.

To assess the relative density through the different steps of processing, cylindrical parts were printed with a diameter of 14 mm and a length of 28 mm in the case of BJP, and diameter of 6,35 mm and length of 12,7 mm, in the case of SLS. Complex shaped parts were printed as well, named as chess pawn in this work (Figure 6.1). The chess pawn with a hollow complex shape (Figure 6.1 A) was originally designed by JaaYoo [1] and the design of the second pawn was adapted to a bulk form (Figure 6.1 B).

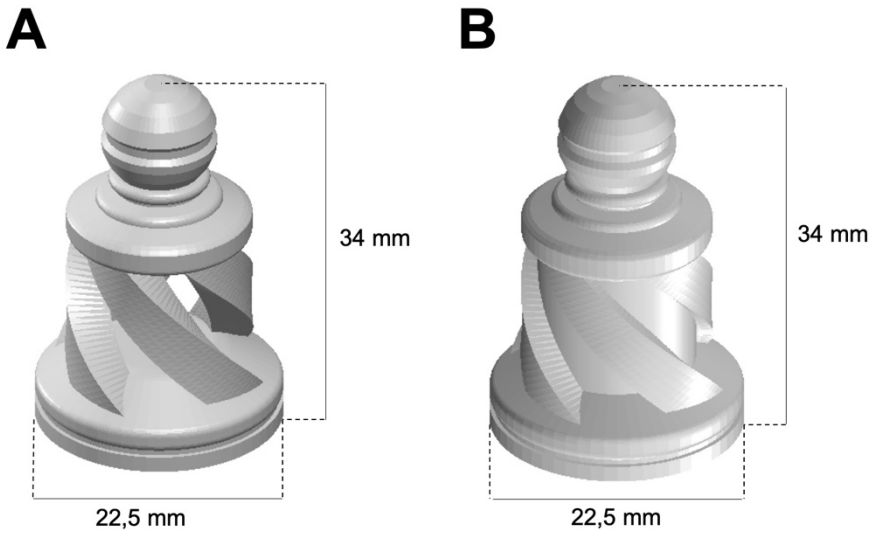


**Figure 6.1:** Virtual designs of complex shaped parts, named as chess pawns, in the hollow form (A) and bulk form (B).

The post-conformation processes used in this work were industrial sintering cycles, cold isostatic pressing and pressureless infiltration with porcelain suspension.

The sintering cycles were performed in continuous industrial kilns, from *Porcelanas da Costa Verde, S.A.* (Portugal) facilities, with a maximum temperature of 1178 °C (PTCR), for 2,5 h, for the 1st sintering, and 1358 °C (PTCR), for 5,5 h, for the 2nd sintering process.

For CIP, green printed parts were protected with a rubber bag, in vacuum, and then processed in cold isostatic presser using an oil medium to apply 196 MPa, for 5 min.

The pressureless infiltration consisted in soaking the printed parts, after the 1st sintering cycle, in a water based suspension, produced by *Costa Verde, S.A.* (Portugal), varying the agitation method, soaking time, suspension density and the use of deflocculant, in the case Dolapix (Zschimmer & Schwarz Chemie GmbH, Germany). The different tests and its parameters are presented in Table 6.I.

**Table 6.I:** Pressureless infiltration conditions used to infiltrate printed parts with porcelain suspension, with variation in the agitation method, soaking time and suspension characteristics.

| Test | Agitation method | Soaking time (min) | Density (g/cm$^3$) | Deflocculant (wt.%) |
|---|---|---|---|---|
| I1 | Not used | 10 | 1350 ± 5 | Not used |
| I2 | Ultrassounds | 10 | 1350 ± 5 | Not used |
| I3 | Magnetic stirring | 10 | 1350 ± 5 | Not used |
| I4 | Magnetic stirring | 10 | 1350 ± 5 | Not used |
| I5 | Magnetic stirring | 30 | 1350 ± 5 | Not used |
| I6 | Magnetic stirring | 60 | 1350 ± 5 | Not used |
| I7 | Magnetic stirring | 10 | 1350 ± 5 | 0,2 |
| I8 | Magnetic stirring | 10 | 1250 ± 5 | 0,2 |
| I9 | Magnetic stirring | 10 | 1150 ± 5 | 0,2 |

The diameter variation ($\Delta D$), the length variation ($\Delta L$) and the geometric relative density ($\%\rho_{geom}$) of the green printed cylinders was calculated using the procedure described in Chapter 2. In addition, the relative density measured by Archimedes method, $\%\rho_{Arc}$, and the microstructure of the sintered parts were assessed as described in Chapter 2 as well.

## 6.3. Results and discussion

In this chapter the aim of study is the post-conformation steps towards densification of porcelain parts produced by BJP and SLS. In addition, a comparison between BJP and SLS techniques in the production of porcelain parts, printed in the conditions studied in previous chapters of this thesis, focusing on the relative density of sintered parts.

The formulation of the porcelain powders feedstock for each technique was studied in previous chapters of this thesis. In this chapter, the formulation 0HT is composed by 90 wt.% of porcelain spray dried powders and 10 wt.% of PVA as *in-bed* binder and the formulation 50HT is composed by 45 wt.% of spray dried porcelain powders, 45 wt.% of heat-treated porcelain powders and 10 wt.% of PVA as *in-bed* binder. The amount of PVA (10 wt.%) was found, in Chapter 3 of this thesis, to be the one that have the best combination

of relative density and design features of porcelain printed parts, after industrial sintering. Concerning the fraction of porcelain powders, as discussed in Chapter 4 of this thesis, the use of only spray dried powders (0HT) leads to sintered parts with the highest relative density, while a mixture with equal amount of spray dried and heat-treated porcelain powders (50HT) was the one leading to design defect free ones. In the case of feedstock for SLS of porcelain powders, studied in the Chapter 5 of this thesis, the feedstock formulation with 84 wt.% of heat-treated porcelain powders and 16 wt.% of polyamide 12 as *in-bed* binder was the one that presented the highest values of relative density for sintered parts.

### *6.3.1. Industrial sintering cycles*

The relative density of printed parts, produced by BJP and SLS, after each step of processing, measured by geometric and Archimedes method is presented in Table 6.II. In the green state, the parts produced by SLS present the highest value of geometric relative density (44 %), followed by the parts produced with 0HT (39 %) and 50HT (35 %). This difference is attributed to the higher amount of *in-bed* binder used in the porcelain powers feedstock for SLS (16 wt.%) than the one for BJP (10 wt.%), which promotes better filling of the void space between porcelain particles by fused polyamide 12, leading to an increase in the green relative density. In addition to the difference in the amount of *in-bed* binder, factors such as the penetration of the *in-bed* binders in the void space between ceramic particles may also contribute to the increase in the green relative density, i.e., after the laser scan, in the case of polyamide 12 for SLS, and after the deposition of the liquid binder, in the case of PVA for BJP. In this case, further investigation regarding the penetration behavior of both *in-bed* binders is needed.

After the 1$^{st}$ industrial sintering cycle, performed at 1174 °C for 2 h 30 min, the parts produced by SLS presented the lowest value of geometric relative density (35 %) while the BJP parts exhibit 39 % and 38 %, for the formulations 0HT and 50HT, respectively. The relative density assessed by Archimedes method exhibit values with the same trend, where the highest one was observed for 0HT formulation (42 %) followed by the 50HT (41 %) and SLS parts (39 %). It is noticeable that in the case of parts produced by BJP there is a slight increase in the relative density from the green part to the part after the 1$^{st}$ sintering, while in the case of SLS parts a decrease of 8 % in the relative density was observed. This result is explained by the thermal removal of the *in-bed* binder in both cases, however, the higher

amount of *in-bed* binder used for SLS porcelain feedstock than for BJP, leads to a higher porosity in the printed part than for the BJP ones. Even though the *in-bed* binder was removed, the parts produced by BJP present similar values as green part and after the 1st sintering. This result suggests that, after the PVA is removed, densification is occurring and compensates the void space that the *in-bed* binder leaves after degradation. However, the temperature and time of the thermal cycle is not enough to fully densify the porcelain bodies.

The green printed parts were also directly processed in the 2nd industrial sintering cycle, at 1358 °C for 5 h 30 min, and it is possible to observe that both parts printed in by BJP presented higher geometric relative density, 60 % and 62 % for 0HT and 50HT feedstocks, respectively, when compared with the SLS part which presents 51 % of relative density. In the case of the relative density assessed by Archimedes method, the same trend was observed, with similar values of 67 % for 0HT and 50HT feedstock, and the lowest value of 55 % for SLS parts. As discussed above, the higher amount of *in-bed* binder in SLS feedstock than for BJP, leads more void space in the parts after its thermal removal and decreases the relative density of the porcelain bodies. However, as opposed to the 1st sintering cycle, an increase of relative density, higher than 20 %, was observed for the BJP parts and around 15 % for the SLS ones. This difference for the 1st sintering cycle is attributed to its higher maximum temperature and duration, which promotes matter diffusion inside the porcelain bodies and increases their density.

At the same time, printed parts were processed in both 1st and 2nd sintering cycles, and its relative density is also presented in Table 6.II. The parts produced by BJP present geometric relative densities of 65 % and 63 % for 0HT and 50HT feedstocks and 51 % for parts produced by SLS. In the case of relative density assessed by Archimedes method, the same trend was observed with similar values for 0HT (71 %) and 50HT (68 %), while the parts produced by SLS present the lowest value, 56 %. The parts produced by BJP present values of relative density, after both sintering cycles, slightly higher than the ones observed for parts processed by only the 2nd sintering. This result suggests that most of the densification occurs during the 2nd sintering cycle, attributed to the maximum temperature and duration of the cycle. The increase of relative density by 5 %, for 0HT, and 2 %, for 50HT, using two sintering cycles, is attributed to the fact that the debinding process, i.e., the thermal removal of the *in-bed* binder, which occurs in the 1st sintering cycle does not jeopardizes the densification process during the 2nd sintering cycle, as opposed to the use of only the 2nd sintering cycle, in which the *in-bed* binder needs to be removed. In the case

of the parts produced by SLS, there is not significative difference of using only the 2nd cycle or both 1st and 2nd cycles combined. This is attributed to the fact that the use of 16 wt.% of polyamide in the feedstock leads to higher porosity than for BJP parts, which jeopardizes the matter diffusion during the sintering process and, as consequence, leads to lower relative density of sintered parts. Another factor that may influence the SLS parts to have lower relative density than the BJP ones is the use of only heat-treated porcelain powders in its feedstock. Once the porcelain powders were already thermal treated may influence the behavior during densification processes which occurs during sintering. In addition, properties of the *in-bed* binders, such as its particles size distribution and thermal degradation behavior can also contribute to the differences in the relative density of SLS and BJP parts, however, these characteristics were not addressed in this work.

The SEM micrographs of the printed parts microstructure after the 1st and 2nd sintering cycles is presented in Figure 6.2. As it is possible to observe, the microstructures of 0HT (Figure 6.2 A) and 50HT (Figure 6.2 B) parts are similar, while the one of SLS parts presents higher porosity than the other two (Figure 6.2 C). The microstructures are in accordance with the relative densities of the printed parts, after the two sintering cycles, where the SLS part exhibits the lowest relative density, while the BJP present similar values, as presented in Table 6.II.

**Table 6.II:** Relative density of 0HT, 50HT and SLS printed parts, measured by geometric and Archimedes method, at the different stages of processing: green part, 1st sintering (1178 °C, 2 h 30 min), 2nd sintering (1358 °C, 5 h 30 min) and both 1st and 2nd sintering.

| | **0HT** | | **50HT** | | **SLS** | |
|---|---|---|---|---|---|---|
| | $\%\rho_{geom}$ (%) | $\%\rho_{Arc}$ (%) | $\%\rho_{geom}$ (%) | $\%\rho_{Arc}$ (%) | $\%\rho_{geom}$ (%) | $\%\rho_{Arc}$ (%) |
| Green part | 39,0 ± 0,7 | --- | 35,3 ± 0,5 | --- | 43,5 ± 0,2 | --- |
| 1st Sintering | 39,4 ± 0,5 | 42,2 ± 0,5 | 37,9 ± 0,3 | 40,7 ± 0,1 | 35,3 ± 0,2 | 39,1 ± 0,2 |
| 2nd Sintering | 60,0 ± 1,1 | 67,4 ± 0,8 | 61,6 ± 0,4 | 66,5 ± 1,2 | 50,6 ± 0,2 | 55,4 ± 0,2 |
| 1st Sintering + 2nd Sintering | 64,9 ± 0,8 | 71,0 ± 0,6 | 62,9 ± 1,0 | 68,4 ± 0,8 | 50,7 ± 0,2 | 55,6 ± 0,2 |

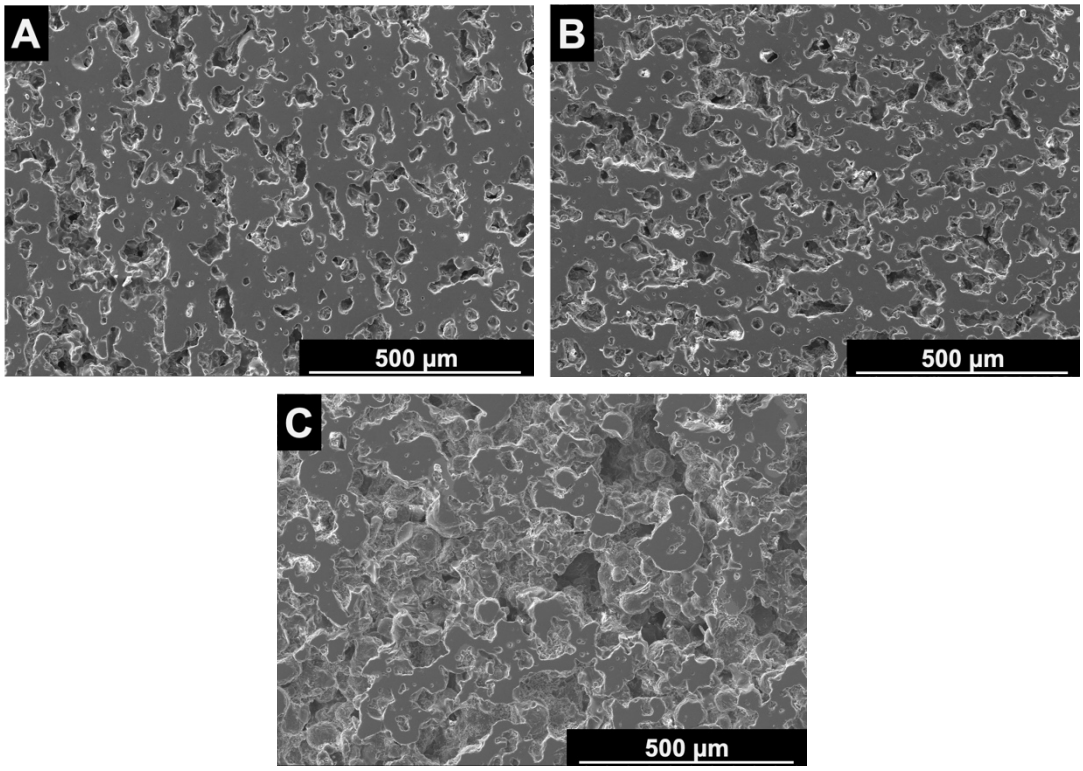


**Figure 6.2:** SEM micrographs of polished fracture zone, after the two sintering cycles, of (A) 0HT, (B) 50HT and (C) SLS parts. The images illustrate similar microstructures of BJP parts (A and B) and a microstructure with more porosity for the SLS one.

The diameter and length variation of the printed cylinders to the virtual design dimensions was also assessed and is presented in Table 6.III. In green state, the parts produced by BJP present lower dimensions than the virtual design, while the SLS printed part exhibit higher dimensions than the virtual design. This effect was presented and discussed in Chapters 4 and 5 of this thesis and was attributed to the use of porcelain powders feedstock in commercial printers which are not prepared for them. In this chapter the focus is the dimensions variations after the post-conformation steps.

After the 1$^{st}$ sintering cycle, the parts produced by BJP using the 0HT exhibit a diameter and length variation of - 11 % and - 9 %, respectively, while the ones produced using the 50HT present - 9 % and - 8 % for diameter and length variations, respectively. In the case of SLS parts, the diameter and length variation have similar values of - 8 %. These results are in accordance with the relative density measured for the parts (Table 6.II), which was higher for 0HT than for 50HT and SLS parts. In the case of the parts processed by the 2$^{nd}$ sintering, the variations of 0HT and 50HT parts increased to - 23 % and - 26 % in the diameter and length directions, respectively. In the case of SLS parts, the diameter and

length variation are - 18 %. These values suggest anisotropy in the linear retraction during the 2nd sintering cycle for BJP parts, which was not observed for the 1st sintering cycle. In one hand, this result supports the idea that most of the densification occurs during the 2nd sintering cycle, as discussed above, on the other hand, it suggests that the BJP parts have higher porosity in the printing direction than in the layer one. This fact may be attributed to the layer by layer printing process, which promotes the interparticle contact in layer direction rather than in the printing direction, and, as consequence, promotes the matter diffusion within the layer (in this work, in the diameter of the cylinder direction) as opposed to the printing direction (in this work, in the length direction) as reported in the literature by Shanjani *et al.* [2]. In the case of SLS this effect was not as prominent as in BJP parts and may be related with higher space between porcelain particles in the same layer, created by the higher amount of *in-bed* binder used in SLS than in the BJP.

The same trend was observed for parts processed using both 1st and 2nd sintering cycles, with similar values as the ones exhibited for printed parts sintered using only the 2nd cycle. The BJP parts presented similar values of diameter variation (- 23 %) for both 0HT and 50HT feedstocks, while in the case of the length variation 0HT exhibit slightly higher variations (- 27 %) than the one observed for 50HT parts (- 26 %). Concerning the SLS parts, a diameter variation of - 19 % and a length variation of - 18 % were observed. These results support and are in accordance with the relative densities (Table 6.II) of the printed parts sintered using both sintering cycles, which are similar to the ones for printed parts sintered using only the 2nd sintering cycle.

**Table 6.III:** Diameter and length variation of 0HT, 50HT and SLS printed parts, to the virtual design dimensions, at the different stages of processing: green part, 1st sintering (1178 °C, 2 h 30 min), 2nd sintering (1358 °C, 5 h 30 min) and both 1st and 2nd sintering

| | **0HT** | | **50HT** | | **SLS** | |
|---|---|---|---|---|---|---|
| | ΔD (%) | ΔL (%) | ΔD (%) | ΔL (%) | ΔD (%) | ΔL (%) |
| Green part | - 3,2 ± 0,2 | - 1,6 ± 1,4 | - 1,6 ± 0,1 | - 0,3 ± 0,1 | 3,3 ± 0,2 | 2,8 ± 0,1 |
| 1st Sintering | - 10,8 ± 0,1 | -9,4 ± 0,2 | - 8,7 ± 0,2 | - 8,4 ± 0,2 | - 7,7 ± 0,2 | - 7,6 ± 0,6 |
| 2nd Sintering | - 22,6 ± 0,2 | - 26,2 ± 0,4 | - 22,5 ± 0,3 | - 25,1 ± 0,1 | - 18,0 ± 0,5 | - 17,6 ± 0,5 |
| 1st Sintering + 2nd Sintering | - 23,4 ± 0,2 | - 26,8 ± 0,3 | - 23,4 ± 0,1 | - 26,4 ± 0,3 | - 19,0 ± 0,2 | -17,8 ± 0,7 |

In Figure 6.3 the complex shaped parts, illustrated in Figure 6.1, produced by BJP using 0HT (Figure 6.3 A) and 50HT (Figure 6.3 B) feedstocks and sintered using both 1st and 2nd sintering cycles are presented. It is noticeable a defect in the bottom of the part printed with 0HT (Figure 6.3 A) which is attributed to layer shifting during the printing process and already discussed in Chapter 4 of this thesis. Regardless of this defect, both parts were industrially sintered without major problems of design deformation. In the case of SLS, it was not possible to produce complex shaped parts due to materials availability constrains, however, it is expected that the same behavior is observed. Nevertheless, the study of industrial sintering of complex shaped porcelain parts produced by SLS, using industrial porcelain powders from Costa Verde, is needed.

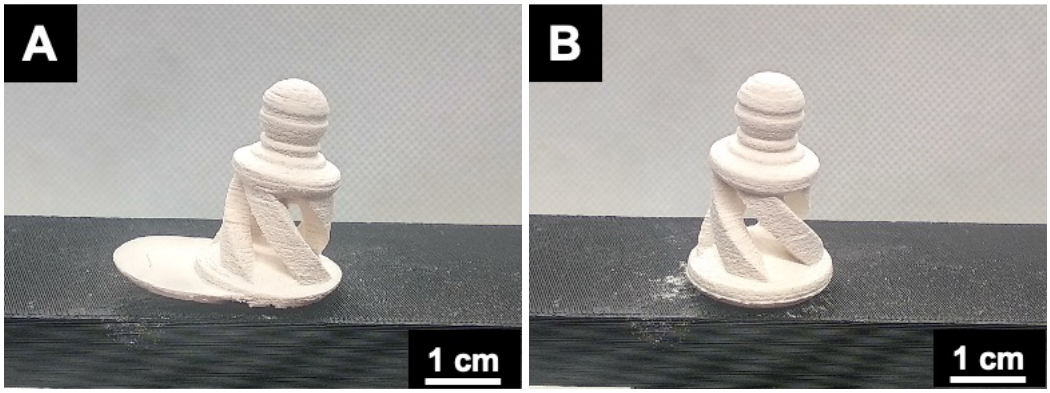


**Figure 6.3:** Complex part, hollow chess pawn, produced by BJP, using (A) 0HT and (B) 50HT feedstocks, after the two sintering cycles. The part produced with 0HT formulation exhibits design defects in the bottom, attributed to layer shifting, as discussed in Chapter 4.

Although using a different *in-bed* binder, the use of sintering process to densify porcelain parts produced by BJP is reported in the literature [3]. The authors used maltodextrin in a fraction 16,7 wt.%, with the addition of sugar powder also in 16,7 wt.%, mixed in 66,7 wt.% of dry clay powder. The ceramics were sintered at 1316 °C for 2 h, producing sintered ceramics with a minimum of porosity of 58 %. In comparison, a higher relative density of the sintered parts was obtained in our work and this fact may be attributed to the lower amount of *in-bed* binder (10 wt.%) which leads to lower porosity, when compared with the work of the authors. However, this difference may also be attributed to the thermal degradation of the used maltodextrin and the different sintering cycles. Maleksaeedi *et al.* [4] present a maximum of 38,4 % of relative density after, sintering at 1650 ºC for 2 h, for alumina parts produced by BJP, using 10 wt.% of PVA as *in-bed* binder. Although the authors used alumina and a different sintering cycle, the feedstock used was also prepared with the same content of *in-bed* binder as ours and by dry mixing alumina and PVA powders, and for this reason was chosen for comparison. The BJP parts produced in our work lead to higher relative density (~ 70 %) than the ones from the authors. This fact may be attributed to the suitable industrial sintering cycles for porcelain parts, but also by the sintering kinetics of both materials.

Sintering processes after the SLS of porcelain are also reported in the literature. Danezan *et al.* [5] studied the direct SLS of a commercial porcelain followed by sintering process. The authors reached a minimum of total porosity of 45 ± 5 %, after sintering at 1350 ºC for 2 h, under vacuum atmosphere. These results are similar to the ones obtained in our work,

however, they have used direct SLS, i.e., without the use of an *in-bed* binder. Tian *et al.* [6] also used laser sintering to produce porcelain objects, however, in this case the material form was a slurry. The authors reached parts with a minimum porosity of 13 % in the parts, after sintering at 1380 ºC for 1 h. In this case, the results obtained by the authors exhibit higher relative densities than ours and it may be explained by the material form, since the use of slurry promotes the approximation of the ceramic particles and, as consequence, matter diffusion during the sintering process. The work of Shahzad *et al.* [7] was chosen due to the use of the same type of *in-bed* binder, polyamide, in similar contents with alumina powders. The authors produced alumina parts, after sintering, with a relative density of 43 %, while in our work the maximum relative density obtained for SLS parts after industrial sintering was 51 %. This difference may be related with the feedstock preparation, in which for our work we dry mixed the porcelain powders with the polyamide ones, while Shahzad *et al.* produced $Al_2O_3$-PA composite particles, where the *in-bed* binder was used as coating of ceramic particles.

Summarizing, the use of industrial sintering cycles towards densification of printed porcelain parts produced by powder bed AM techniques was assessed. For all the parts used in this study, an increase of relative density was observed from the green part to the final sintered one and its application to complex shaped parts is suitable without major design deformations. However, as the porcelain parts produced by *Porcelanas da Costa Verde* should have near full dense microstructures, the use of industrial sintering cycles does not fulfill this requirement and other post-conformation steps must be study and used to reach fully dense porcelain parts.

### *6.3.2. Cold Isostatic Pressing*

The relative density assessed by geometric and Archimedes methods, of the printed parts by BJP and SLS, after each post-conformation step is presented in Table 6.IV. As for the relative density of the green parts was already discussed, the geometric relative density of the parts after CIP was higher for the 0HT feedstock (86 %) than for the 50HT (80 %), while SLS parts have a relative density of 64 %. These values represent an increase in the relative density of the green parts of 45 % for BJP and 20 % for the SLS ones. This difference may be explained by the amount and type of the *in-bed* binders used for each feedstock. Firstly, the amount of polyamide in feedstock for SLS is higher (16 wt.%) than for the BJP (10 wt.%). In this case, there is less void space between porcelain particles, as supported by the higher

relative density as green part of SLS than for BJP parts, which jeopardizes the matter movement during CIP process to fill the porosity. Also, polyamide is a rigid thermoplastic which will resist to plastic deformation during CIP, as opposed to PVA, and, as consequence, the CIP process will be more efficient promoting higher approximation of particles in BJP parts than for SLS ones.

The printed parts were industrially sintered in the 1st sintering cycle after the CIP process, presenting a geometric relative density of 80 % and 77 % for 0HT and 50HT parts, respectively, while for SLS parts the relative density is 51 %. The relative density assessed by Archimedes method exhibits the same trend, with the maximum of 83 % observed for 0HT parts, followed by 80 % for 50HT ones and 53 % for the parts produced using SLS. Overall, the relative density decreased after the 1st sintering cycle. This fact is related with the thermal removal of the *in-bed* binders which lead porosity in the porcelain bodies. As opposed to the values observed for the sintering cycles without CIP (Table 6.II), in which the parts presented similar relative density before and after the 1st sintering, here the decrease observe was 5 % and 3 % for 0HT and 50HT parts and 14 % for SLS parts. This difference is attributed, once again, to the higher content of *in-bed* binder used for SLS feedstock than for the BJP one. In addition, the fact that the relative density did not increase, supports the idea that the 1st sintering cycle does not promote as much densification as the 2nd cycle, as discussed in the study of the sintering cycles, even though the interparticle contact increased due to the CIP processing.

In the case of printed parts after the complete process of CIP followed by 1st and 2nd sintering, the 0HT and 50HT parts presented similar values of geometric relative density with 92 % and 93 %, respectively, while SLS parts have 73 % of geometric relative density. The same trend was observed when the relative density of sintered parts was assessed by Archimedes method, with 97 % for parts produced by BJP with both 0HT and 50HT feedstocks, while the SLS parts exhibit values of 78 %. The effect of CIP is noticeable at this stage of processing with the maximum relative densities observed in this work. CIP process leads to an approximation of particles inside the printed part, which increases the interparticle contact, promoting the matter diffusion during the 2nd sintering cycle, leading to an increase in the relative density of the porcelain parts.

The microstructures of the parts produced with 0HT and 50HT feedstocks in BJP and by SLS are presented in Figure 6.4. It is noticeable that 0HT and 50HT parts have a denser

microstructure than the one of SLS, which is in accordance with the relative densities discussed above. The porosity present in SLS parts is attributed to the higher amount of *in-bed* binder used in the feedstock than the amount in feedstock for BJP.

**Table 6.IV:** Relative density of 0HT, 50HT and SLS printed parts, measured by geometric and Archimedes method, at the different stages of processing: green part, after CIP, CIP followed by 1st sintering (1178 °C, 2 h 30 min) and CIP followed by both 1st and 2nd sintering.

| | **0HT** | | **50HT** | | **SLS** | |
|---|---|---|---|---|---|---|
| | $\%\rho_{geom}$ (%) | $\%\rho_{Arc}$ (%) | $\%\rho_{geom}$ (%) | $\%\rho_{Arc}$ (%) | $\%\rho_{geom}$ (%) | $\%\rho_{Arc}$ (%) |
| Green part | 39,0 ± 0,7 | --- | 35,3 ± 0,5 | --- | 43,5 ± 0,2 | --- |
| CIP | 85,7 ± 1,2 | --- | 80,3 ± 0,4 | --- | 64,1 ± 0,3 | --- |
| CIP + 1st Sintering | 80,0 ± 0,5 | 82,9 ± 0,2 | 77,0 ± 0,6 | 79,8 ± 0,2 | 50,5 ± 0,2 | 52,6 ± 0,1 |
| CIP + 1st Sintering + 2nd Sintering | 92,4 ± 2,0 | 96,7 ± 0,2 | 93,0 ± 0,5 | 96,6 ± 0,2 | 72,7 ± 0,3 | 78,2 ± 0,4 |

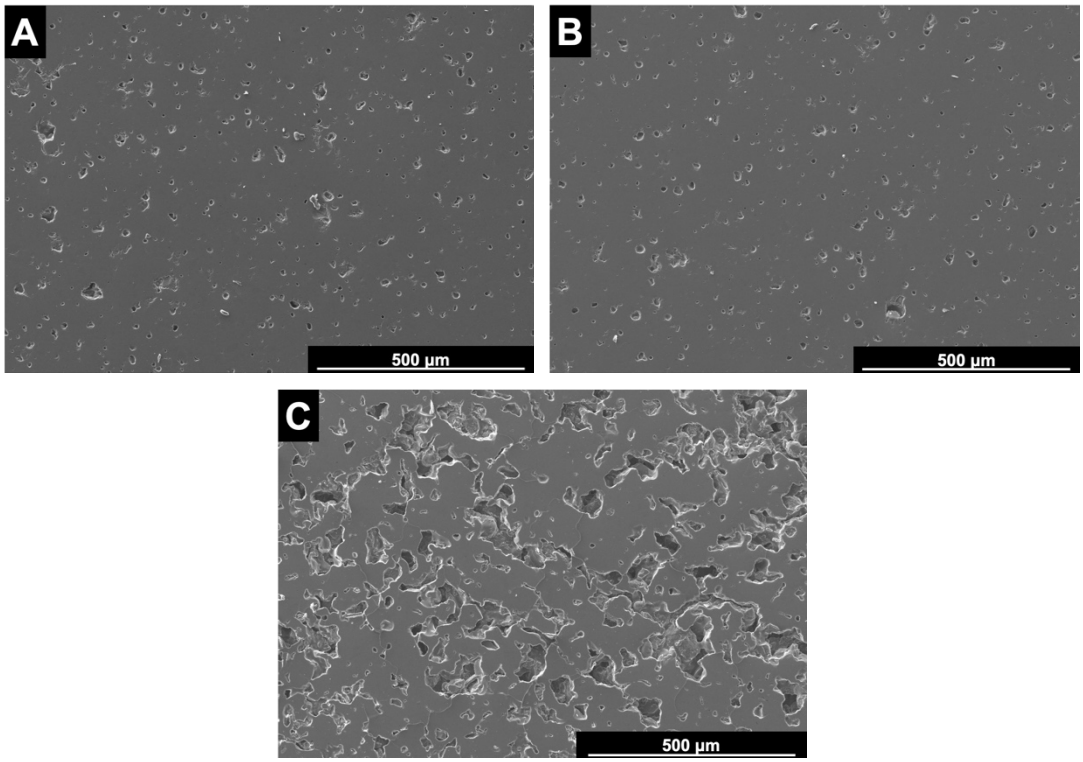


**Figure 6.4:** SEM micrographs of polished fracture zone, of parts processed by CIP followed by both industrial sintering cycles, using (A) 0HT, (B) 50HT and (C) SLS feedstocks and processing. The images of 0HT and 50HT parts present a denser microstructure than SLS parts.

Comparing the printed parts with the CIP process (Table 6.IV), with the previous ones, for which were only processed by sintering cycles (Table 6.II), it is noticeable an increase of 27 % in the relative density of 0HT parts and 30 % in 50HT parts while for SLS parts the increase is 22 %. Here we advocate, that the CIP promotes the particle approximation and the interparticle contact inside the printed parts, which increases the relative density of the parts before the thermal cycles, leading to an increase in densification during sintering.

The diameter and length variations to the virtual design of the parts processes by CIP is presented in Table 6.V. While for the green parts the variations were already discussed, after CIP the parts produced with 0HT exhibit a variation of - 25 % and - 32 % for diameter and length, respectively. In the case of 50HT the diameter and length variation are - 23 % and - 29 %, respectively, while for SLS parts after CIP the diameter and length variations have similar values of - 10 %. The first observation concerns in the anisotropy of the variation in the BJP, which present higher variation in the length direction rather than in the diameter one. This effect is attributed to the higher porosity between layers than within each

layer, resulting from the layer by layer process. A second major observation regards in the higher variations for BJP parts than for SLS ones, which supports the previous statement that the fact that polyamide is a rigid plastic, which hinders the rearrangement of particles inside the printed part during CIP, leaving more void space between particles than for BJP parts, which have PVA as *in-bed* binder. The consequence of this difference is an increase in the interparticle contact in BJP parts which promotes the matter diffusion during sintering and the increase of relative density in the final parts.

After the 1$^{st}$ sintering cycle, 0HT exhibit a diameter and length variation to the virtual design dimensions of - 28 % and - 36 %, respectively, and 50HT parts present - 27 % and - 33 % of diameter and length variations, respectively. In the case of SLS parts, the diameter variation is - 17 % and the length one is - 18 %. Concerning the parts after the CIP followed by the two sintering cycles, the 0HT and 50HT parts exhibit a diameter variation of - 31 %, while the length variation is - 40 % and - 38 %, respectively. The SLS parts present similar values of diameter and length variation of - 27 %. Comparing these values with the ones without sintering (Table 6.III) it is noticeable an increase in the diameter variation around 7 % for all the printed parts with 0HT, 50HT and SLS and an increase around 13 % in the length variation of BJP parts and 10 % in SLS parts. This increase in the dimensions variations, i.e., increase in the retraction of the parts, may justify the increase in the relative density of the sintered parts by using CIP. As said above, CIP promotes the approximation of particles in the part which increases the densification process during sintering. Also, the fact that the variations are higher in the length direction than in the diameter one, promotes even more the approximation interlayers and decreases the porosity in these regions.

**Table 6.V:** Diameter and length variation of 0HT, 50HT and SLS printed parts, at the different stages of processing: green part, after CIP, CIP followed by 1st sintering (1178 °C, 2 h 30 min) and CIP followed by both 1st and 2nd sintering.

| | **0HT** | | **50HT** | | **SLS** | |
|---|---|---|---|---|---|---|
| | ΔD (%) | ΔL (%) | ΔD (%) | ΔL (%) | ΔD (%) | ΔL (%) |
| Green part | - 3,2 ± 0,2 | - 1,6 ± 1,4 | - 1,6 ± 0,1 | - 0,3 ± 0,1 | 3,3 ± 0,2 | 2,8 ± 0,1 |
| CIP | - 24,5 ± 0,3 | - 31,7 ± 0,5 | - 23,3 ± 0,1 | - 28,9 ± 0,3 | - 9,5 ± 0,1 | - 9,7 ± 0,1 |
| CIP + 1st Sintering | - 28,2 ± 0,3 | - 35,5 ± 0,6 | - 26,8 ± 0,1 | - 33,0 ± 0,3 | - 16,9 ± 0,2 | - 18,0 ± 0,1 |
| CIP + 1st Sintering + 2nd Sintering | - 30,6 ± 0,4 | - 39,5 ± 0,5 | - 31,0 ± 0,2 | - 38,0 ± 0,2 | - 26,6 ± 0,2 | - 27,4 ± 0,2 |

Although the isostatic pressing has been studied for additively manufactured parts and reported in the literature, most of them have simple shapes, as Liu *et al.* [8] did with alumina parts. Based on one of the main advantages of AM, which is the production of highly complex shaped parts, the chess pawns (Figure 6.1) were processed in CIP as well. In Figure 6.5 the parts produced by BJP using the 50HT feedstock are presented before and after CIP. It is noticeable that the part in hollow form, as defined in Figure 6.1, was completely damaged after, while the part in bulk form did not suffer any major deformation. This is explained by the process of CIP, where a rubber bag is used to protect the part from the oil bath. However, using the bag leads to a defective isostatic pressing application due to the impossibility of the oil to reach the inner faces of the part. The same effect was observed for the complex shaped parts produced using the 0HT feedstock.

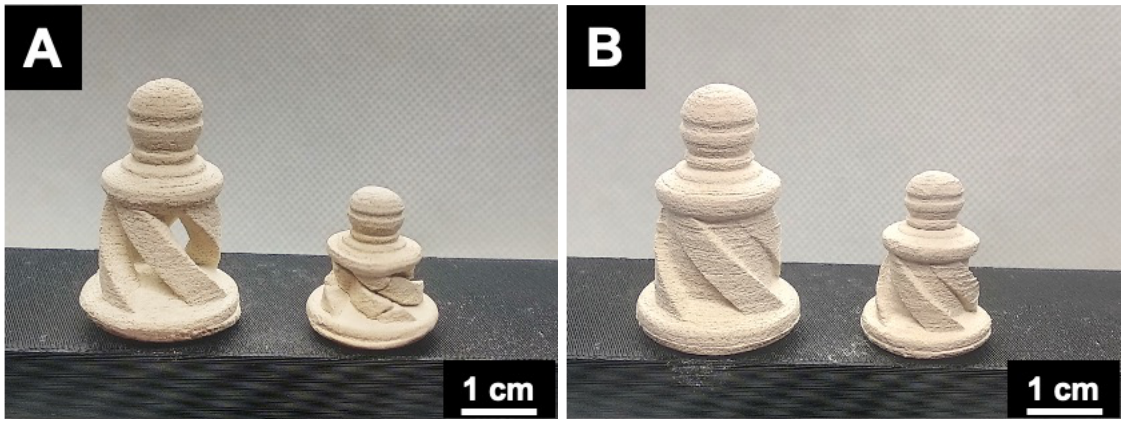


**Figure 6.5:** Complex shaped chess pawns produced by BJP using 50HT feedstock, in (A) hollow form and (B) bulk form, as illustrated in Figure 6.1. In each image the part on the left is before CIP and the one on the right is after CIP. It is noticeable that for the hollow form the part is completely damaged (A) while for bulk form the part retains its relative shape (B).

Although the use of isostatic pressing for porcelain parts additively manufactured is not reported in the literature, Shahzad *et al.* [9], used CIP with alumina parts produced by SLS, using polypropylene as binder. Warm Isostatic Pressing (WIP), where temperature is applied at the same time as pressure is, was used and a sintered relative density of 89 % was reported. However, the main difference to our work regards in the increase of relative density from green part to the stage after isostatic pressing, which was 59 %, comparing with the one in our work of 20 %. This difference may be attributed to the fact that temperature was used during isostatic pressing, promoting the softening of the binder and leading to higher movement of particles and an increase in the relative density. Other factors such as the type of *in-bed* binder (polypropylene) may contribute as well to the higher effectiveness of isostatic pressing in part produced by SLS than in our work. Deckers *et al.* [10] also used CIP process in printed alumina parts produced in SLS with polyamide as *in-bed* binder (22 wt.%). The results of the group exhibit a maximum relative density of 59 % after the CIP process and a maximum of 88 % for parts after CIP followed by sintering at 1600 °C for 2 h. Although the parts in our work present a higher relative density in the green state (64 %), the relative density after the sintering is lower (78 %) than the one observed by the authors of the work. This difference may be related with the feedstock preparation, in which Deckers *et al.* mixed the alumina powders with the polyamide by ball milling, creating composite particles. Liu *et al.* [8] reached 92 % of relative density after CIP and sintering, of $Al_2O_3$ and resin epoxy composite powders, which are comparable results to the ones of our work.

Summarizing, the use of CIP combined with the industrial sintering cycles for porcelain parts produced by powder bed AM techniques leads to an increase in the relative density of final parts than the use of only the sintering cycles. While showing very promising results of relative density of simple shaped parts or parts without inner faces, the process is not yet suitable for highly complex shaped parts.

### *6.3.3. Pressureless infiltration with porcelain suspension*

As discussed in the introduction, the use of infiltration may be a process to increase the relative density of parts produced by powder bed AM techniques. In this sense, based in the availability in production of porcelain parts by conventional methods, the use of a porcelain suspension to infiltrate printed parts was tested. In this part of the work, the results concerning the 50HT parts are presented, although 0HT, 50HT and SLS parts were used, but the same observations were similar for the three groups of parts.

The pressureless infiltration was performed by soaking printed parts after the 1$^{st}$ sintering cycle in the porcelain suspension. Initially, the process was done without any agitation method for the suspension and the resultant part is presented in Figure 6.6 A. Different parts were then soaked in the suspensions using ultrasounds (Figure 6.6 B) and magnetic stirring (Figure 6.6 C). As it is possible to observe, the part soaked in the porcelain suspension without any agitation and using ultrasounds exhibits an irregular surface while the part soaked using the magnetic stirring presents a homogenous surface without major defects. The soaking of printed parts in porcelain suspension without any agitation leads to the deposition of the solids in the bottom of the beaker, where the printed part also settled, after 10 min, preventing the part to be infiltrated. Based on this observation, the ultrasounds were used in order to avoid the sedimentation of the solids, however the opposite effect was observed, and the part was also buried in the solids fraction deposited in the bottom of the beaker. Finally, with the use of magnetic stirring, the sedimentation of the solids was prevented, and the final part presents a homogenous surface.

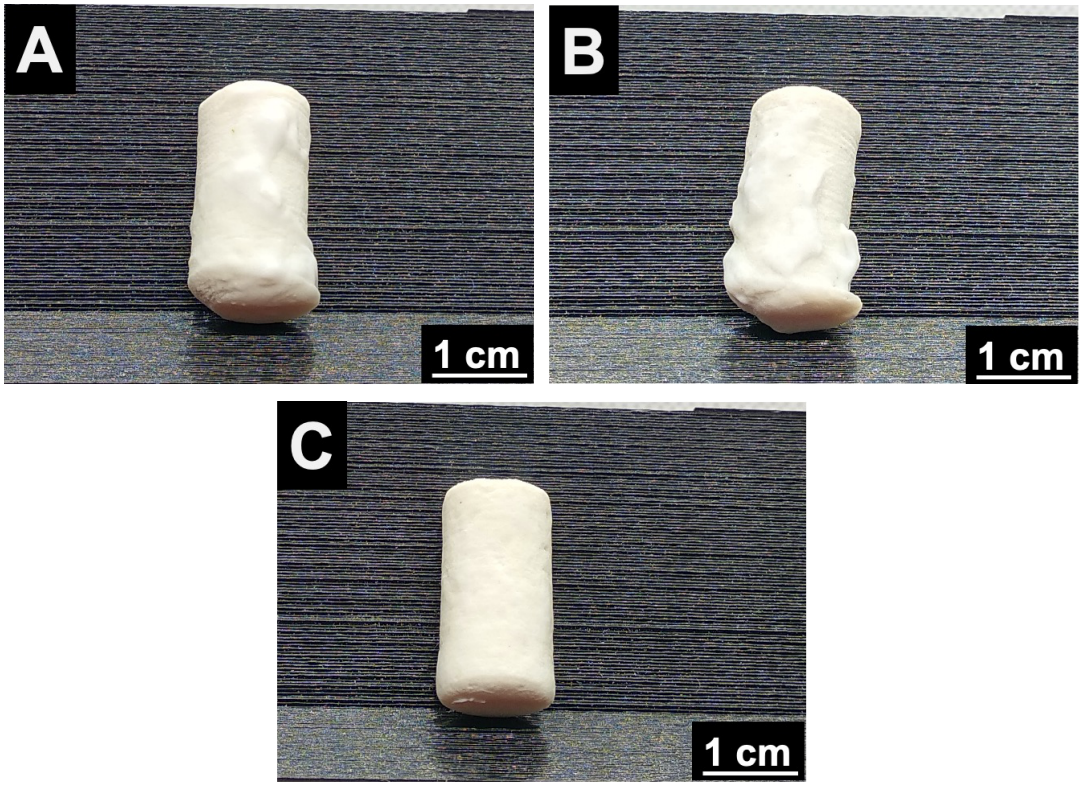


**Figure 6.6:** Cylindrical parts, produced by BJP, using 50HT feedstock, after the two sintering cycles, soaked in porcelain suspension with 1350 g/cm$^3$ for 10 min, after the 1$^{st}$ sintering cycle, using different agitation conditions: (A) no agitation, (B) ultrasounds and (C) magnetic stirring.

Magnetic stirring was the agitation method used to keep the particles in suspension. In Figure 6.7 the 50HT sintered parts after the soaking with porcelain suspension with magnetic stirring during 60, 30 and 10 min are presented. While for parts soaked for 10 min (Figure 6.7, A) any major damage was observed, the parts in the tests with 30 min (Figure 6.7, B) and 60 min (Figure 6.7, C) exhibit damages. This fact is attributed to the collisions with the magnetic stirrer and between the printed parts. This result is supported with the reduction in the diameter after the infiltration of 5 %, in the case of 30 min, and 9 %, in the case of the 60 min. However, it is possible to observe that the deposition of the porcelain particles from the suspension occurs on the surface of the part, creating a layer of porcelain. This effect may be related with the fact that the particles in the suspension are not fully dispersed, leading to the clog of the open porosity of the printed part and preventing the infiltration to continue.

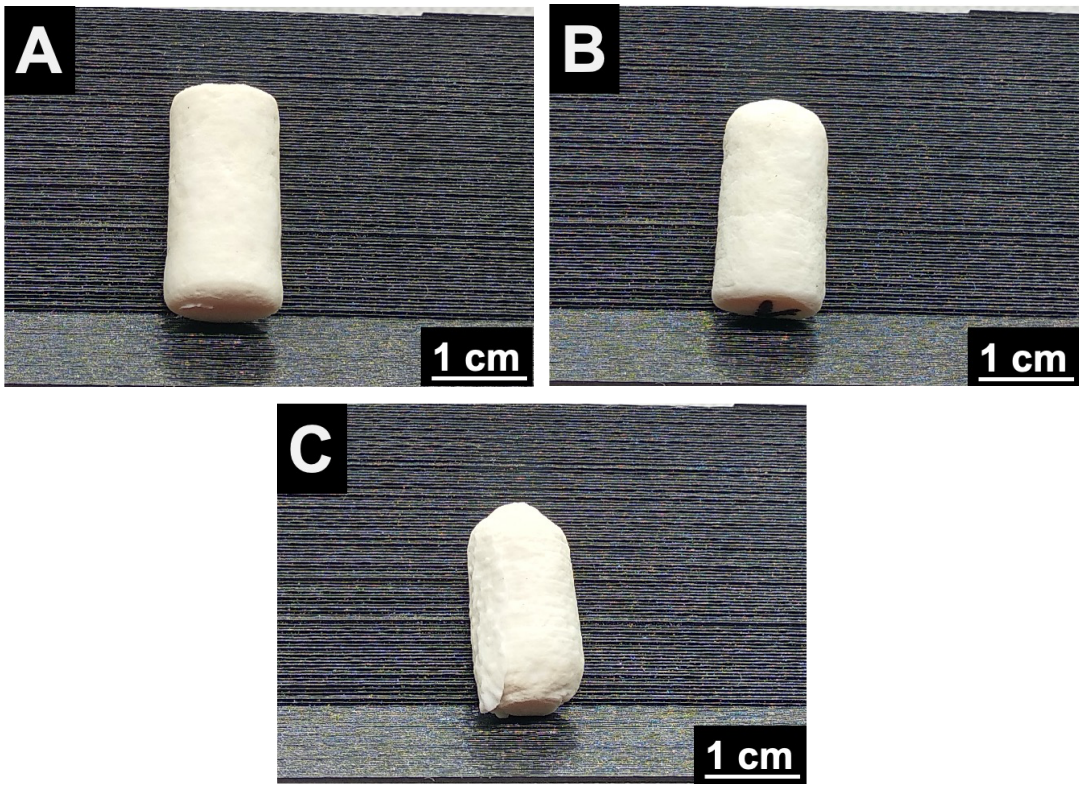


**Figure 6.7:** Cylindrical parts, produced by BJP, using 50HT feedstock, after the two sintering cycles, soaked in porcelain suspension with 1350 g/cm$^3$ using magnetic stirring, after the 1$^{st}$ sintering cycle, during different times: (A) 10 min, (B) 30 min and (C) 60 min.

Based in the results above, the suspension was prepared with the addition of 0,2 wt.% of deflocculant, to improve the dispersion of the ceramic particles in the suspension, and a reduction in the density of the suspension was done as well. The soaking of the printed parts was done under the same conditions as above. The parts soaked without and with the addition of deflocculant are illustrated in Figure 6.8. Both parts exhibit a layer of deposited ceramic particles on its surface. While in the case of the tests using different densities of suspension exhibit the same defects as well (Figure 6.9). In addition, the diameter variation exhibits an increase of 2 % in average for all the parts in the different tests and the relative density of the parts varies between 67 % and 70 %, which is a similar value for the parts sintered in both sintering cycles, without any infiltration process, as presented in Table 6.II.

Based on this observations, we advocate that several reasons are contributing to this effect: 1) the size of porous of the printed parts is too small in order to be infiltrated by the ceramic particles from the suspension; 2) the solid content in the suspension is too high, jeopardizing the dispersion of the ceramic particles and 3) the materials used, specifically the porcelain

suspension, is prepared to use in an opposite way, i.e., is suitable to use in slip casting processes, in which the particles are deposited in the surface of a mold and the water is removed by capillarity of the porous, forming the ceramic body.

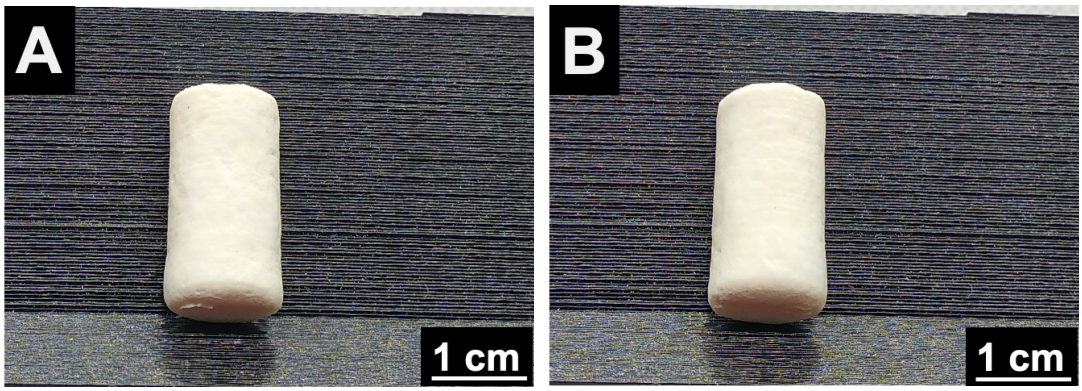


**Figure 6.8:** Cylindrical parts, produced by BJP, using 50HT feedstock, after the two sintering cycles, soaked in porcelain suspension with 1350 g/cm$^3$ using magnetic stirring for 10 min, after the 1$^{st}$ sintering cycle: (A) without and (B) with the addition of 0,2 wt.% of deflocculant to the ceramic suspension.

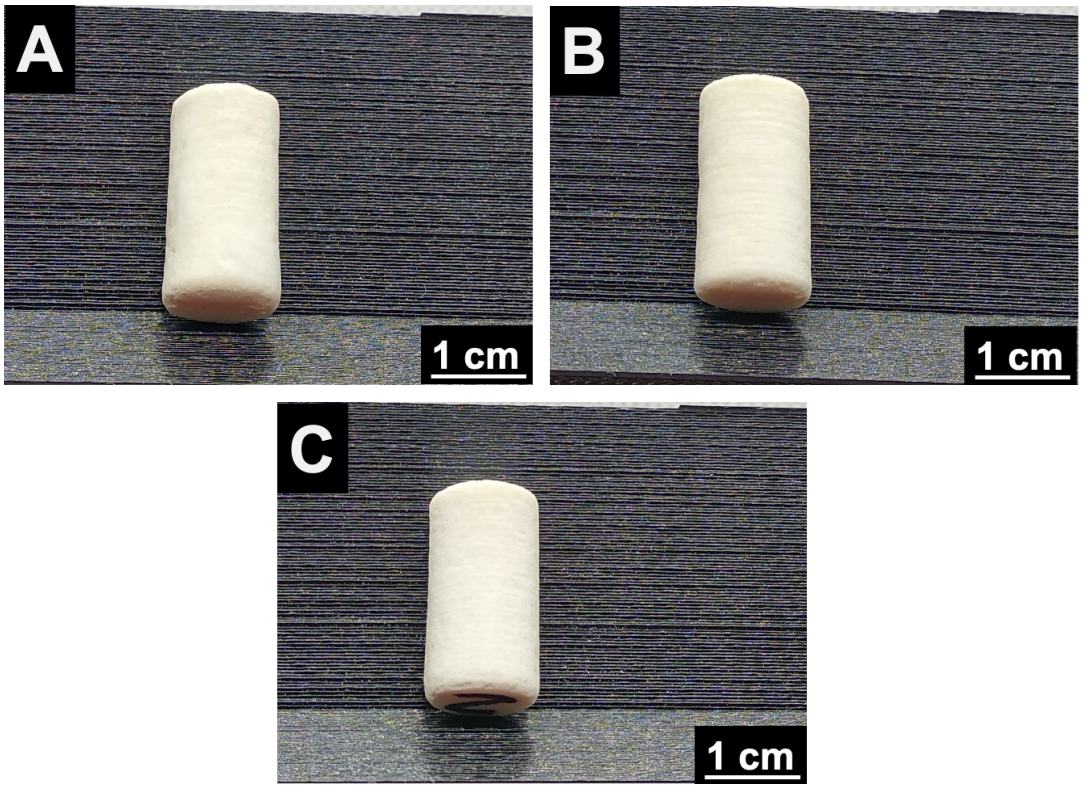


**Figure 6.9:** Cylindrical parts, produced by BJP, using 50HT feedstock, after the two sintering cycles, soaked in porcelain suspension with deflocculant using magnetic stirring

for 10 min, after the 1st sintering cycle, using (A) 1350 g/cm$^3$, (B) 1250 g/cm$^3$ and (C) 1150 g/cm$^3$ as porcelain suspension density.

Summarizing, the infiltration of printed parts produced by powder bed AM techniques with porcelain suspension was not possible. In order to achieve so, a porous size of printed parts study must be done, in order to prepare a suspension with ceramic particles size lower than the porous size. In a different perspective, the infiltration of the printed parts may be done with different materials, such as preceramic solutions or TEOS (tetraethyl orthosilicate), i.e., materials that convert into ceramics after pyrolysis, or the infiltration must be done using different approaches, such as vacuum infiltration, to promote the movement of ceramic particles to inside the printed parts. However, within the goal of this project, the porcelain suspension was chosen in order to use the raw materials of porcelain as much as possible, in order to keep the composition of Costa Verde porcelain after sintering and the pressureless infiltration was chosen due to the ease to apply at industrial scale.

In conclusion, in this work we compared three different ways to improve the relative density of porcelain printed parts, produced using powder bed AM techniques. In Table 6.VI we present the main advantages and drawbacks of each of these processes. Concerning the sintering cycles, while they are already settled in the conventional production of porcelain parts and, in addition, its parameters such as temperature, time and atmosphere are already optimized for the porcelain composition used by *Porcelanas da Costa Verde*, the final sintered parts exhibit lower relative density than the conventionally produced porcelain parts and far from fully dense microstructure (maximum of 71 % of relative density was obtained for 0HT parts). In the case of using CIP, the main advantage is the production of near full dense printed parts, with a maximum relative density of 97 %. However, as presented in Figure 6.5, the process is yet not suitable for highly complex shaped parts. Finally, the infiltration process of printed parts with porcelain suspension, although have the advantage of its easy implementation at industrial scale, based on the results obtained, the suspension as produced, combined with the process used, is not suitable to infiltrate porcelain parts, once the ceramic particles deposit on the surface of the part as opposed to reach its interior.

**Table 6.VI:** Advantages and drawbacks of sintering cycles, cold isostatic pressing and pressureless infiltration processes, studied in this work, to improve the relative density of porcelain printed parts.

| Process | Advantages | Drawbacks |
|---|---|---|
| Sintering cycles | Already used for conventionally produced porcelain parts<br><br>Suitable for complex shaped parts<br><br>Otimized for porcelain composition (*Porcelanas da Costa Verde*) | Parts do not reach full densification |
| Cold Isostatic Pressing | High relative density | Not suitable for complex shaped parts |
| Pressureless Infiltration | Easy to implement at industrial scale | Porcelain suspensions and process are not suitable for infiltration |

## 6.4. Conclusions

In this work we presented post-conformation processes for porcelain printed parts by BJP and SLS, in order to increase the density of the sintered porcelain bodies. For this purpose, the post processing steps included the industrial thermal cycles of *Porcelanas da Costa Verde*, cold isostatic pressing and pressureless infiltration with porcelain suspension.

The industrial sintering cycles lead to porcelain final parts with 71 % of relative density for parts produced by BJP with 0HT feedstock and 68 % using the 50HT one. While in the case of SLS parts the maximum relative density reached was 56 %. The lowest value of relative density of SLS parts was attributed to the amount of polyamide 12 used as *in-bed* binder which hinders the densification of the porcelain body by creating porosity after its thermal removal. In addition, it was concluded that the 2$^{nd}$ sintering cycle promotes higher densification of the parts than the 1$^{st}$ cycle, due to higher temperature and time of cycle.

CIP was the process that promoted the best results combined with the thermal sintering cycles, increasing the relative density of the final parts by almost 30 %, for the parts prepared by BJP and almost 20 % of SLS ones. In addition, using CIP the parts reached the highest relative density of 97 % for BJP parts and 78 % of SLS ones. Although, CIP leads to almost full dense simple shaped parts, such as cylinders, it is not suitable for highly

complex shaped parts, once the method damages the green parts. In addition, the CIP process was more efficient in the case of BJP parts in the green state than for SLS parts, and this result was attributed to the type of *in-bed* binder used. Polyamide 12 is a rigid plastic which prevents the elimination of the porosity by pressure application, as opposed to PVA.

The pressureless infiltration process with porcelain suspension was also studied, however the results were far from the desired, once the solid fraction of the porcelain suspensions deposited on the surface of the part instead of reaching the interior of the part. In this sense, different approach must be studied by changing the infiltration process conditions or the infiltrant suspension used.

In conclusion, we proved that the relative density of porcelain printed parts, produced by powder bed AM techniques using industrial porcelain powders, can be successfully improved by using industrial sintering cycles combined with CIP process.

## 6.5. References

[1] JaaYoo, “Thingiverse, Thing: 1094870,” 2015. [Online]. Available: https://www.thingiverse.com/thing:1094870. [Accessed: 25-Nov-2018].

[2] Y. Shanjani, Y. Hu, R. M. Pilliar, and E. Toyserkani, “Mechanical characteristics of solid-freeform-fabricated porous calcium polyphosphate structures with oriented stacked layers,” *Acta Biomater.*, vol. 7, no. 4, pp. 1788–1796, Apr. 2011.

[3] G. Marchelli, M. Ganter, and D. Storti, “New material systems for 3D ceramic printing,” in *Solid Freeform Fabrication Symposium*, 2009, pp. 477–487.

[4] S. Maleksaeedi, H. Eng, F. E. Wiria, T. M. H. Ha, and Z. He, “Property enhancement of 3D-printed alumina ceramics using vacuum infiltration,” *J. Mater. Process. Technol.*, vol. 214, no. 7, pp. 1301–1306, 2014.

[5] A. Danezan *et al.*, “Selective laser sintering of porcelain,” *J. Eur. Ceram. Soc.*, vol. 38, no. 2, pp. 769–775, 2018.

[6] X. Tian, D. Li, and J. G. Heinrich, “Rapid prototyping of porcelain products by layer-wise slurry deposition (LSD) and direct laser sintering,” *Rapid Prototyp. J.*, vol. 18, pp. 362–373, 2012.

[7] K. Shahzad, J. Deckers, S. Boury, B. Neirinck, J.-P. Kruth, and J. Vleugels, “Preparation and indirect selective laser sintering of alumina/PA microspheres,”

*Ceram. Int.*, vol. 38, no. 2, pp. 1241–1247, Mar. 2012.

[8] K. Liu, Y. Shi, C. Li, L. Hao, J. Liu, and Q. Wei, “Indirect selective laser sintering of epoxy resin-$Al_2O_3$ ceramic powders combined with cold isostatic pressing,” *Ceram. Int.*, vol. 40, no. 5, pp. 7099–7106, 2014.

[9] K. Shahzad, J. Deckers, J. P. Kruth, and J. Vleugels, “Additive manufacturing of alumina parts by indirect selective laser sintering and post processing,” *J. Mater. Process. Technol.*, vol. 213, no. 9, pp. 1484–1494, 2013.

[10] J. Deckers, K. Shahzad, J. Vleugels, and J. P. Kruth, “Isostatic pressing assisted indirect selective laser sintering of alumina components,” *Rapid Prototyp. J.*, vol. 18, no. 5, pp. 409–419, 2012.

# *Chapter 7: Towards powder bed Additive Manufacturing industrialization of porcelain parts*

**Abstract**

In this chapter we exploit the possibility of the use of binder jet printing (BJP) as a production route for porcelain parts at industrial scale. The industrialization of a new conformation process requires the study of three main stages of industrial production: the materials and feedstock preparation, the conformation step and the post conformation process. Here we proved that the feedstock preparation for BJP is possible with the facilities of *Porcelanas da Costa Verde*, although few modifications both in the spray drying process and in the sieving of porcelain powders are required. The printing process was assessed using a commercial BJP printer and several limitations of the commercial printers are highlighted and suggestions for the improvement of the printing process are presented. The existent post conformation steps such as industrial sintering cycles, glazing and decoration are suitable for BJP porcelain parts, however a different 1$^{st}$ sintering cycle is required, and the final parts do not reach full densification. A comparison with the conventional production routes used by *Porcelanas da Costa Verde* regarding the density of parts, and with selective laser sintering (SLS) in terms of materials preparation, printing process and properties of produced parts is also part of this study. This work proves the feasibility of the use of BJP as a production route for porcelain products using the equipments of materials preparation, printing and post conformation steps, already existing at facilities of *Porcelanas da Costa Verde*. However, in some processing steps there is still room for improvement, especially regarding the efficiency of the processes. Finally, we present printed parts with shapes that are expensive or impossible to produce in any conventional way, and the potential of BJP for porcelain parts production is exhibited.

**Keywords**

Industrialization, production, additive manufacturing, porcelain

## 7.1. Introduction

The development of additive manufacturing (AM) processes as conformation method to produce 3D objects, promoted the interest of the industry in the technology, looking for this route as an opportunity to produce new objects and reach new markets [1]. The opportunity to produced objects with complex shapes, high level of personalization with minimal materials used at industrial scale and small lot production sizes [2], is hold by its lack of

reproducibility and lack of knowledge regarding the characteristics of the materials for AM, especially in traditional products companies. Stavropoulos *et al.* [3] propose hybrid systems of additive and subtractive manufacturing of metal parts in order to reduce the limitations of AM implementation at industrial scale, such as, reproducibility, process control and part volume limitations.

In the case of ceramics and according to Levi *et al.* [4], there are a lot of difficulties to overcome, especially when compared with sectors as polymers and metals with several decades of research and innovation. Oropallo *et al.* [5] presents ten challenges in the future for AM, which are among others, the design for AM, the development of new software and dedicated printers and the pre and post-processing required steps, subjects discussed in this chapter.

The production flowchart of the existing processes available at *Porcelanas da Costa Verde* facilities is depicted in Figure 7.1.The process starts with the preparation of the batch using the following raw materials: quartz, feldspar, ball clay and kaolin. Quartz, feldspar and ball clay are milled together, and kaolin is diluted in water. Then, all the materials are mixed together followed by a sieving process. The suspension is processed either in the spray dryer to produce powders for isostatic pressing, filter pressed to produce plastic paste for jiggering or directly used in automatic, manual or pressure casting. Depending on the conformation process that will follow, additives, such as binder or deflocculant are added to the mixture.

The post conformation processing comprise the first firing in an industrial continuous furnace for 15,5 – 18 h and a maximum temperature of 980 – 1020 °C, to reach enough mechanical resistance and proper porosity of the objects for following glazing process and at the same time that all the organic matter is burned out. The second firing is performed in another continuous furnace, for 5 - 7 h and a maximum temperature of 1360 - 1380 °C. This cycle is done under oxidant atmosphere, for low temperatures, and reductant atmosphere at high temperatures.

The first quality assessment is performed after the high temperature sintering cycle, and, if the quality of the parts obeys to the standards of the company, the decoration step takes place, followed by the decoration firing. This third firing process occurs at 1180 - 1230 °C, if the decoration is in-glaze, or at 880 – 950 °C if the decoration is on-glaze.

The production process finishes with another quality assessment, followed by packing and shipping to the client.

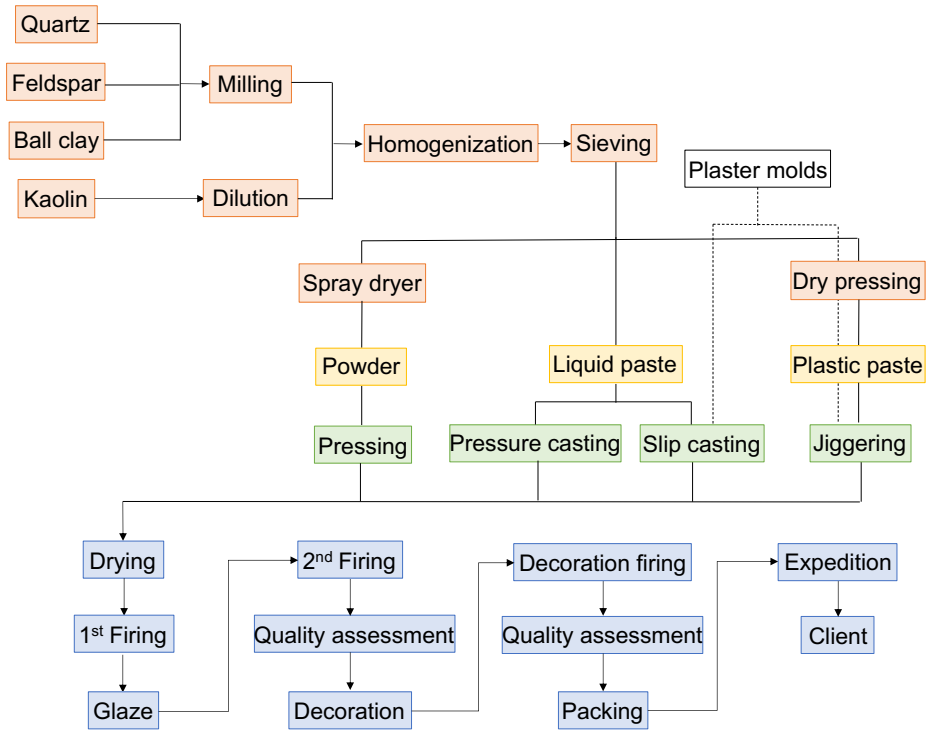


**Figure 7.1:** Production flowchart of Porcelanas da Costa Verde, for objects produced through conventional methods.

As discussed in Chapter I, an object may be produced through four main groups of manufacturing processes: formative, subtractive, bonding and additive. In Table 7.I, formative, bonding and subtractive manufacturing processes used in porcelain production by *Porcelanas da Costa Verde*, are presented. The formative processes, which are the most used ones, comprise pressure casting, slip casting, isostatic pressing and jiggering. In the case of subtractive and bonding processes, used in combination with the first group, comprises holes drilling, for subtractive, and handles applications for bonding. In this work we explore the use of BJP and SLS for porcelain parts production.

**Table 7.I:** Conformation classes and processes in the porcelain parts production used by Porcelanas da Costa Verde, and the potential new conformation AM processes.

| **Conformation processes** | |
|---|---|
| Formative | Slip Casting, Pressure Casting, Isostatic Pressing, Jiggering |
| Subtractive | Drilling |
| Bonding | Handles application |
| Additive | Binder Jet Printing, Selective Laser Sintering |

The idea of this project comes from the interest of *Porcelanas da Costa Verde* in exploiting and ultimately implementing a disruptive way to produce complex shaped and personalized porcelain parts: additive manufacturing (AM), adding this group of processes to the conformation methods already used for porcelain parts production, as illustrated in Figure 7.2.

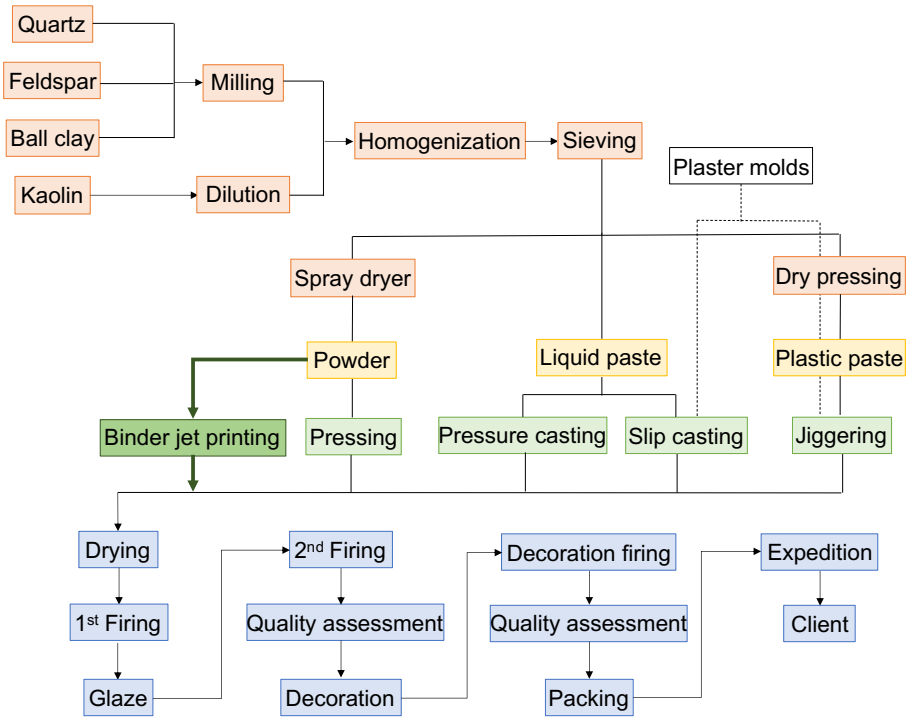


**Figure 7.2:** Production flowchart of Porcelanas da Costa Verde, including new conformation method: Binder Jet Printing.

This technique was implemented in the company in early 2000's as a rapid prototyping tool, using plaster based commercial powders, to produce 3D models of new products, which are used to produce plaster molds for automatic and manual slip casting process.

However, the interest of the company goes beyond prototyping, willing to turn it in a production process. From the industrial point of view and based on the results previously shown in this thesis, the technique may be used as a conformation process with porcelain powders produced by *Porcelanas da Costa Verde*. With AM porcelain products, the company may reach new markets and costumers with alternative products, that may be difficult or even impossible to be produced through the conventional means or even use the process for small production series and highly customized products.

The adequation of the materials and feedstocks, equipments and facilities of *Porcelanas da Costa Verde*, for the use of BJP as industrial production route needs also to be addressed. In this chapter we will discuss and exploit the implementation of BJP as production route for porcelain products, with focus on the three different stages of the production route: materials and feedstock preparation, the conformation process and the post conformation steps, using the existent composition, equipments and facilities of *Porcelanas da Costa Verde*.

The materials and feedstock preparation include the processes of spray drying, sieving and mixing of dry porcelain powders with the *in-bed* binder ones. The conformation step focus in the printing parameters, the printer feeding system and the reuse of powders. The post conformation steps comprise drying, sintering and glazing of the printed parts. A comparison of properties of printed parts with SLS ones and conventional processes already used by *Porcelanas da Costa Verde* are also presented, regarding the density of the final parts.

With this in consideration some information will be protected due to proprietary information. However, the provided information is enough to understand the work.

## 7.2. Materials and methods

As discussed above, three main subjects were addressed in this work, to assess the viability of the BJP industrialization for porcelain parts manufacturing: feedstock preparation, printing process and post-conformation steps. In the feedstock preparation we address the production of porcelain powders for BJP by spray drying, followed by industrial sieving. The feedstock is then prepared by dry mixing porcelain powders and PVA ones. The second subject addressed is the printing process, with a brief study regarding the printing parameters: layer thickness and binder saturation. The powder feeding system of the printer and the reuse of powders was assessed as well. The post-conformation as sintering cycles were also subject of study and the density of the parts was compared with the ones for conventionally produced porcelain parts. Finally, complex shaped printed parts were processed by sintering cycles and another part was glazed and decorated, in order to present the potential of BJP for porcelain parts production. Experimental details regarding these subjects are presented in this section.

### *7.2.1. Materials and feedstock preparation*

The powders used in this work, here after defined as porcelain powders, were produced by industrial spray drying using a ceramic suspension, with 50 % of kaolin and clay, 25 % of quartz and 25 % of feldspar in water medium, here after defined as porcelain suspension.

The industrial spray dryer used in *Porcelanas da Costa Verde* is schematically illustrated in Figure 7.3, with most important spray drying conditions and its values identified. The spray dryer is an industrial size mixed flow type, equipped with hydraulic nozzles (also known as one-fluid) [6], where the hot air is inserted in the chamber from the top side, while the ceramic suspension is pulverized from the bottom towards the top of the spray dryer. The powders used for conventional production processes are collected after sieving (identified as collect point coarse in Figure 7.3).

The spray dryer was adapted to produce porcelain powders for powder bed AM processes, as illustrated in Figure 7.4. The main adaptation done in the spray dryer for this work was the removal of the fine powder reintroduction system. The powders used for AM processes are collected after the cyclone system (identified in Figure 7.4 as collect point fine) and are here after defined as fine porcelain powders. The powders collected after the sieve

(identified in Figure 7.4 as collect point coarse) are here after designated as coarse porcelain powders.

For powders characterization, the coarse and fine porcelain powders were collected in the collect points identified in Figure 7.3 and Figure 7.4, using the spray drying setup of Figure 7.3 in the case of production spray drying conditions, and using the setup illustrated in Figure 7.4 in the case of porcelain powders for AM processes.

The main conditions of spray drying to produce powders for conventional manufacturing processes, Figure 7.3, are 10 - 20 bar for the feeding pump pressure, 49 - 147 Pa for the depression of the cyclone, 300 - 400 °C for the air temperature and nozzles with a diameter higher than 1,5 mm. The density of the porcelain suspension is 1600 - 1640 g/L with the addition of 0,5 – 2,5 wt.% of proprietary additives. To note as well that for the conventional production processes, fine powder particles in the spray dryer chamber, are removed using a cyclone, but these particles are injected back in the drying chamber.

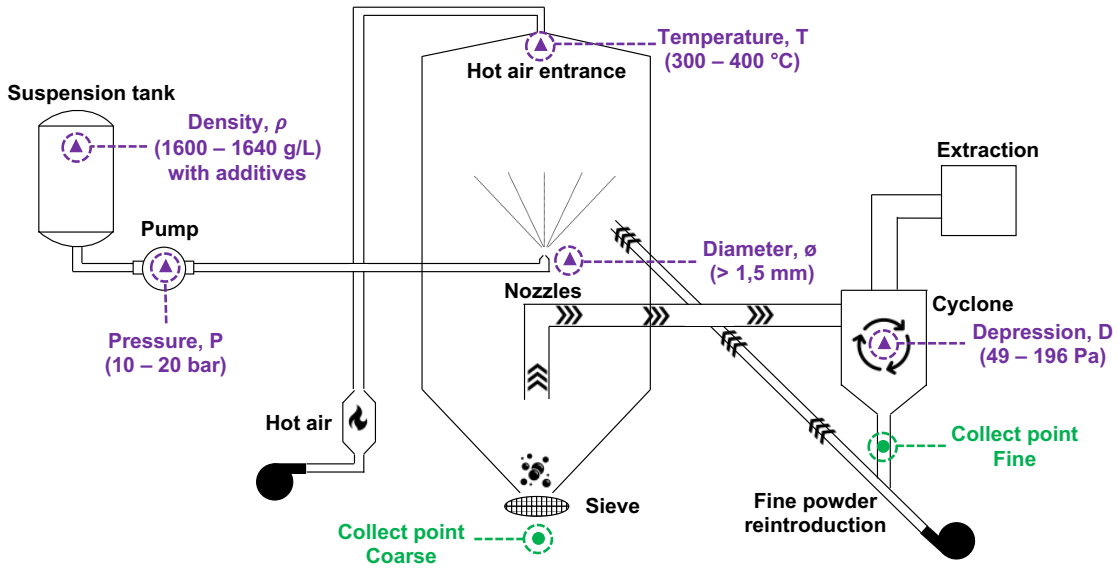


**Figure 7.3:** Schematic representation of the industrial spray dryer used to produce porcelain powder for conventional methods of porcelain manufacture. The controlled parameters identified in purple, with the conventional values used, are the density and the additives of the porcelain suspension, the air temperature, the feeding pump pressure, the nozzles diameter and the cyclone depression. The collect points of coarse and fine porcelain powders are identified in green.

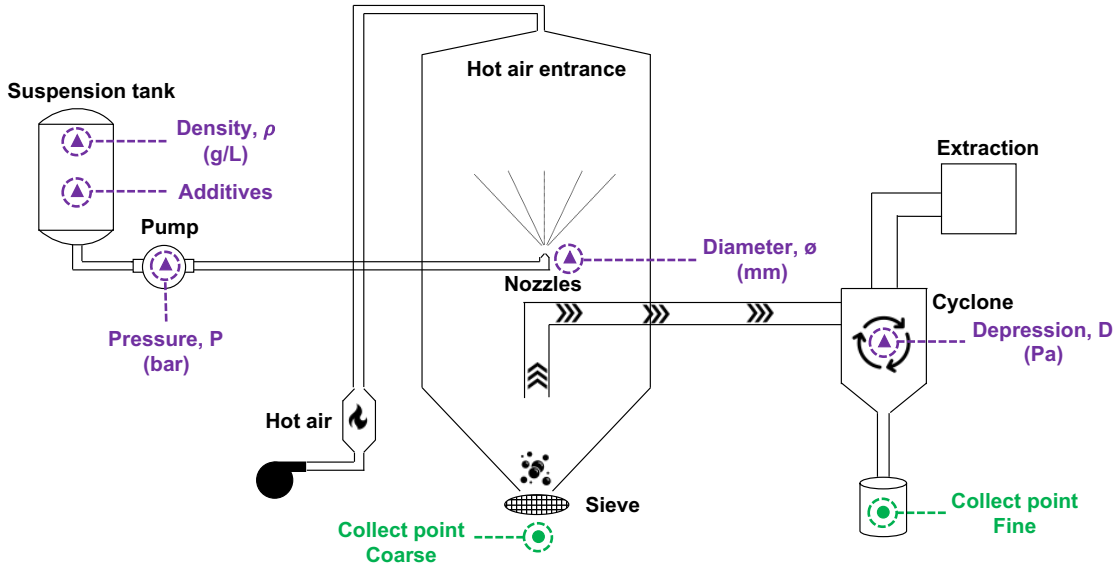


**Figure 7.4:** Schematic representation of the industrial spray dryer used to produce porcelain powder for powder bed AM processes. The controlled parameters identified in purple, are the density and the additives of the porcelain suspension, the feeding pump pressure, the nozzles diameter and the cyclone depression. The collect points of coarse and fine porcelain powders are identified in green.

A study at industrial scale was done varying operation conditions as feeding pressure, cyclone depression and nozzle diameter of the spray dryer operation process and porcelain suspension characteristics as density and use of additives, as presented in Table 7.II, in order to study its influence in the porcelain powders characteristics. Porcelain powders produced were also produced using the conditions for conventional porcelain manufacturing processes, identified in Table 7.II as production.

**Table 7.II:** Spray dryer operation conditions (nozzle, depression and pressure) and porcelain suspension characteristics (density and additives), used in the different spray drying studies.

| Name | Operation conditions | | | Suspension | |
|---|---|---|---|---|---|
| | Nozzle, ø (mm) | Depression, D (Pa) | Pressure, P (bar) | Density, $\rho$ (g/L) | Additives (wt.%) |
| Production | > 1,5 | 49 - 196 | 10 - 20 | 1600 - 1640 | 0,5 – 2,5 |
| SD1 | 0,9 | 147 | 10 | 1625 | 0,5 – 2,5 |
| SD2 | 0,9 | 147 | 10 | 1580 | 0,5 – 2,5 |
| SD3 | 0,9 | 147 | 10 | 1580 | --- |
| SD4 | 0,7 | 147 | 10 | 1580 | --- |
| SD5 | 0,9 | 49 | 10 | 1580 | --- |
| SD6 | 0,9 | 147 | 20 | 1580 | --- |

Some of the industrial porcelain powders, produced using SD3 conditions (Table 7.II) and collected from the fine powder collect point, were heat treated, in an industrial continuous kiln, with a maximum temperature of 980 - 1020 ºC, for 15 h 30 min, under oxidant atmosphere.

The powders were then industrially sieved separately, using a sieve with a mesh of 80 µm with 1 m diameter, in an industrial sieving equipment regularly used to sieve porcelain suspensions, as schematically presented in Figure 7.5. The porcelain powders after the industrial sieving, produced by spray drying and without the heat treatment are named in this work as raw porcelain powders, and the ones after the heat treatment are named as heat-treated porcelain powders.

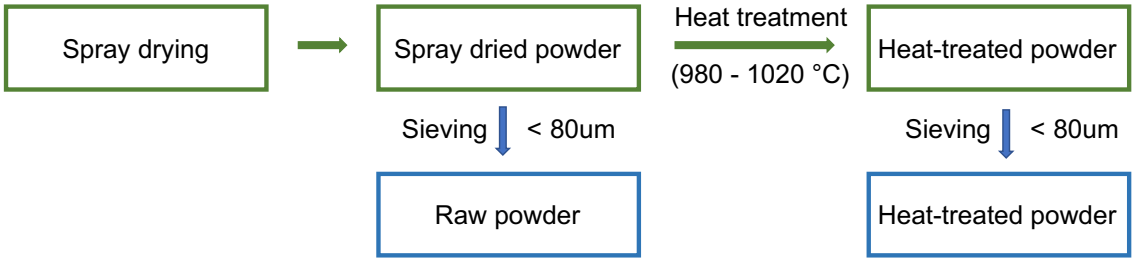


**Figure 7.5:** Preparation of raw and heat-treated porcelain powders.

The *in-bed* binder used in the BJP of porcelain powders was PVA (Zschimmer & Schwarz), based in the results of Chapter 3. In order to be used in this process, PVA as received was dry milled for 27 h at 60 rpm and dry sieved, as schematically represented in Figure 7.6.


**Figure 7.6:** Flowchart of the PVA powders preparation.

Porcelain and PVA sieved powders were dry mixed, using a dry rotational mixer at pilot scale, to produce the feedstock for BJP. The feedstock used in this chapter, chosen based on the results of Chapter 3 and Chapter 4, is composed by 45 wt.% of raw porcelain powders, 45 wt.% of heat-treated porcelain powders and 10 wt.% of PVA powders, as schematically presented in Figure 7.7. The feedstock produced is here after named as 50HT.

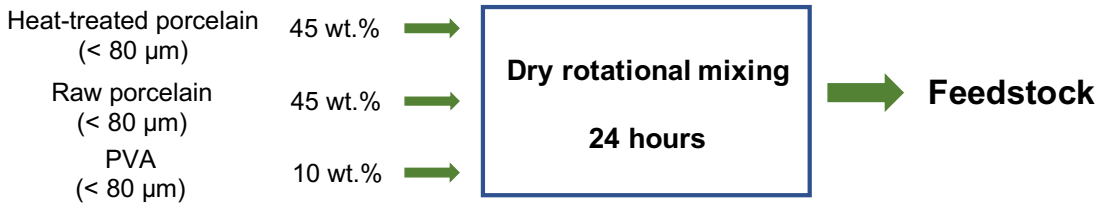


**Figure 7.7:** Feedstock preparation for BJP of porcelain parts, using raw porcelain (45 wt.%), heat-treated porcelain (45 wt.%) and PVA (10 wt.%) powders, mixed by dry rotational mixing.

The dried coarse and fine porcelain powders were characterized regarding their particle size distribution and morphology, using the procedure described in Chapter 2.

### 7.2.2. Additive manufacturing process

Printing process was performed in a ZPrinter 650 (ZCorp) to study the influence of layer thickness and binder saturation parameters in the production of defect free parts, programmed using the 3DPrint Software, version 1.03.8 (3DSystems). The conditions of layer thickness and binder saturation used are despite in Table 7.III. The 50HT feedstock, described above, was used to produce the porcelain printed parts and commercial powders Visijet PXL Core (3DSystems) were used with the standard set of parameters, as a control printed part. The virtual design of the printed part with different wall thicknesses is illustrated in Figure 7.8.

**Table 7.III:** Process parameters and its variations tested in ZPrinter 650 with 50HT feedstock.

| | Layer thickness (µm) | Binder saturation | | |
|---|---|---|---|---|
| | | (%) | Core ratio | Shell ratio |
| **Standard** | 100 | 100 | 0,12 | 0,24 |
| **Fine layer** | 87,5 | 100 | 0,12 | 0,24 |
| **Coarse layer** | 112,5 | 100 | 0,12 | 0,24 |
| **Binder high** | 100 | 180 | 0,21 | 0,43 |
| **Binder low** | 100 | 50 | 0,06 | 0,12 |

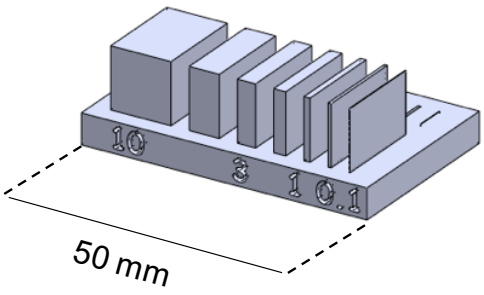


**Figure 7.8:** Illustration of the virtual design, used to assess the influence of printing parameters, with different wall thicknesses: 10 mm, 5 mm, 3 mm, 2 mm, 1 mm, 0,5 mm and 0,1 mm (from left to right, respectively)

Using the binder high conditions of Table 7.III, cylinders, with diameter of 7 mm and length of 14 mm, were printed with the 50HT feedstock. The feedstock was removed from the powder bed using the vacuum system of ZPrinter 650 and the feedstock was reused one time, named as 50HTx1. The same process was performed for a second time, named as 50HTx2.

In addition, a Z310 printer (ZCorp) was also used to study the influence of the powder feeding system. In this sense, the system used in the ZPrinter 650 was defined as dynamic feeding system, as represented in Figure 7.9, and the one of Z310 was defined as static feeding system, represented in Figure 7.10. Cylinders, with diameter of 7 mm and length of 14 mm were used as printed parts.

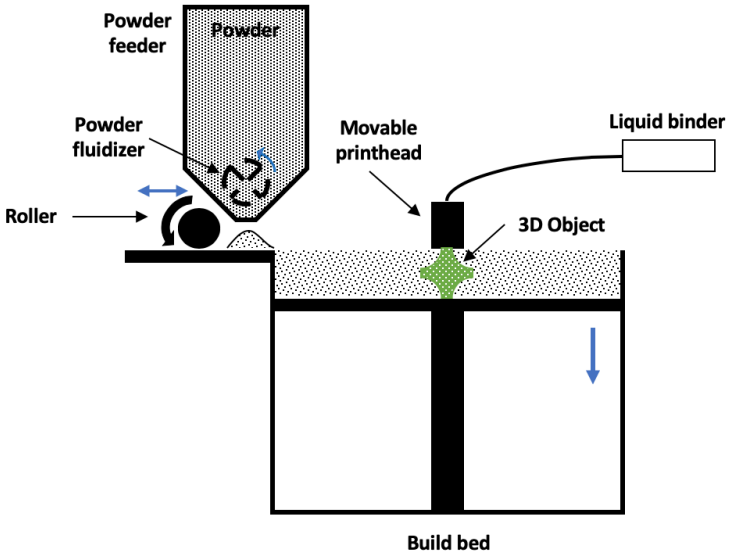


**Figure 7.9:** Schematic representation of commercial printer ZPrinter 650 (ZCorporation), with a dynamic feeding system.

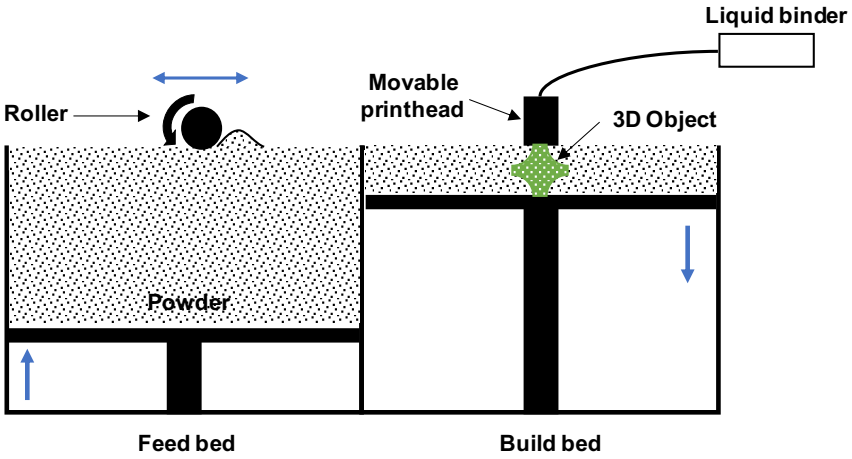


**Figure 7.10:** Schematic representation of commercial printer Z310 printer (ZCorporation), with a static feeding system.

The geometric relative density ($\%\rho_{geom}$) of the green printed cylinders produced using the different printing parameters and the reused feedstock, was calculated as described in Chapter 2.

Finally, the ZPrinter 650, using binder high printing conditions of Table 7.III and 50HT feedstock, was used to print a set of complex shaped parts, named as chess set, illustrated in Figure 7.11, an original design by JaaYoo [7], and a statue to assess the decoration process of a printed part in the different post-conformation industrial processes, illustrated in Figure 7.12, an original design of BerlinRockz [8].

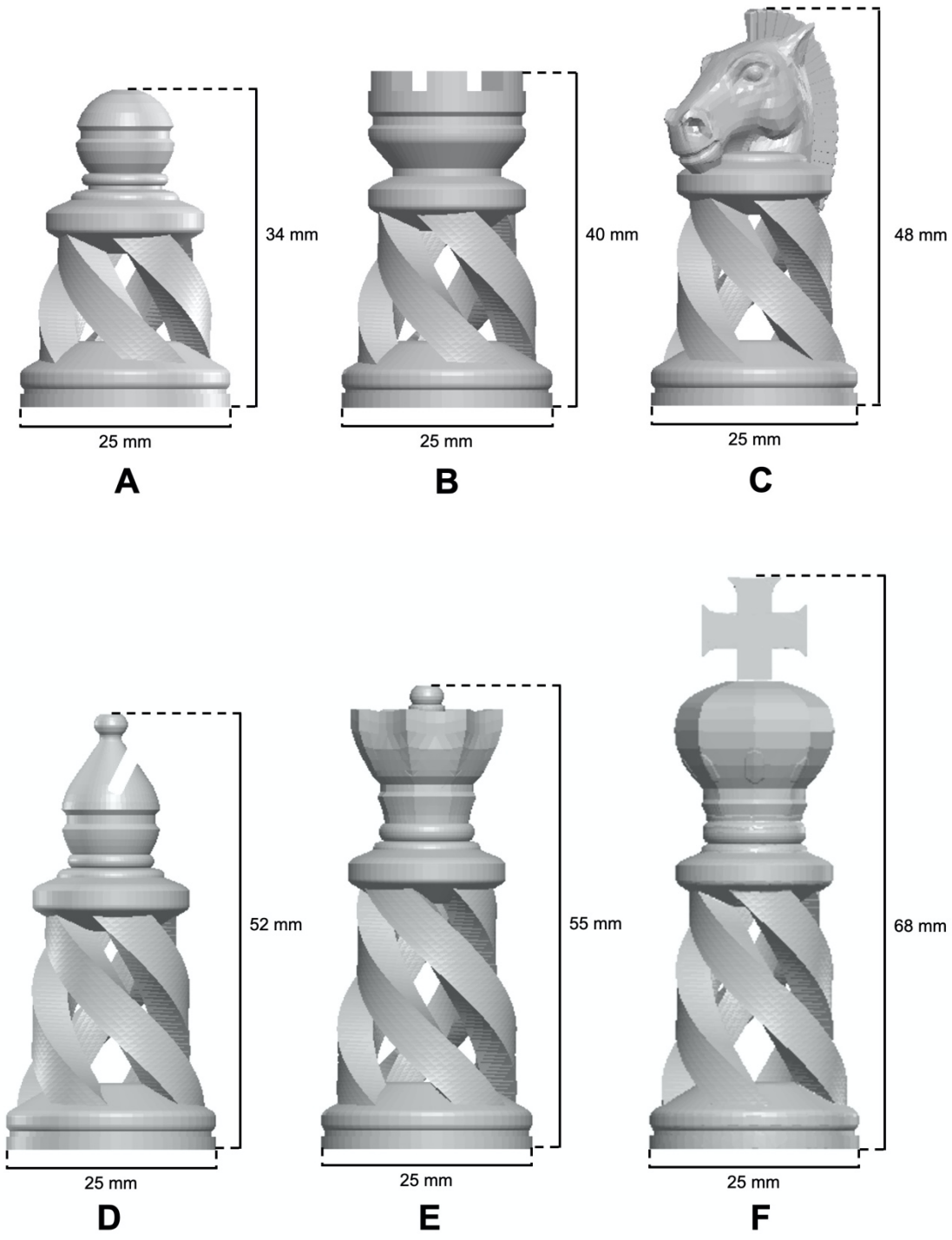


**Figure 7.11:** Illustration of the virtual design of the complex shaped parts of a chess set, with the following parts: (A) Pawn, (B) Rock, (C) Knight, (D) Bishop, (E) Queen and (F) King.

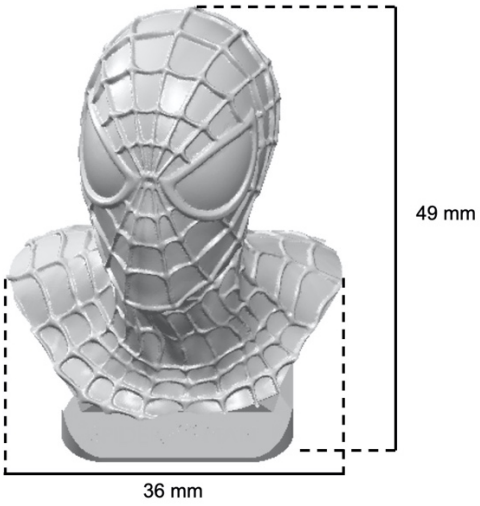


**Figure 7.12:** Illustration of the virtual design of the statue, used to assess the decoration process.

### *7.2.3. Post conformation*

The post conformation processes for the printed parts included the drying of the parts. The first drying step was done in the powder bed of the ZPrinter 650 for 24 h, after the printing process is finished. A second drying step was done at 90 °C for 16 h, in an oven.

For comparison with additively manufactured parts, parts from the conventional methods of porcelain manufacture, used by *Porcelanas da Costa Verde* were processed in the conventional route, presented in Figure 7.13. For the parts produced by BJP and SLS, as schematically represented in Figure 7.13, the results of relative density from Chapter 6 were used for the comparison.

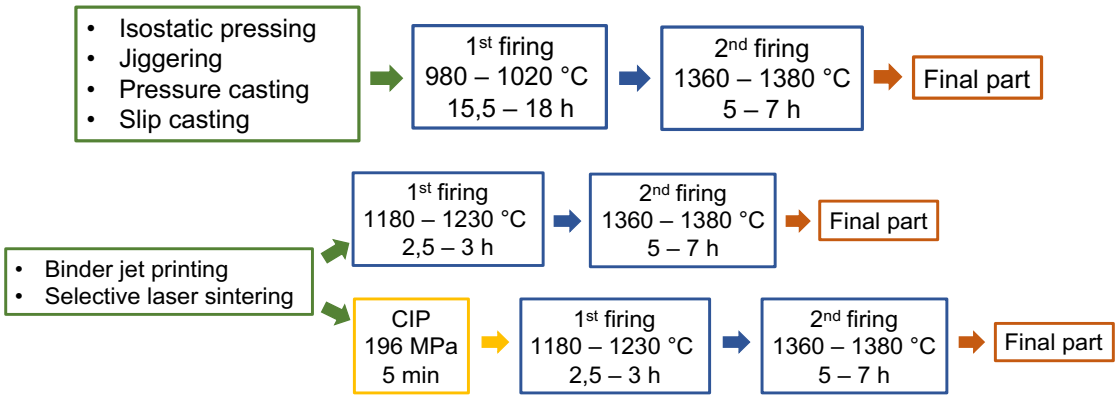


**Figure 7.13:** Sintering (firing) cycles flowchart of conventional manufactured porcelain parts by isostatic pressing, jiggering and pressure casting and additively manufactured ones by BJP and SLS, with and without CIP process. The main difference is the 1st firing cycle used for the second group.

The sintered parts, produced by the conventional methods, were also characterized regarding their relative density measured by Archimedes method as described in Chapter 2.

The complex shaped parts of the chess set, illustrated in Figure 7.11, were processed according with the described in Figure 7.13 for additively manufactured parts, without the CIP process. In the case of the statute, illustrated in Figure 7.12, besides the same process as the first group, the part was glazed and decorated by hand painting and process in the on-glaze firing cycle of *Porcelanas da Costa Verde,* at 890 °C for 2 h 30 min.

## 7.3. Materials and feedstock preparation

One of the most important aspects in AM of powders is the powder feedstock, as shown in Chapters 3 and 4. In the case of porcelain, due to the limitations in the mechanical strength of the green parts, an *in-bed* powder binder is needed in the powder formulation for BJP. As found in Chapter 3, PVA powders have a good performance for the production of porcelain parts by BJP, keeping an interesting cost for the industrial application. In the same chapter we conclude that an amount between 10 and 15 wt.% of PVA, mixed with porcelain powders presents a good balance between printing quality and properties of porcelain products.

In Chapter 4, we found that the use of heat-treated porcelain powders, mixed with the raw porcelain powders and *in-bed* binder powders, improve the quality of printed parts avoiding design defects. It was found that the preferred amount of heat-treated porcelain powders is 50 wt.% of the porcelain powders fraction. In this sense, a feedstock composed by 45 wt.% of raw porcelain, 45 wt.% of heat-treated porcelain and 10 wt.% of PVA powders was the chosen one to assess the industrialization of BJP for porcelain parts production.

Powders for porcelain parts production at industrial scale are prepared using a spray dryer, and varying processing parameters, such as feeding pressure, depression of cyclone and diameter aperture of the nozzles, allows to produce porcelain powders with different characteristics. The density and the addition of binders to the porcelain suspension will lead to powders with different morphological characteristics, as well.

In this section we present studies regarding the materials and the feedstock preparation for BJP of porcelain powders, focusing in the porcelain powders preparation by industrial spray drying and industrial dry sieving. The feedstock preparation was performed using dry mixing of porcelain and PVA powders.

### *7.3.1. Spray drying*

Considering the relevance of keeping as much as possible the current technological process of the company, the process used to produce porcelain powders for BJP, at an industrial scale, was spray drying, the one already in use to produce the porcelain powders for the isostatic pressing, a conventional manufacturing process of *Porcelanas da Costa Verde*.

The spray dryer used in *Porcelanas da Costa Verde* described above and presented in Figure 7.3, is an industrial size mixed flow type, equipped with a hydraulic (also known as one-fluid) nozzle atomizer. In mixed-flow spray dryers, the hot air is insert in the chamber from the top side, while the ceramic suspension is pulverized from the bottom towards the top of the spray dryer. When the suspension drops reach the hot air, the water from each droplet is removed, leaving only the solid content, and forms a particle or an agglomerate [6]. In the case of porcelain suspension, composed of clay, feldspar and quartz, the result is an agglomerate of these raw materials particles.

The main operation parameters are the nozzle diameter, the feeding pump pressure and the temperature of the air. The use of small orifices apertures of the nozzle leads to smaller suspension drops formed in the chamber, and as consequence the particles or agglomerates formed are smaller. In the same way, the increase in the feeding pressure decreases the size of the suspension drops, an as consequence, the decrease in the particle size formed [6]. The temperature of the air has the most impact in the moisture of the particles or agglomerates formed in spray drying, where the increase of the temperature increases the kinetics of solvent evaporation and decreases the moisture content in the particle or agglomerate. It has an impact as well in surrounding temperature of the droplet, for which low temperatures prevent thermal degradation of the formed particles [6]. Excessive high temperatures may also contribute for shape irregularities and deformations (i.e. non spherical shaped particles) [9]. Although the temperature has an important role in the spray drying process, in this work it was not possible to control the temperature, once the spray drying runs performed using the conditions despite in Table 7.II were short in time and in suspension and the temperature of the chamber was not stable enough, varying 40 to 50 °C during the process, in order to control it and do a systematic study. Regarding the fine particles separation, industrial spray dryers may use a cyclone to collect fine particles. In the cyclone is based on centrifugal force, which pushes the hot air containing ceramic agglomerates or particles. A vortex is created in the cyclone system, expelling the air from the top and the particles settled in the bottom [6]. The depression referred in this work is the low pressure created by the vortex of the cyclone, which can be controlled in the industrial spray dryer of Costa Verde. In the case of suspension characteristics, the high solid content, i.e., high density of the ceramic suspension, which leads to an increase in the density of the granules and as consequence high ceramic content in the green ceramic bodies, and the addition of organic additives, such as dispersants, to proper dispersion of the ceramic particles in the suspensions, and binders, to provide enough mechanical strength of the green bodies produced in the following production steps, are also typically controlled in the spray drying of ceramic suspensions [9]. Other spray drying operation parameters such as, feeding rate, gas flow rate and type of nozzle have also an impact in the morphology of the particles produced, but were not subject of study in this work.

The study of production of porcelain powders by spray drying was initiated using the spray drying conditions used for conventional production. As despite in Table 7.II, the density used was 1600 - 1640 g/L with 0,5 – 2,5 wt.% of proprietary additives. The feeding pressure used was 10 - 20 bar, with > 1,5 mm nozzles and depression of 49 - 147 Pa. The

morphology of the coarse and fine porcelain powders is presented in Figure 7.14 and the PSD curves are exhibited in Figure 7.15. Both powders exhibit mostly spherical shape and monomodal PSD, peaking at 330 μm in the case of coarse powders and at 174 μm in the case of fine powders.

Comparing with commercial powders for BJP, which have irregular shaped particles, as presented in Chapter 4, the coarse and fine porcelain powders here produced have mostly spherical shape and it may jeopardize the quality of the printed parts, promoting shifting of layers, as presented and discussed in Chapter 4. In addition, the size of both porcelain powders may be too big for the BJP process, where a typical 100 μm layer thickness is used, and small size is preferable to avoid defects during printing, as discussed in Chapter 4 as well.

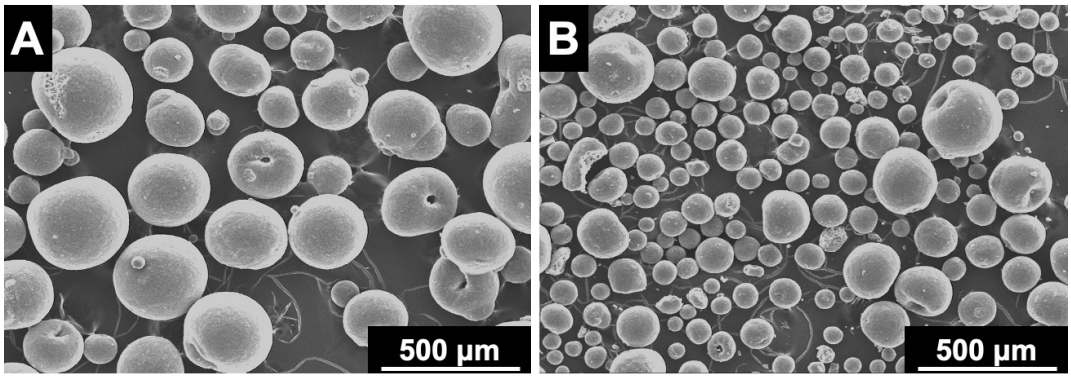


**Figure 7.14:** SEM micrographs of spray dried porcelain, using the production spray drying conditions, despite in Table 7.II, of (A) coarse and (B) fine powders. Both powders are composed of spherical shape particles.

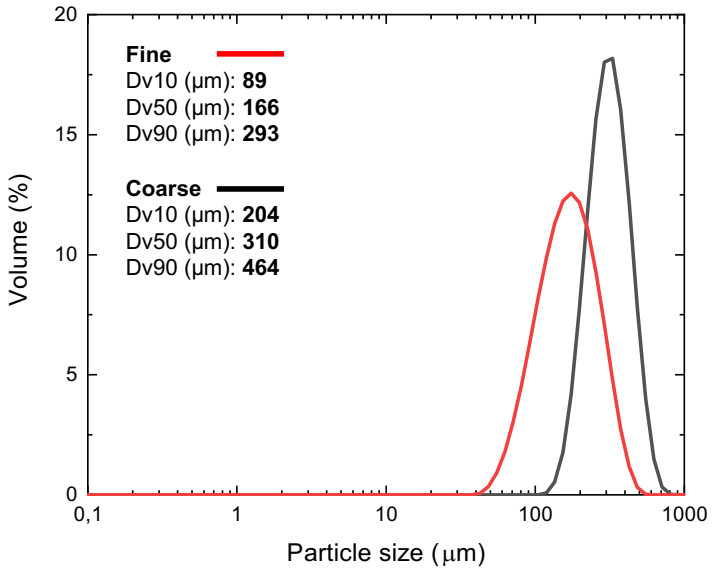


**Figure 7.15:** Particle size distribution of spray dried porcelain using the production spray drying conditions, despite in Table 7.II, of coarse (black) and fine (red) powders, with the insert presenting the values of Dv10, Dv50 and Dv90. Both powders exhibit a monomodal distribution.

The porcelain powders produced for conventional methods may be not suitable for BJP and there is a need to study how to produce porcelain powders with small particle size, using the industrial spray dryer already available. Having this in consideration, the fine porcelain powders, which are collected after the cyclone of the spray dryer may exhibit morphologies closer to the desired ones. In this sense, the effect of porcelain suspension characteristics, as density and the use of additives, and the effect of operation conditions, as feeding pressure, cyclone depression and nozzle orifice diameter, is presented next.

**Characteristics of porcelain suspension**

As despite in Table 7.II, the use of proprietary additives and the density of the porcelain suspension for the spray drying process was assessed, using 1625 g/L with additives, 1580 g/L with and without additives, while the nozzle diameter, the feeding pressure and the cyclone depression were kept constant at 0,9 mm, 10 bar and 147 Pa, respectively. The morphology of the coarse and fine porcelain powders produced is presented in Figure 7.16. It is noticeable that in the case of the three coarse powders (Figure 7.16 A, C and E) the porcelain agglomerates are mostly shaped, while in the case of fine powders (Figure 7.16 B, D and F) there is both spherical and irregular shaped particles. The PSD curves of the

coarse and fine porcelain powders is presented in Figure 7.17. In the case of coarse porcelain powders (Figure 7.17 A), the three curves present a monomodal distribution peaking at 352 μm, for the 1625 g/L with additives suspension, at 272 μm and 197 μm , for the 1580 g/L with and without additives, respectively. The fine porcelain powders (Figure 7.17 B) present a monomodal distribution with a shoulder in the small particles side for the suspensions with additives, peaking at 163 μm and a shoulder between 20 μm and 60 μm, in the case of 1625 g/L, and a peak at 127 μm and a shoulder between 10 μm and 30 μm, in the case of 1580 g/L. The suspension without additives and 1580 g/L of density, the PSD of fine porcelain powders is bimodal, with a major peak at 92 μm and a minor one at 18 μm. During the spray drying process was often observed the clog of the nozzles for the suspensions with the additives, requiring the process of nozzles unclog for the process to continue. This effect is attributed to the small nozzle orifice diameter (0,9 mm) which, combined with the use of additives in the porcelain suspension, promotes solid accumulation in the nozzle and clog the orifice.

Based on these results, we advocate that the use of additives and higher porcelain suspension density promote the formation of bigger agglomerates when compared with suspension without additives and with lower densities, for both coarse and fine porcelain powders. This effect may be explained by: i) the behavior of the additives, which comprises organic binders promoting the bond between raw materials particles increasing the size of the agglomerates and explains the nozzle clog observed during the spray drying of these porcelain suspensions, and ii) the increase in density, i.e., the increase in the solid content in the suspension, promotes agglomerates with more solid fraction. In addition, the three fine powders curve (Figure 7.17 B) tend to be monomodal with a shoulder in the small particles side or bimodal and this effect may be attributed to the size of the nozzle, once for the case of the porcelain powders for conventional methods (Figure 7.15), the bimodal distribution was not observed for both fine and coarse powders, and the main difference in the processing was the use of 0,9 mm diameter nozzles. In addition, the bimodal distribution is emphasized for suspensions without any additives due to the lack of organic binders in the mixture, and as consequence, lack bond between the raw materials particles.

As presented in Figure 7.16 B, D and F, the fine porcelain powders have both spherical and irregular shaped agglomerates, which is not observed for the fine porcelain powders produced using the production conditions (Figure 7.14 B). In this sense, the smaller orifice diameter of the nozzles, may contribute to the appearance of the irregular shaped particles.

However, this type of particles were not observed in the case of coarse powders (Figure 7.16 A, C and E) and here we advocate that the cyclone collector system has a major contribution for the formation of this type of agglomerates. In Figure 7.18 we schematically represent porcelain agglomerates inside the cyclone chamber. When the cyclone pushes the finer agglomerates from the main chamber of the spray dryer, the agglomerates will stay in movement inside the cyclone. While this process is happening, agglomerate-agglomerate and agglomerate-walls collisions will happen, leading to the fracture of the agglomerates, creating irregular shaped agglomerates. In addition, this explanation is supported by the PSD curves of the fine porcelain powders produced with these conditions (Figure 7.17), for which a shoulder in the small particles side and a second peak was observed, as opposed to the PSD curve observed for conventional production methods (Figure 7.15). Also, in the case of the suspension without additives, it is noticeable a bimodal distribution for fine porcelain powders, suggesting an increase in the small particles fraction evolving from a shoulder for suspension with additives to a second peak for suspension without additives. Here we advocate that the lack of binders in the suspension combined with the collisions in the cyclone described above, smaller particles are formed when compared with the suspension with the use of additives. As a matter of fact, the use of binders during the spray drying improves the resistance to deformation of the agglomerates [9]. As discussed before, the formation of irregular shape particles occurs inside the cyclone of the spray dryer due to agglomerate-agglomerate and agglomerate-wall collisions. Thus, the fact that the use of binders promote particles with higher resistance to deformation and fracture, leads to more spherical particles in the collection of fine particles, due to the higher fracture resistance of the particles, supported by the PSD (Figure 7.17) and the SEM images of the fine porcelain powders (Figure 7.16 B and D), for which is possible to observe more spherical agglomerates than for the suspensions without additives (Figure 7.16 F).

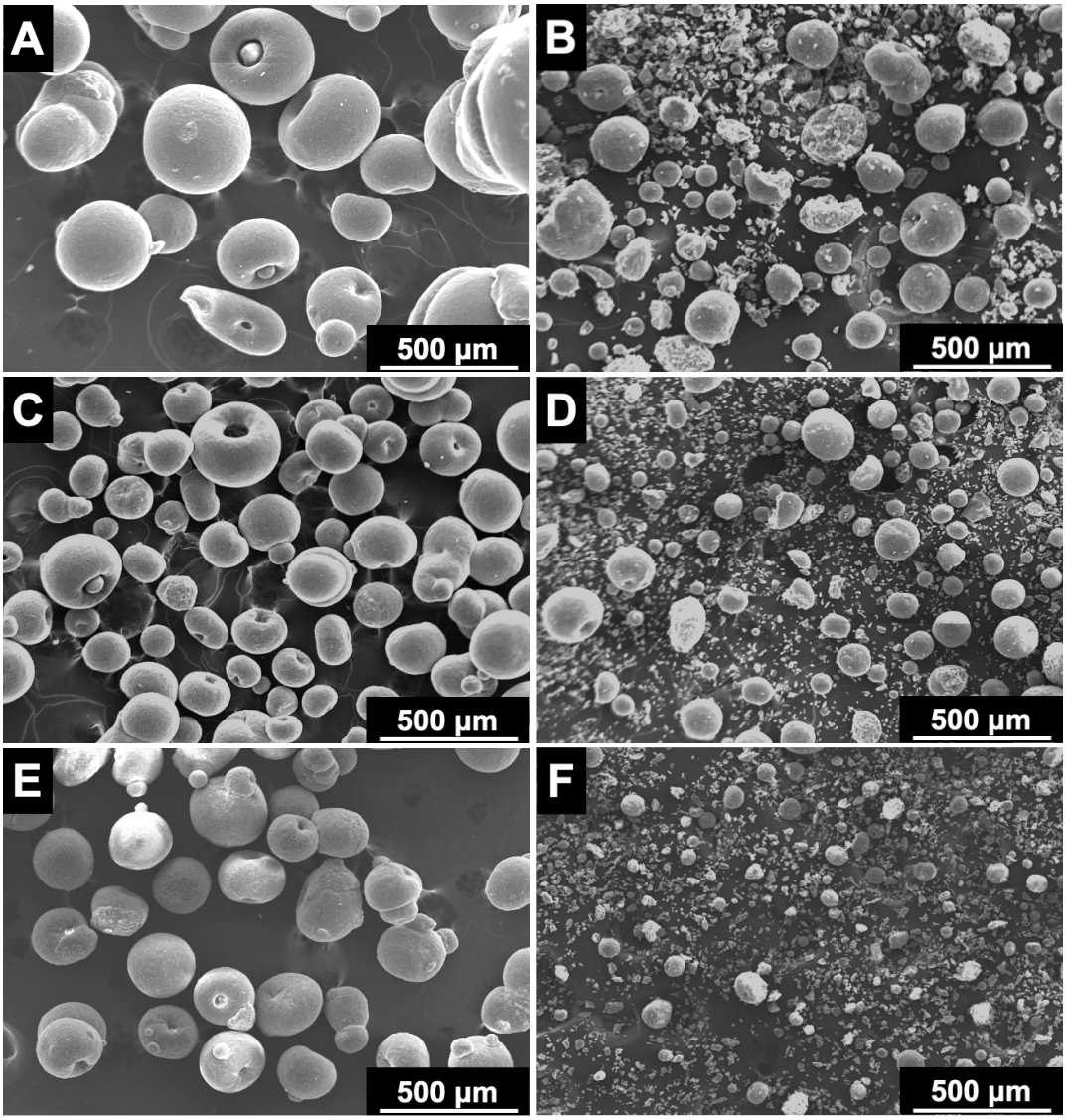


**Figure 7.16:** SEM micrographs of porcelain powders produced by spray drying under different conditions of porcelain suspension characteristics: (A) coarse and (B) fine powders of 1625 g/L with additives, (C) coarse and (D) fine powders of 1580 g/L with additives and (E) coarse and (F) fine powders of 1580 g/L without additives. The powders have spherical shape in the case of coarse powders and a mixture of spherical and irregular shaped particles in the case of fine powders.

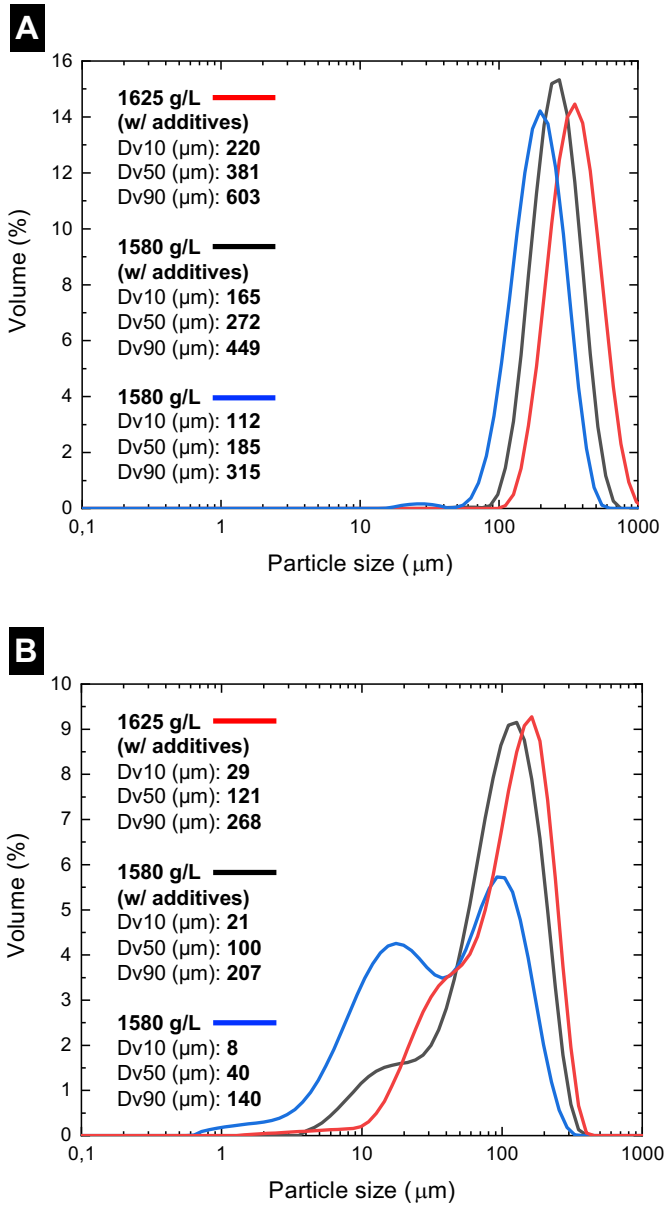


**Figure 7.17:** Particle size distribution of (A) coarse and (B) fine spray dried porcelain powders using the SD1, SD2 and SD3 spray drying conditions, as despite in Table 7.II, with the insert presenting the values of Dv10, Dv50 and Dv90. While the coarse powders exhibit a monomodal distribution, the fine powders present a bimodal distribution for suspension without additives and monomodal distribution with a shoulder in the small particles side for the suspensions with additives.

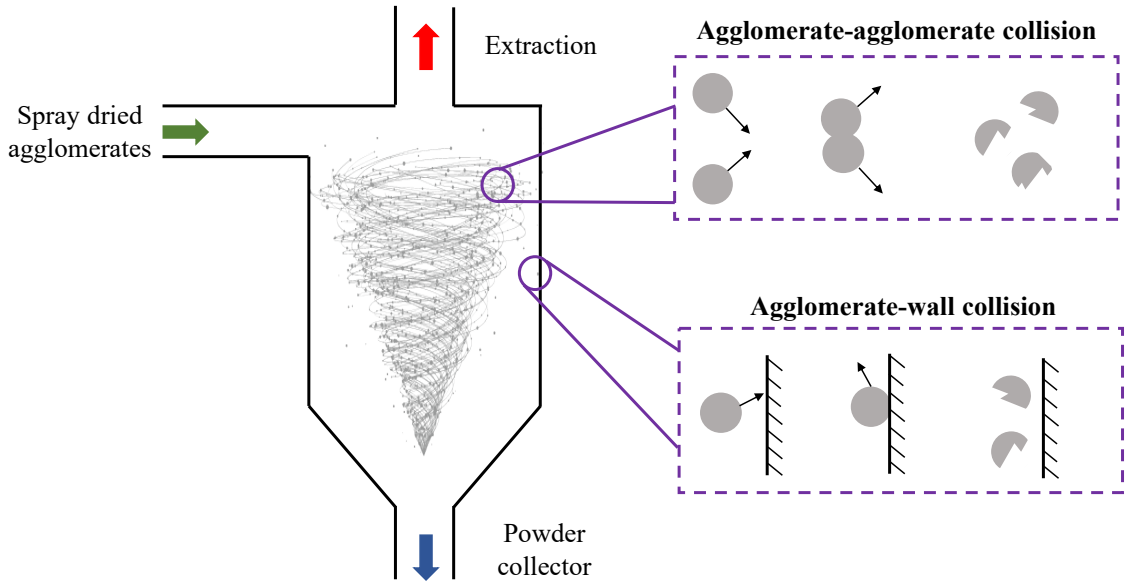


**Figure 7.18:** Schematic representation of the agglomerate-agglomerate and agglomerate-wall collisions happening inside the cyclone of the spray dryer.

Based on these results, we advocate that the use of additives and higher porcelain suspension density promote the formation of bigger agglomerates when compared with suspension without additives and with lower densities, for both coarse and fine porcelain powders. This effect may be explained by: i) the behavior of the additives, which comprises organic binders promoting the bond between raw materials particles increasing the size of the agglomerates and explains the nozzle clog observed during the spray drying of these porcelain suspensions, and ii) the increase in density, i.e., the increase in the solid content in the suspension, promotes agglomerates with more solid fraction. In addition, the three fine powders curve (Figure 7.17 B) tend to be monomodal with a shoulder in the small particles side or bimodal and this effect may be attributed to the size of the nozzle. In the case of the porcelain powders for conventional methods (Figure 7.15), the bimodal distribution was not observed for both fine and coarse powders, and the main difference in the processing was the use of 0,9 mm diameter nozzles. In addition, the bimodal distribution is emphasized for suspensions without any additives due to the lack of organic binders in the mixture, and as consequence, lack bond between the raw materials particles.

**Operation conditions of the spray dryer**

The use of a nozzle with an orifice diameter of 0,7 mm was also assessed and the porcelain powders were compared with the ones produced with 0,9 mm. The suspension

characteristics were kept constant using 1580 g/L of density without additives. The feeding pressure and the cyclone depression were kept constant at 0,9 mm, 10 bar and 147 Pa, respectively. The morphology of the porcelain powders produced is presented in Figure 7.19, where is noticeable that there is no significative difference between the powders produced, which present spherical shaped coarse porcelain powders and both spherical and irregular shaped fine porcelain powders, for both 0,7 mm and 0,9 mm nozzles. In the case of the PSD curves, the same trend was observed, both presenting monomodal distributions in the case of coarse powders (Figure 7.20 A), peaking at 197 μm with the 0,9 mm and at 174 μm with the 0,7 mm nozzles, and bimodal distributions for the fine powders, with a major peak at 92 μm and a minor one at 18 μm, for both 0,7 mm and 0,9 mm nozzles. However, a major difference was observed during the spray drying process, in which the use of 0,7 mm promotes the clog of the nozzles, right after the process starts, jeopardizing the production of powders, as opposed for the 0,9 mm nozzles. We conclude that the use of 0,7 mm is not suitable for the spray dryer of *Porcelanas da Costa Verde*, once it is impossible to keep the spray drying process running without the nozzles clog.

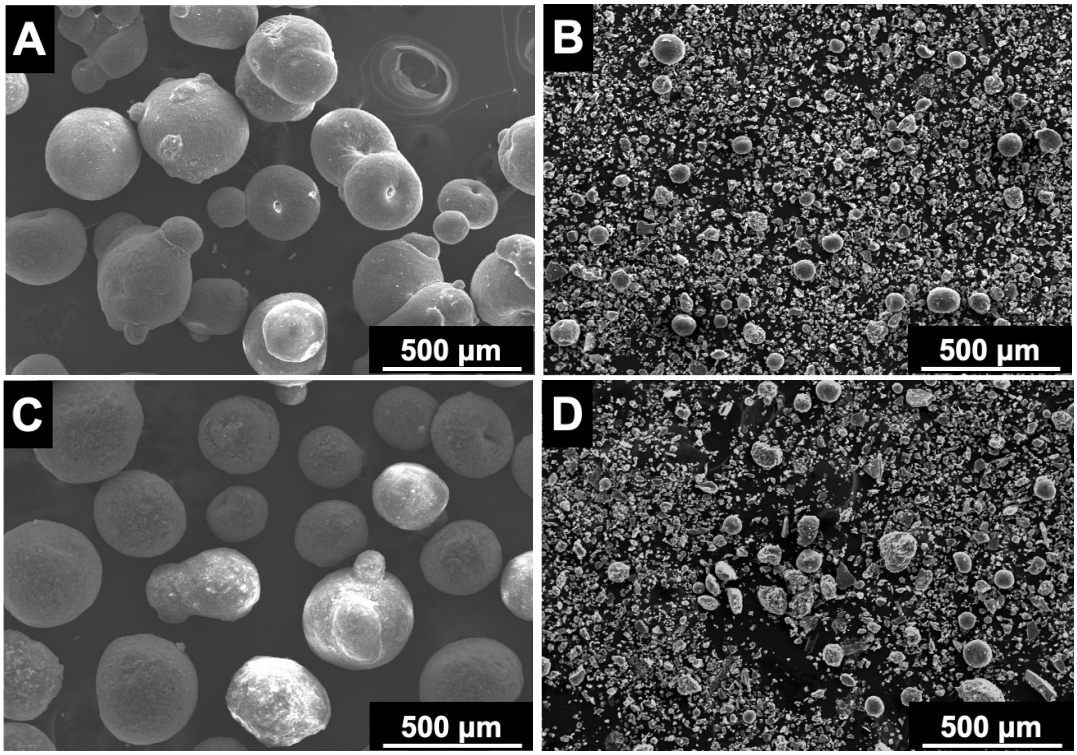


**Figure 7.19:** SEM micrographs of porcelain powders produced by spray drying using different nozzles diameters: (A) coarse and (B) fine powders of 0,9 mm nozzles and (C) coarse and (D) fine powders of 0,7 mm nozzles. The powders have mostly spherical

shape in the case of coarse powders and a mixture of spherical and irregular shaped particles in the case of fine powders.

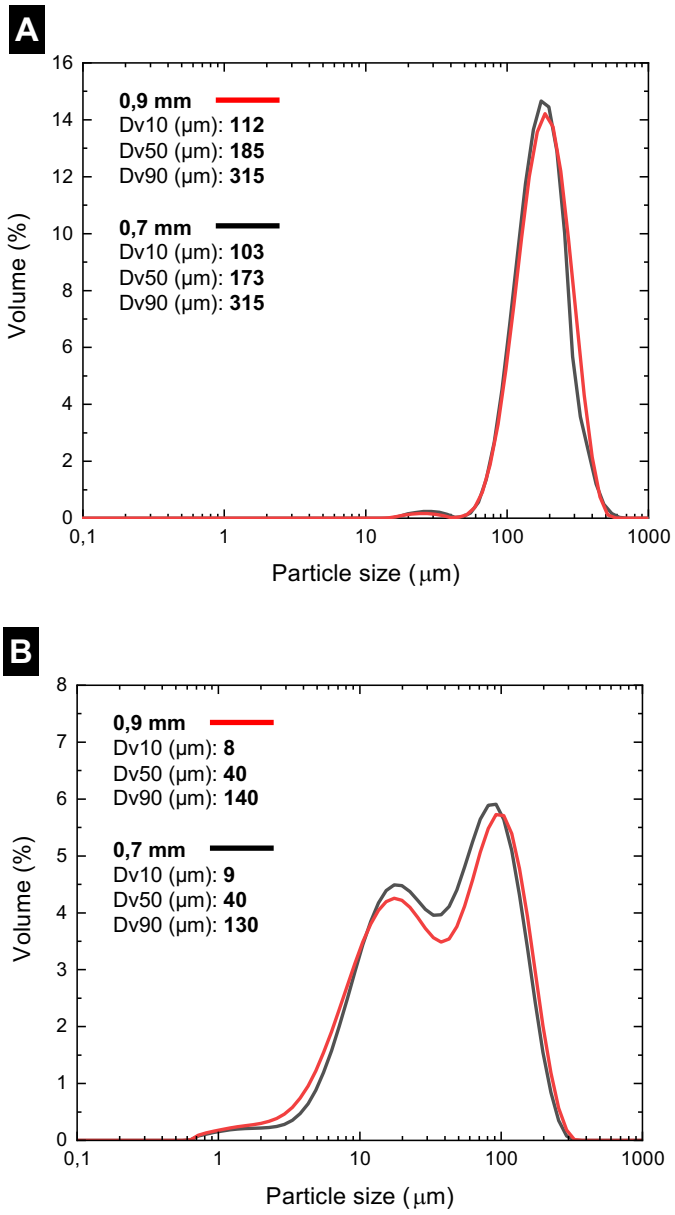


**Figure 7.20:** Particle size distribution of (A) coarse and (B) fine spray dried porcelain powders using the SD3 and SD4 spray drying conditions, as despite in Table 7.II, with the insert presenting the values of Dv10, Dv50 and Dv90. While the coarse powders exhibit a monomodal distribution, the fine powders present a bimodal distribution.

Based on the previous results, the 0,9 mm nozzles were chosen to assess the effect of the other operation conditions: feeding pump pressure and cyclone depression, using the same porcelain suspension (Table 7.II). In Figure 7.21 the SEM images of the powders are presented. A first main observation is regardless of the pressure and depression used, the

coarse porcelain powders exhibit spherical shaped agglomerates (Figure 7.21 A, C and E) while the fine porcelain powders present both irregular and spherical agglomerates (Figure 7.21 B, D and F), the same trend as observed above for different porcelain suspension characteristics and different nozzles diameters. In the case of the PSD curves, the coarse porcelain powders produced using the different conditions, exhibit a monomodal distribution (Figure 7.22 A), peaking at 197 μm with a feeding pressure of 10 bar and a cyclone depression of 147 Pa, at 174 μm with a pressure of 10 bar and a depression of 49 Pa, while with 20 bar pressure and 147 Pa of depression, the peak was observed at 153 μm. The main difference observed using the different operation conditions was the PSD curves of the fine porcelain powders (Figure 7.22 B). In the case of the spray drying using 10 bar of pressure and 147 Pa of depression, the curve presents a bimodal distribution, already discussed above. However, for both the spray drying with 20 bar of pressure and 147 Pa of depression and the one with 10 bar of pressure and 49 Pa of depression, the curve presents a monomodal distribution with a shoulder in the big particles side. In the case using the 20 bar pressure, the curve peaks at 12 μm and exhibits a shoulder between 40 μm and 60 μm, while for the use of 49 Pa the curve presents a peak at 18 μm and a shoulder between 40 μm and 100 μm. The first curve is explained by the use of 20 bar of feeding pressure, which promotes the formation of small suspension drops during the spray drying and leads to small agglomerates formed [10]. In one hand the agglomerates are smaller than the ones formed with 10 bar and on the other hand, because more agglomerates are pushed to the cyclone due to its small size, more agglomerate-agglomerate and agglomerate-wall collisions happen inside the cyclone chamber and decrease even more the agglomerate size. In the case of the conditions using 49 Pa of depression, the lower depression than for the other spray drying conditions, will be able to push smaller agglomerates, i.e., lighter agglomerates, from the main chamber of the spray dryer. In this sense, the powders collected after the cyclone system will be composed of smaller agglomerates than the ones using higher depression.

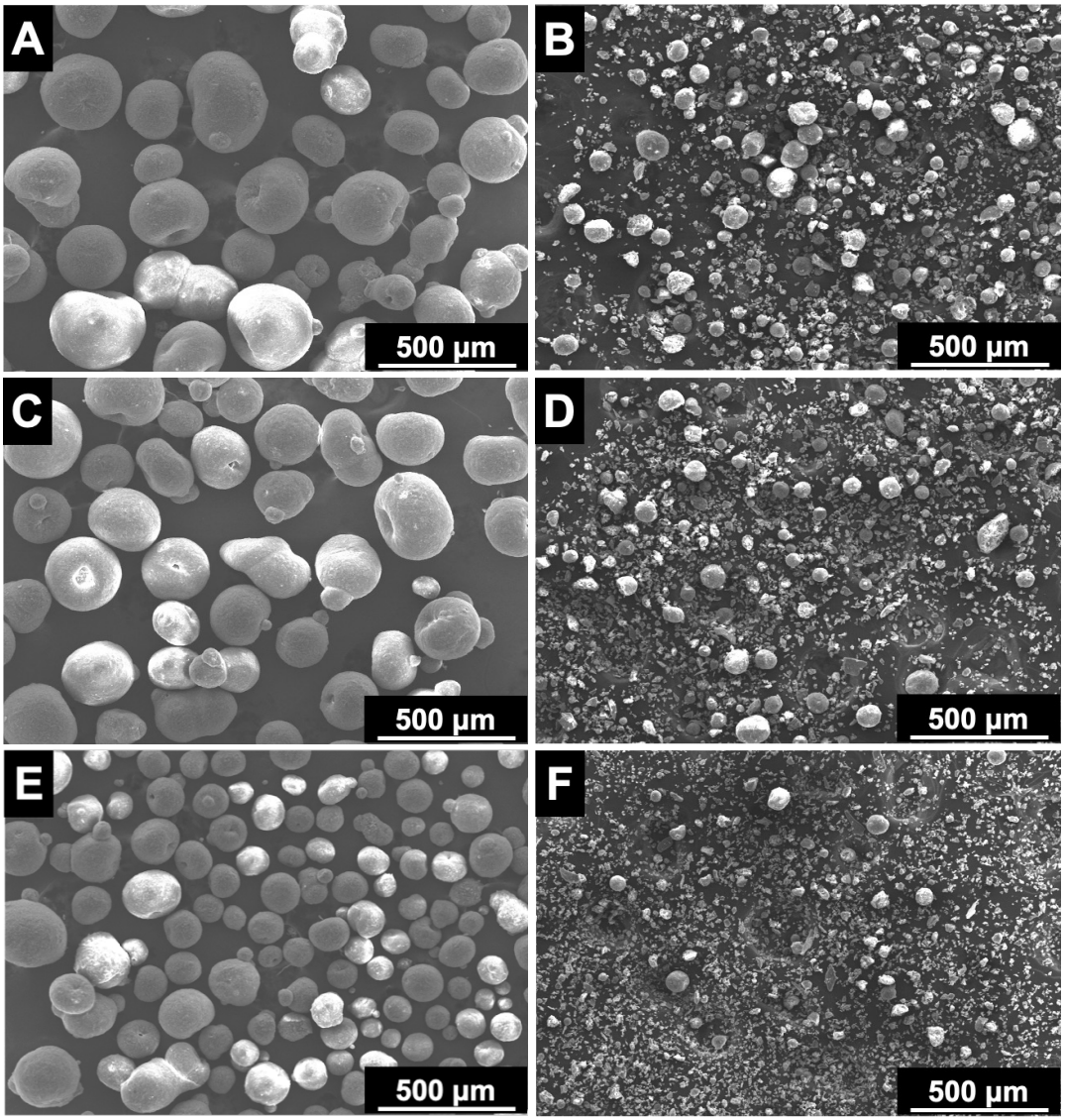


**Figure 7.21:** SEM micrographs of porcelain powders produced by spray drying under different conditions of feeding pressure and cyclone depression: (A) coarse and (B) fine powders produced with 10 bar pressure and 147 Pa of depression, (C) coarse and (D) fine powders produced with 10 bar pressure and 49 Pa of depression and (E) coarse and (F) fine powders produced with 20 bar pressure and 147 Pa of depression. The powders have spherical shape in the case of coarse powders and a mixture of spherical and irregular shaped particles in the case of fine powders.

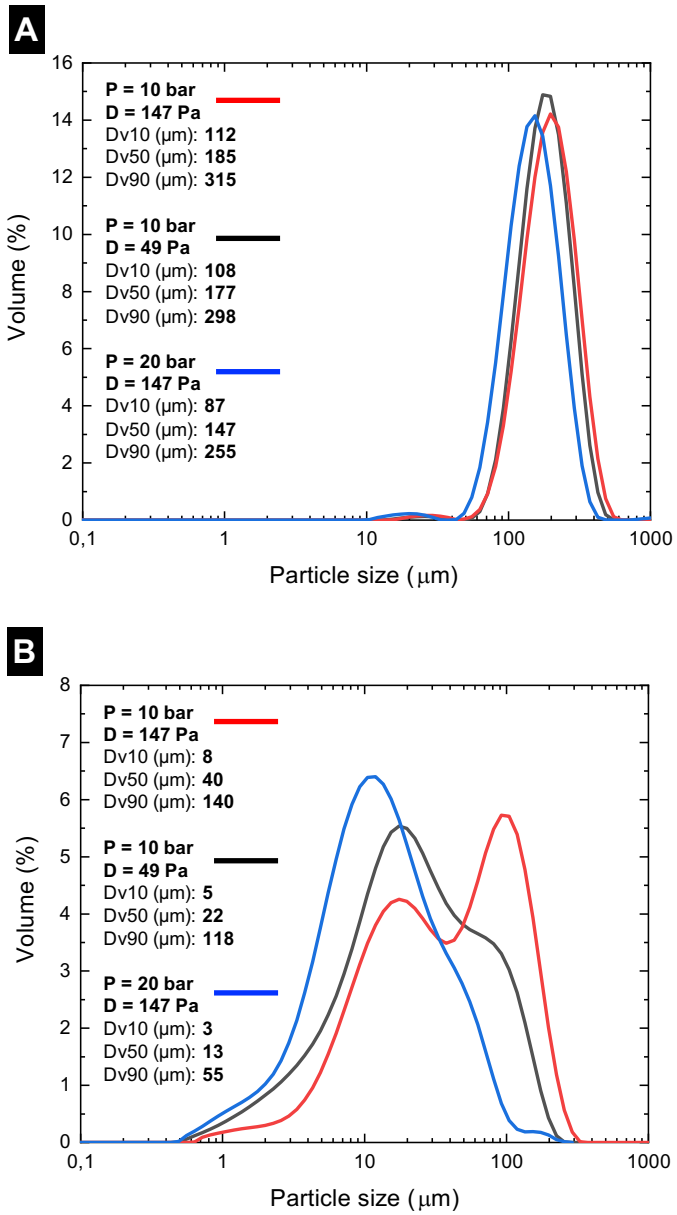


**Figure 7.22:** Particle size distribution of (A) coarse and (B) fine spray dried porcelain powders using the SD3, SD5 and SD6 spray drying conditions, as despite in Table 7.II, with the insert presenting the values of Dv10, Dv50 and Dv90. While the coarse powders exhibit a monomodal distribution, the fine powders present a bimodal distribution in the case of 10 bar pressure and 147 Pa depression, while for 10 bar pressure and 49 Pa depression and 20 bar pressure and 147 Pa depression exhibits a monomodal distribution with a shoulder in the large particles side.

Summarizing, in this section we proved that it is possible to produce porcelain powders suitable for BJP process due to its smaller size than the ones produced for conventional methods, in combination with the production of irregular shaped powders, which, as

discussed in Chapter 4, are similar to the ones of commercial powders. These results were possible by using a nozzle with a 0,9 mm of orifice diameter with a 1580 g/L porcelain suspension without additives. In addition, the operation conditions present higher influence in the morphology of fine porcelain powders than in the coarse ones. Also, the irregular shaped particles observed in the fine porcelain powders was attributed to a combination of three factors: the use of a small orifice diameter of the nozzles, the lack of additives in the porcelain suspension and especially to the agglomerate-agglomerate and agglomerate-walls collisions that happen inside the cyclone system chamber. However, there is still a need of sieving the fine porcelain powders, once they exhibit a fraction of agglomerates above 80 μm, which is the desired size for porcelain powders for BJP, as discussed in Chapter 4.

### *7.3.2. Sieving and feedstock preparation*

The sieving process of porcelain powders is necessary in order to have a PSD of powders suitable for BJP. In this sense, the sieving was done using an industrial scale sieving system, with 80 μm mesh sieve, conventionally used for sieving porcelain suspension for conventional manufacturing processes. The morphology of the fine porcelain powders, produced by spray drying using the SD3 conditions of Table 7.II, before the sieving process is presented in Figure 7.23 A, while the powders after sieving are exhibited in Figure 7.23 B, for porcelain powders above the sieve, and Figure 7.23 C for powder under the sieve. With a first overall observation it is noticeable that the porcelain powder above the sieve still contain fine agglomerates of porcelain. The PSD analysis, Figure 7.24, supports this result, as the powder above the sieve exhibits a monomodal distribution, peaking at 104 μm with a shoulder in the small particles side. In addition, this curve presents a Dv50 of 81 μm, which means that 50 vol.% of the powders above the sieve have lower size than the mesh aperture, while the powder under the sieve exhibits a monomodal distribution with a shoulder in the small particle size. Also, the PSD curve of the porcelain powder under the sieve exhibits a Dv90 of 96 μm, which means that the powder has some agglomerates bigger than the mesh aperture. This effect may be explained by the orientation of irregular particles which may have a dimension smaller than the aperture. The same effect was observed and discussed in Chapter 3 of this thesis.

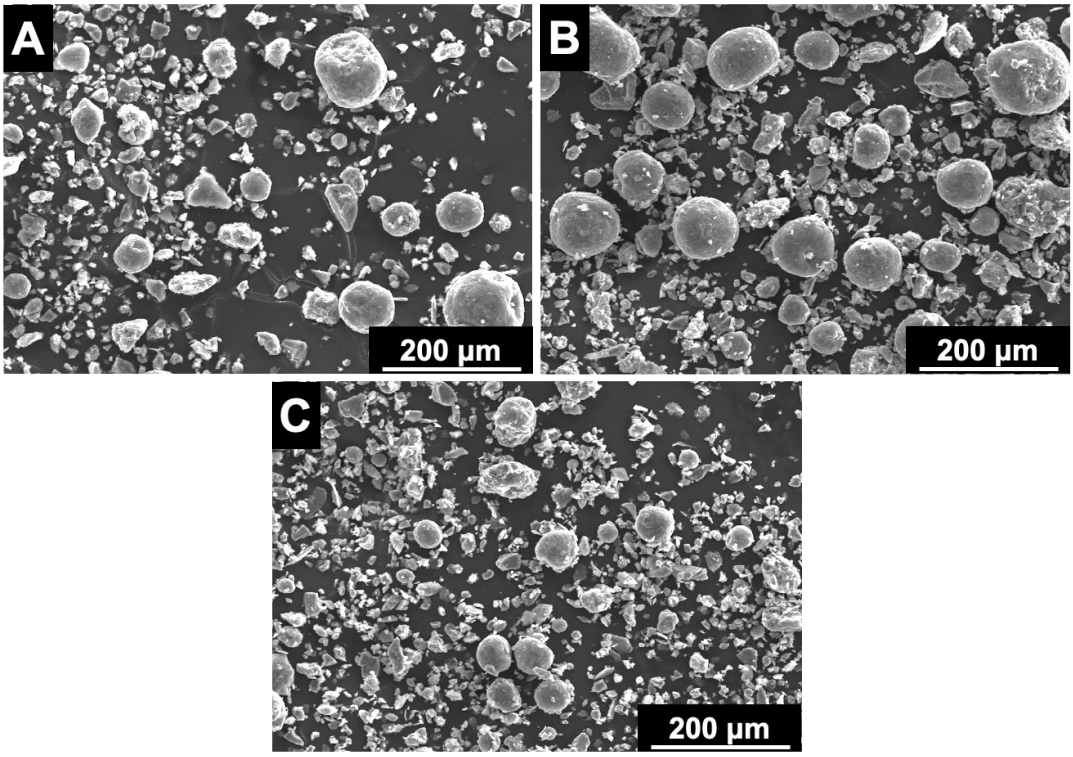


**Figure 7.23:** SEM micrographs of spray dried porcelain powders (A) before sieving and (B) above and (C) under sieve, after sieving, using an industrial mesh with 80 µm.

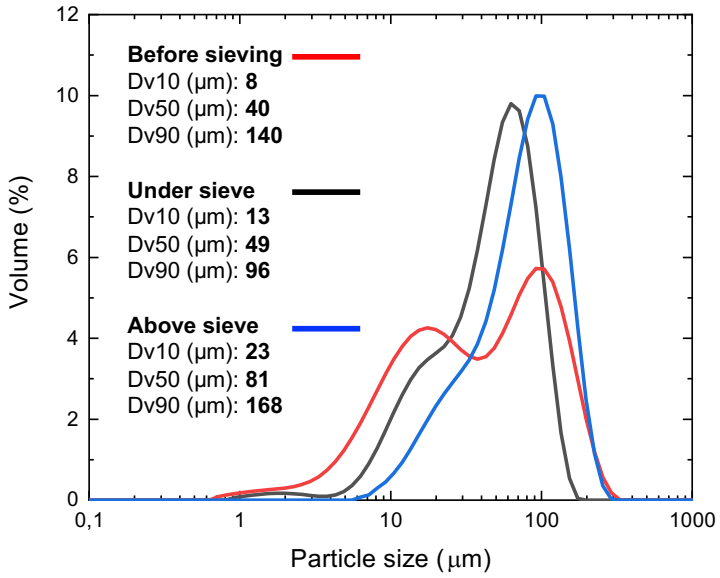


**Figure 7.24:** Particle size distribution of spray dried porcelain powders before and under and above sieve, after industrial sieving with a mesh of 80 µm.

Based on these results, we advocate that the sieving process using the industrial equipment of *Porcelanas da Costa Verde* is not fully efficient. Even though the powder under the sieve may be used for BJP, the powder above the sieve still has a fraction (50 vol.%) that could

be used as well and may affect the PSD of fine porcelain powders once it may lead to more sieved powders in different sieving runs. This is explained by two main reasons: i) the industrial sieving system is prepared for wet sieving, i.e., sieving of porcelain suspensions which is more efficient due to better dispersion of particles and the water medium acts as a carrier for the solid fraction and ii) the industrial system has an extraction for the solid fraction of the suspension above the mesh and, using it for dry sieving of powders, this extraction of the powder leads to a fast removal of the powder above the sieve and do not gives time to the complete sieve of the powders, decreasing the efficiency of the process due to remotion of fine porcelain powder. However, the sieve of porcelain powders for BJP must be done in dry state once the porcelain powders are composed of agglomerates which deagglomerate in water and affects its PSD. In this sense, further investigation must be done to improve the dry sieve process at industrial scale of porcelain powders for BJP.

The feedstock preparation must also to be done in dry state as in addition to the porcelain powders which are deagglomerable in water, the *in-bed* binder, in this case PVA, is water soluble. Based on the results of Chapter 3 and Chapter 4, the feedstock used for porcelain parts production is composed of 45 wt.% of raw porcelain powders, 45 wt.% of heat-treated porcelain powders and 10 wt.% of PVA powders. The heat-treated powders allow the printing of defect free parts and is performed in the industrial continuous kiln of *Porcelanas da Costa Verde*. The batches of feedstock for BJP were mixed by rotational mixing for 24 h, in batches of 4 kg, using the three powders sieved individually at 80 μm. In the case of PVA, the powder as received has large particle size and dry milling for 27 h, is required in order to reach the desired PSD.

Summarizing, although for this work, done at pilot and industrial scale, the sieving and mixing scale was not a problem, in the case of fully industrialization the amount of feedstock required may increase and a more efficient sieving system may be required. In addition, the is also the need to assess the economic viability and comparison of milling the PVA as received or buyng the powder already with the desired PSD (< 80 μm).

## 7.4. Printing process

In this section we discuss the printing process with focus in the printing parameter layer thickness and binder saturation, the feedstock feeding system and the reuse of feedstock. A ZPrinter 650 (ZCorporation) with the 3DPrint Software, version 1.03.8 (3DSystems) was

used to print the parts and the liquid binder was the commercial Visijet PXL clear (3DSystems).

Concerning the printing parameters, the commercial software used only allows the variation of layer thickness and binder saturation. The standard layer thickness is 100 µm for commercial powders. The minimum layer thickness allowed by the software is 87,5 µm. In order to study the effect of the layer thickness we used the minimum layer thickness and a coarser layer thickness, 112,5 µm, to keep the same difference to the standard value. The binder saturation refers to the ratio of binder volume to the powder volume. In this work we used the minimum binder saturation value (50 %) and the maximum value (180 %). The set of parameters (Table 7.III) was used to print a part with different thicknesses of walls (Figure 7.8) to evaluate the print of defect free parts. The 50HT feedstock was used.

The printed parts are presented in Figure 7.25, starting with a control part, produced with the standard parameters and Visijet PXL Core commercial powders (Figure 7.25 A). The minimum wall thickness printed without defects has 1 mm while the one with 0,5 mm was printed, but has defects formed during its removal from the powder bed. Concerning the porcelain parts, the first observation concerns the use of binder low parameters, i.e., 100 µm and 50 % of binder saturation, which was not possible to print. This result is explained by the low amount of liquid binder which is not enough to dissolve the in-bed binder PVA, leading to the lack of bond of porcelain powders. In the case of porcelain parts printing using the standard parameters (Figure 7.25 B), layer coarse (Figure 7.25 C) and layer fine (Figure 7.25 D) there was not significative differences, with the minimum wall thickness printed of 2 mm. In the case of printing with binder high parameters (Figure 7.25 E) the minimum wall thickness printed is 1 mm, comparable with the printed part with commercial powders and standard printing parameters.

Based on these results we advocate that the main printing parameter for a defect free part with small design features is the binder saturation. The minimum binder saturation (50 %) does not provide enough bond of porcelain powders in the printed part and the standard value (100 %) does not allow the printing of small design features, such as a wall with 1 mm thickness. The maximum binder saturation (180 %) is the one which provides the best results concerning the design features of the printed part. This is explained by the higher amount of liquid binder, which penetrates in the powder bed and dissolves the *in-bed* binder PVA, providing enough mechanical resistance to porcelain printed part, when compared

with the minimum and standard values of binder saturation. In addition, these study supports the fact that the reduction in binder saturation, although might reduce the layer shifting effect observed in Chapter 4, it will have an impact in the mechanical resistance of the green parts. The layer thickness and the binder saturation were also aim of study by Vaezi *et al.* [11] with ZP102 commercial powder and ZB60 commercial liquid binder, using 0,1 and 0,0875 mm of layer thickness and 90 % and 125 % of binder saturation. The group found that the decrease in the layer thickness lead to an increase in the tensile strength and a decrease in the flexural strength of the parts, followed by a decrease in the surface quality. The group also found that the use of lower binder saturations leads to a smoother surface of the parts. However, in the case of the porcelain powder feedstock, the most important effect of the binder saturation was the mechanical strength in order to be handled.

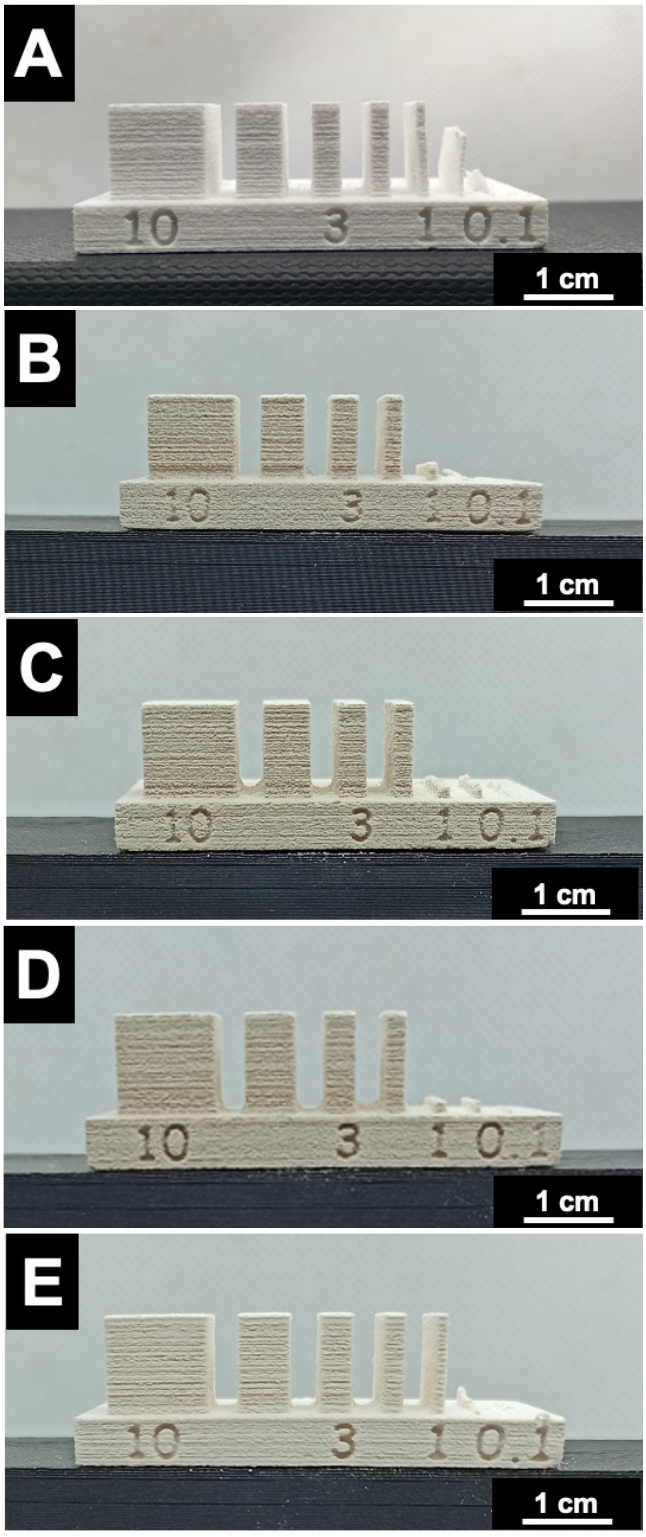


**Figure 7.25:** Printed parts in green state, with different thicknesses of walls, using the printing parameters of Table 7.III. A control printed part using Visijet PXL Core commercial powder was printed (A), and the porcelain 50HT feedstock was used with (B) standard, (C) Layer coarse, (D) Layer fine and (E) Binder high printing parameters.

The feeding system of the binder jet printer was also studied, using a dynamic feeding system, Figure 7.9, of ZPrinter 650, i.e., the feedstock is in a vat, and a static feeding system, Figure 7.10, of Z310, i.e., the feedstock is a powder bed. In the static mode, the powder feedstock is pushed from a surface of a powder bed to the build bed. In this system, there are friction forces between particles which is being pushed and the ones adjacent to them. In the case of the dynamic system, the powder is released from the vat, by gravitational forces, in front of the roller which pushes the powder to the build bed. Also, in the dynamic mode there is a powder fluidizer responsible to fluidize the powder.

In Table 7.IV the geometrical relative density printed parts with 50HT feedstock in green state and after 1st and 2nd industrial sintering cycles is presented for both feeding systems. In the case of static system, the green parts exhibit 32 % of relative density which increases up to 57 % after industrial sintering, while for the dynamic feeding system the green parts exhibit 35 % of relative density and 63 % in the case of final parts. The dynamic feeding system leads to an increase in both green and industrially sintered parts. As said above, in the case of static feeding system, the powder is pushed from a powder bed and friction forces of the pushed powder and the powder in the bed leads to a worse spread of the powder in the build bed, and as consequence, the green density of the printed parts is lower than the ones using a dynamic system. After the industrial sintering, the same trend is observed as consequence of the low relative density of the green parts. Another factor that may affect the powder distribution in the static feeding system is the powder segregation, well discussed by Mostafaei *et al.* [12] which is typically for powders with coarse and fine particles, and relates with the downward movement of fine particles in the void space between large particles, leading to higher fraction of fine particles in the bottom of the powder bed as compared with the top of the powder bed. This effect may lead to heterogeneity in the PSD of powders and has an impact in the density of green parts. In the case of dynamic feeding system, the impact is low, once the powder is deposited by gravitational forces in front of the roller, previous to the spread of the powder.

**Table 7.IV:** Geometric relative density of printed parts with 50HT feedstock, using static and dynamic feeding systems.

| **Feeding system** | $\%\boldsymbol{\rho}_{geom}$ **(%)** | |
|---|---|---|
| | **Green part** | **Sintered part** |
| Static | 32,1 ± 0,4 | 57,2 ± 0,7 |
| Dynamic | 35,3 ± 0,5 | 62,9 ± 1,0 |

In addition to the feeding system, the reuse of powders was also assessed for the ZPrinter 650 with the 50HT. The reuse was performed using the vacuum system of the printer to push the exceeding powder from the powder bed and from the overflow bins, i.e., bins which are at the end of the powder bed to collect the exceeding powder from each layer after the spread by the roller. The reused powders were name as 50HTx1, after one reuse, and as 50HTx2, after the second reuse. The geometric relative density of the printed parts in green state and after 1st and 2nd industrial sintering cycles is presented in Table 7.V. Although a small decrease in the green density from 35,3 % to 34,7 % and in sintered parts from 62,9 % to 62,1 % after the two reused feedstocks, it is not significative and here we advocate that the reuse of feedstock powders in the ZPrinter 650 is possible and do not jeopardize the printed parts properties.

**Table 7.V:** Geometric relative density of printed parts with 50HT feedstock and reused feedstock.

| Feedstock | $\%\rho_{geom}$ (%) | |
|---|---|---|
| | **Green part** | **Sintered part** |
| 50HT | 35,3 ± 0,5 | 62,9 ± 1,0 |
| 50HTx1 | 34,9 ± 0,4 | 62,3 ± 0,7 |
| 50HTx2 | 34,7 ± 0,4 | 62,1 ± 0,6 |

Summarizing, for 50HT porcelain feedstock a combination of 100 μm and a binder saturation of 180 % should be used in a BJP printer with a dynamic feeding system. The binder saturation present higher influence in the design features able to be printed than the layer thickness, at the same time that provides enough mechanical resistance to the green parts in order to be printed.

During the practical work for this thesis, several challenges and limitations were found in the use of commercial BJP printers for porcelain feedstocks. In this sense, the interest in the development of a BJP printer dedicated for porcelain feedstock of *Porcelanas da Costa Verde* increased and a group of recommendations were registered after the limitations and challenges found.

The first challenge with the commercial BJP printers concerns in the piezoelectric printheads. In the case of Z310 printer, a printhead No 10 from Hewlett-Packard (HP) is

used. However, in the last years the production of this printhead model stop and turned the Z310 printer difficult to use due to the lack of printheads available in the market. The ones remaining were not reliable once some of them do not work well, leading to fails in the printing process. In the case of ZPrinter 650, the model of printhead is the No 11 (HP) and are still available in the market.

In Table 7.VI some of the most common errors found during the printing process with porcelain feedstock in the ZPrinter 650 are presented and reported in the user manual of the BJP printer. The first one, described above concerns in the high temperature reached in the printhead and is attributed to low binder flow, electric circuits failure and clog of the printhead orifices which may lead the print process to fail. The last one was observed and presented in Chapter 3, when printing with CMC as *in-bed* binder and its effects in the quality of the prints was discussed.

Other common error happening during the printing process regards in the axis position, which is calibrated every time that the printer is rebooted. However, if there is accumulation of powder in the guides of the axis, as shown in Figure 7.26, the axis will lose the position information, leading to a fail printer, corresponding to the 2303(0), 60300 and 60301 errors in Table 7.VI. This error is only solved if the printer is rebooted, making it impossible to recover a print in the middle of the job and leading to a failure in the printing.

Regarding the powder, two main errors occur: stop feeding powder (error 5001) and loose of position of the feeder (error 60100). The feeding powder error happens when the printer thinks it is out of powder, as reported in the printer user manual. The fact that the printer is prepared for commercial powders, which have a different density of the porcelain feedstock, leads to the need of the calibration of the feeder balance. This calibration is not possible to do by the operator for commercial printers, leading the only option to increase the weight in the balance by adding external weights. The second problem with the powder is the loose of position by the feeder, mainly due to the compaction of powder at the bottom of the feeder. Even though the feeder has its own fluidize system, when the powder is to compact, as shown in Figure 7.27, leads to the clog of the feeding orifices and stops the print process, and the only option is to remove the powder by hand.

**Table 7.VI:** Most common errors that happen during the printing with ZPrinter 650 (from printer manual user).

| Error | Description |
|---|---|
| 1006: Head x temperature too high | Caused by a print head overheating due to low binder flow, poor cleaning of the print head by the service station or a failed electrical circuit including the print head. |
| 2303(0): MOVER: axis 0 excessive position error | This error is caused by the presence of or the appearance of excessive friction on the slow axis rails front to back. |
| 60300: REZERO: fast axis length out of tolerance | This error is caused by the fast axis length being out of tolerance while rebooting. The length of travel is measured while booting. |
| 60301: REZERO: Slow axis length out of tolerance | This error is caused by the slow axis length being out of tolerance while rebooting. The length of travel is measured while booting. |
| 5001: POWDER: no more feed | This error occurs when the feeder runs out of powder or it thinks it is out of powder |
| 60100: Feeder timeout | This error occurs when the feeder drive motor is not responding or when the powder is packed in the bottom of the VAT. |

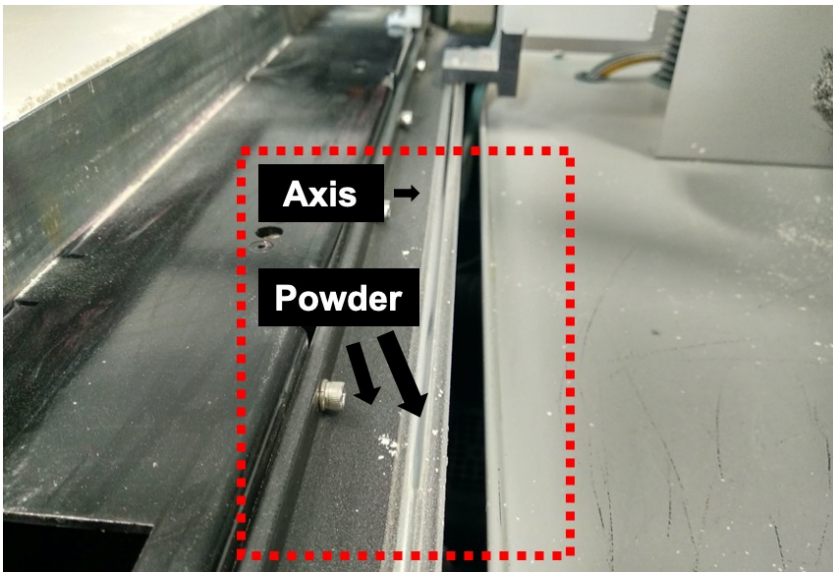


**Figure 7.26:** Powder accumulation in the guides of axis, leading to 2303(0), 60300 and 60301 errors.

**Figure 7.27:** Compacted 50HT feedstock powder in the bottom of the feeder, leading to the 60100 error.

Another limitation found was the accumulation of feedstock powder in the inner walls of the feeder after the printing, as illustrated in Figure 7.28. After the printing process is finished and all the powder is deposited in the build bed, it is noticeable that some powder was accumulated in the inner walls of the vat. A PSD analysis to this powder exhibits a broad monomodal distribution peaking at 15 μm. This means that a fraction of small particles is not deposited in the build bed, affecting the PSD of the printed powder and may lead to lower density of green and sintered parts and distortions of the sintered final part. However, all the parts produced with this printer were affected by this effect.

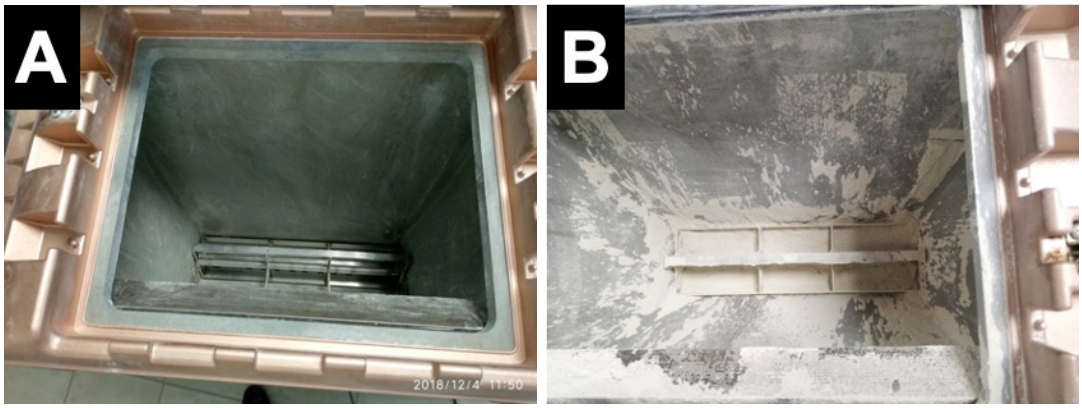


**Figure 7.28:** Powder feeder of ZPrinter 650 before (left) and after (right) printing with 50HT feedstock.

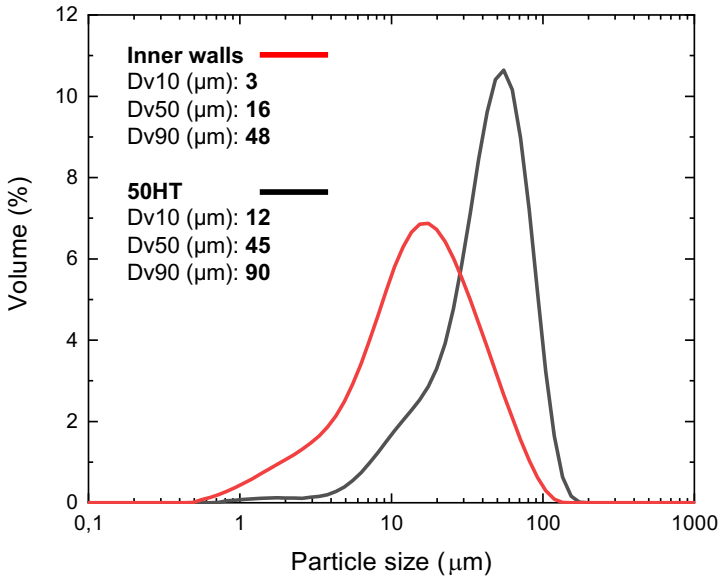


**Figure 7.29:** Particle size distribution of 50HT feedstock and of the powder in the inner walls of the feeder.

The final major limitation during the printing process regards in the software used. The software, 3DPrint Software, version 1.03.8 (3DSystems), is dedicated to the commercial printers and optimized for commercial powders. The software is limited to the use of porcelain feedstock and only allows variations in the layer thickness and binder saturation, as discussed above. The need of a more flexible software is clear and it is present by Oropallo *et al.* [5] by one of the ten challenges in additive manufacturing.

Summarizing, several limitations were found in the use of commercial BJP printers for porcelain parts production. Based on the discussion above, we advocate that a dedicated BJP printer should be developed for the full industrialization of BJP for porcelain parts production in order to have full control of the printer and the printing process, its maintenance and possible variations in the future.

The printer should comprise a liquid binder deposition system able to be easily clean or replaced without depending on commercial providers, a protection for the axis to avoid accumulation of powder in the rails, a feedstock fluidizer system to avoid the compaction of powder in the bottom of the feeder, smooth inner walls in the feeder to avoid accumulation of fine particles, the feeding system should be dynamic to keep the homogeneity of the PSD

of the feedstock in each layer and a vacuum system should be used to recover the exceeding powder after the print as it has low impact in the density of the printed parts. In addition, a dedicated software allowing full control of printing parameters should be subject of development, and if possible, the ability to use different printing parameters in different sections of the part to be printed, for instance, using different binder saturations in different sections may reduce the amount of liquid binder without jeopardizing the mechanical strength of the printed part.

## 7.5. Post conformation process

The post conformation processes comprise the drying of printed parts and the processing in industrial sintering cycles, as discussed in Chapter 6. The in bed drying time settle by the firmware of the printer ZPrinter 650 is 90 min for parts printed using commercial powders and standard printing parameters. We found that this time is too short when for the print with porcelain feedstock, due to the use of 180 % of binder saturation, which means more liquid binder is deposited to print the part and as consequence, more time is needed to fully dry the printed part. If the drying time is too short, the parts will deform during its removal from the powder bed because the *in-bed* binder is saturated with the liquid binder and is still in a viscous state. In this sense, the printed parts with the porcelain feedstock should dry in bed for 24 h, to make sure that the part has enough mechanical resistance and can be removed from the powder bed without breaking.

The post printing drying was also assessed using a laboratorial oven. The parts were dried at 90 °C, for 16 h. The differences of sintered parts without and with oven drying are shown in Figure 7.30 A and B. It is noticeable that the drying step in the oven avoid the crack of printed parts. In addition, deformations were observed after the industrial sintering of the printed parts in Figure 7.30 B. This effect was attributed to the friction between the base of the printed part and the plate inside the industrial kiln. In this sense, a fine alumina powder layer was used between the part bottom and the furnace plate to reduce the friction and the part was sintered without major deformation as presented in Figure 7.30 C.

These results show the importance of the drying in the quality of the final porcelain parts. The parts should dry for 24 h in the powder bed, and in an oven for 90 °C, for 16 h. A fine particle alumina powder layer should be used during sintering in order to produce crack free porcelain parts.

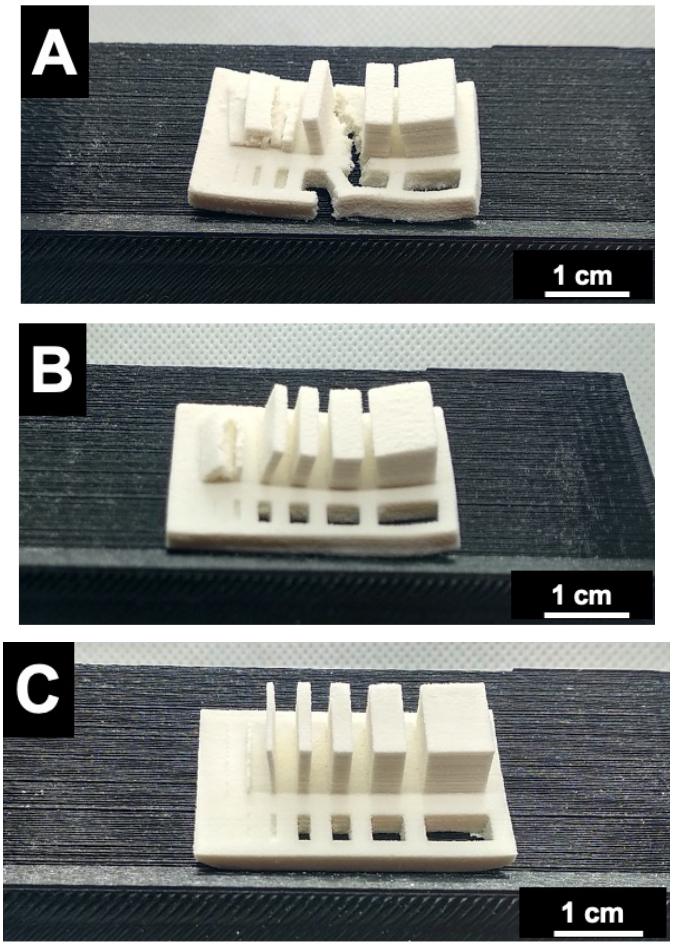


**Figure 7.30:** Printed part, after high temperature sintering, (A) using drying at room temperature for 16 h, (B) using a drying step in an oven at 90 °C, for 16 h and (C) using fine alumina between the part and the support, with drying at 90 °C, for 16 h.

The conventional produced porcelain parts by Porcelanas da Costa Verde comprises two step sintering in industrial continuous kilns, as illustrated in Figure 7.13, with the 1st sintering cycle with a maximum temperature of 980 - 1020 °C for 15 - 18 h, and the 2nd sintering with maximum temperature of 1360 - 1380 °C for 5 - 6 h. Using the same process for BJP parts, during the 1st sintering the *in-bed* binder is removed, however there is no significative densification, i.e., matter diffusion and no bonds between porcelain agglomerates is created, the parts are not consolidated and lead to poor mechanical resistance of parts, which broke by handling as presented in Figure 7.31, where a complex shaped part was processed by the sintering at 980 - 1020 °C for 15 - 18 h. In this sense, for the 1st sintering a different sintering cycle was used, as presented in Figure 7.13, with a maximum

temperature of 1180 - 1230 °C for 2,5 - 3 h. This thermal cycle is typically used for in-glaze decoration firing.

**Figure 7.31:** Complex part, produced by BJP with 50HT feedstock, after the firing cycle at 980 - 1020 °C for 15 - 18 h.

In Table 7.VII the relative density, assessed by Archimedes method, is presented for parts produced with different conformation methods, after processing in the 1st sintering cycle and after both 1st and 2nd sintering cycles. It is noticeable that for conventional methods, isostatic pressing, jiggering and pressure casting, produced parts have a relative density between 64 and 68 %. However, the parts produced by AM techniques only reached a maximum of 41 %. Even though the relative density was considerable low, the parts were consolidated enough to be handled during following processes. In the case of AM printed parts subject to CIP, the relative density increased up to 80 %, however, as discussed in Chapter 6, the processing in CIP is not suitable for complex shaped parts.

Regarding the second firing cycle, the parts produced by conventional processes reach a relative density of 99 %, near 100 %. This is not the case of the parts produced by powder bed AM techniques, which reached a maximum relative density of 68 %. The high porosity of the green parts jeopardizes the densification of the parts during the second sintering. The use of CIP lead to products with similar relative density (97 %), However, as demonstrated before, the CIP process is only possible in parts without complex shape. Considering that one of the main advantages of AM is the production of complex shaped products, the use of CIP is limited. Nevertheless, with the innovation in several techniques, in the future the use of CIP may be possible, if the medium (usually liquid) do not affect the porcelain products.

**Table 7.VII:** Relative density assessed by Archimedes method, after 1st sintering and after 1st and 2nd sintering, of porcelain parts produced through different conformation processes. In the case of AM produced parts the 1st sintering is different from the conventional ones.

| Process | $\%\rho_{Arc}$ | |
|---|---|---|
| | **1st sintering** | **1st + 2nd sintering** |
| **Isostatic pressing** | 68,0 | 99,1 |
| **Jiggering** | 67,8 | 99,9 |
| **Pressure casting** | 64,3 | 99,6 |
| **Binder jet printing (*)** | 40,7 | 68,4 |
| **Binder jet printing (+ CIP) (*)** | 79,8 | 96,6 |
| **Selective laser sintering (*)** | 39,1 | 55,6 |
| **Selective laser sintering (+ CIP) (*)** | 52,6 | 78,2 |

*(*) The firing cycle used was different for the parts of powder bed AM techniques, as discussed previously.*

Summarizing, the AM produced parts, especially the ones produced by BJP require a drying step in order to avoid deformations during industrial sintering, and a different base inside the kiln to reduce the friction between the base of the part and the plate. In addition, AM produced parts do not reach full densification after the two sintering cycles as opposed to the conventional ones.

## 7.6. Comparison of process with selective laser sintering

In this work two powder bed AM techniques were used: BJP and SLS. In this section we compare both regarding its possible industrialization for porcelain parts production, with focus in the feedstock, the printing process and the properties of final parts. Due to the higher interest in the BJP, because it is already available in the company, a more complete understanding of BJP was done in this work, however, a brief study of SLS was also done allowing the comparison between the techniques. Both techniques require the use of the feedstock in powder form, however, the process differ in the method of part construction: in the case of BJP a liquid binder is deposited for each cross-section, which bonds the particles

in the powder bed, while in the case of SLS a laser is responsible to sinter or melt the powder in the powder bed, promoting the bond between particles.

In the feedstock, there is a need of an *in-bed* binder for both techniques: in the case of BJP the *in-bed* binder must be water soluble and in the case of SLS the *in-bed* binder must be thermoplastic. However, both binders must have enough viscosity to penetrate in the void space between porcelain powder and provide enough mechanical resistance to the printed parts in order to be handled. In the case of BJP the viscosity is reached by the deposition of a liquid binder and the solubility of the *in-bed* binder in the liquid one, while in SLS the viscosity is reached after the laser scan, which melts the binder and provide the viscosity. In addition, based on the results of this work, the use of heat-treated porcelain powder is required in both techniques in order to reach defect free printed parts, as discussed in Chapter 4 and Chapter 5.

Concerning the printing process, as compared above, the BJP uses a liquid binder to bond particles while the SLS uses a laser for the same purpose. The use of the laser requires a controlled inert atmosphere in the chamber in order to prevent oxidation and burning of the *in-bed* binder powders and a controlled temperature of the powder bed in order to keep the powder near the melting temperature. In the case of ceramic powders, the use of temperature to process each layer may be a limitation due to thermal stress formed and possible delamination of the printed part. In the case of BJP the whole process is performed at room temperature without any atmosphere. This difference may increase the cost of the production of porcelain parts by SLS when compared with the ones produced by BJP. As the reuse of powders was assessed for both SLS (Chapter 5) and for BJP (in this Chapter) it is also noticeable that the reuse of powders does not have an impact in the BJP parts properties as opposed to the ones produced by SLS, for which deformations were observed after sintering, related with the decrease of small particles fraction in the feedstock. Although this fact may be attributed to the handle of powders, which in the case of BJP were recovered by a vacuum system and in the case of SLS were manually removed, it depends on the commercial printers features. The thermal processing of the feedstock in the case of SLS may also contribute for defective parts, once it affects properties of feedstock such as PSD, thermal behavior and flowability [13][14].

The printed parts have also differences, mainly concerning its density, when comparing parts produced by BJP and SLS. As discussed in Chapter 6, the parts produced by SLS

have higher content of *in-bed* binder than the ones produced by BJP, leading to higher porosity after the industrial sintering. In addition, even the use of CIP process, which is not suitable for complex shape parts, have also higher impact in the relative density of porcelain parts produced by BJP than the ones by SLS.

Summarizing, from the industrial point of view, the BJP have higher potential for its implementation at industrial scale for porcelain parts production than SLS. The reduced costs of BJP, the properties of the produced parts and the ease to scale up are advantages of BJP when compared with SLS. However, SLS present also the possibility to produce porcelain parts. Further investigation regarding the use of different *in-bed* binders and its content and the printing parameters in SLS is still needed for porcelain parts production.

## 7.7. Demonstration parts

As discussed previously, one of the main advantages of AM technologies is the ability to produce highly complex shaped parts, which can be difficult or even impossible to produce by conventional processes. In this section, we present complex shaped porcelain parts produced by BJP (Figure 7.11). The chosen objects are impossible to produce by conventional routes in one piece at Costa Verde facilities, based on their design. In addition, a small statue (Figure 7.12) was chosen to process in the glazing and decoration by hand painting steps of porcelain production, in order to present the adequation of the printed parts to the full process of porcelain parts production. All the parts were produced by BJP using the 50HT feedstock with 10 wt.% of PVA as *in-bed* binder.

The printing process of the chess set is illustrated in Figure 7.32. The process starts with parts positioning in the construction bed, using the appropriate software (Figure 7.32 A). The printing is then performed in a layer by layer process by the deposition of the liquid binder (Figure 7.32 B to E). Once the printing process is finished and after the parts dry in the powder bed for 24 h, the parts are removed by hand (Figure 7.32 F), followed by the depowdering process in a compressed air station, to remove all the exceeding powder out of the parts (Figure 7.32 G). The parts are then ready for the post conformation processes. The obtained parts were design defect free at the end of the printing, as presented in (Figure 7.32 H). In addition, one of the advantages of the powder bed AM processes is well noticeable in these images: the ability to print several parts at the same time.

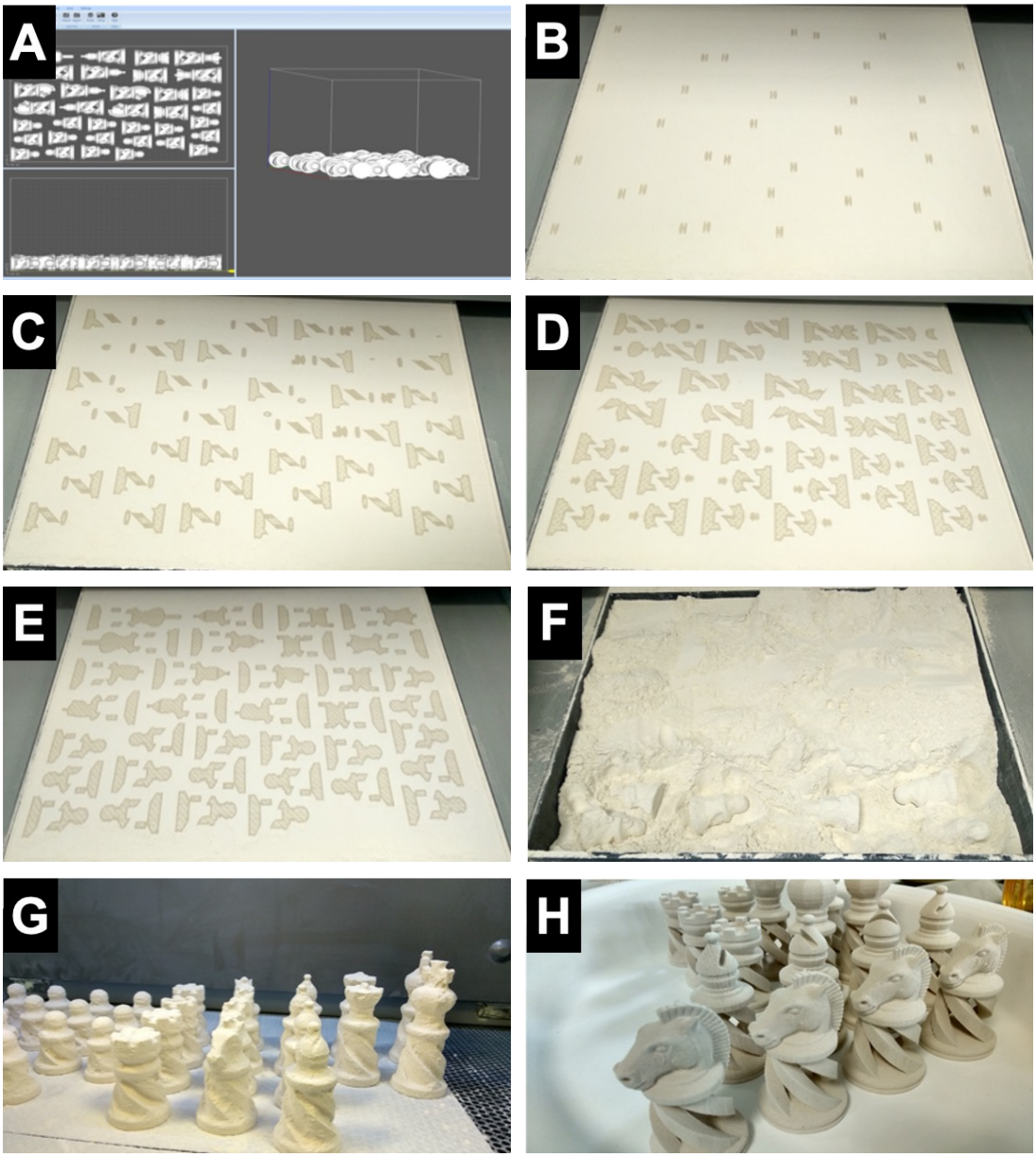


**Figure 7.32:** Chess set produced by BJP using 50HT feedstock, through the different stages of the process: (A) part positioning in construction bed using the software, (B) layer 2, (C) layer 63, (D) layer 109, (E) layer 201, (F) part removal from powder bed, (G) before depowdering with compressed air and (H) before post conformation processing.

The printed parts after the industrial sintering cycles, as illustrated in Figure 7.13 without the CIP process, are presented in Figure 7.33. Some of the parts were produced without major design defects (Figure 7.33 A), while others suffer major deformation and fracture during the industrial sintering (Figure 7.33 B). This defect is attributed to the design of the parts: firstly a major fraction of the weight are in the top side of the printed parts, i.e., in the

head of the chess parts, and also the ones presented in Figure 7.33 A are smaller in height (lower than 50 mm) than the ones in Figure 7.33 B (higher than 50 mm), as presented in Figure 7.11. Here we advocate that this fact contributed to the deformation during sintering, once the body structure was not suitable to hold the mass weight of the part top section of the taller parts, promoting its deformation and fracture.

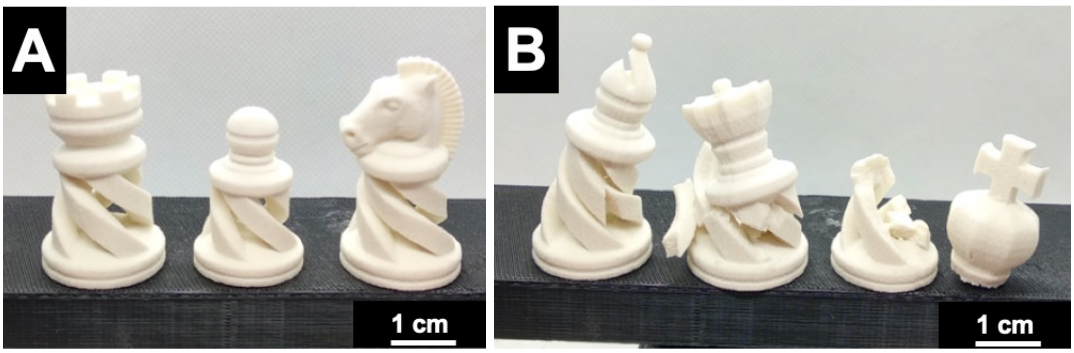


**Figure 7.33:** Printed parts by BJP after 1st and 2nd industrial sintering cycles, as presented in Figure 7.13 without CIP process. The parts presented in (A) were defect free after the sintering processing, while the parts presented in (B) suffer major deformation during the sintering.

The statue with detail features is presented in Figure 7.34 after different stages of post conformation steps: after 1st and 2nd industrial sintering (Figure 7.34 A) unglazed, after the 1st and 2nd sintering glazed (Figure 7.34 B) and after decoration followed by decoration firing (Figure 7.34 C). With a first general overview we can conclude that high detail parts and the ability to produce personalized objects is possible by BJP followed by post conformation processes. In addition, the decorated part leads us to advocate that the printed parts are also suitable for the glazed decoration as well.

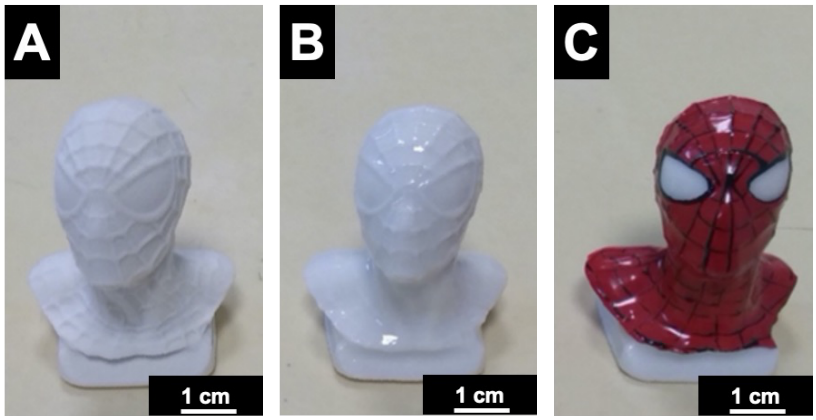


**Figure 7.34:** Porcelain printed part by BJP, using 50HT feedstock, through different stages of industrial porcelain printed parts processing: (A) after 1st and 2nd sintering without glaze, (B) after 1st and 2nd sintering with glaze and (C) after glazing followed by decoration and decoration firing.

Summarizing, we proved that it is possible to produce highly complex shaped parts by BJP and processed in the post conformation processes available at *Porcelanas da Costa Verde*, such as industrial sintering cycles and decoration processes. However, major deformations were observed for some of the complex shaped parts (Figure 7.33 B) and these defects were attributed to the design of the parts. As reported in the literature, Design for Additive Manufacturing (DfAM) is one of the challenges in AM [5] and one of the emerging fields in design engineering [15] and, in the case of the AM use for porcelain parts production is on exception. The object design optimization may also have an impact in post conformation processes reducing the number of assemblies and cost [2]. Thus, further investigation is needed focused on design for BJP of porcelain parts in order to avoid such defects and reach the full potential of AM for complex shaped objects.

## 7.8. Conclusions

The major conclusion of this work is the proof that powder bed AM techniques, especially BJP, can be used as production route for porcelain products. We also proved that the facilities of the company are suitable for both preparation of feedstock and post-conformation process of printed porcelain products.

In the case of feedstock, the use of spray drying to produce porcelain powders for BJP is suitable, and varying porcelain suspensions and operation conditions the company is able to produce powders with different characteristics regarding its PSD and morphology.

However, some modification to the spray dryer must be done, with the main one the collection of fine porcelain powders after the cyclone system. Based on our results, the powder should be produce using a 1580 g/L porcelain suspension without the use of additives and a nozzle with 0,9 mm, a feeding pressure of 10 bar and depression of 147 Pa in the cyclone. In the case of the industrial sieving of porcelain powders, even though it is possible to reach the desired PSD of porcelain powders, the efficiency of the process is jeopardized by the equipment used. In this sense, an equipment dedicated to sieve dry powders should be used.

Concerning the printing process, the commercial printers may be used to produced porcelain parts, however several limitations were found during the work and we recommend a development of a BJP printer dedicated for porcelain feedstock. In this sense, the printer should have a vacuum system to recover the exceeding powder for its reuse, the dynamic feeder should have smooth inner walls to avoid the variation in PSD of feedstock and the construction should allow the easy clean of the printheads and avoid the powder to reach the axis rails of the printer. In addition, a software which allows full control of the printing process and its main parameters may be an advantage.

The post conformation steps, conventionally used for porcelain parts production, are suitable to produce defect free printed parts. However, the full densification of the printed parts was not possible and further investigation in post-conformation processes should be done in order to produce printed parts with full densification without major deformations.

Summarizing, the industrialization of BJP process to produced porcelain printed parts is possible and was proven so. However, further investigation in the different steps of production is needed to reach the full potential of AM processing. In the next section we recommend several future works.

## 7.9. References

[1] E. Rauch, M. Unterhofer, and P. Dallasega, “Industry sector analysis for the application of additive manufacturing in smart and distributed manufacturing systems,” *Manuf. Lett.*, vol. 15, pp. 126–131, 2018.

[2] C. Klahn, B. Leutenecker, and M. Meboldt, “Design strategies for the process of additive manufacturing,” *Procedia CIRP*, vol. 36, pp. 230–235, 2015.

[3] P. Stavropoulos, P. Foteinopoulos, A. Papacharalampopoulos, and H. Bikas, “Addressing the challenges for the industrial application of additive manufacturing: Towards a hybrid solution,” *Int. J. Light. Mater. Manuf.*, vol. 1, no. 3, pp. 157–168, 2018.

[4] H. Levi, “Changing the way we manufacture – AM in technical ceramics,” *Met. Powder Rep.*, vol. 73, no. 6, pp. 314–315, 2018.

[5] W. Oropallo and L. A. Piegl, “Ten challenges in 3D printing,” *Eng. Comput.*, vol. 32, no. 1, pp. 135–148, 2015.

[6] D. Santos, A. C. Maurício, V. Sencadas, J. D. Santos, M. H. Fernandes, and P. S. Gomes, “Spray Drying: An Overview,” *Biomater. - Phys. Chem. - New Ed.*, 2018.

[7] JaaYoo, “Thingiverse, Thing: 1094870,” 2015. [Online]. Available: https://www.thingiverse.com/thing:1094870. [Accessed: 25-Nov-2018].

[8] BerlinRockz, “Thingiverse, Thing: 1692007,” 2016. [Online]. Available: https://www.thingiverse.com/thing:1692007. [Accessed: 25-Nov-2018].

[9] S. J. Lukasiewicz, “Spray-Drying Ceramic Powders,” *J. Am. Ceram. Soc.*, vol. 72, no. 4, pp. 617–624, 1989.

[10] V. One and A. S. Mujumdar, *Spray Drying Technology*.

[11] M. Vaezi and C. K. Chua, “Effects of layer thickness and binder saturation level parameters on 3D printing process,” *Int. J. Adv. Manuf. Technol.*, vol. 53, no. 1–4, pp. 275–284, 2011.

[12] A. Mostafaei, A. M. Elliott, J. E. Barnes, C. L. Cramer, P. Nandwana, and M. Chmielus, “Binder jet 3D printing – process parameters, materials, properties, and challenges,” *Prog. Mater. Sci.*, p. 100684, 2020.

[13] L. C. Ardila *et al.*, “Effect of IN718 recycled powder reuse on properties of parts manufactured by means of Selective Laser Melting,” *Phys. Procedia*, vol. 56, no. C, pp. 99–107, 2014.

[14] H. Asgari, C. Baxter, K. Hosseinkhani, and M. Mohammadi, “On microstructure and mechanical properties of additively manufactured AlSi10Mg_200C using recycled powder,” *Mater. Sci. Eng. A*, vol. 707, no. September, pp. 148–158, 2017.

[15] W. Gao *et al.*, “The status, challenges, and future of additive manufacturing in engineering,” *Comput. Des.*, 2015.

# Conclusions and final remarks

The main goal of this project was to assess the industrialization of powder bed AM techniques, with special focus in BJP technology. For that, several studies were performed concerning the feedstock preparation and characteristics, and the post-conformation processing. Although the AM process itself has a crucial role in the properties of the final parts, currently the commercial BJP printers available at Costa Verde have limited access to the printing parameters.

Overall, the results obtained in this project support the argument that the BJP process can be used as a conformation route for the production of porcelain objects, using industrial porcelain powders produced at Costa Verde. However, several limitations concerning the BJP equipment were found, and we advocate that, in order to have full control in the process, a BJP printer should be developed and constructed by the company.

In addition, SLS was also aim of study however we advocate that for industrial production of porcelain parts, BJP is a more suitable option mainly due to the energy consumption and the cost of the equipment.

The highlight of this whole project regards on the use of heat-treated porcelain powders. This subject, not reported in the literature under our scope, was a key part of this work, once the use of heat-treated porcelain powders in the feedstock lead to defect free porcelain objects for both BJP and SLS. In that sense, a feedstock using 10 wt.% of PVA as *in-bed* binder, 45 wt.% of raw porcelain powder and 45 wt.% of heat-treated porcelain powder shown promising results for production of industrial porcelain parts by BJP. In the case of SLS, the formulation with the most promising results is composed of 16 wt.% of polyamide 12 as *in-bed* binder and 84 wt.% of heat-treated porcelain powders.

The industrialization of additive manufacturing at Costa Verde, especially BJP allows the company to produce objects that are impossible or expensive to manufacture by any other process available at Costa Verde. In this sense, the company may reach new markets and customers using this technology to produce small size production batches, personalized objects and differentiated porcelain objects.

# Future work

In this exploratory project we demonstrated the possibility of the use of BJP for the production of porcelain parts. However, because this was the first work of this type in the company, there were several subjects approach. In this sense, in this section, we present what we think it should be the focus of following research, in order to bring a deeper knowledge in this area.

## Feedstock

In the case of the feedstock preparation, a deeper study should be done regarding the industrial spray drying process. A comprehensive study regarding the influence of the properties of the ceramic suspension in the characteristics of the powders produced should be done in detail for the spray dryer available in *Porcelanas da Costa Verde*. The optimization of the operation conditions such as nozzle orifice diameter, feeding pressure and cyclone depression should be assessed in order to maximize the production of fine porcelain powders, reducing the waste of coarse porcelain powders and improving its efficiency. Other factors that may influence the process and were not addressed in this work are the chamber temperature, in the case of operations parameters, and the viscosity of the ceramic suspension, in the case of the suspension characteristics.

The dry sieving process should be performed using a different system in order to increase the efficiency of the process for dry powders, once it was observed that a fraction of fine powders (50 vol.%) is not sieved using the existent system. In this way the waste of powders may be reduced and its efficiency increased.

The mixing of the powders should also be aim of study, in order to improve the blend of dry powders, reducing the time to prepare the feedstock keeping its homogeneity regarding the mixture of the *in-bed* binders with the porcelain ones. Also, an increase in the amount of feedstock may also be aim of study, once for full industrialization, the amount of feedstock available for industrial production must increase.

A detailed cost analysis should also be performed in the preparation of the *in-bed* binder for AM, once the cost of milling and sieving could be less than the order of the binder already with the desired granulometric properties. In addition, although the goal of this work was

based on the idea of not changing the porcelain composition *of Porcelanas da Costa Verde*, the addition of materials able to reduce the sintering temperature may be interesting in order to use the conventional process route for AM parts.

**Printing process**

The development of an equipment and software dedicated for porcelain feedstock should also be done. As demonstrated in this chapter, commercial BJP printers have several limitations regarding the hardware and the software. In this sense, a development of a fully equipment will give the company the opportunity to have full control of the process and do a proper maintenance without the need of the technical support. The software should also have some flexibility regarding the type of formulation used during the printing. The software should also allow the use of different parameters (layer thickness and binder saturation) in different sections of a part, in order to increase the quality of the part and its densification as well. The printer should also comply a bigger printing volume, in order to compensate the elevated retraction of porcelain products during the sintering process.

Also, in the printing process, the high cost of the liquid binder leads to the need to study homemade liquid binders for the printing of porcelain parts. During this work, we approach the study of the liquid binder, however, due to the limits of the commercial printers, it was noticed that for new binders, the liquid binder system should be changed, in order to avoid clogs and deterioration of the system, for instance, the deterioration of the polymeric tubes, as reported in the literature [1]. Two main directions can be taken regarding this subject: i) the use of a simple liquid binder, such as distilled water, once the *in-bed* binder used, PVA, is water soluble and the use of distilled water may be enough to solubilize the PVA powder and provide enough mechanical resistance, as reported in literature using maltodextrin and clay powders [2] and ii) as reported in the literature [3]-[6], the use of liquid binder suspensions with ceramic nanoparticles may increase the density of the printed parts by filling the void space between porcelain agglomerates with ceramic powders after drying. However, in this case, the use of this type of liquid binders may change the composition of the final sintered porcelain part and increase the cost of printing.

**Post conformation processing**

In the post-conformation processes, the biggest limitation is to reach full densification of the parts. Although the printed parts were produced using the existent thermal cycles of *Porcelanas da Costa Verde*, it was proven that, for instance, the 1st sintering cycle is not appropriated for BJP parts as it is for conventionally produced ones. The study of appropriate sintering cycles is needed. The use of CIP was approached and shown to have high influence in the densification of the parts. However, as discussed before, the technique has limitations regarding complex shaped products. In this sense, different post-conformations steps towards higher densification should also be subject of a detailed study for instance, the infiltration of the printed parts with ceramic suspensions.

The deformations during the post-conformations processes and the design compensations should be also subject of study, in order to reduce defective parts, as it is one of the challenges in the future for AM produced parts [7]. However, even for conventional processes, the design compensation is not the same for all the products, being influenced by the design of the part. So, a previous study for each part, must be always done.

**Economic viability of BJP**

Finally, a cost analysis must be done to understand the economic viability of the industrialization of BJP for porcelain parts production. The development of the equipment and changes in the feedstock preparation, turns a detailed analysis of costs indispensable in order to fully industrialize this process as production route. In addition, a market research should be done as well, in other to understand the type of products, clients and markets for which BJP produced porcelain parts may exhibit full potential.

## References

[1] J. a Inzana *et al.*, “3D printing of composite calcium phosphate and collagen scaffolds for bone regeneration.,” *Biomaterials*, vol. 35, no. 13, pp. 4026–34, Apr. 2014.

[2] G. Marchelli, M. Ganter, and D. Storti, “New material systems for 3D ceramic printing,” in *Solid Freeform Fabrication Symposium*, 2009, pp. 477–487.

[3] H. Zhao, C. Ye, Z. Fan, and C. Wang, “3D printing of CaO-based ceramic core using nanozirconia suspension as a binder,” *J. Eur. Ceram. Soc.*, vol. 37, no. 15, pp. 5119–

5125, 2017.

[4] Y. Bai and C. B. Williams, “Binder jetting additive manufacturing with a particle-free metal ink as a binder precursor,” *Mater. Des.*, vol. 147, no. 2017, pp. 146–156, 2018.

[5] Y. Bai and C. B. Williams, “The effect of inkjetted nanoparticles on metal part properties in binder jetting additive manufacturing,” *Nanotechnology*, 2018.

[6] H. Zhao, C. Ye, S. Xiong, Z. Fan, and L. Zhao, “Fabricating an effective calcium zirconate layer over the calcia grains via binder-jet 3D-printing for improving the properties of calcia ceramic cores,” *Addit. Manuf.*, vol. 32, no. June 2019, 2020.

[7] W. Oropallo and L. A. Piegl, “Ten challenges in 3D printing,” *Eng. Comput.*, vol. 32, no. 1, pp. 135–148, 2015.